

6-16-2011

Simulations for the Test Flight of an Experimental HALE Aircraft

Brooke E. Kaszynski

Follow this and additional works at: <https://scholar.afit.edu/etd>

Part of the [Aerospace Engineering Commons](#)

Recommended Citation

Kaszynski, Brooke E., "Simulations for the Test Flight of an Experimental HALE Aircraft" (2011). *Theses and Dissertations*. 1334.
<https://scholar.afit.edu/etd/1334>

This Thesis is brought to you for free and open access by the Student Graduate Works at AFIT Scholar. It has been accepted for inclusion in Theses and Dissertations by an authorized administrator of AFIT Scholar. For more information, please contact richard.mansfield@afit.edu.



**SIMULATIONS FOR THE TEST FLIGHT OF AN EXPERIMENTAL HALE
AIRCRAFT**

THESIS

Brooke E. Kaszynski, 1st Lieutenant, USAF

AFIT/GAE/ENY/11-J02

**DEPARTMENT OF THE AIR FORCE
AIR UNIVERSITY**

AIR FORCE INSTITUTE OF TECHNOLOGY

Wright-Patterson Air Force Base, Ohio

APPROVED FOR PUBLIC RELEASE; DISTRIBUTION UNLIMITED.

The views expressed in this thesis are those of the author and do not reflect the official policy or position of the United States Air Force, Department of Defense, or the United States Government. This material is declared a work of the U.S. Government and is not subject to copyright protection in the United States.

AFIT/GAE/ENY/11-J02

**SIMULATIONS FOR THE TEST FLIGHT OF AN EXPERIMENTAL HALE
AIRCRAFT**

THESIS

Presented to the Faculty

Department of Aeronautics and Astronautics

Graduate School of Engineering and Management

Air Force Institute of Technology

Air University

Air Education and Training Command

In Partial Fulfillment of the Requirements for the
Degree of Master of Science in Aeronautical Engineering

Brooke E. Kaszynski

1st Lieutenant, USAF

June 2011

APPROVED FOR PUBLIC RELEASE; DISTRIBUTION UNLIMITED.

**SIMULATIONS FOR THE TEST FLIGHT OF AN EXPERIMENTAL HALE
AIRCRAFT**

Brooke E. Kaszynski

1st Lieutenant, USAF

June 2011

Approved:

Lt Col Christopher M. Shearer, USAF (Chairman)

date

Dr. Donald L. Kunz (Member)

date

Dr. Mark F. Reeder (Member)

date

Abstract

Recent events, such as the crash of NASA's Helios aircraft during a test flight, show that more must be known about the nonlinear control of HALE aircraft. Shearer, Cesnik and their co-workers have developed a code that is a practical solution to the coupled nonlinear aeroelasticity and flight dynamics of very flexible aircraft called the University of Michigan's Nonlinear Aeroelastic Simulation Toolbox (UM/NAST). They are also in the process of developing a model HALE aircraft called X-HALE which will be used to validate this code experimentally. This research performs flight simulations with UM/NAST so as to make predictions about X-HALE's future test flights and subsequently uncover the strengths and weaknesses of UM/NAST when X-HALE is finally flown. These simulations include simulations of straight and level flight and rolling flight. Rolling simulations involve periodic changes in the angle of the ailerons. Both the 6 meter and the 8 meter models of X-HALE are studied. Two control models are compared. These include the linear and non-linear models of UM/NAST.

Acknowledgements

I would like to say thank you to my loving husband and our beautiful son; both of whom have been with me the whole way on this journey, and to God for all the wonderful blessings He has given me in life.

Brooke E. Kaszynski

Table of Contents

	Page
Abstract.....	v
Acknowledgements.....	vi
Table of Contents.....	vii
List of Figures.....	ix
List of Symbols.....	xx
List of Abbreviations.....	xxiii
I. Introduction.....	1
II. Theoretical Development.....	5
II.1 Previous Research and Motivation.....	5
II.2 The Early Work of Van Schoor, Von Flotow and Jones.....	5
II.3 The Development and Use of ASWING.....	6
II.4 The Development of UM/NAST.....	7
II.5 RCAS.....	9
II.6 NATASHA.....	10
II.7 Other Recent Work on Nonlinear Aeroelastic Solvers.....	10
II.8 Present Motivation and Problem.....	12
III. Model Development.....	13
III.1 The X-HALE Aircraft.....	13
III.2 The Coordinate Systems of UM/NAST.....	16
III.3 A Study of the Governing Differential Equations of Motion.....	21
III.3.1 The Equations of Motion.....	22
III.3.2 A Retrieval of the Rigid-Body Equations of Motion.....	25
III.4 Numerical Integration and the Trim Solution.....	27
III.5 Solution of the Governing Equations of Motion.....	29
IV. Results.....	32
IV.1 The Assumptions Made.....	32
IV.2 Running the Simulations and Initial Complications.....	34
IV.3 The Chosen Simulations.....	38
IV.4 The Completed Simulations and Their Results.....	43
IV.4.1 The 6 Meter X-HALE Results.....	43
IV.4.2 The 8 Meter X-HALE Results.....	55
V. Conclusions and Recommendations.....	83

V.1	Conclusions.....	83
V.2	Recommendations for Future Research.....	87
V.3	General Remarks.....	88
Appendix A.	Additional Figures.....	90
	Case 1: 6 m Linear Type 15 sec Simulation, No Aileron Input.....	90
	Case 2: 6 m Linear Type 10 sec Simulation, No Aileron Input.....	94
	Case 3: 6 m Nonlinear Type 10 sec Simulation, No Aileron Input.....	98
	Case 4: 6 m Linear Type 10 sec Simulation, 2 deg Aileron Input.....	102
	Case 5: 6 m Linear Type 10 sec Simulation, 5 deg Aileron Input.....	106
	Case 6: 6 m Linear Type 10 sec Simulation, 10 deg Aileron Input.....	110
	Case 7: 8 m Linear Type 15 sec Simulation, No Aileron Input.....	114
	Case 8: 8 m Linear Type 15 sec Simulation, 2 deg Aileron Input.....	118
	Case 9: 8 m Nonlinear Type 15 sec Simulation, 2 deg Aileron Input.....	122
	Case 10: 8 m Linear Type 15 sec Simulation, 5 deg Aileron Input.....	126
	Case 11: 8 m Nonlinear Type 15 sec Simulation, 5 deg Aileron Input.....	130
	Case 12: 8 m Linear Type 15 sec Simulation, 10 deg Aileron Input.....	134
	Case 13: 8 m Nonlinear Type 15 sec Simulation, 10 deg Aileron Input.....	138
	Case 14: 8 m Linear Type 15 sec Simulation, 15 deg Aileron Input.....	142
	Case 15: 8 m Nonlinear Type 15 sec Simulation, 15 deg Aileron Input.....	146
	Case 16: 8 m Linear Type 15 sec Simulation, 20 deg Aileron Input.....	150
	Case 17: 8 m Linear Type 15 sec Simulation, 25 deg Aileron Input.....	154
Appendix B.	Input File for the 6 Meter, 5 Degree Aileron Input Linear Case, Case 5.	158
Appendix C.	Input File for the 8 Meter, No Aileron Input Linear Case, Case 7.....	180
Bibliography	201

List of Figures

Figure	Page
Figure 1. Wing-Body-Tail Configuration [4]	2
Figure 2. Single-Wing Configuration [4].....	2
Figure 3. Joined-Wing Configuration [4]	2
Figure 4. Aerovironment's Helios [4].....	3
Figure 5. X-HALE: 6 Meter Model (Top) and 8 Meter Model (Bottom) [24]	14
Figure 6. Body Fixed Reference Frame B [22].....	17
Figure 7. The Rigid-body Reference Frame [22].....	18
Figure 8. The Body Reference Frame B and the Vehicle Coordinates [22]	19
Figure 9. Trim Solution Flow Chart [22].....	29
Figure 10. UM/NAST Model of the 8 Meter X-HALE Aircraft [4].....	33
Figure 11. Deformed Shape at the Trim Condition for the 8 Meter X-HALE [4].....	34
Figure 12. Case 1 Longitudinal Velocity v_y versus Time	35
Figure 13. Case 6 Aileron Input versus Time	39
Figure 14. Case 1 Longitudinal Velocity v_y versus Time	44
Figure 15. Case 1 Lateral Velocity v_x versus Time.....	45
Figure 16. Case 1 Vertical Velocity v_z versus Time	45
Figure 17. Case 1 Pitch Rate ω_x versus Time	46

Figure 18. Case 1 Roll Rate ω_y versus Time.....	46
Figure 19. Case 1 Yaw Rate ω_z versus Time	47
Figure 20. Case 3 Lateral Velocity v_x versus Time.....	48
Figure 21. Case 3 Longitudinal Velocity v_y versus Time	49
Figure 22. Case 3 Vertical Velocity v_z versus Time	49
Figure 23. Case 3 Pitch Rate ω_x versus Time	50
Figure 24. Case 3 Roll Rate ω_y versus Time.....	50
Figure 25. Case 3 Yaw Rate ω_z versus Time	51
Figure 26. Case 6 Aileron Input versus Time	52
Figure 27. Case 6 Lateral Velocity v_x versus Time.....	52
Figure 28. Case 6 Longitudinal Velocity v_y versus Time	53
Figure 29. Case 6 Vertical Velocity v_z versus Time	53
Figure 30. Case 6 Pitch Rate ω_x versus Time	54
Figure 31. Case 6 Roll Rate ω_y versus Time.....	54
Figure 32. Case 6 Yaw Rate ω_z versus Time	55
Figure 33. Case 7 Lateral Velocity v_x versus Time.....	56
Figure 34. Case 7 Longitudinal Velocity v_y versus Time	57
Figure 35. Case 7 Vertical Velocity v_z versus Time	57
Figure 36. Case 7 Pitch Rate ω_x versus Time	58

Figure 37. Case 7 Roll Rate ω_y versus Time.....	58
Figure 38. Case 7 Yaw Rate ω_z versus Time	59
Figure 39. Case 8 Aileron Input versus Time	60
Figure 40. Case 8 Lateral Velocity v_x versus Time.....	61
Figure 41. Case 8 Longitudinal Velocity v_y versus Time	61
Figure 42. Case 8 Lateral Velocity v_z versus Time.....	62
Figure 43. Case 8 Pitch Rate ω_x versus Time	62
Figure 44. Case 8 Roll Rate ω_y versus Time.....	63
Figure 45. Case 8 Yaw Rate ω_z versus Time	63
Figure 46. Case 12 Aileron Input versus Time	65
Figure 47. Case 12 Lateral Velocity v_x versus Time.....	66
Figure 48. Case 12 Longitudinal Velocity v_y versus Time	66
Figure 49. Case 12 Vertical Velocity v_z versus Time	67
Figure 50. Case 12 Pitch Rate ω_x versus Time	67
Figure 51. Case 12 Roll Rate ω_y versus Time.....	68
Figure 52. Case 12 Yaw Rate ω_z versus Time	68
Figure 53. Case 13 Aileron Input versus Time	69
Figure 54. Case 13 Lateral Velocity v_x versus Time.....	69
Figure 55. Case 13 Longitudinal Velocity v_y versus Time	70

Figure 56. Case 13 Vertical Velocity v_z versus Time	70
Figure 57. Case 13 Pitch Rate ω_x versus Time	71
Figure 58. Case 13 Roll Rate ω_y versus Time.....	71
Figure 59. Case 13 Yaw Rate ω_z versus Time	72
Figure 60. Case 14 Aileron Input versus Time	73
Figure 61. Case 14 Lateral Velocity v_x versus Time.....	74
Figure 62. Case 14 Longitudinal Velocity v_y versus Time	74
Figure 63. Case 14 Vertical Velocity v_z versus Time	75
Figure 64. Case 14 Pitch Rate ω_x versus Time	75
Figure 65. Case 14 Roll Rate ω_y versus Time.....	76
Figure 66. Case 14 Yaw Rate ω_z versus Time	76
Figure 67. Case 15 Aileron Input versus Time	77
Figure 68. Case 15 Lateral Velocity v_x versus Time.....	77
Figure 69. Case 15 Longitudinal Velocity v_y versus Time	78
Figure 70. Case 15 Vertical Velocity v_z versus Time	78
Figure 71. Case 15 Pitch Rate ω_x versus Time	79
Figure 72. Case 15 Roll Rate ω_y versus Time.....	79
Figure 73. Case 15 Yaw Rate ω_z versus Time	80
Figure 74. Case 1 Lateral Velocity v_x versus Time.....	90

Figure 75. Case 1 Longitudinal Velocity v_y versus Time	91
Figure 76. Case 1 Vertical Velocity v_z versus Time	91
Figure 77. Case 1 Pitch Rate ω_x versus Time	92
Figure 78. Case 1 Roll Rate ω_y versus Time.....	92
Figure 79. Case 1 Yaw Rate ω_z versus Time	93
Figure 80. Case 2 Lateral Velocity v_x versus Time.....	94
Figure 81. Case 2 Longitudinal Velocity v_y versus Time	95
Figure 82. Case 2 Vertical Velocity v_z versus Time	95
Figure 83. Case 2 Pitch Rate ω_x versus Time	96
Figure 84. Case 2 Roll Rate ω_y versus Time.....	96
Figure 85. Case 2 Yaw Rate ω_z versus Time	97
Figure 86. Case 3 Lateral Velocity v_x versus Time.....	98
Figure 87. Case 3 Longitudinal Velocity v_x versus Time	99
Figure 88. Case 3 Vertical Velocity v_z versus Time	99
Figure 89. Case 3 Pitch Rate ω_x versus Time	100
Figure 90. Case 3 Roll Rate ω_y versus Time.....	100
Figure 91. Case 3 Yaw Rate ω_z versus Time	101
Figure 92. Case 4 Aileron Input versus Time	102
Figure 93. Case 4 Lateral Velocity v_x versus Time.....	103

Figure 94. Case 4 Longitudinal Velocity v_y versus Time	103
Figure 95. Case 4 Vertical Velocity v_z versus Time	104
Figure 96. Case 4 Pitch Rate ω_x versus Time	104
Figure 97. Case 4 Roll Rate ω_y versus Time.....	105
Figure 98. Case 4 Yaw Rate ω_z versus Time	105
Figure 99. Case 5 Aileron Input versus Time	106
Figure 100. Case 5 Lateral Velocity v_x versus Time.....	107
Figure 101. Case 5 Longitudinal Velocity v_y versus Time	107
Figure 102. Case 5 Vertical Velocity v_z versus Time	108
Figure 103. Case 5 Pitch Rate ω_x versus Time	108
Figure 104. Case 5 Roll Rate ω_y versus Time.....	109
Figure 105. Case 5 Yaw Rate ω_z versus Time	109
Figure 106. Case 6 Aileron Input versus Time	110
Figure 107. Case 6 Lateral Velocity v_x versus Time.....	111
Figure 108. Case 6 Longitudinal Velocity v_y versus Time	111
Figure 109. Case 6 Vertical Velocity v_z versus Time	112
Figure 110. Case 6 Pitch Rate ω_x versus Time	112
Figure 111. Case 6 Roll Rate ω_y versus Time.....	113
Figure 112. Case 6 Yaw Rate ω_z versus Time	113

Figure 113. Case 7 Lateral Velocity v_x versus Time.....	114
Figure 114. Case 7 Longitudinal Velocity v_y versus Time	115
Figure 115. Case 7 Vertical Velocity v_z versus Time	115
Figure 116. Case 7 Pitch Rate ω_x versus Time	116
Figure 117. Case 7 Roll Rate ω_y versus Time.....	116
Figure 118. Case 7 Yaw Rate ω_z versus Time	117
Figure 119. Case 8 Aileron Input versus Time	118
Figure 120. Case 8 Lateral Velocity v_x versus Time.....	119
Figure 121. Case 8 Longitudinal Velocity v_y versus Time	119
Figure 122. Case 8 Vertical Velocity v_z versus Time	120
Figure 123. Case 8 Pitch Rate ω_x versus Time	120
Figure 124. Case 8 Roll Rate ω_y versus Time.....	121
Figure 125. Case 8 Yaw Rate ω_z versus Time	121
Figure 126. Case 9 Aileron Input versus Time	122
Figure 127. Case 9 Lateral Velocity v_x versus Time.....	123
Figure 128. Case 9 Longitudinal Velocity v_y versus Time	123
Figure 129. Case 9 Vertical Velocity v_z versus Time	124
Figure 130. Case 9 Pitch Rate ω_x versus Time	124
Figure 131. Case 9 Roll Rate ω_y versus Time.....	125

Figure 132. Case 9 Yaw Rate ω_z versus Time	125
Figure 133. Case 10 Aileron Input versus Time	126
Figure 134. Case 10 Lateral Velocity v_x versus Time.....	127
Figure 135. Case 10 Longitudinal Velocity v_y versus Time	127
Figure 136. Case 10 Vertical Velocity v_z versus Time	128
Figure 137. Case 10 Pitch Rate ω_x versus Time	128
Figure 138. Case 10 Roll Rate ω_y versus Time.....	129
Figure 139. Case 10 Yaw Rate ω_z versus Time	129
Figure 140. Case 11 Aileron Input versus Time	130
Figure 141. Case 11 Lateral Velocity v_x versus Time.....	131
Figure 142. Case 11 Longitudinal Velocity v_y versus Time	131
Figure 143. Case 11 Vertical Velocity v_z versus Time	132
Figure 144. Case 11 Pitch Rate ω_x versus Time	132
Figure 145. Case 11 Roll Rate ω_y versus Time.....	133
Figure 146. Case 11 Yaw Rate ω_z versus Time	133
Figure 147. Case 12 Aileron Input versus Time	134
Figure 148. Case 12 Lateral Velocity v_x versus Time.....	135
Figure 149. Case 12 Longitudinal Velocity v_y versus Time	135
Figure 150. Case 12 Vertical Velocity v_z versus Time	136

Figure 151. Case 12 Pitch Rate ω_x versus Time	136
Figure 152. Case 12 Roll Rate ω_y versus Time.....	137
Figure 153. Case 12 Yaw Rate ω_z versus Time	137
Figure 154. Case 13 Aileron Input versus Time	138
Figure 155. Case 13 Lateral Velocity v_x versus Time.....	139
Figure 156. Case 13 Longitudinal Velocity v_y versus Time	139
Figure 157. Case 13 Vertical Velocity v_z versus Time	140
Figure 158. Case 13 Pitch Rate ω_x versus Time	140
Figure 159. Case 13 Roll Rate ω_y versus Time.....	141
Figure 160. Case 13 Yaw Rate ω_z versus Time	141
Figure 161. Case 14 Aileron Input versus Time	142
Figure 162. Case 14 Lateral Velocity v_x versus Time.....	143
Figure 163. Case 14 Longitudinal Velocity v_y versus Time	143
Figure 164. Case 14 Vertical Velocity v_z versus Time	144
Figure 165. Case 14 Pitch Rate ω_x versus Time	144
Figure 166. Case 14 Roll Rate ω_y versus Time.....	145
Figure 167. Case 14 Yaw Rate ω_z versus Time	145
Figure 168. Case 15 Aileron Input versus Time	146
Figure 169. Case 15 Lateral Velocity v_x versus Time.....	147

Figure 170. Case 15 Longitudinal Velocity v_y versus Time	147
Figure 171. Case 15 Vertical Velocity v_z versus Time	148
Figure 172. Case 15 Pitch Rate ω_x versus Time	148
Figure 173. Case 15 Roll Rate ω_y versus Time.....	149
Figure 174. Case 15 Yaw Rate ω_z versus Time	149
Figure 175. Case 16 Aileron Input versus Time	150
Figure 176. Case 16 Lateral Velocity v_x versus Time.....	151
Figure 177. Case 16 Longitudinal Velocity v_y versus Time	151
Figure 178. Case 16 Vertical Velocity v_z versus Time	152
Figure 179. Case 16 Pitch Rate ω_x versus Time	152
Figure 180. Case 16 Roll Rate ω_y versus Time.....	153
Figure 181. Case 16 Yaw Rate ω_z versus Time	153
Figure 182. Case 17 Aileron Input versus Time	154
Figure 183. Case 17 Lateral Velocity v_x versus Time.....	155
Figure 184. Case 17 Longitudinal Velocity v_y versus Time	155
Figure 185. Case 17 Vertical Velocity v_z versus Time	156
Figure 186. Case 17 Pitch Rate ω_x versus Time	156
Figure 187. Case 17 Roll Rate ω_y versus Time.....	157
Figure 188. Case 17 Yaw Rate ω_z versus Time	157

List of Tables

Table	Page
Table 1. X-HALE's Characteristics [12]	16
Table 2. A Summary of Discussed Simulations	40
Table 3. A Summary of Discussed 6 Meter X-HALE Simulations.....	84
Table 4. A Summary of Discussed 8 Meter X-HALE Simulations.....	86

List of Symbols

Symbol	
a	An arbitrary point in the vehicle with respect to the origin of the inertial frame G
B	The body-fixed reference frame
b	Displacements and rotations as the time integral of β
C	A generalized damping matrix
F	An externally applied state-dependent force
$f(\cdot)$	Generic function
f	A vector used to trim the aircraft
f_{dst}, f_{pt}	Distributed and point forces
G	The inertial reference frame
g^B	B reference frame resolved gravity vector
g_0	Gravity column vector
h	The position and orientation vector of the flexible structure
I_B	Inertia matrix
J	Jacobian matrix
J_{trim}	Trim cost function
K	A generalized stiffness matrix
M	An externally applied state-dependent moment or a generalized mass matrix
m	Mass per unit span
O	The origin of the B reference frame
p_a	Position of an arbitrary point in the vehicle with respect to the origin of the inertial frame G
p_B	Inertial position vector of the B reference frame
p_r	Position from the B reference frame origin to the local w reference frame
$p_{r_{cm}}$	Vector from the B reference frame origin to the center of mass
q	Generalized displacement column vector

R	Either the a generalized force column vector, or the residual value computed at each subiteration when UM/NAST is run
R_B	Generalized force applied to the B reference frame states
R_F	Generalize force applied to elastic states
S	Search variable column vector
s	Undeformed beam spatial dimension
t	Time
u	Control surface and external inputs for a function
v_B	Linear velocity vector of the B reference frame
w	Local elastic reference frame
δW	The total virtual work
x, y, z	The x , y and z directions
α	Angle of attack
β	Column vector of the B reference frame linear and angular velocities
δ_e	Elevator deflection angle
δ_t	Thrust
ϵ	Column vector of the elastic strain state
ζ	Quaternion column vector used for the B reference frame orientation
Θ_B	Generalized B reference frame rotation vector
λ	Column vector of inflow states
$\bar{\Omega}_\zeta$	The finite element discretization of the ω_B matrix
ω_B	Angular velocity vector of the B reference frame
(\cdot)	Skew-symmetric matrix operator
$(\tilde{\cdot})$	Transpose of the skew-symmetric matrix operator

Subscript or superscript

<i>aero</i>	Related to aerodynamic effects
B	A reference to the body-fixed reference frame B
BB, BF	Contributions of a particular matrix to the body and body/flexible differential equations of motion
<i>dst</i>	Distributed

<i>(e)</i>	Element number
<i>ext</i>	External
<i>F</i>	A reference to the flexible degree of freedom
<i>FF, FB</i>	Contributions of a particular matrix to the body and flexible/body differential equations of motion
<i>G</i>	A reference to the global matrix
<i>k</i>	A member, which is a collection of elements, index
<i>pt</i>	Point
<i>T</i>	Transpose operator

List of Abbreviations

Abbreviation

AFIT	Air Force Institute of Technology
AVL	Athena Vortex Lattice
CFD	Computational Fluid Dynamics
ESC	Electronic Speed Controller
GPS	Global Positioning System
HALE	High Altitude Long Endurance
INS	Inertial Navigating System
ISR	Intelligence, Surveillance and Reconnaissance
MC	Phoenix Integration's Model Center Software
NASA	National Aeronautics and Space Administration
NATASHA	Nonlinear Aeroelastic Trim and Stability for HALE aircraft
Nastran	NASA Stress Analysis Program
NPRF	Navy Pacific Range Facility
ONERA	Office National d'Etudes et Recherches Aéropatiales
SBC	Single Board Computer
SSC	Servo Switch Controller
RCAS	Rotorcraft Comprehensive Analysis System
RPA	Remotely Piloted Aircraft
THWIL	True Hardware in the Loop
UM/NAST	University of Michigan's Nonlinear Aeroelastic Simulation Toolbox
X-HALE	Experimental High Altitude Long Endurance

SIMULATIONS FOR THE TEST FLIGHT OF A HALE AIRCRAFT

I. Introduction

High Altitude Long Endurance (HALE) aircraft have great potential as Intelligence, Surveillance and Reconnaissance (ISR) platforms [35]. Additionally, they can also be used as network communication nodes for military or civilian purposes, or perform general atmospheric research [39]. The US Air Force has been developing a new type of ISR aircraft called “SensorCraft”, which are large HALE aircraft with wings spans in excess of 60 meters. These highly flexible aircraft ideally have high-aspect-ratio wings, slender fuselages and high aircraft performance to handle long loiter times and heavy payloads [22]. SensorCraft generally have high structural performance, high aerodynamic efficiencies and low structural weight fractions. As a result, they also generally have low frequency natural structural vibration modes, and geometrically-nonlinear structural and flight dynamics. The three platform shapes that have been considered for SensorCraft are wing-body-tail (Figure 1), single-wing (Figure 2) and joined-wing (Figure 3) configurations [34]. Because very flexible aircraft have very low frequencies for their natural vibration modes, the structural dynamics and the rigid-body characteristics of these aircraft are strongly coupled [4].

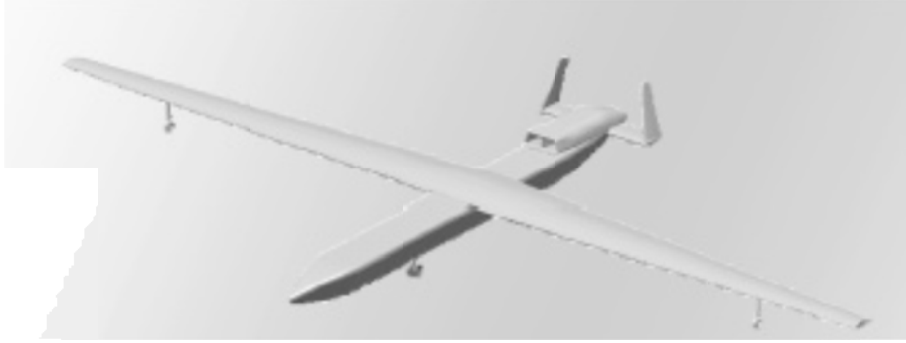


Figure 1. Wing-Body-Tail Configuration [4]



Figure 2. Single-Wing Configuration [4]

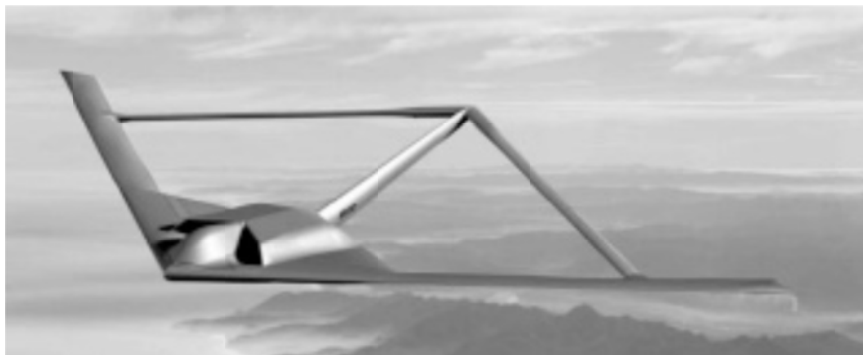


Figure 3. Joined-Wing Configuration [4]

Aurora Flight Sciences, Boeing Co. and Lockheed-Martin Co. have developed very long duration HALE aircraft concepts for the DARPA's Vulture Program [40]. However, recent events show that more must be known about the nonlinear control of HALE aircraft. For example, NASA developed the Helios aircraft (Figure 4) as a forerunning HALE Remotely Piloted Aircraft (RPA).



Figure 4. Aerovironment's Helios [4]

During a flight test on 26 June 2003, Helios experienced turbulence on a test flight at the Navy Pacific Missile Range Facility (PMRF) near Kauai, Hawaii, and developed high wing dihedral which resulted in an unstable pitching mode. The resulting high speed caused parts of the aircraft wing and solar cells to rip off. The aircraft then crashed in to the ocean. One of the primary causes of the accident was that Helios' engineers did not fully understand the nonlinear flight dynamics of the aircraft [14]. Several codes, such as NATASHA (Nonlinear Aeroelastic Trim and Stability for HALE

aircraft), RCAS (Rotorcraft Comprehensive Analysis System) and ASWING have been developed for the use of modeling nonlinear aeroelastic and flight dynamics of an aircraft but none have been completely validated with real flight data from a HALE aircraft [4].

Shearer, Cesnik and their co-workers [4] have developed a Matlab program that is a practical solution to the coupled nonlinear aeroelasticity and flight dynamics of very flexible aircraft called the University of Michigan's Nonlinear Aeroelastic Simulation Toolbox (UM/NAST). This code serves as a plant representation for HALE aircraft control design. It focuses on a reduced number of states to represent the complex nonlinear problem. This code addresses the following issues: nonlinear aeroelastic modeling, integral wing actuation for generating maneuver loads, flutter boundary enhancement, gust load alleviation and overall nonlinear vehicle optimization of unconventional high aspect ratio aircraft. Shearer, Cesnik and their co-workers are also in the process of developing a scaled test HALE aircraft called X-HALE which will be used to validate UM/NAST. The goal of this research is to perform flight simulations with UM/NAST so as to make predictions about X-HALE's future test flights and subsequently uncover the strengths and weaknesses of UM/NAST when X-HALE is finally flown.

II. Theoretical Development

II.1 Previous Research and Motivation

Recent events such as the crash of NASA's Helios aircraft show that more must be known about the nonlinear control of HALE aircraft. This is the motivation of this research. Nonlinear aeroelastic solvers have been under development since the 1990's; however, the problem of nonlinear aeroelasticity coupled with nonlinear flight dynamics is still not completely understood. Several codes, such as UM/NAST, NATASHA, ASWING and RCAS, have been developed for the use of modeling nonlinear aeroelastic and flight dynamics of an aircraft but none have been completely validated with real flight test data from a HALE aircraft; they have been validated in a piecemeal fashion against beam models such as a simple cantilevered beam model and wind tunnel data. This is because there currently is no aircraft flight data available for validation [4]. A history of progress made on the problem of nonlinear aeroelasticity coupled with nonlinear flight dynamics will be explored.

II.2 The Early Work of Van Schoor, Von Flotow and Jones

Van Schoor and von Flotow were two of the first to study nonlinear aeroelasticity for very flexible aircraft in the 1990's. They demonstrated that when flexible structural modeling is included the classic rigid-body modes change significantly by using linearized analysis about nonlinear equilibrium points. Their work confirmed the importance of taking aircraft structural dynamics, as well as other aeroelastic effects such as gust response and flutter instability, into account when analyzing the flight dynamics of very flexible aircraft [36]. Jones and his co-workers [11] have worked on the approach of designing HALE aircraft. Their work describes some of the challenges with the design

approach of HALE aircraft and demonstrates that standard aircraft control design methods are not valid for the high-aspect-ratio and low Reynolds number wings of HALE aircraft. They concluded that this is because of the lack of data and methods that allow the prediction of a HALE aircraft's structure mass, engine performance at high altitudes and aerodynamic parameters. They explained that the high-aspect-ratio and low Reynolds number wings of HALE aircraft are associated with nonlinear structural dynamics and are frequently subject to aeroelastic phenomena such as flutter making typical design approaches unreliable.

II.3 The Development and Use of ASWING

Drela [6] was the first to begin developing the ASWING code and is currently working to improve its design. ASWING models an entire flexible aircraft as a structure of joined nonlinear beams. ASWING uses a compressible vortex type source-lattice with wind-aligned trailing vorticity. It also uses the full Newton method to solve the nonlinear equation.

Love et al. [13] used ASWING to model the aeroelastic effects on a swept flying wing SensorCraft. The aeroelastic analysis focused on body freedom flutter. A Nastran finite element model of the aircraft was used to provide an initial aeroelastic flutter analysis. Love explored tradeoffs with wing stiffness, altitude and center of gravity locations in order to better understand whether passive means can increase flutter speed to acceptable levels.

González [9] modeled the Unmanned Airplane for Ecological Conservation as a flexible-body using the ASWING code and compared it with results from an analytical-empirical method and potential flow codes. The goal was to evaluate the aerodynamic

and static stability of the aircraft. The results show that the flexible-body and rigid-body results show slight differences.

II.4 The Development of UM/NAST

Patil et al. [16] studied the aeroelasticity and flight dynamics of HALE aircraft. Their work showed that the behavior of HALE aircraft can vary dramatically due to the flexible nature of the wings. They also showed that modeling a HALE aircraft using a linear aeroelastic analysis in which the structure is assumed to be rigid can lead to significant errors. Furthermore, there is a significant difference between rigid body, linear aeroelastic and nonlinear aeroelastic dynamics when it comes to the short period and the phugoid modes of very flexible aircraft. The short period and phugoid modes were acquired by linearizing the nonlinear dynamics about a nonlinear equilibrium.

Cesnik and Brown [3] started the strain-based approach for modeling the dynamics of highly flexible aircraft. This method is solved in the time domain and was validated against the Goland wing [2]. Cesnik and Brown [3] modeled a HALE aircraft using a rigid fuselage and a highly flexible high-aspect-ratio composite wing. They analyzed the time-marching aeroelastic and aeroservoelastic behavior of HALE aircraft and cantilevered wings under constrained reference frame motion with imbedded actuation. They used the finite state two-dimensional strip theory developed by Peters et al. [19] for unsteady aerodynamics.

By adding a flexible fuselage and developing a split beam formulation, Cesnik and Su [5] continued the work of Cesnik and Brown. They emphasized roll performance and nonlinear-flutter during their study. Patil and Hodges [17], Su and Cesnik [31], and Patil and Taylor [18] all used 1-D beam modeling for slender structures to study the

nonlinear structural flight dynamics of a flying wing type aircraft. They also used the finite state two-dimensional strip theory developed by Peters et al. [19] for unsteady aerodynamics just as Cesnik and Brown did [3]. Su and Cesnik also studied how the wrinkling of the skin of a flying wing type aircraft affected its torsional stiffness. Wang et al. [37] used the unsteady vortex lattice method and the geometrically exact beam modeling method to study a flying wing type aircraft.

Palacios and Cesnik [15] developed nonlinear aeroelastic tools. Their high-fidelity code used 3-D Euler equations to model the air flow. They used a split 1-D and 2-D model to model the 3-D structural deformation. The 1-D model follows traditional 1-D beam bending theory where the cross section of the beam remains undeformed. The 2-D model allows for changes in the cross section of the beam as the beam undergoes various internal and external loads. Palacios and Cesnik's high-fidelity code can only produce results for steady-state solutions because of the large computational size and the coupled structure of the CFD solution; the code is not suitable to run full aircraft simulations. Garcia [8] added to Palacios and Cesnik's code and created a nonlinear finite element model which includes the full Euler/Navier-Stokes solution. Garcia's results are significant because he showed that there are significant differences between the results of the linear and the nonlinear structural modeling of a swept cantilevered wing.

Shearer and Cesnik [22] developed a method for the characterization of the response of a very flexible aircraft that is used in the UM/NAST code. The geometrically nonlinear structural response of the aircraft was modeled using six-degree of freedom equations of motion. They used a low-order strain-based nonlinear structural analysis

method and an unsteady finite state potential-flow aerodynamics analysis method to formulate their aerodynamic model. Shearer and Cesnik used their modified Generalized- α Method for integrating the governing equations of a very flexible aircraft. Su and Cesnik [32] used the UM/NAST code to model the nonlinear aeroelasticity of a flapping wing Micro Air Vehicle (MAV), however, the code has not been validated by any experimental means at this time.

Shearer, Cesnik and their co-workers have begun the development of a very flexible RPV aircraft called X-HALE for this purpose. This aircraft has two configurations: the 6 meter and 8 meter span configurations. Cesnik et al. [4] have performed gust and roll simulations for the 8 meter model of X-HALE. Their results suggest that when a 1-cosine gust is symmetrically applied to the 8 meter model X-HALE with a maximum gust speed of 4 m/s, while the nominal flight speed is 14 m/s at 30 m altitude, the aircraft is stable. Also, when a single period of a left-wing-down sinusoidal aileron input is applied the aircraft is stable for aileron inputs with a 2 degree amplitude, but not for inputs with a 5 degree amplitude or greater.

II.5 RCAS

Saberi et al. [21] of the Aeroflightdynamics Directorate of the U.S. Army developed an integrated computational fluid and non-linear structural dynamics software system called RCAS for comprehensive rotorcraft analysis and simulation. The software uses computational fluid dynamics, rotorcraft comprehensive analysis and computational structural dynamics on parallel high performance computer systems. According to Strawn et al. [30], RCAS was validated with data taken from full-scale helicopters. The results of the validation showed that the computational fluid approach provides an

accurate model for the non-linear aerodynamics and dynamic forces experienced by a rotorcraft. No validation has been done using fixed-wing aircraft [4].

II.6 NATASHA

NATASHA is a software system that analyzes the nonlinear aerodynamics and nonlinear structural dynamics of HALE aircraft. NATASHA is based on geometrically exact, fully intrinsic beam equations. Sotoudeh and Hodges [26] updated NATASHA so that it is capable of analyzing joined-wing aircraft configurations. This was done using fully intrinsic equations and an incremental form of kinematical equations. This updated version of the NATASHA code was validated using a joined-wing structure. The program can also now provide trim and stability analyses. Sotoudeh and Hodges [27] also studied the effects of joint position and sweep angle of the aft wing of a joined-wing aircraft. Sotoudeh et al. [28] validated NATASHA with a range of results from well known solutions of beam stability and vibration problems, experimental data from scaled wind tunnel tests and results from RCAS. NATASHA uses 2-D aerodynamics and the finite state induced flow model of Peters and Johnson [19] to analyze the nonlinear aeroelastic characteristics of flying wings. Sotoudeh and Hodges have stated that they hope that NATASHA's results can be used as benchmarks for their own codes since the NATASHA model is limited in its capabilities.

II.7 Other Recent Work on Nonlinear Aeroelastic Solvers

Blair and Canfield [1] created a method for estimating the weight of a joined-wing HALE aircraft. Their method is based on the nonlinear static aeroelastic formulations and structural constraints of a given joined-wing HALE aircraft. It also incorporates the structures, aerodynamics and aeroelasticity of the aircraft. The static aerodynamics are

modeled using vortex lattice formulations. Recently, Richards, et al. [20] began designing a scaled joined-wing SensorCraft model for the purpose of validating an existing analytical nonlinear aeroelastic model which is based on the Matlab Aerospace Blockset and the Unmanned Dynamics Aerosim v1.2 Blockset. The simulator uses a set of first order terms and multi-dimensional lookup tables, which allow for the input of different angles of attack and sideslip angles, to model nonlinear aerodynamics. The simulator also uses vortex lattice software called AVL and a parametric model based on the software Phoenix Integration's Model Center Software (MC). The data is then outputted into a Matlab m-file. The model can very quickly produce a flight simulation using the flight simulator FlightGear for visualization. An optional aircraft autopilot was also integrated into the model using the Micropilot 2128 THWIL system.

Weishaar and Lee [38] studied how the weight and center of gravity of a high-aspect-ratio joined-wing HALE aircraft affect body-freedom flutter. Additionally, Tang et al. [33] used the finite state aerodynamic model to experimentally validate linear structural modeling when nonlinear trailing-edge flap deflections occur. Their results showed a strong correlation between their model and their experimental results; therefore, their results validated their model well. Tang and Dowell [34] experimentally validated an ONERA unsteady aerodynamic model using nonlinear structural modeling. Their results also validated their model well for cantilevered wings similar to HALE wings when the wings are exposed to limit-cycle oscillations. Dowell and Tang [7] also created a review of cantilevered structures with nonlinear aeroelasticity in which they discuss HALE aircraft.

II.8 Present Motivation and Problem

While all of the previous research discussed contributes to the problem of nonlinear aeroelasticity coupled with nonlinear flight dynamics, the problem is still not completely understood. Several codes have been developed for the use of modeling nonlinear aeroelastic and flight dynamics of an aircraft but none have been completely validated with real flight data from a fixed-wing aircraft [4]. This research will continue the work of Shearer, Cesnik and their co-workers and perform flight simulations with UM/NAST in order to make predictions about X-HALE's future test flights. This is all done with the hope of eventually experimentally validating the UM/NAST code with the X-HALE aircraft.

III. Model Development

This research involved running various simulations with UM/NAST in order to predict the behavior of the X-HALE test vehicle. Initial simulations have been run by Shearer and are described in [23]. These initial simulations predicted that X-HALE will show instabilities in flight under certain conditions; further simulations need to be run in order to explore what other conditions will cause unstable flight. Also, more simulations are necessary in order to potentially validate the UM/NAST code. These simulations will include straight and level flight, and rolling flight performed by simulating aileron deflections.

III.1 The X-HALE Aircraft

Shearer, Cesnik and their co-workers have are developing a very flexible RPV aircraft called X-HALE, shown in Figure 5, at the University of Michigan in order to experimentally validate the UM/NAST code. X-HALE can be converted from a 6 meter test vehicle to an 8 meter test vehicle. This is done by removing two wing segments from the aircraft. During flight, X-HALE's middle elevator can rotate 90 degrees to become a vertical stabilizer. This will be done in order to observe the vertical stabilizer's effects on the aircraft's stability [25].

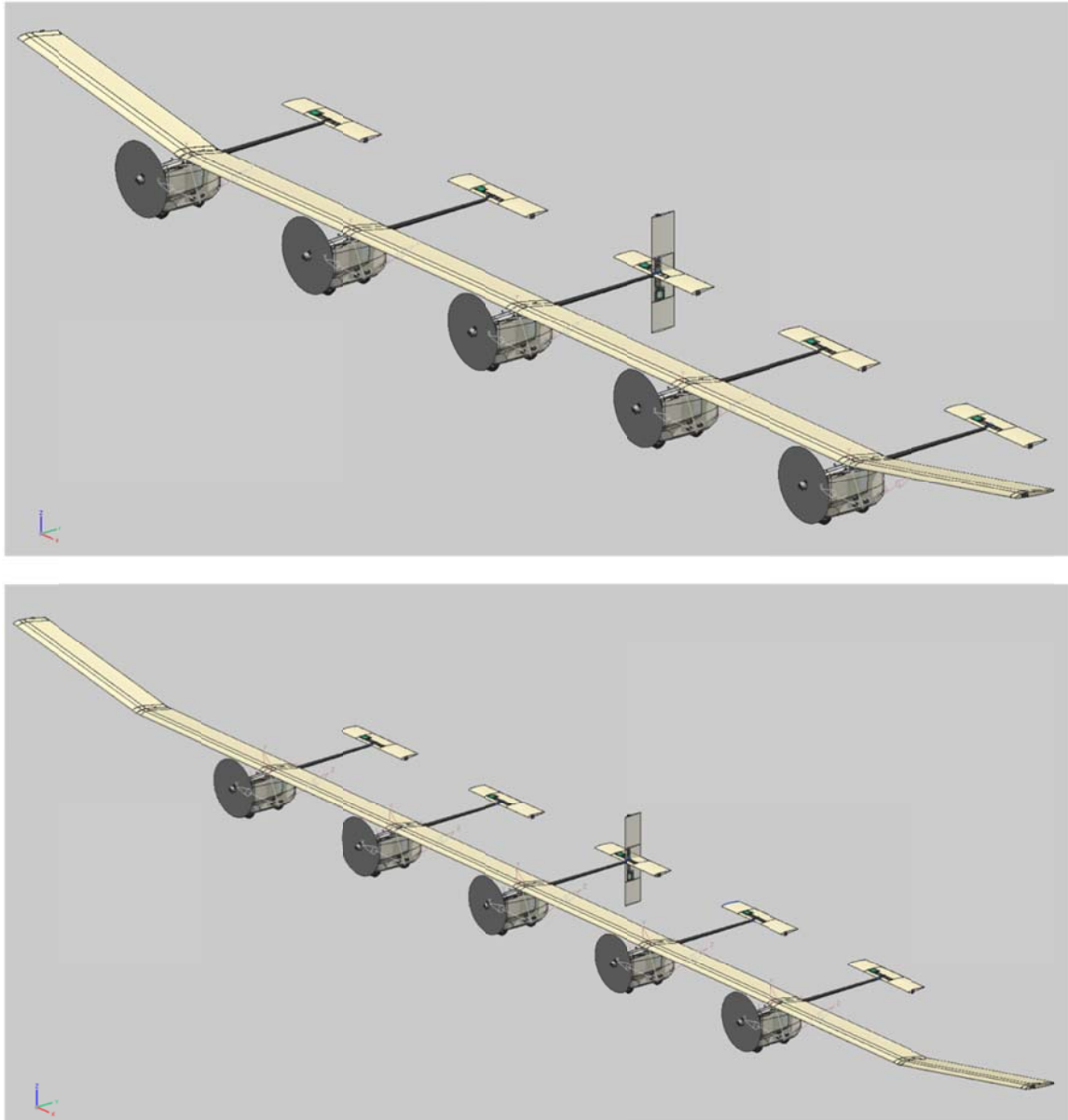


Figure 5. X-HALE: 6 Meter Model (Top) and 8 Meter Model (Bottom) [25]

This aircraft will collect data of its geometrically nonlinear aeroelastic response when it is test flown in the hope of validating the UM/NAST code. The aircraft has rigid and elastic body instabilities with large deflections during gusts. The airframe will be designed so that its elastic, inertial and geometric properties correlate well with its

UM/NAST model [4]. The aircraft can be configured either as a 6 m flight test vehicle (FTV) or an 8 m aeroelastic test vehicle (ATV) [25].

Both the 6 meter and the 8 meter models include five fuselages, which are each mounted to a joiner block that connects two wing modules. The wing modules are all 1 meter long. Each fuselage is composed of a fairing pod, a tail boom, and an elevon. Remote control aircraft propellers attach to the motors for propulsion. Each fairing pod has a carbon spine which holds an electric motor with two batteries and other components such as a GPS/INS, a GPS antenna, a transmitter, electronic speed controllers (ESC's), a glitch buster, a servo switch controller, an Ethernet hub and landing gear. The first battery powers the motor and the second powers the electronics contained in the fuselage. These electronics include a single board computer (SBC), an analog to digital converter module, and several scientific sensors such as strain gauges, accelerometers, a pitot probe and a tail potentiometer. These sensors vary in number and type depending on the wing module and the aircraft configuration [12].

The majority of the X-HALE flight components have been manufactured by the X-HALE program. Currently, the X-HALE program is integrating these components at the University of Michigan and is developing software for the networking of the onboard computers. Table 1 summarizes X-HALE's characteristics [12].

Table 1. X-HALE's Characteristics [12]

Wing Span	6 m or 8 m
Chord	0.2 m
Planform Area	1.2 m ²
Aspect Ratio	30 or 40
Length	0.96 m
Propeller Diameter	12 in
Gross Takeoff Weight	11 kg or 12 kg
Power/Weight	30 W/kg
Airspeed	12-18 m/s
Max Range	3 km
Endurance	45 min

III.2 The Coordinate Systems of UM/NAST

The UM/NAST controller was developed based on the known physics of the situation that is being modeled; that is, how a very flexible aircraft flies. The controller uses closed-loop reference tracking of a body fixed reference frame B (Figure 6) at a point O while also including the properties of nonlinear aeroelasticity. This point O is typically is not the aircraft's center of mass but may be at some points in time during a simulation. The point O is chosen to be at a convenient location on the aircraft so that both linear and angular velocities can be tracked. Usually, the x-axis is chosen to be out the right wing and the y-axis is tangent to the undeformed fuselage's longitudinal axis and extends in the direction of the front of the aircraft. As a result, the x-y plane of the B reference frame is parallel to the x-y plane of the inertial frame G when the aircraft is undeformed. The z-axis extends out the top of the aircraft and is the cross product of the x-axis and y-axis. The flexible members of the aircraft are modeled as beams that propagate from the origin O or that are rigidly offset from the point O . In order to determine the orientation of the B reference frame, one of three methods is used: an Euler

angle transformation using three nonorthogonal Euler angles, a transformation using a four-parameter quaternion, or a transformation using a nine-parameter set of the unit vectors that define the x -, y - and z -axes of the B reference frame [23].

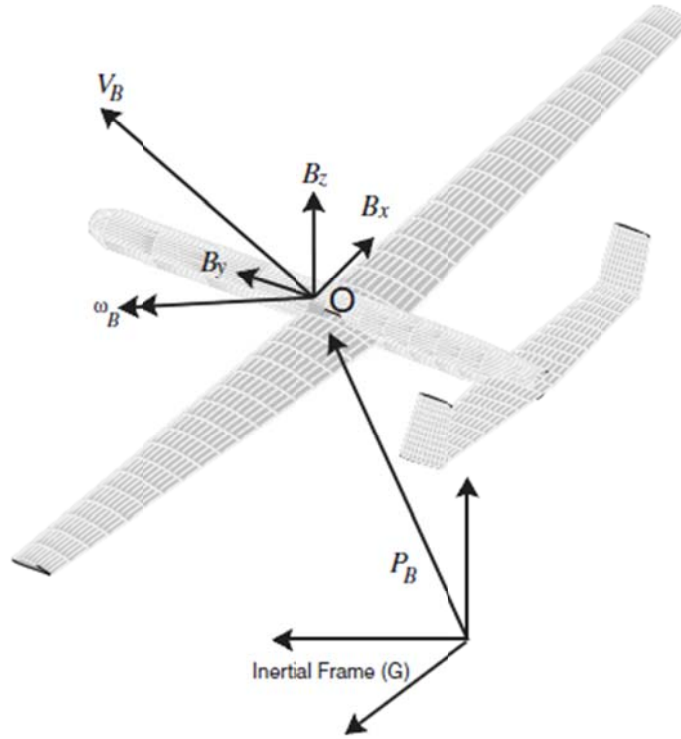


Figure 6. Body Fixed Reference Frame B [23]

Here p_B is the inertial position of the B reference frame. Also, v_B and ω_B are the linear and angular velocity variables of the B reference frame and can be represented by the vector shown in Equation (1).

$$\beta = \begin{Bmatrix} v_B \\ \omega_B \end{Bmatrix} \quad (1)$$

Figure 7 depicts the B reference frame if the aircraft is assumed to be a rigid-body. For this case, the elastic members are modeled as beams that propagate from the B reference

frame origin or with rigid offsets from the origin. The position vector $p_{r_{cm}}$ extends from the body-fixed B reference frame to the center of mass of a rigid fuselage piece. Note that the origin O of the B reference frame is not the center of mass of the fuselage piece [23].

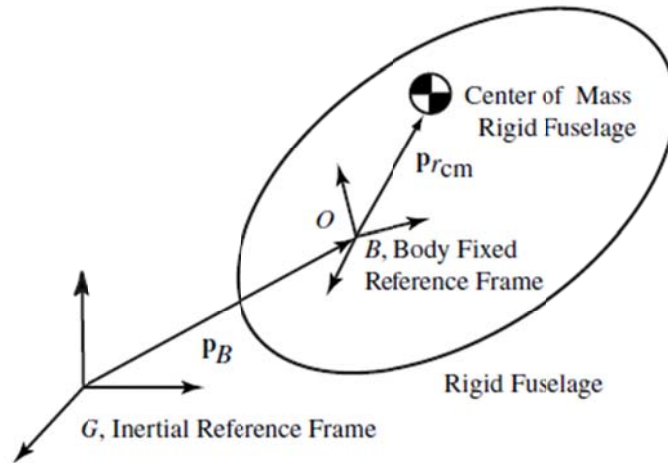


Figure 7. The Rigid-body Reference Frame [23]

During a simulation, the B reference frame moves forward with the aircraft, allowing the movement of the aircraft to be modeled. This is done by deriving and integrating a set of first-order differential equations. These equations are of the form of Equation (2) below.

$$\dot{x} = f(x, u) \quad (2)$$

These nonlinear differential equations are time-invariant and nonlinear. When the aircraft is assumed to be a rigid-body, the first-order equations take the form of Equation (3).

$$\begin{aligned}
\dot{v}_B &= f_{v_B}(v_B, \omega_B, \zeta, p_B, g_0, m, F_{ext}) \\
\dot{\omega}_B &= f_{\omega_B}(\omega_B, I_B, \zeta, p_B, M_{ext}) \\
\dot{\zeta}_B &= f_{\zeta_B}(\omega_B, \zeta) \\
\dot{p}_B &= f_{p_B}(\zeta, v_B)
\end{aligned} \tag{3}$$

The forces F_{ext} and the moments M_{ext} are state-dependent externally applied. Additionally, I_B is the inertia matrix of the aircraft about the origin O of the B reference frame, ζ is the quaternion vector containing the four quaternion elements used to find the orientation of the B reference frame with respect to the inertial reference frame G and g_0 represents the gravitational field effects on the aircraft [23].

Figure 8 shows the B reference frame and the coordinates of the flexible aircraft wing.

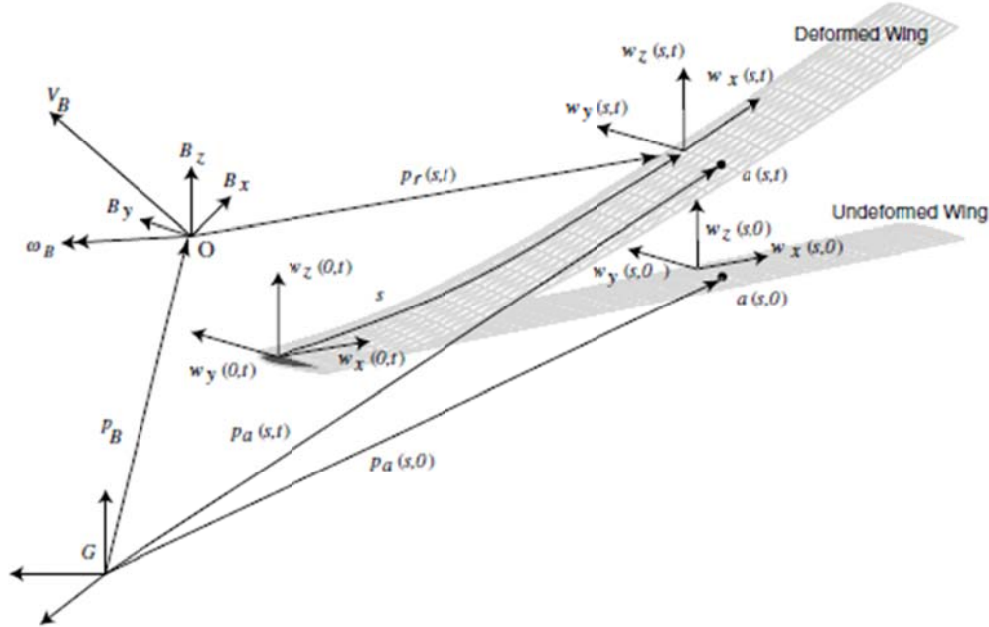


Figure 8. The Body Reference Frame B and the Vehicle Coordinates [23]

Here w represents the local elastic reference frame, p_r is the position of the B reference frame origin to the local w reference frame, s represents the undeformed beam spatial dimension, a represents an arbitrary point in the vehicle with respect to the origin of the inertial frame G and t represents time [23].

The position and the orientation vector h at a point in the flexible body is given in Equation (4 below.

$$h = \{p^T \quad w_x^T \quad w_y^T \quad w_z^T\}^T \quad (4)$$

The vector function h is a function of only ϵ , the column vector of the elastic strain state and b , displacements and rotations as time integral of β , the B reference frame linear and angular velocities. Equation (5 gives expressions that relate h to ϵ and b .

$$\begin{aligned} \delta h &= J_{h\epsilon} \delta \epsilon + J_{hb} \delta b \\ dh &= J_{h\epsilon} d\epsilon + J_{hb} db \end{aligned} \quad (5)$$

In these equations, $J_{h\epsilon}$ and J_{hb} , which are given in Equation (6, are Jacobian matrices which link the flexible position and orientation vectors and the independent coordinates of ϵ and β .

$$\begin{aligned} J_{h\epsilon} &= \frac{\partial h}{\partial \epsilon} \\ J_{hb} &= \frac{\partial h}{\partial b} \end{aligned} \quad (6)$$

Equation (7 gives the value of \dot{h} , which further explains the connection between the vectors ϵ and β .

$$\dot{h} = J_{h\epsilon} \dot{\epsilon} + J_{hb} \dot{b} = J_{h\epsilon} \dot{\epsilon} + J_{hb} \beta \quad (7)$$

The relative acceleration of h due to the vectors ϵ and its first and second derivatives with respect to time is given in Equation (8 [23].

$$\ddot{p}_a = \ddot{p} + x\ddot{w}_x + y\ddot{w}_y + z\ddot{w}_z = \begin{Bmatrix} 1 \\ x \\ y \\ z \end{Bmatrix}^T [J_{h\epsilon}\dot{\epsilon} + J_{h\epsilon}\ddot{\epsilon}] \quad (8)$$

III.3 A Study of the Governing Differential Equations of Motion

By assuming that an aircraft is a rigid body when creating a controller, three things are assumed:

1. The inertia properties of the aircraft are either constant or time-varying.
2. The inertial force caused by a rotating coordinate frame in conjunction with the relative velocity of the aircraft's flexible members can be neglected.
3. Any external forces, such as F_{ext} and M_{ext} , or moments are founded on a constant aircraft geometry.

These assumptions are invalid for vey flexible aircraft because of the changing geometry of the aircraft. Instead, for a flexible aircraft a set of differential equations of motion that allow for changing aircraft geometry are used. These equations are shown in Equation (9) and Equation (10).

$$M\ddot{q} + C\dot{q} + Kq = R(q, \dot{q}, \lambda) \quad (9)$$

$$q = \begin{Bmatrix} \epsilon \\ p_B \\ \Theta_B \end{Bmatrix} \quad \dot{q} = \begin{Bmatrix} \dot{\epsilon} \\ v_B \\ \omega_B \end{Bmatrix} \quad \ddot{q} = \begin{Bmatrix} \ddot{\epsilon} \\ \dot{v}_B \\ \dot{\omega}_B \end{Bmatrix} \quad (10)$$

In these equations, M represents the mass properties of the aircraft and C represents the structural damping and the nonlinear terms created by a rotating coordinate frame and its effects on relative position and velocity, such as v_B and ω_B . Additionally, K represents the stiffness matrix of the aircraft, and q represents a set of coordinates which contain both strain ϵ , which is linked with the inertial position p_B , and an orientation vector Θ_B . The function $R(q, \dot{q}, \lambda)$ represents forces, such as aerodynamic forces, that are a function

of finite state flow velocities λ . This function is further described in [19]. Because the variables M , C and R are dependent on each other, the rigid-body and flexible structural dynamics are also dependent on each other. The program UM/NAST uses a constant strain-based approach to predict the movement of the aircraft. This approach, which is further described in [2, 3], allows for nonlinear geometric changes and changes to the inertia matrix I_B , and the matrices M , C and R [23].

III.3.1 The Equations of Motion

The equations of motion are further derived from Equation (9) and Equation (10) using unsteady aeroelastic modeling. This is done by applying the principle of virtual work to the B reference frame while assuming the aircraft wings are flexible beams and the body of the aircraft is composed of rigid bodies. Equation (11) below is the total virtual work expression based on both the B reference frame, and the flexible beams and the rigid bodies of the aircraft.

$$\delta W = [\delta\epsilon^T \quad \delta b^T]^T \left(- \begin{bmatrix} M_{FF} & M_{FB} \\ M_{BF} & M_{BB} \end{bmatrix} \begin{bmatrix} \ddot{\epsilon} \\ \ddot{\beta} \end{bmatrix} - \begin{bmatrix} C_{FF} & C_{FB} \\ C_{BF} & C_{BB} \end{bmatrix} \begin{bmatrix} \dot{\epsilon} \\ \dot{\beta} \end{bmatrix} - \begin{bmatrix} K_{FF} & K_{FB} \\ K_{BF} & K_{BB} \end{bmatrix} \begin{bmatrix} \epsilon \\ b \end{bmatrix} + R \right) \quad (11)$$

In this equation, R is the vector described below in Equation (12) where R_F is the force vector component pertaining to the flexible body degree of freedom and R_B is the force vector component pertaining to the fixed-body degree of freedom.

$$R = \begin{Bmatrix} R_F \\ R_B \end{Bmatrix} \quad (12)$$

Equation (13) provides the mass and damping matrices that apply to Equation (11) [23].

$$\begin{aligned}
M_{FF} &= J_{h\epsilon}^T M_G J_{h\epsilon} \\
M_{FB} &= J_{h\epsilon}^T M_G J_{hb} \\
M_{BF} &= J_{hb}^T M_G J_{h\epsilon} \\
M_{BB} &= J_{hb}^T M_G J_{hb} + M_B \\
C_{FF} &= J_{h\epsilon}^T M_G \dot{J}_{h\epsilon} + C_G \\
C_{FB} &= J_{h\epsilon}^T M_G H_{hb} + 2J_{h\epsilon}^T M_G H_{h\epsilon\dot{b}} \\
C_{BF} &= J_{hb}^T M_G \dot{J}_{h\epsilon} \\
C_{BB} &= J_{hb}^T M_G H_{hb} + 2J_{hb}^T M_G H_{h\epsilon\dot{\beta}} + C_B \\
K_{FF} &= K_G \\
K_{FB} &= K_{BF} = K_{BB} = 0
\end{aligned} \tag{13}$$

Here M_G , C_G and K_G are the generalized flexible-element mass, damping and stiffness matrices about the G reference frame, while M_B and C_B are the generalized rigid-element mass and damping matrices associated with the B reference frame rigid-element portion. Also, H_{hb} and $H_{h\epsilon\dot{\beta}}$ incorporate the effects of a rotating coordinate frame. M_G , C_G and K_G are the assembled flexible-element generalized mass, damping and stiffness matrices. They are of the form of Equation (14).

$$\begin{aligned}
M_G &= \begin{bmatrix} M_{(1)} & 0 & \dots & 0 \\ 0 & M_{(2)} & \dots & 0 \\ 0 & 0 & \ddots & 0 \\ 0 & 0 & \dots & M_{(e)} \end{bmatrix} \\
C_G &= \begin{bmatrix} C_{(1)} & 0 & \dots & 0 \\ 0 & C_{(2)} & \dots & 0 \\ 0 & 0 & \ddots & 0 \\ 0 & 0 & \dots & C_{(e)} \end{bmatrix}
\end{aligned} \tag{14}$$

M_B and C_B are the mass and damping matrices associated with the B reference frame element portion. They are given in Equation (15).

$$M_B = \begin{bmatrix} m & m\tilde{p}_{r_{cm}} \\ m\tilde{p}_{r_{cm}} & I_B \end{bmatrix} \quad (15)$$

$$C_B = \begin{bmatrix} m\tilde{\omega}_B & m\tilde{\omega}_B\tilde{p}_{r_{cm}} \\ m\tilde{p}_{r_{cm}}\tilde{\omega}_B & \tilde{\omega}_B I_B \end{bmatrix}$$

Here m represents mass per unit span and $p_{r_{cm}}$ represents the position vector from the B reference frame origin to the center of mass. Additionally, $(\tilde{\cdot})$ is a skew-symmetric matrix operator on the given matrix and $(\tilde{\cdot})^T$ is the transpose of the given matrix's skew-symmetric matrix [23].

Equation (16 below can be derived from Equation (11), the total virtual work expression and the principle of virtual work.

$$\begin{bmatrix} M_{FF} & M_{FB} \\ M_{BF} & M_{BB} \end{bmatrix} \begin{bmatrix} \ddot{\epsilon} \\ \dot{\beta} \end{bmatrix} + \begin{bmatrix} C_{FF} & C_{FB} \\ C_{BF} & C_{BB} \end{bmatrix} \begin{bmatrix} \dot{\epsilon} \\ \beta \end{bmatrix} + \begin{bmatrix} K_{FF} & K_{FB} \\ K_{BF} & K_{BB} \end{bmatrix} \begin{bmatrix} \epsilon \\ b \end{bmatrix} = \begin{Bmatrix} R_F \\ R_B \end{Bmatrix} \quad (16)$$

This equation comprises the set of elastic equations of motion and could be written in the form of Equation (9) where the mass matrix is a function of strain, $M = f_M(\epsilon)$, the damping matrix is a function of strain, strain rate and the B reference frame velocity, $C = f_C(\epsilon, \dot{\epsilon}, \beta)$, the stiffness matrix K is constant and R contains all other nonlinearities. Equation (17 provides the expanded form of Equation (16) and the complete set of governing differential equations.

$$\begin{aligned}
M_{FF}\ddot{\epsilon} &= -M_{FB}\dot{\beta} - C_{FF}\dot{\epsilon} - C_{FB}\beta - K_{FF}\epsilon + R_F \\
M_{BB}\dot{\beta} &= -M_{BF}\ddot{\epsilon} - C_{BB}\beta - C_{BF}\dot{\epsilon} + R_B \\
\dot{\zeta} &= -\frac{1}{2}\bar{\Omega}_\zeta\zeta \\
\dot{p}_B &= [C^{BG} \quad 0]\beta \\
\dot{\lambda} &= F_1\ddot{q} + F_2\dot{q} + F_3\lambda
\end{aligned} \tag{17}$$

Here ζ is a vector of four quaternion parameters used to determine the orientation of the B reference frame, $\bar{\Omega}_\zeta$ is the finite element discretization of the ω_B matrix, \dot{p}_B is the time rate of change of the inertial position vector of the B reference frame, C^{BG} is a transformation matrix between the B reference frame and the inertial G reference frame, and λ is a set of unsteady aerodynamic inflow velocities. F_1 , F_2 and F_3 are differential equation matrices associated with λ [23].

III.3.2 A Retrieval of the Rigid-Body Equations of Motion

It is valuable to identify that the standard rigid-body equations of motion for an aircraft can be retrieved from the total virtual work expression, Equation (11), by holding the elastic degrees of freedom constant. This results in the expression for R in Equation (18).

$$\begin{aligned}
R = \begin{Bmatrix} R_F \\ R_B \end{Bmatrix} &= \begin{bmatrix} K_{FF} \\ K_{BF} \end{bmatrix} \epsilon_{initial} + \begin{bmatrix} B_{gF} \\ B_{gB} \end{bmatrix} g^B + \begin{bmatrix} B_{dstF}^F \\ B_{dstB}^F \end{bmatrix} F^{dst} + \begin{bmatrix} B_{dstF}^M \\ B_{dstB}^M \end{bmatrix} M^{dst} \\
&+ \begin{bmatrix} B_{ptF}^F \\ B_{ptB}^F \end{bmatrix} F^{pt} + \begin{bmatrix} B_{ptF}^M \\ B_{ptB}^M \end{bmatrix} M^{pt}
\end{aligned} \tag{18}$$

In this equation, $\epsilon_{initial}$ is the initial strain vector and g^B is the body-fixed reference frame B resolved gravity vector. Also, F^{dst} , M^{dst} , F^{pt} and M^{pt} are the body-resolved

distributed and point forces and moments. F^{aero} and M^{aero} are functions of control surface inputs u and are included in F^{dst} and M^{dst} . Any propulsion related forces such as propeller forces or motor forces are modeled as if they were evenly distributed along the vehicle and are included in F^{pt} and M^{pt} . The values for the influence matrices are explained further in [2] and are given in Equation (19).

$$\begin{aligned}
B_{dst_F}^F &= J_{p\epsilon}^T B_F \\
B_{dst_B}^F &= J_{p\beta}^T B_F \\
B_{dst_F}^M &= J_{\theta\epsilon}^T B_M \\
B_{dst_B}^M &= J_{\theta\beta}^T B_M \\
B_{p_F}^F &= J_{p\epsilon}^T \\
B_{p_B}^F &= J_{p\beta}^T \\
B_{p_F}^M &= J_{\theta\epsilon}^T \\
B_{p_B}^M &= J_{\theta\beta}^T
\end{aligned} \tag{19}$$

Here B_F and B_M are constant matrices characterized by an elastic element's undeformed mass [23]. If $\epsilon_{initial}$ and M^{pt} are assumed to be zero, and the finite strain formulation given in [19] for any aerodynamic forces and moments is assumed to be linear in the discrete trailing edge surface deflections, Equation (18) can be simplified to Equation (20) [3].

$$\begin{aligned}
R &= [B_g]g^B + B_{dst}^F F^{aero} + [B_{dst}^M]M^{aero} + [B_{dst}^M] \frac{\delta F^{aero}}{\delta u_{flap}} u_{flap} \\
&\quad + [B_p^F]u_{thrust}
\end{aligned} \tag{20}$$

III.4 Numerical Integration and the Trim Solution

For both the zero thrust and the thrust required for 1-g level flight cases, trimming is performed in UM/NAST and is based upon techniques described in [23]. A cost function given in Equation (21) is used.

$$J_{trim} = f^T \cdot f \quad (21)$$

Equation (22) gives the zero thrust or gliding cases value for f , the vector used to trim the aircraft.

$$f = \{\text{pitching moment about the origin of the } B \text{ frame lift weight}\} \quad (22)$$

Equation (23) gives the thrust required for 1-g level flight case value for f . Here the longitudinal B reference frame linear and angular accelerations are used for f .

$$f = \begin{Bmatrix} \dot{v}_{B_y} \\ \dot{v}_{B_z} \\ \dot{v}_x \end{Bmatrix} \quad (23)$$

UM/NAST minimizes the cost function J over the solution space using the elevator deflection angle δ_e , the body angle of attack α and the thrust δ_t . The local minimum of the search variable is discovered using a basic numerical Newton-Raphson method, which is given in Equation (24).

$$\Delta S_k = -\frac{\delta f^{-1}}{\delta S_k} f_k \quad (24)$$

Here S_k is given in Equation (25).

$$S_k = \begin{Bmatrix} \delta_e \\ \alpha \\ \delta_t \end{Bmatrix}_k \quad (25)$$

The search variable S_k is recomputed using Equation (26).

$$S_{k+1} = S_k + \Delta S \quad (26)$$

Furthermore, f_{k+1} and

$$\left[\frac{\partial f}{\partial S}\right]_{k+1}^{-1}$$

are recomputed at each iteration using S_{k+1} . This minimization process continues until a desired tolerance is met. Divergence of the solution is avoided by checking S_{k+1} at each iteration step and is limited to prescribed bounds. Equation (27) provides the Jacobian matrix which is computed numerically through finite differences.

$$J_{trim} = \frac{\delta f}{\delta S} \quad (27)$$

Figure 9 outlines this entire trimming solution procedure [23].

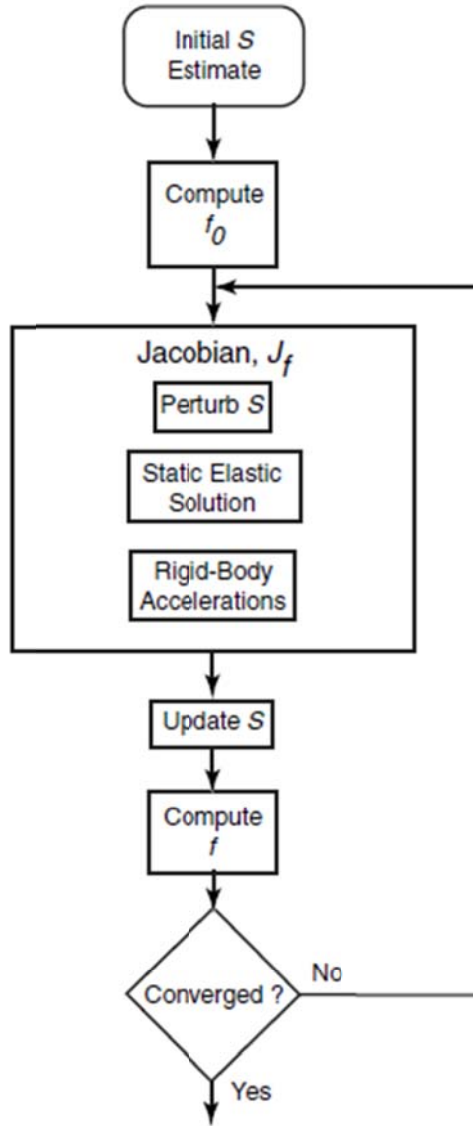


Figure 9. Trim Solution Flow Chart [23]

III.5 Solution of the Governing Equations of Motion

A high-frequency dissipative time-stepping approach is used to solve the governing nonlinear differential equations given in Equation (17). This involves a modified Newark method, which is further described in [23]. The modified Newark method was selected because it can integrate large systems of equations, including ones

with repeated eigenvalues, its ease of use with the equations of motion used, and means by which its first-order and second-order methods were derived [10].

UM/NAST can produce three different types of solutions: a reduced order solution, a linear solution and a nonlinear solution. For a reduced order solution, all elastic degrees of freedom are removed once the vehicle flexes into a steady-state deflection. For this type of simulation the inertia matrices is fixed but the Jacobian matrices change at each subiteration. For a linear solution, the elastic degrees of freedom remain intact and the inertia matrices change at each subiteration, but the Jacobian matrices obtained from the steady-state solution that UM/NAST computes at the beginning of each simulation are used; therefore, they are fixed. For a nonlinear solution, the elastic degrees of freedom remain intact, the inertia matrices change at each subiteration and the Jacobian matrices are updated at each subiteration, resulting in a full time-marching simulation based on Equation (17).

A few issues with UMNAST should be noted: UM/NAST begins a simulation by first going through a routine that determines the steady-state solution. It then continues into a time-marching simulation. The code is also sensitive to the time step selected, how long the simulation is run for and how big the tolerance for the R , or the residual, value is. Additionally, the predictor-corrector method used to find the S values can create a problem where certain matrices have values that are very large or very small, making it difficult to invert these matrices. The simulation may fail before it is complete because the values selected are inappropriate. In general, smaller time steps work better, but often a smaller time step means the simulation may take longer to finish. A time step that is too large can also cause the simulation to take a longer amount of time to finish. Also, a

larger residual value tolerance helps the simulation to finish sooner, although a residual value that is too large may cause the simulation to diverge from the actual solution. The longer the simulation time, the more difficult it is for the simulation to complete without issues. If these values are selected properly, a complete simulation can be accomplished. The ease at which a simulation will complete depends on the simulation type selected; the reduced-order type simulation is the least sensitive to selected values and is the most likely to complete, while the linear type is less likely to complete and the nonlinear type is the least likely to complete because it is the least sensitive to the selected values.

IV. Results

IV.1 The Assumptions Made

This research performed a set of simulations using the UM/NAST code to predict the flight behavior of the 6 meter and 8 meter models of X-HALE. The UM/NAST code was provided by Shearer, Cesnik and their co-workers. In order to model the X-HALE aircraft using UM/NAST, several assumptions were made. These assumptions involve how X-HALE is modeled in the UM/NAST code. For example, the NACA 4415 airfoil used for the main wing segments in these simulations is not identical to the EMX-07 airfoil used for the physical X-HALE aircraft, but it is similar enough to the EMX-07 airfoil for the purposes of this research because it has similar lifting and moment characteristics. The NACA 0012 airfoil used to model the tail elevons is the actual airfoil used on the physical X-HALE. The fairing pods are modeled with a NACA 0018 airfoil. The fairings are also modeled with applied follower concentrated forces to simulate motor thrust.

Each motor is simulated with a constant force. The tails are modeled as all-movable horizontal surfaces. All booms, tails and fairings are modeled as rigid members with inertias placed at points best suitable to model the two physical X-HALE aircrafts. Furthermore, the outer 1 meter long members are modeled with a dihedral of 10 degrees just like the physical X-HALE aircrafts. The ailerons are modeled on the outer dihedral members and occupy 25% of the chord also just like the physical X-HALE aircrafts. The inertias of the spine and the pod covers are neglected and instead the concentrated inertias are placed inside the pods. This is done primarily to model the electronic equipment inside the pods. The masses of aircraft models are programmed to be the estimated

completed 6 meter and 8 meter X-HALE weights. Figure 10 illustrates the UM/NAST model of the 8 meter X-HALE [4].

The actual X-HALE aircraft has a center tail and elevon, as seen in Figure 5. The UM/NAST model does not include a center tail and elevon, as seen in Figure 10. However, because the tail is in the center and it is a symmetric airfoil, its absence is unlikely to make a difference in the results of the simulations. Also, the actual X-HALE can flip the center tail 90 degrees so that it becomes a vertical stabilizer. However, this is not done in any of the simulations performed for this research.

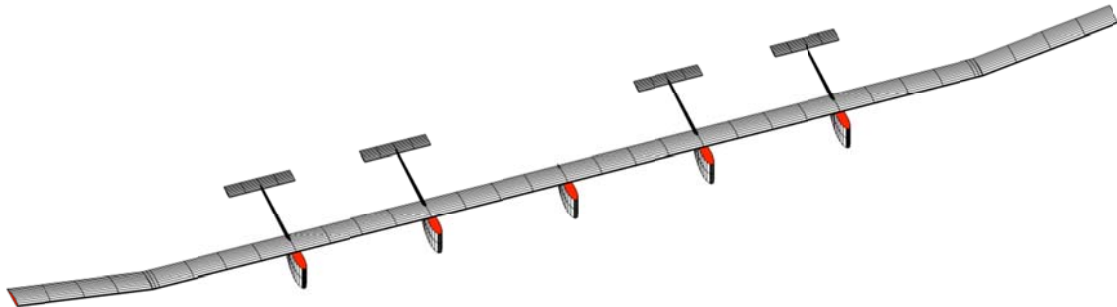


Figure 10. UM/NAST Model of the 8 Meter X-HALE Aircraft [4]

The X-HALE aircraft is trimmed for equal lift and weight, and also for a zero pitching moment about its center of gravity at level flight at 30 meters altitude. The normal flight velocity for the aircraft ranges from 12 to 20 m/s. Figure 11 shows the deformed shape at the trimmed condition for the 8 meter X-HALE model. The 8 meter X-HALE trims at 14 m/s and its tip deflection is about 37% its half span [4]. The X-HALE aircraft's starting speed is its trim speed, the flights are assumed to be gust free and the starting altitude is assumed to be 30 meters above sea level.

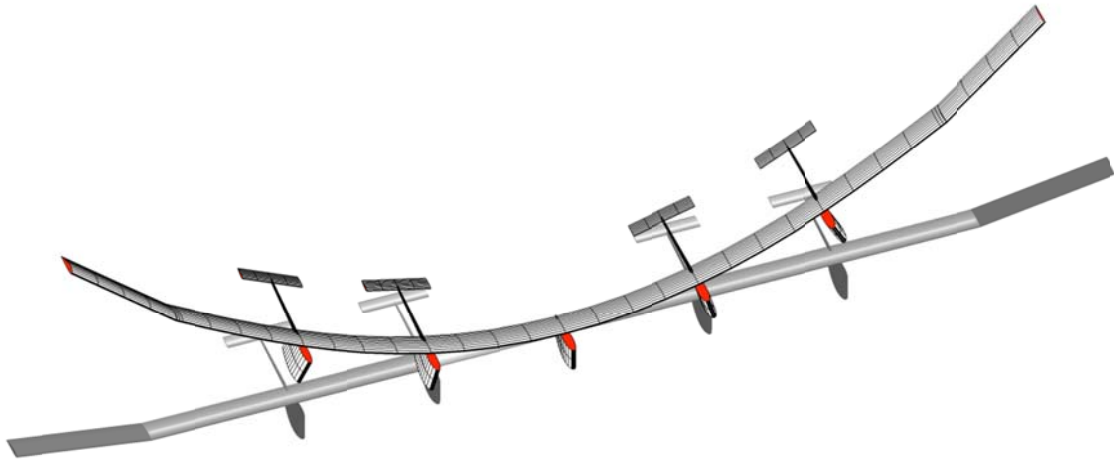


Figure 11. Deformed Shape at the Trim Condition for the 8 Meter X-HALE [4]

IV.2 Running the Simulations and Initial Complications

This research was performed by altering pre-existing input files for the UM/NAST code in order to meet the specified simulation parameters. Initial complications arose when completing the simulations because the code is sensitive to the simulation type selected (the reduced-order, linear or nonlinear cases), the time step selected, how long the simulation flight is and how big the tolerance for the R (the residual) value is. Many simulations failed before they completed because the values selected were inappropriate and calculations became very difficult for the computer to perform.

This research ran two types of simulations: the linear and nonlinear solution types. Initially the simulations were set for the 6 meter aircraft and a 15 second flight time involving constant thrust flight with no other inputs such as an aileron or control surface input. However, problems occurred completing the simulation after approximately the 9.6 second point, no matter what time step or maximum residual value was selected. After repeatedly failing simulations, a linear type simulation with a time

step of 0.0025 seconds and a maximum residual value of 0.1 completed. The simulation took approximately a week to complete using 64-bit Matlab on a dual core 2.6 GHz personal computer. The results of this simulation revealed why the simulations struggled to complete after approximately 9.6 seconds: the flight of the 6 meter X-HALE model had become highly unstable at that point in time as seen in Figure 12. No nonlinear type simulation attempted for the 6 meter X-HALE would run to completion after approximately the 9.7 second mark because all of these simulations resulted in unstable flight. This will be further discussed in Section IV.4.1.

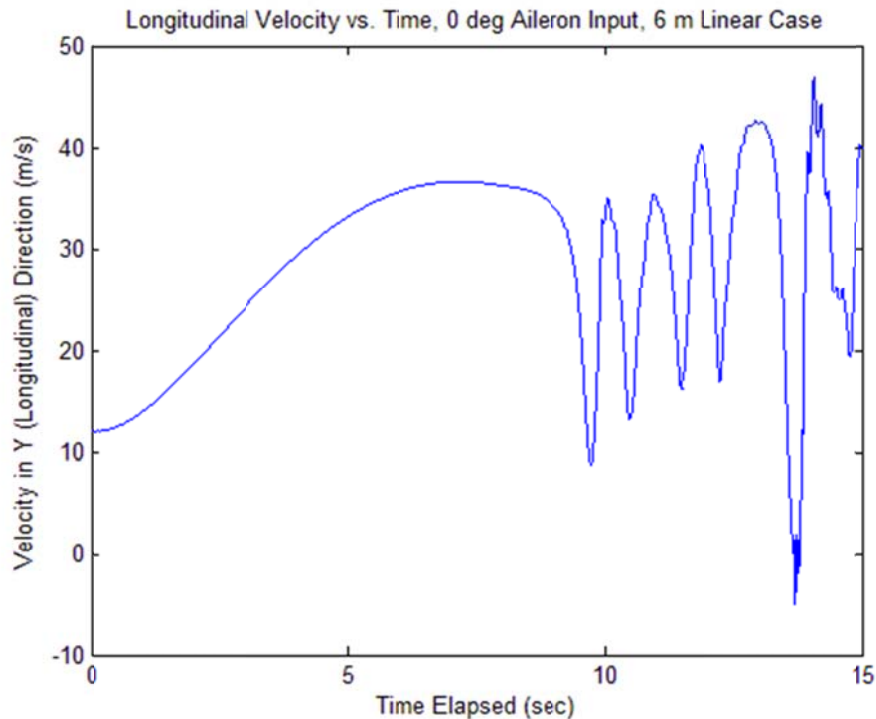


Figure 12. Case 1 Longitudinal Velocity v_y versus Time

The simulation flight time was shortened to 10 seconds in order to ensure the 6 meter X-HALE simulations completed. Several more 6 meter X-HALE simulations were run until a nonlinear simulation involving constant thrust flight with no other inputs, such as an aileron or control surface input, completed a 10 second flight with a time step of

0.0001 seconds and a maximum residual value of 10. All other 6 meter X-HALE simulations and several 8 meter X-HALE simulations were run using this time step and maximum residual value from this point on so that all the simulations run from this point onward would have this time step and maximum residual value in common. Next one linear type simulation involving constant thrust flight with no other inputs was run for the 6 meter X-HALE. After that three linear type simulations involving sinusoidal aileron inputs on both wings were run for the 6 meter X-HALE.

Next the 8 meter X-HALE simulations were run. First, four 8 meter X-HALE model linear type simulations with a 10 second flight time and sinusoidal aileron inputs on both wings were run. Each 10 second flight time simulation took anywhere from three to five days to complete using 64-bit Matlab on a dual core 2.6 GHz personal computer. These simulations had the same time step (0.0001 seconds) and maximum residual value (10) as the 6 meter X-HALE simulations. They ran much smoother than the 6 meter X-HALE simulations because the aircraft did not become extremely unstable by the end of the 10 second runs. However, these 10 second simulations did not provide enough data in order to find what sinusoidal aileron inputs on both wings would make the aircraft unstable, so thirteen more simulations were run for the 8 meter X-HALE using a 0.001 second time step, a maximum residual value of 10 and a time duration of 15 seconds. Therefore, the 10 second 8 meter X-HALE simulations are not discussed in this research because the 15 second simulations provide all of the data needed. The time step was then increased by an order of magnitude for the latter simulations in order to get the simulations to run faster. Two of the 15 second simulations failed because the

amplitudes of the sinusoidal aileron inputs applied to both wings were too large (20 and 25degrees) and caused the aircraft to become unstable.

In general, smaller time steps worked better for the simulations, but often a smaller time step meant the simulation took longer to finish. Also, a larger maximum residual value helped the simulation to finish sooner. However, a maximum residual value that is too large could cause a simulation to diverge from the actual solution. The ease at which a simulation would complete also depended on the simulation type selected; the nonlinear type simulation was more likely to fail than the linear type simulation was. This research first aimed for a time step of 0.05 seconds and a maximum residual value of 0.1 for the 6 meter X-HALE simulations, but these values were changed since the simulations would fail before finishing a 10 second flight with these values. A time step of 0.0001 and a maximum residual value of 10 were used in order to ensure a nonlinear type 6 meter simulation finished the 10 second flight. However, a time step this small caused the simulations to take approximately 3 to 5 days to complete a 6 meter X-HALE simulation, which was much longer than initially anticipated.

In comparison, the 8 meter X-HALE simulations run with a 15 second time duration and a time step of 0.001 seconds each took approximately 7 to 10 hours to complete. These were a mix of linear and nonlinear type simulations. The time step and time duration were changed for these additional 8 meter model X-HALE simulations to allow the simulations to provide more data since the flight was longer but also so that the simulation could run faster. A 10 second 8 meter X-HALE simulation with a time step of 0.0001 seconds took approximately ten times longer than a 10 second simulation with a

time step 0.001 since this large time step still allowed the simulation to run quite smoothly.

IV.3 The Chosen Simulations

The 6 meter model of the aircraft was based off the pre-existing input file 6_meter_baseline_case0.nin which uses a NACA 4415 airfoil. The 8 meter model of the aircraft was based off the pre-existing input file 8_meter_ailerons_case0.nin, which also uses a NACA 4415 airfoil. Examples of these input files can be found in Appendix B and Appendix C. Of all the simulations run, seventeen were chosen to be discussed in detail in this research. The first six simulations, Cases 1 through 6, were simulations for the 6 meter model of X-HALE. The first simulation, Case 1, used a 0.0025 second time step, a maximum residual value of 0.1 and a 15 second time duration. It had no inputs, such as an aileron or control surface input, and had a constant thrust. This was a linear type simulation. The rest of the 6 meter X-HALE simulations used a 0.0001 time step, a maximum residual value of 10 and a 10 second time duration. Except for one nonlinear type simulation, they were all linear type simulations which either used no inputs or they had sinusoidal aileron inputs on both wings. The 8 meter X-HALE simulations had a time duration of 15 seconds, a time step of 0.001 seconds and a maximum residual value of 10. These all had sinusoidal aileron inputs on both wings. These were part linear type and part nonlinear type simulations.

Each of the simulations that used a sinusoidal aileron input on both wings were given an aileron input with a period of 5 seconds on both the left and right ailerons. The input started at 0.1 seconds and finished after 10 seconds. The inputs had amplitudes of 2, 5, 10, 15, 20 or 25 degrees. The aileron input completes approximately two periods

before terminating. An example of a sinusoidal aileron input can be seen in Figure 13. A summary of the simulations discussed in this research is provided in Table 2.

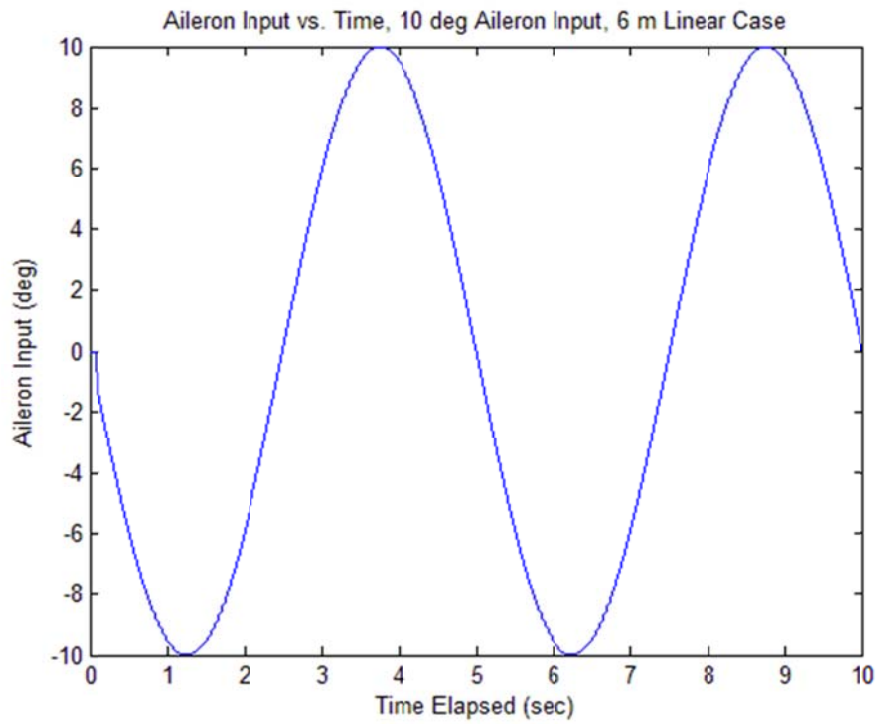


Figure 13. Case 6 Aileron Input versus Time

Table 2. A Summary of Discussed Simulations

Case	Simulation Type	Input	Duration (sec)	Time Step (sec)	Max Residual Value	Sinusoidal Aileron Input Data		
						Period (sec)	Start/End Time (sec)	Amplitude (deg)
1	6 Meter Linear	None	15	0.0025	0.1	N/A	N/A	N/A
2	6 Meter Linear	None	10	0.0001	10	N/A	N/A	N/A
3	6 Meter Nonlinear	None	10	0.0001	10	N/A	N/A	N/A
4	6 Meter Linear	Aileron	10	0.0001	10	5	0.1/10	2
5	6 Meter Linear	Aileron	10	0.0001	10	5	0.1/10	5
6	6 Meter Linear	Aileron	10	0.0001	10	5	0.1/10	10
7	8 Meter Linear	None	15	0.001	10	N/A	N/A	N/A
8	8 Meter Linear	Aileron	15	0.001	10	5	0.1/10	2
9	8 Meter Nonlinear	Aileron	15	0.001	10	5	0.1/10	2
10	8 Meter Linear	Aileron	15	0.001	10	5	0.1/10	5
11	8 Meter Nonlinear	Aileron	15	0.001	10	5	0.1/10	5
12	8 Meter Linear	Aileron	15	0.001	10	5	0.1/10	10
13	8 Meter Nonlinear	Aileron	15	0.001	10	5	0.1/10	10
14	8 Meter Linear	Aileron	15	0.001	10	5	0.1/10	15
15	8 Meter Nonlinear	Aileron	15	0.001	10	5	0.1/10	15
16	8 Meter Linear	Aileron	15	0.001	10	5	0.1/10	20
17	8 Meter Linear	Aileron	15	0.001	10	5	0.1/10	25

This research was performed to predict the in flight behavior of both the 6 meter model and the 8 meter models of X-HALE. The two baseline 6 meter model simulations performed with no inputs were performed using the linear and nonlinear simulation types. This was done in order to compare the linear and nonlinear simulation types and to gain knowledge of their differences. This was also done in order to see how well the 6 meter X-HALE model can fly straight and level. The three sinusoidal aileron input linear type simulations were performed for the 6 meter model in order further understand the aircraft's response to an aileron input. Only the linear type solution was used in order to better compare the simulations performed while also minimizing the time it took to compute the solutions. The one 8 meter model linear type simulation was run with no inputs in order to form an understanding of how well the 8 meter aircraft can fly straight and level. Finally, the ten 8 meter model sinusoidal aileron input simulations were performed in order to understand aircraft's response to an aileron input on both wings. These simulations were a mix of linear and nonlinear type simulations so that the two simulation types could be compared.

Again, for a linear solution, the elastic degrees of freedom remain intact and the inertia matrices change at each subiteration, but the Jacobian matrices obtained from the steady-state solution computed at the beginning of each simulation are used; therefore, they are fixed. For a nonlinear solution, the elastic degrees of freedom remain intact, the inertia matrices change at each subiteration and the Jacobian matrices are updated at each subiteration, resulting in a full time-marching simulation based on Equation (17).

While the Case 1 simulation has a different time step (0.0025 seconds) and maximum residual value (0.1) than the other 6 meter X-HALE simulations, it is included

in the data because it is the only 6 meter X-HALE simulation that runs for 15 seconds; the other simulations only run for 10 seconds. For the rest of the 6 meter X-HALE simulations the time step, maximum residual value, and time duration were chosen based on the limitations of the UM/NAST code and the simulation parameters, as mentioned in Section IV.1. The time step for these simulations, 0.0001 seconds, was the largest time step that actually allowed a 6 meter X-HALE nonlinear type simulation to complete a 10 second run. The residual value tolerance of 10 was chosen because a value smaller than that would cause a simulation to take significantly longer to finish but a value larger than would potentially cause a nonlinear simulation to fail. The time duration of 10 seconds was chosen because after approximately the 9.6 second point, a simulation would struggle to finish, so this time duration value was chosen to make sure simulations could finish. For the 8 meter X-HALE simulations, the time step was changed to 0.001 and the time duration was changed to 15 seconds in order to allow for a longer flight but also so that the simulations could finish more quickly.

For simulations that involved a sinusoidal aileron input on both wings, the period of the input, 5 seconds, and the start and stop time of the input, 0.1 seconds and 10 seconds, were chosen because this periodic input would be similar to the kind of aileron input X-HALE would normally receive in flight. Several different sinusoidal aileron input amplitudes were used: 2, 5, 10, 15, 20 and 25 degrees. These values were chosen in order to find the maximum aileron input amplitude that could be used without the aircraft's flight becoming unstable. These values were also chosen based on the results of Cesnik et al. [4] who, when performing UM/NAST simulations for the 8-meter X-

HALE, discovered that a left aileron input (a rolling maneuver) resulted in unstable flight when a sinusoidal input of 5 degrees or more was used.

IV.4 The Completed Simulations and Their Results

The results of all seventeen chosen simulations are discussed in detail in this section of the research. The results are broken down into results for the 6 meter aircraft and the 8 meter aircraft. Six to seven plots per simulation were generated. Some of them are used in this section and all of them are included in the Appendix.

IV.4.1 The 6 Meter X-HALE Results

All six 6 meter X-HALE simulations had the same primary result; the aircraft over speeds up to approximately 40 m/s and stalls after approximately 9 seconds in all six simulations. After the stall, the aircraft enters highly unstable flight. As stated previously, 12 to 20 m/s is considered the normal flight speed range for X-HALE [4]. This leads to two possible conclusions: Either UM/NAST did not properly model the flight of the 6 meter X-HALE or the 6 meter X-HALE is an unstable aircraft and can be expected to crash soon after takeoff.

Case 1 is a linear type no aileron input simulation run for 15 seconds. The time step was 0.0025 seconds and the residual tolerance value was 0.1. Again, this was the first completed simulation and is the case that has a different time step and residual tolerance value than the other simulations. Figure 14 shows the aircraft's longitudinal velocity v_y versus time. Note that the B reference frame is used for all plots. The x-axis is out the right wing and the y-axis is tangent to the undeformed fuselage's longitudinal axis and extends in the direction of the front of the aircraft. As a result, the x-y plane of

the B reference frame is parallel to the x - y plane of the inertial frame G when the aircraft is undeformed. The z -axis extends out the top of the aircraft and is the cross product of the x -axis and y -axis.

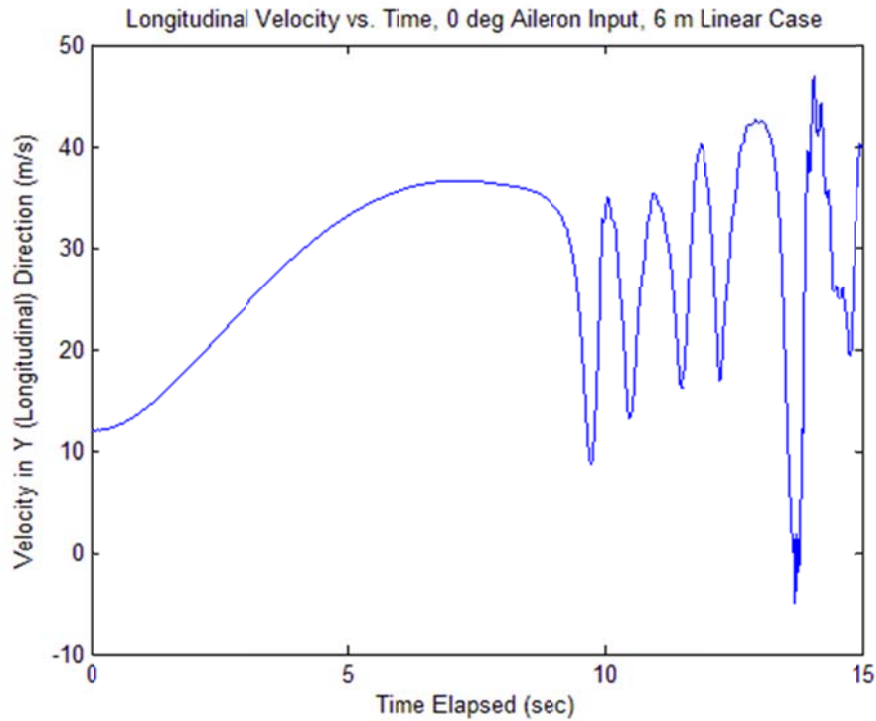


Figure 14. Case 1 Longitudinal Velocity v_y versus Time

This plot shows that the aircraft begins to over speed at approximately 2.5 seconds when its velocity goes over 20 m/s and stalls at approximately 9 seconds. At this point the aircraft becomes highly unstable. Figure 15 and Figure 16 show the velocity of the aircraft in the x and z directions. Figure 17, Figure 18 and Figure 19 show the angular velocity of the aircraft about the x -, y - and z -axes versus time.

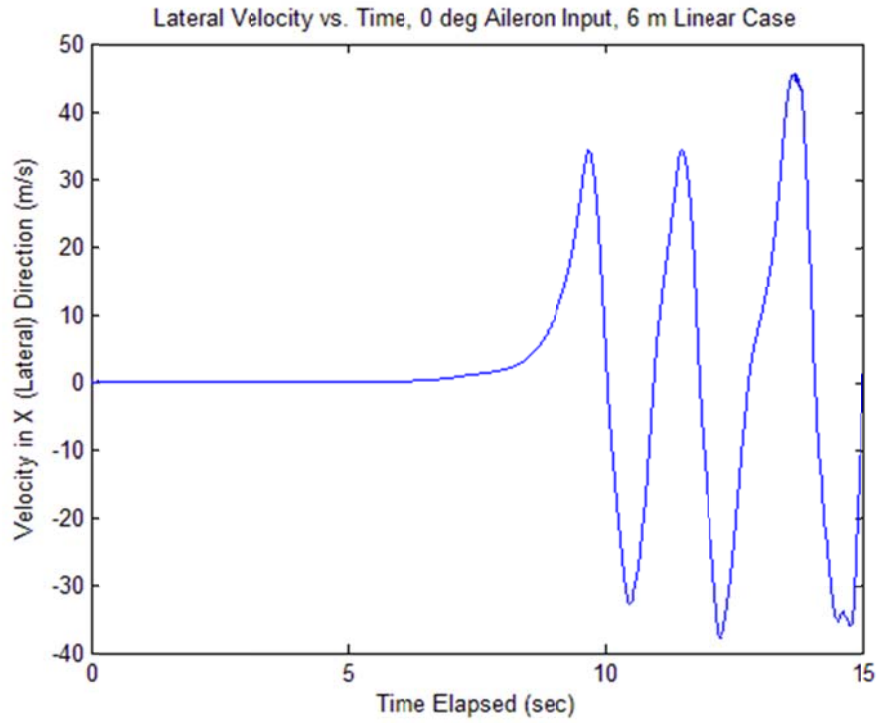


Figure 15. Case 1 Lateral Velocity v_x versus Time

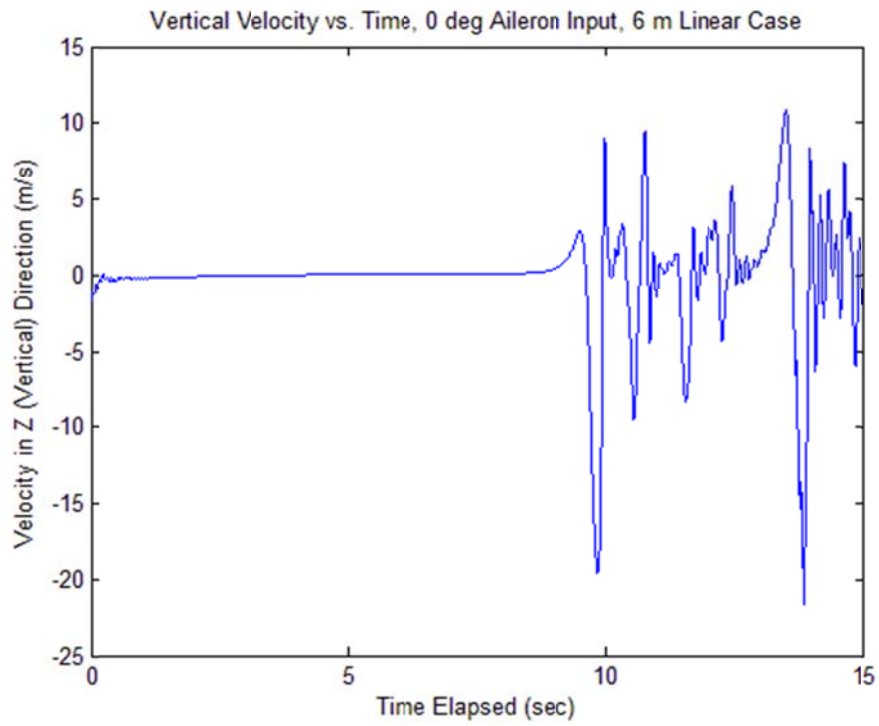


Figure 16. Case 1 Vertical Velocity v_z versus Time

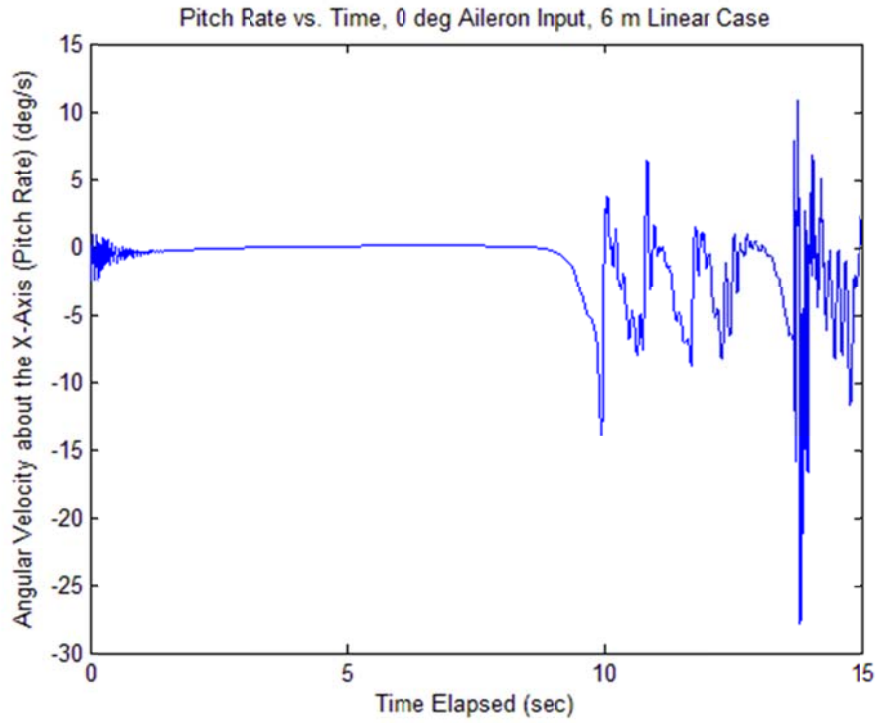


Figure 17. Case 1 Pitch Rate ω_x versus Time

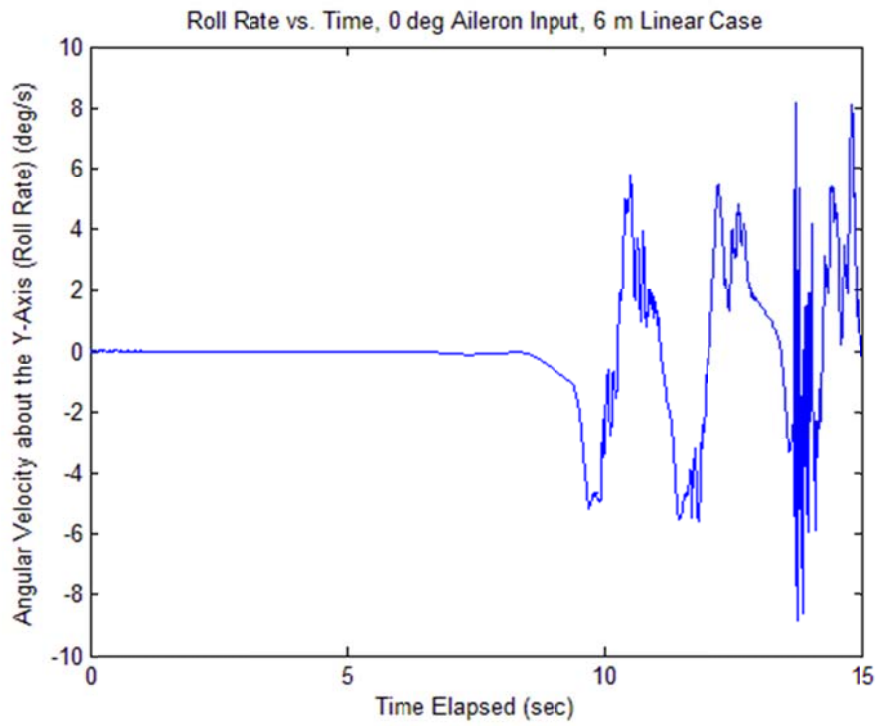


Figure 18. Case 1 Roll Rate ω_y versus Time

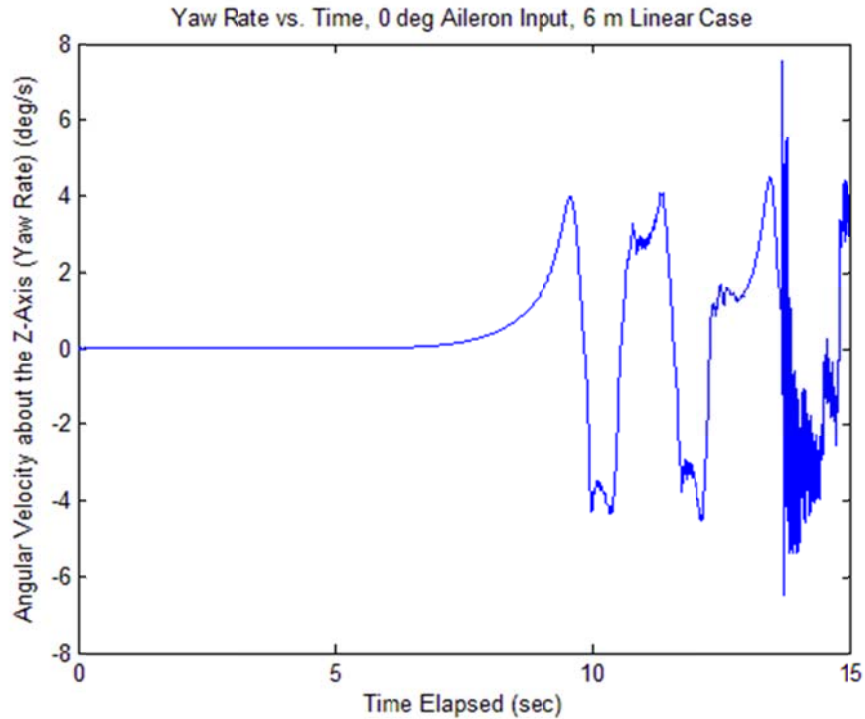


Figure 19. Case 1 Yaw Rate ω_z versus Time

These plots also show that the 6 meter X-HALE becomes highly unstable after approximately 9 seconds. These angular velocity plots show that the 6 meter X-HALE is rotationally stable for approximately the first 9 seconds of the simulation. However, Figure 14 which shows the aircraft's longitudinal velocity v_y , suggests that the aircraft was unstable from the start of the simulation since the aircraft begins to speed up and then over speeds at the beginning of the simulation. Note that many of the results of the simulations run for this research show initial instabilities that quickly dampen out, such as in Figure 17. This is not due to an actual instability of the aircraft but is due to numerical errors caused by the UM/NAST program.

Case 2 is another linear type no aileron input simulation, just like Case 1, but is run for 10 seconds instead of 15 seconds. Also, Cases 2 through 6 have a different time

step (0.0001 seconds), residual tolerance value (10) and time duration (10 seconds) than Case 1. Besides the fact that Case 2 is a shorter simulation than Case 1, there are no apparent differences between the results of the two simulations. Case 3 is a nonlinear version of Case 2 and its results can be viewed in Figure 20, Figure 21, Figure 22, Figure 23, Figure 24 and Figure 25. The Case 2 simulations can be viewed in the Appendix.

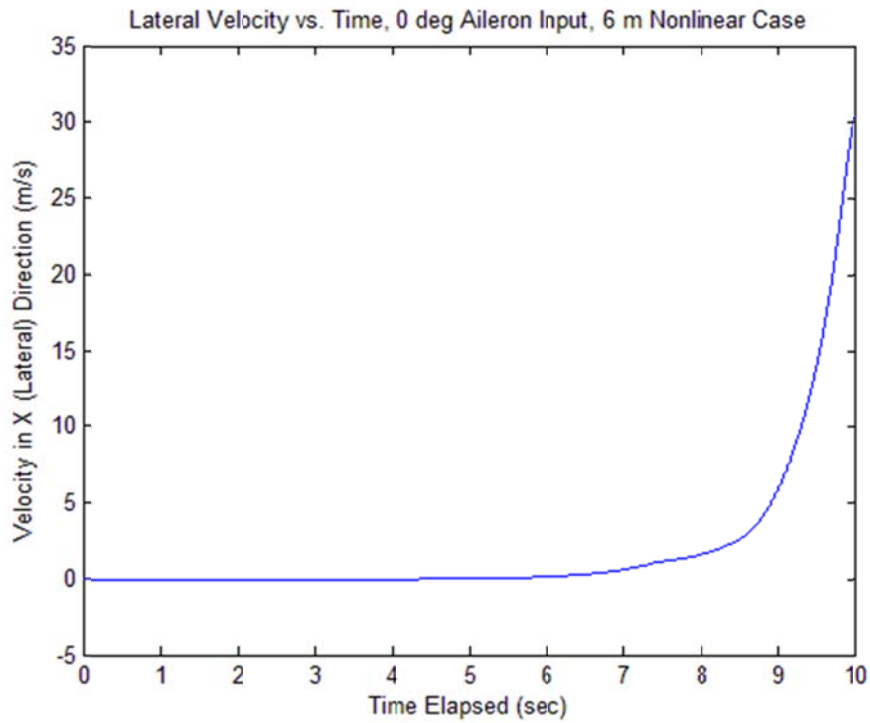


Figure 20. Case 3 Lateral Velocity v_x versus Time

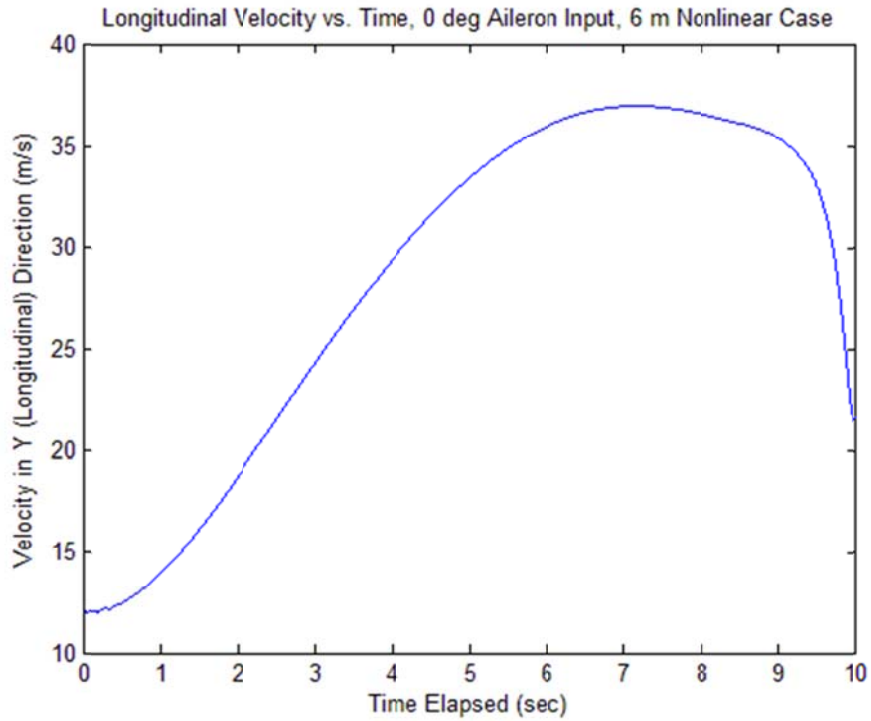


Figure 21. Case 3 Longitudinal Velocity v_y versus Time

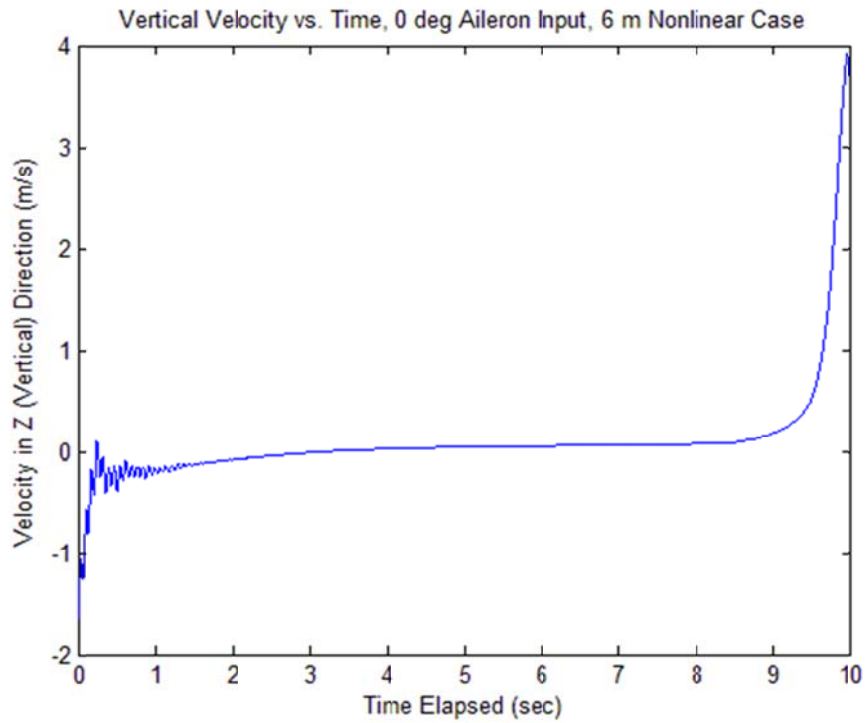


Figure 22. Case 3 Vertical Velocity v_z versus Time

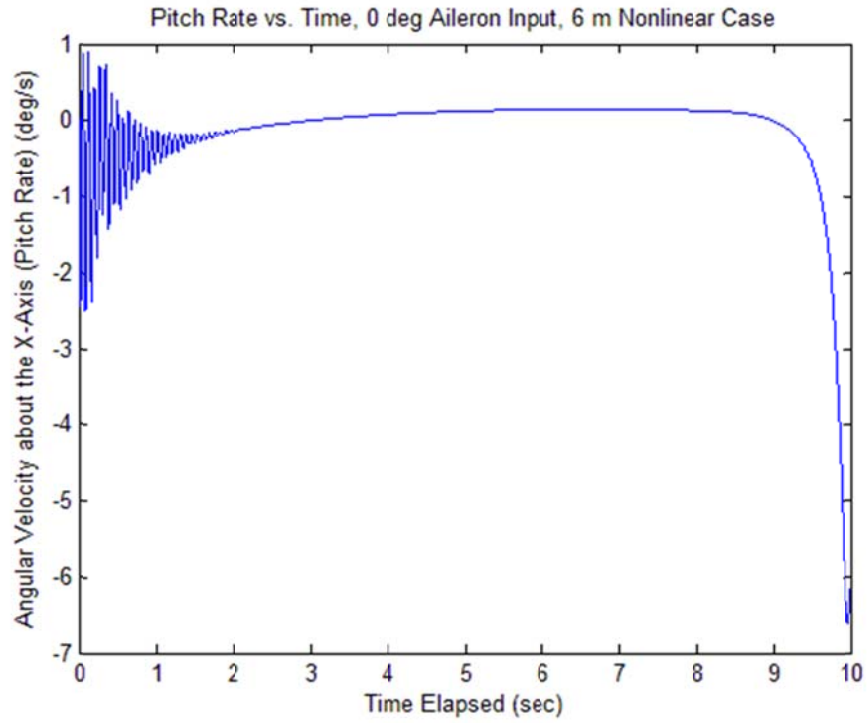


Figure 23. Case 3 Pitch Rate ω_x versus Time

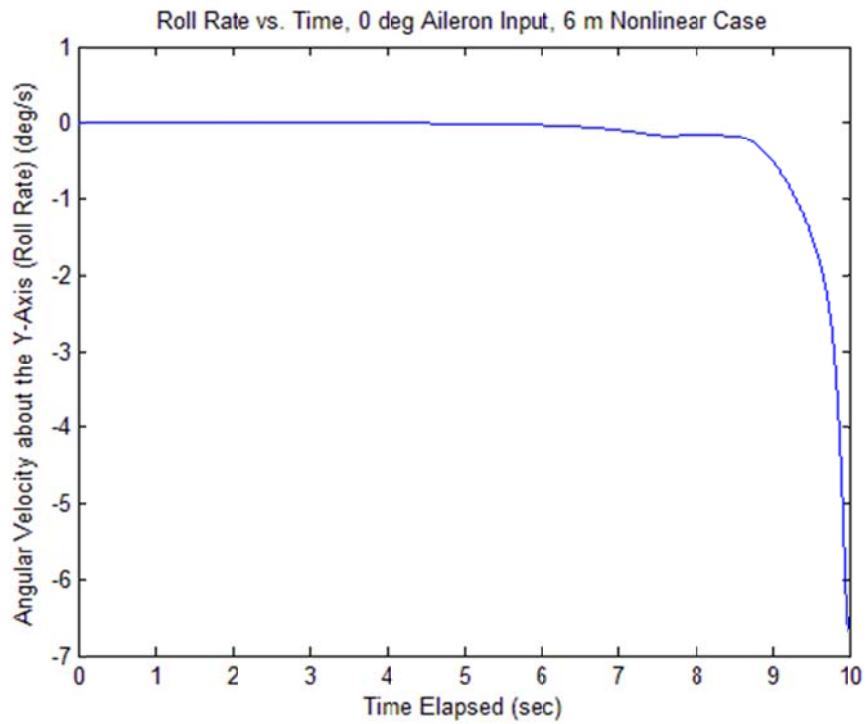


Figure 24. Case 3 Roll Rate ω_y versus Time

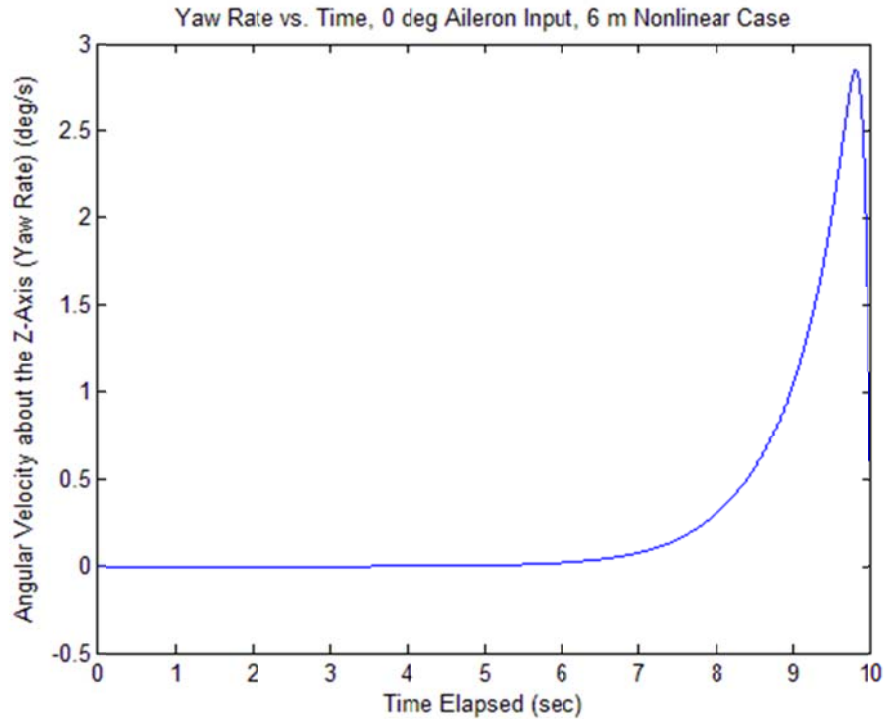


Figure 25. Case 3 Yaw Rate ω_z versus Time

These plots show that there is little difference between the linear and nonlinear simulation types because they are very similar to the results from Case 1 and Case 2.

Case 4, Case 5 and Case 6 are the same linear type 6 meter X-HALE simulation except for the fact that they have different sinusoidal aileron input amplitudes. The input amplitudes are 2, 5 and 10 degrees, respectively. These three cases also show that the 6 meter X-HALE aircraft begins to over speed at approximately 2.5 seconds when its velocity goes over 20 m/s and stalls at approximately 9 seconds. The aileron input for Case 6 can be seen in Figure 26, while the results for Case 6 can be seen in Figure 27, Figure 28, Figure 29, Figure 30, Figure 31 and Figure 32. The aileron inputs and the results for Cases 4 and 5 can be viewed in the Appendix.

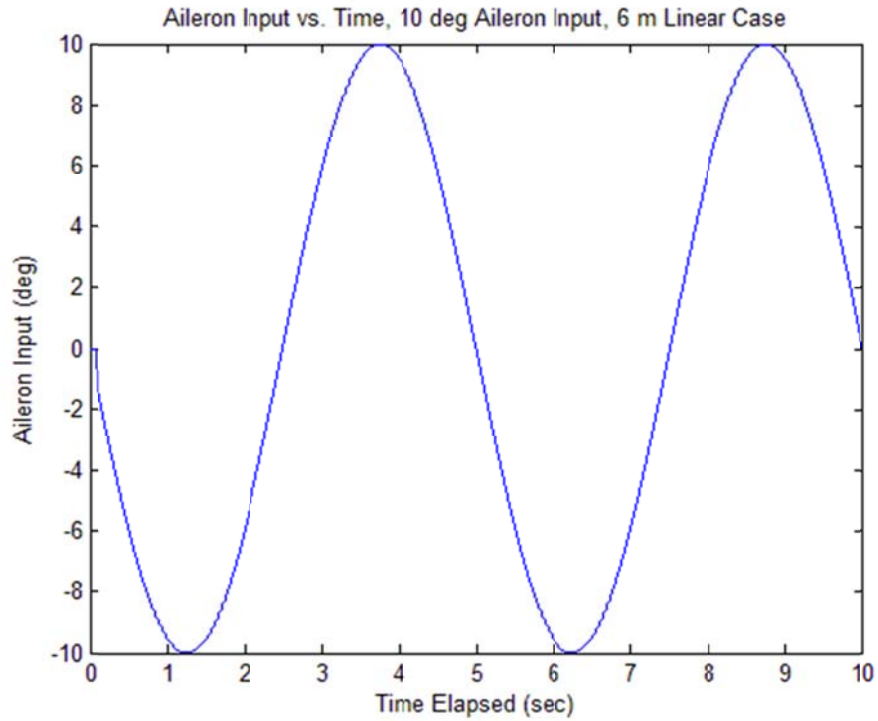


Figure 26. Case 6 Aileron Input versus Time

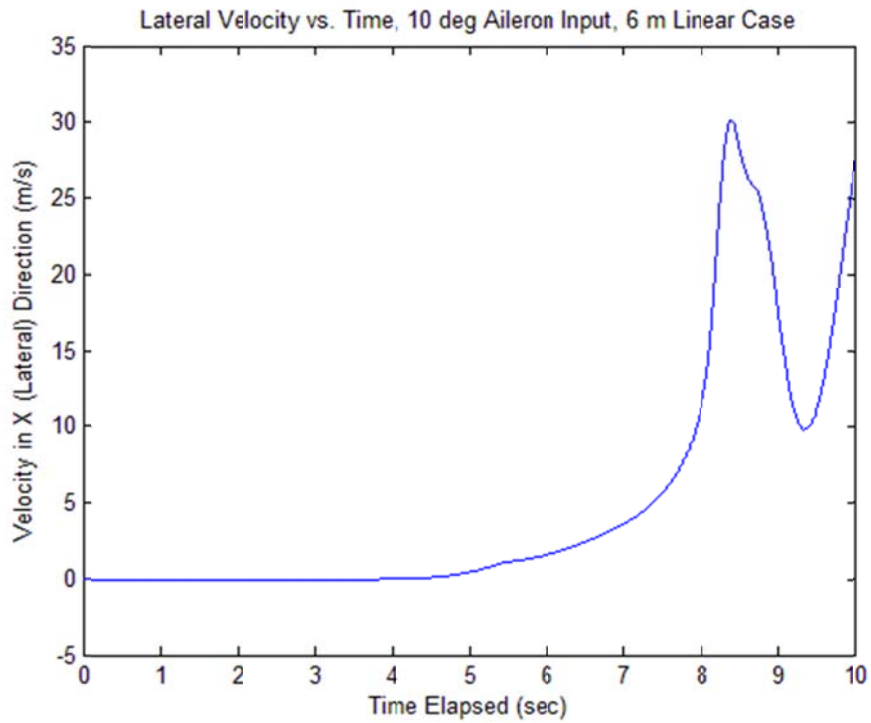


Figure 27. Case 6 Lateral Velocity v_x versus Time

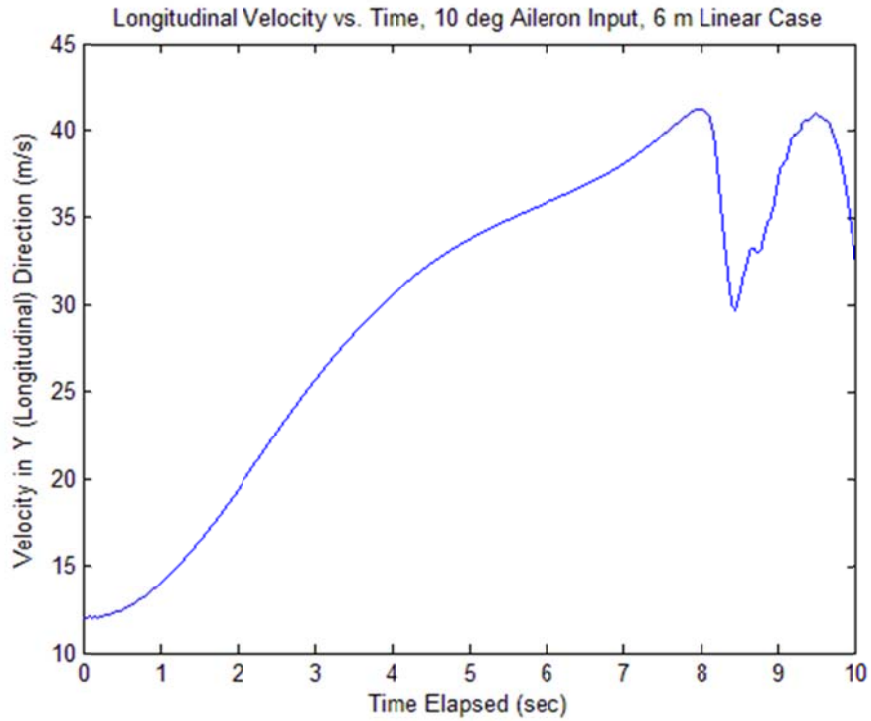


Figure 28. Case 6 Longitudinal Velocity v_y versus Time

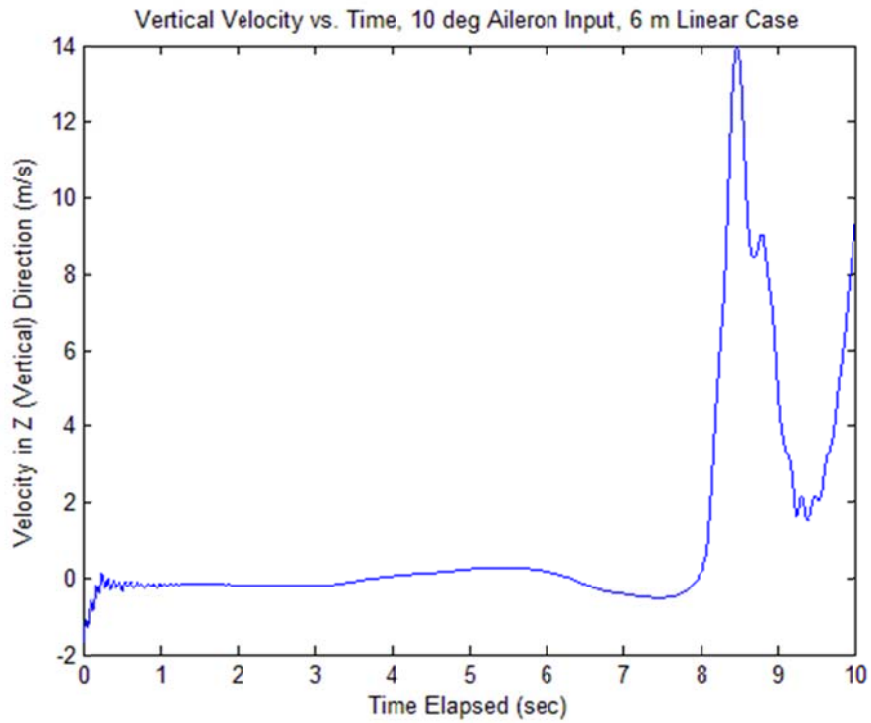


Figure 29. Case 6 Vertical Velocity v_z versus Time

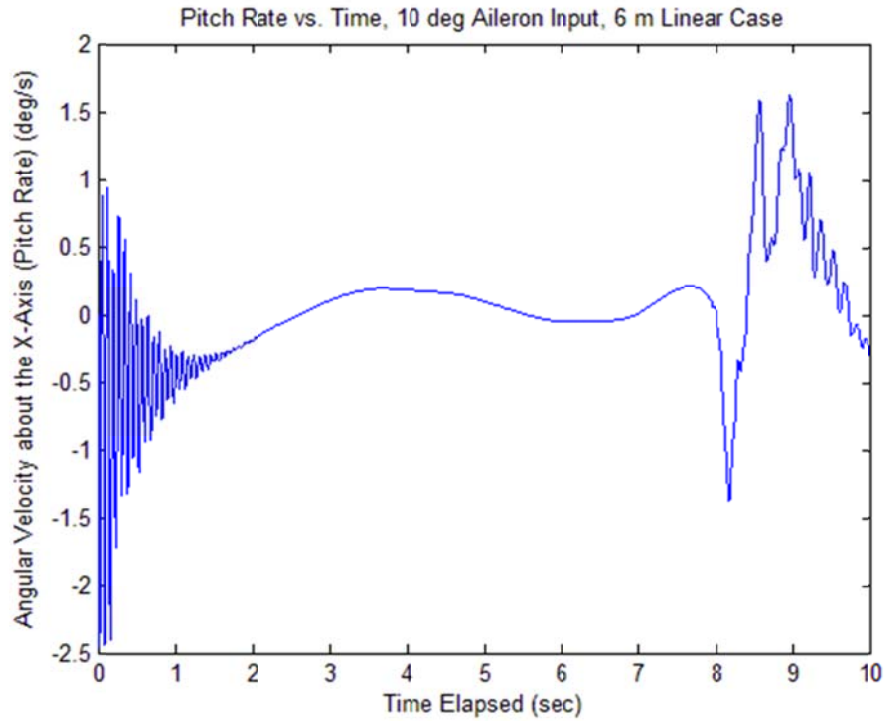


Figure 30. Case 6 Pitch Rate ω_x versus Time

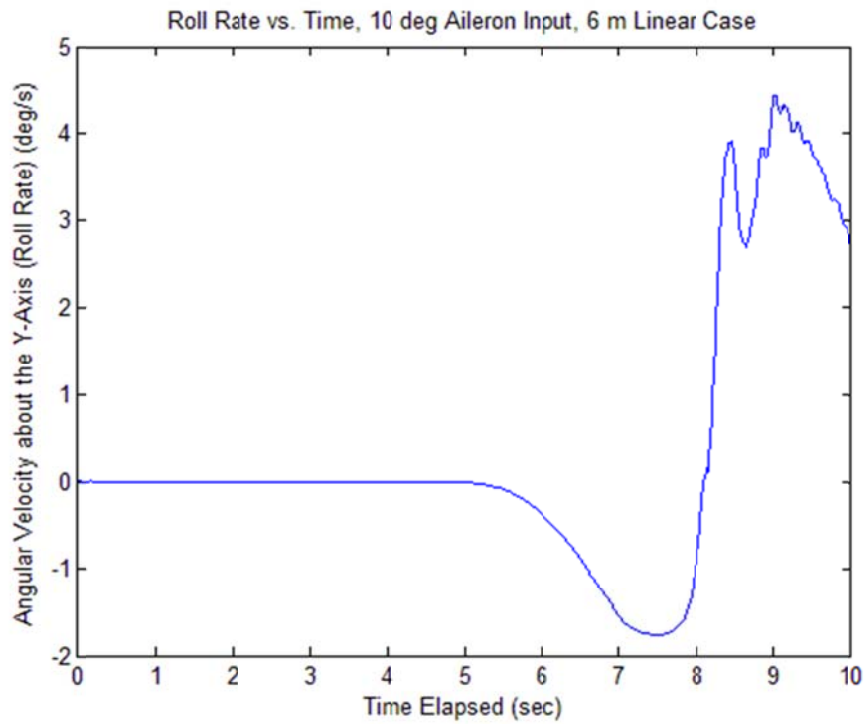


Figure 31. Case 6 Roll Rate ω_y versus Time

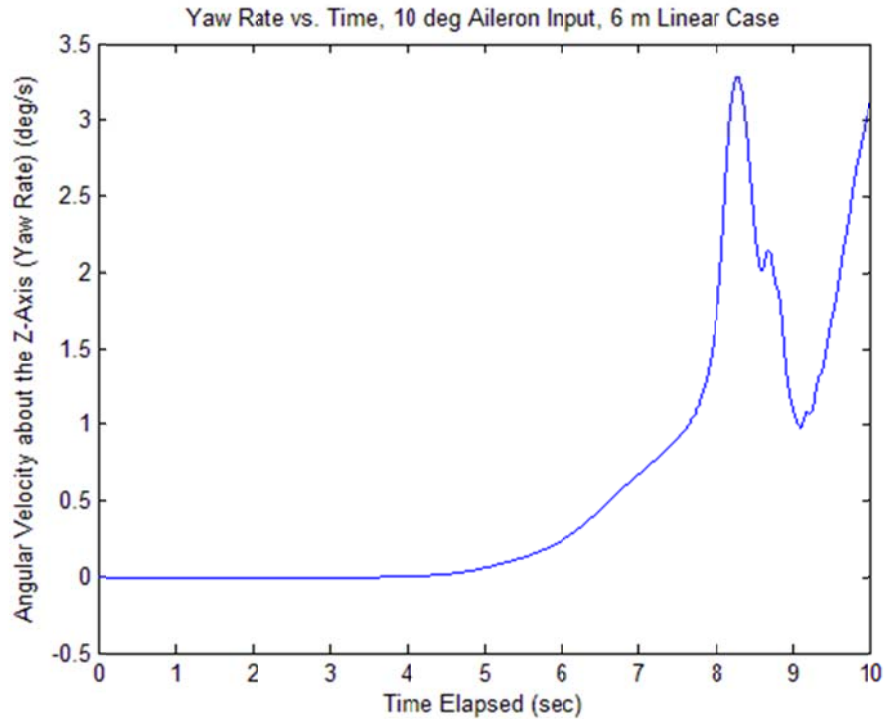


Figure 32. Case 6 Yaw Rate ω_z versus Time

It is clear when comparing the figures from Cases 4, 5 and 6 that the sinusoidal aileron inputs did have an impact on the flight behavior of the aircraft. However, the aileron inputs did not prevent the aircraft from over speeding and stalling. The results from Cases 4, 5 and 6 show that the larger the aileron input amplitude is, the more effect the aileron input has on the flight behavior of the aircraft. The results for Cases 1 through 6 all show that the flight behavior of the 6 meter X-HALE is unstable from the start of the simulations.

IV.4.2 The 8 Meter X-HALE Results

Cases 7 through 17 are the 8 meter X-HALE model simulations preformed. These cases have a 15 second flight time, a 0.0001 second time step and a maximum residual value of 10. They are a mix of the linear and nonlinear solution types. Case 7 is

a linear type simulation and has no inputs, while Cases 8 through 17 have sinusoidal aileron inputs with amplitudes of 2, 5, 10, 15, 20 and 25 degrees. The results for Case 7 can be viewed in Figure 33, Figure 34, Figure 35, Figure 36, Figure 37 and Figure 38.

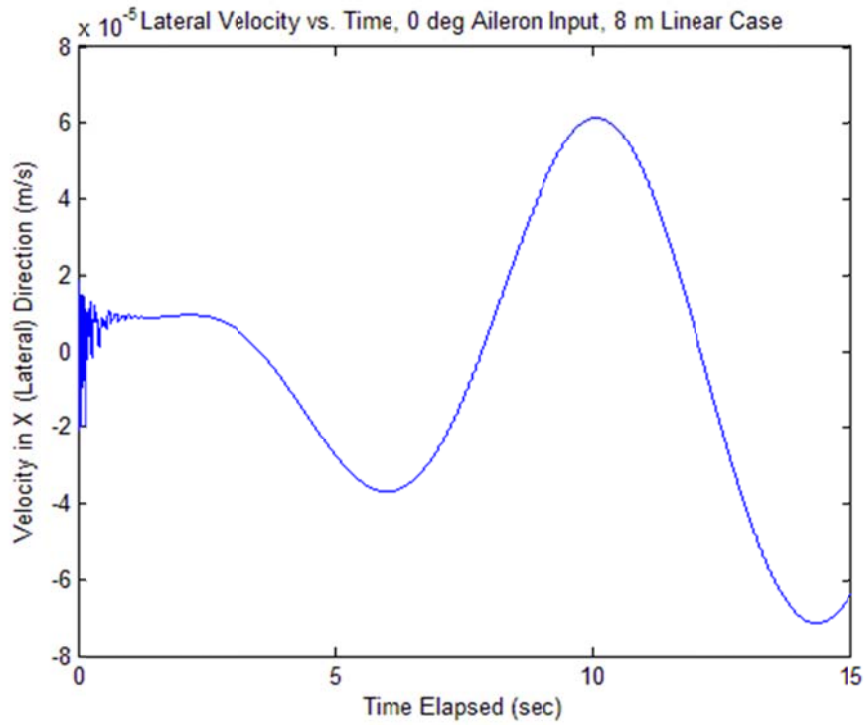


Figure 33. Case 7 Lateral Velocity v_x versus Time

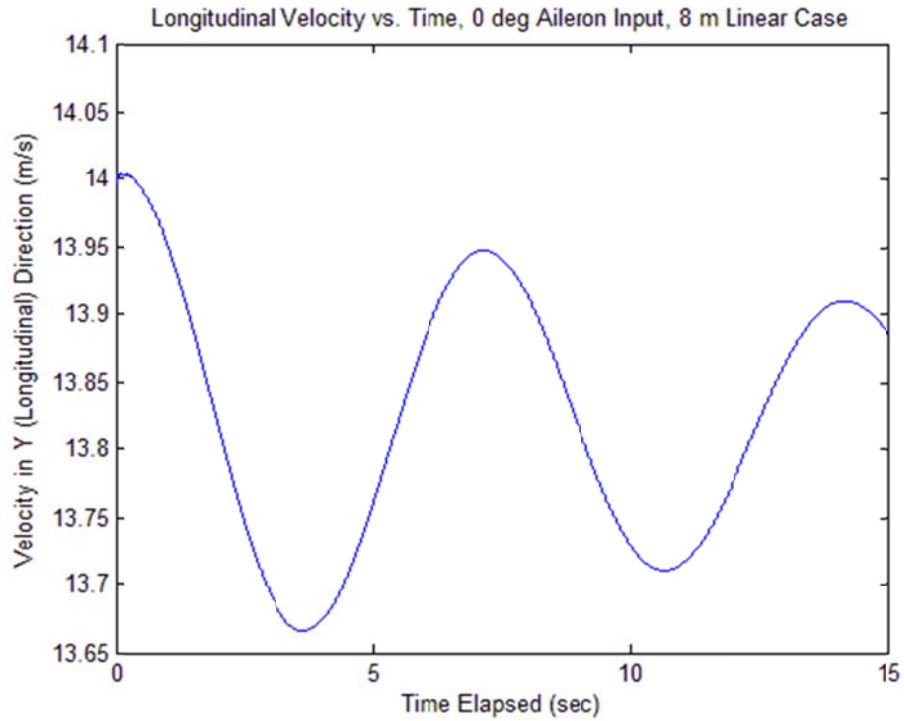


Figure 34. Case 7 Longitudinal Velocity v_y versus Time

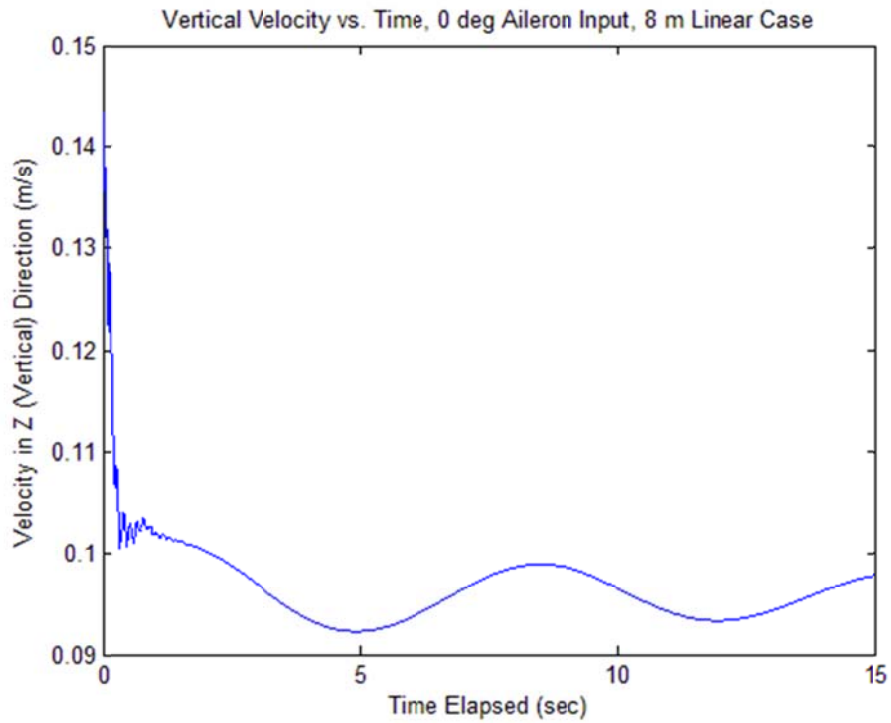


Figure 35. Case 7 Vertical Velocity v_z versus Time

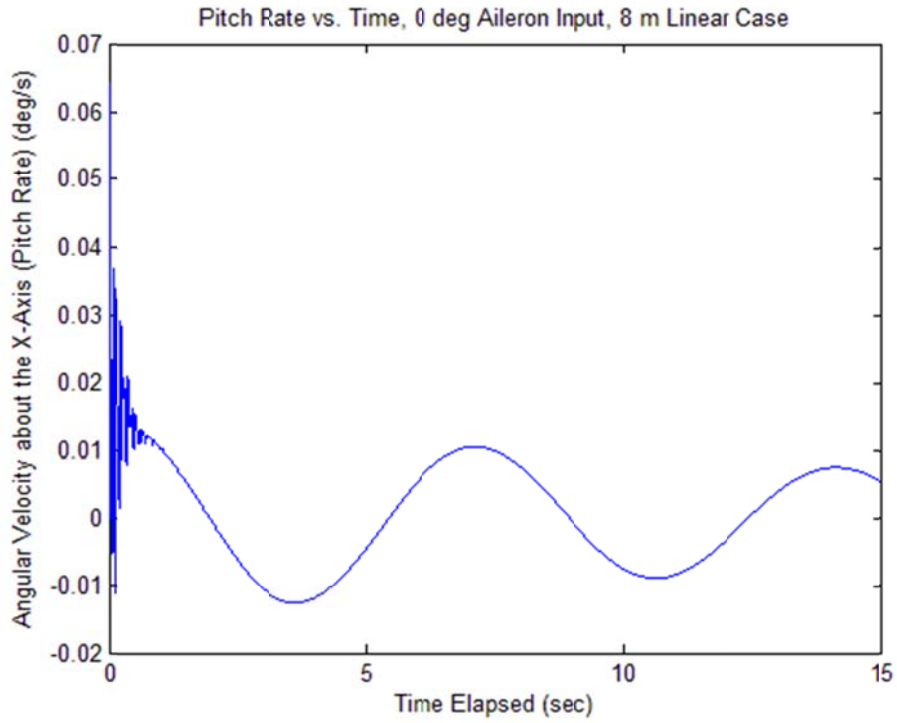


Figure 36. Case 7 Pitch Rate ω_x versus Time

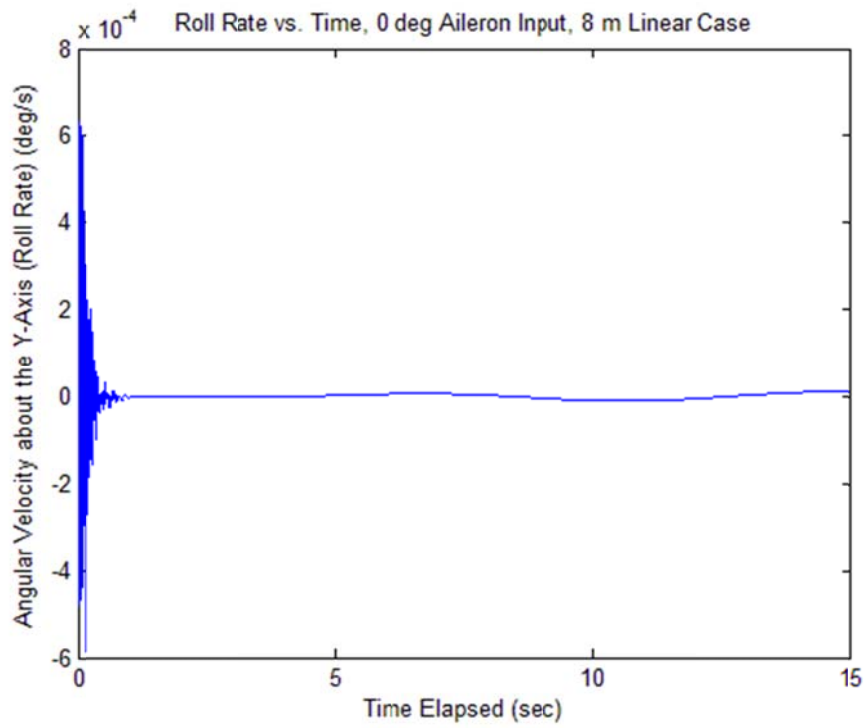


Figure 37. Case 7 Roll Rate ω_y versus Time

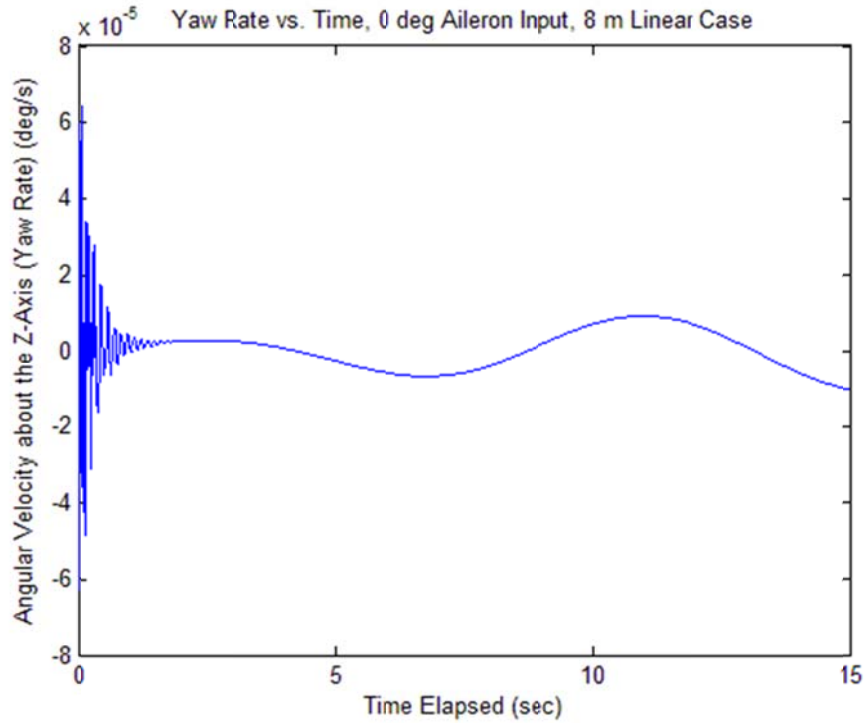


Figure 38. Case 7 Yaw Rate ω_z versus Time

These results show that the 8 meter X-HALE is stable for no aileron inputs. While the plots of the aircraft's velocities in the x, y, and z directions show a sinusoidal pattern, the amplitudes of the peaks and troughs get progressively smaller as the flight progresses. This suggests that the aircraft is approaching a constant velocity in all three directions. For the x direction, this value is near zero. For the z direction, this value appears to be approximately 0.095, which is very close to zero. For the y direction, this value appears to be approximately 13.8 m/s. Additionally, the plot of the angular velocity about the x-axis shows a sinusoidal pattern with the amplitude of the peaks and troughs get progressively smaller as the flight progresses. The plots of the angular velocities about the y- and z- axes also show sinusoidal patterns but their amplitudes are near zero. The aircraft appears to be approaching an angular velocity of zero in all three directions. Combined, this data suggests that the aircraft is stable when no inputs, such as

an aileron input, are given. Again, many of the results of the simulations run for this research show initial instabilities that quickly dampen out, such as in Figure 38. This is not due to an actual instability of the aircraft but is due to numerical errors caused by the UM/NAST program.

Case 8 is a linear simulation run with a sinusoidal aileron input on both wings with an amplitude of 2 degrees. The aileron input for Case 8 can be viewed in Figure 39, and the results for Case 8 can be viewed in Figure 40, Figure 41, Figure 42, Figure 43, Figure 44 and Figure 45.

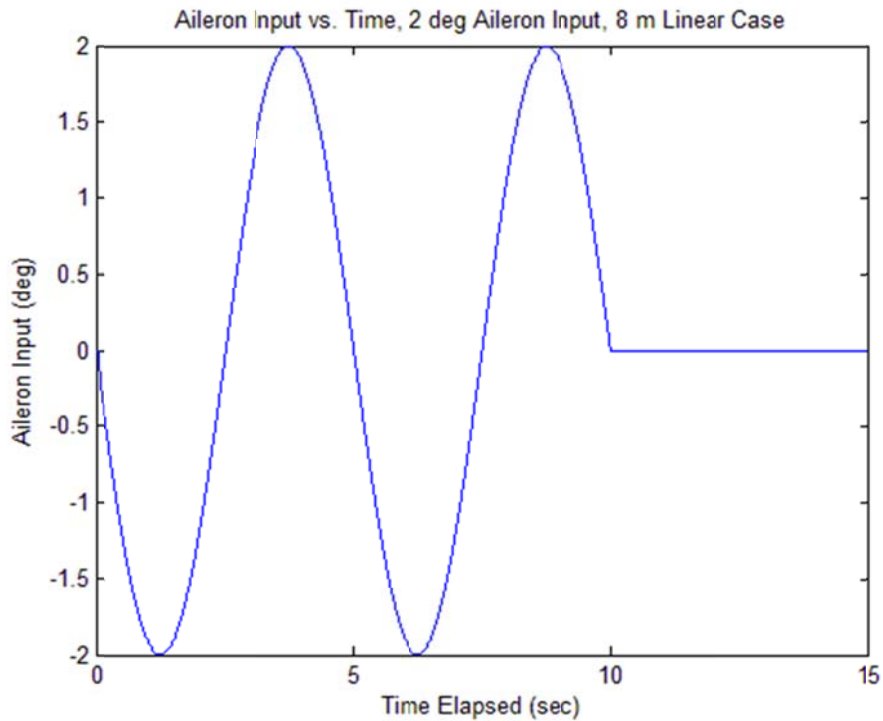


Figure 39. Case 8 Aileron Input versus Time

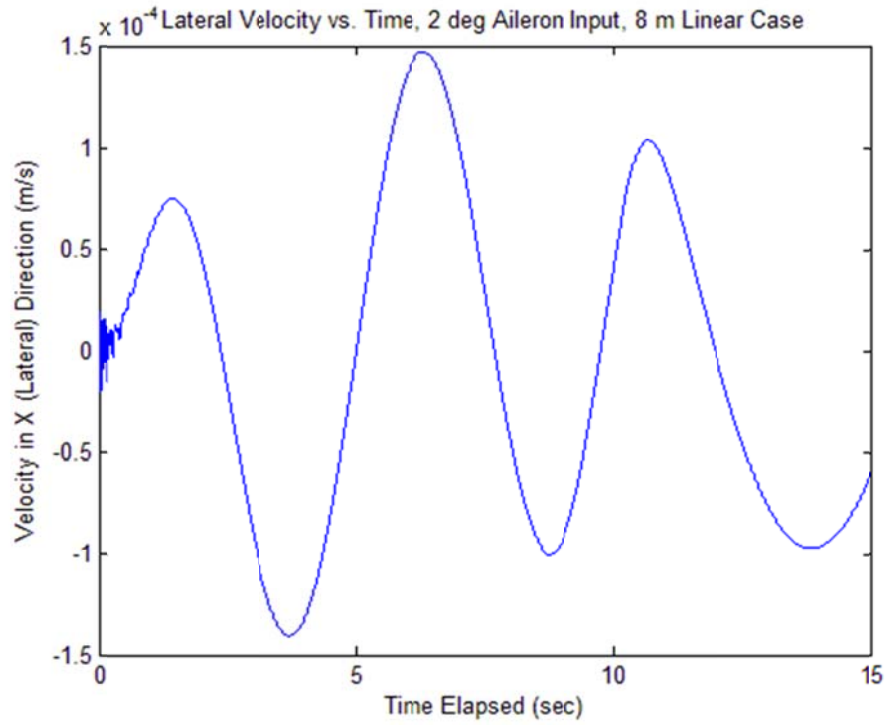


Figure 40. Case 8 Lateral Velocity v_x versus Time

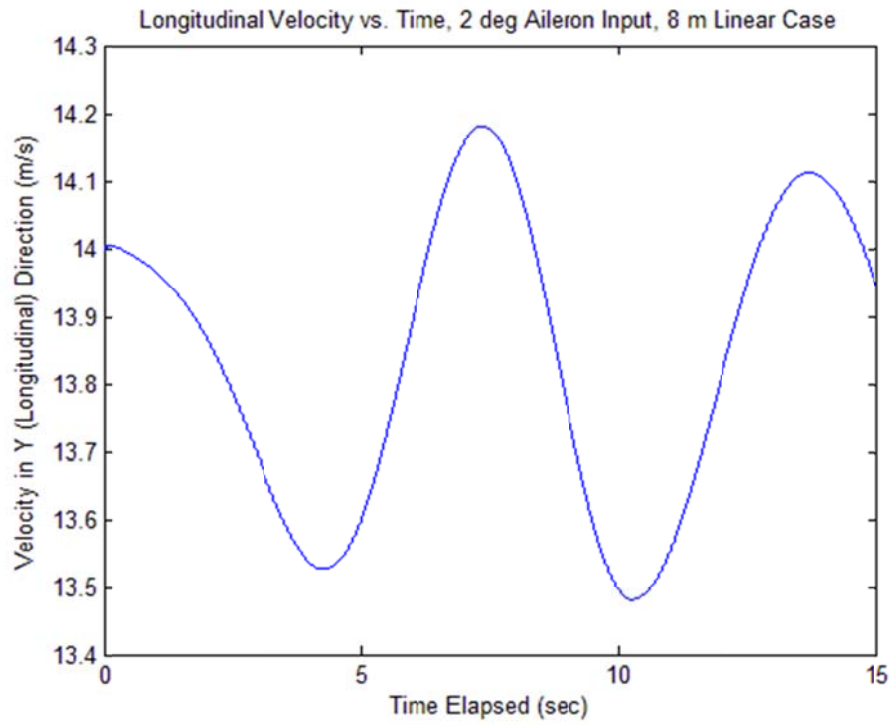


Figure 41. Case 8 Longitudinal Velocity v_y versus Time

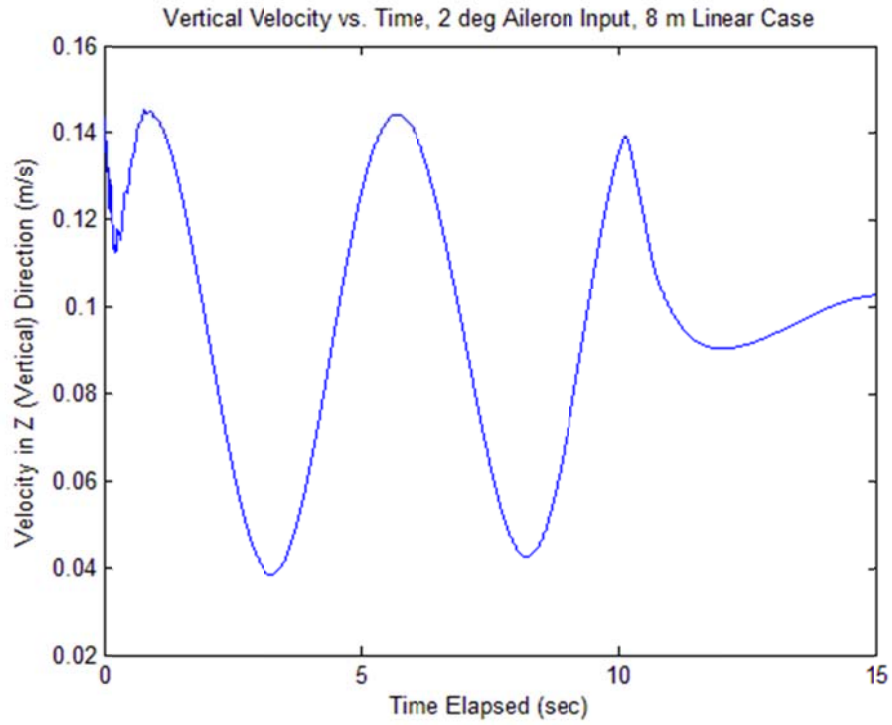


Figure 42. Case 8 Lateral Velocity v_z versus Time

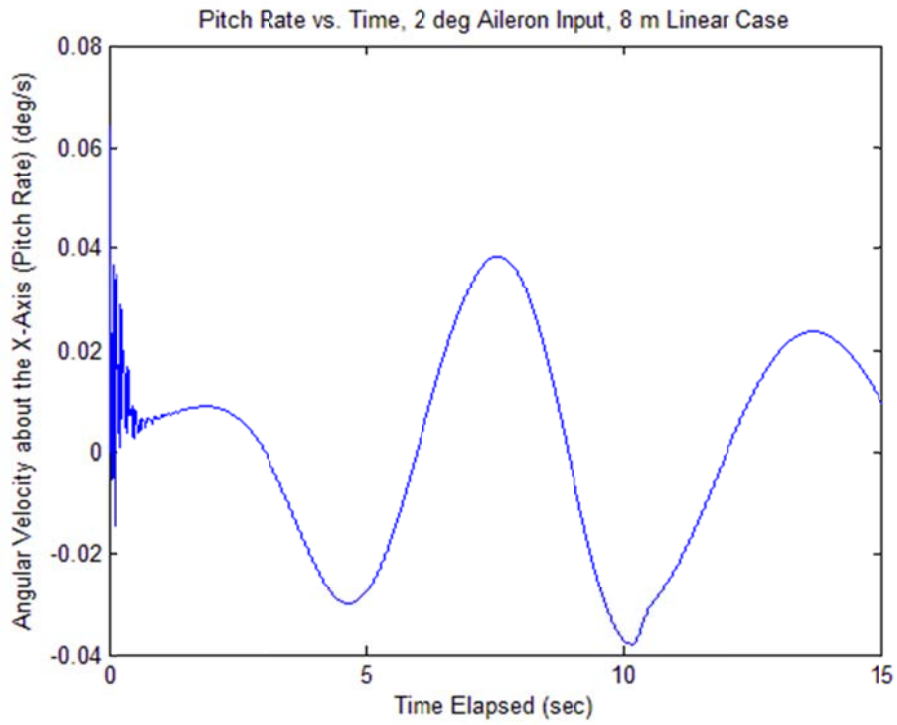


Figure 43. Case 8 Pitch Rate ω_x versus Time

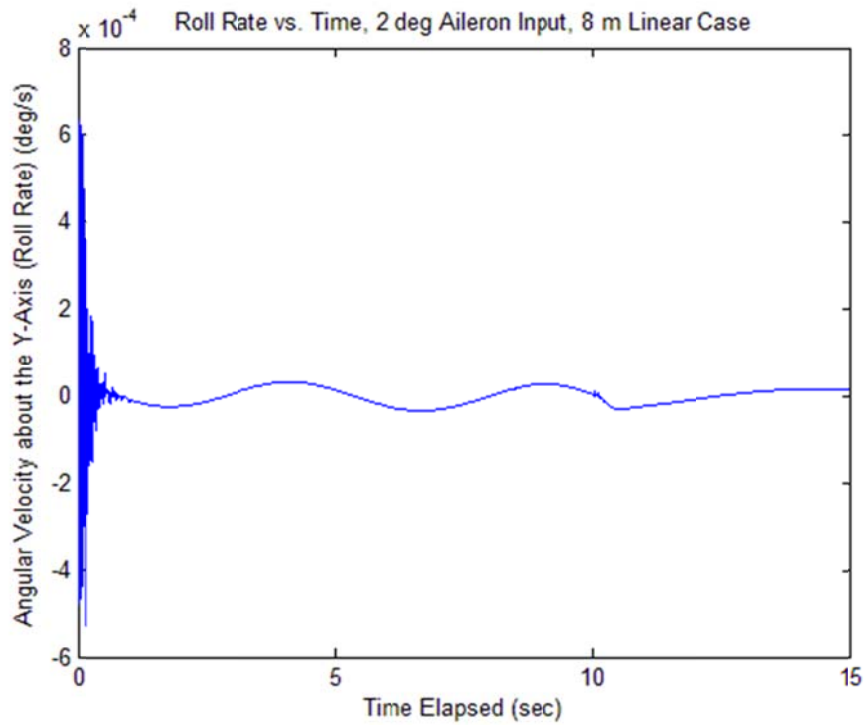


Figure 44. Case 8 Roll Rate ω_y versus Time

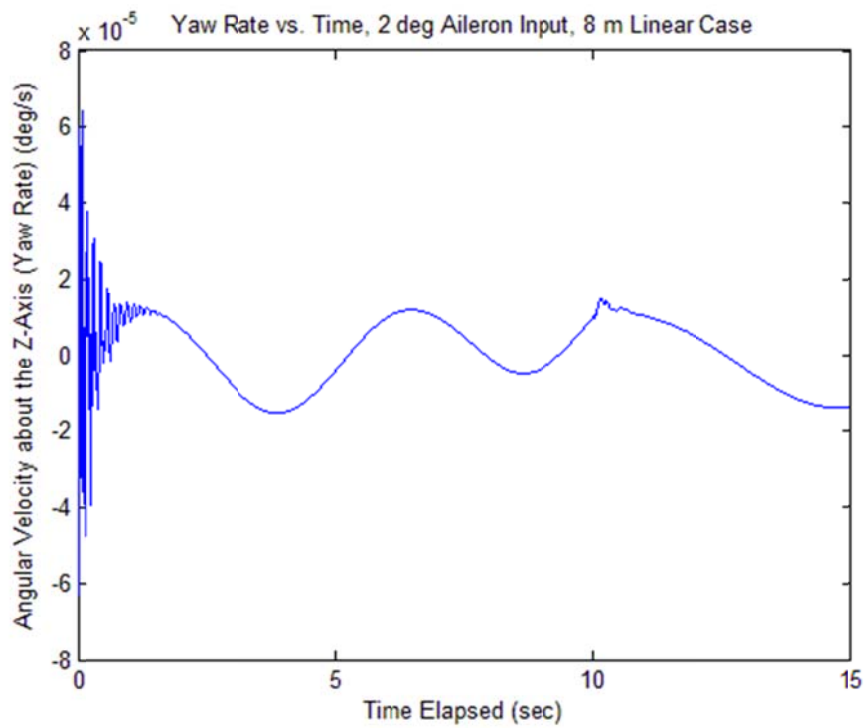


Figure 45. Case 8 Yaw Rate ω_z versus Time

These figures show that the 8 meter X-HALE is stable when a sinusoidal aileron input is performed on both wings with a 2 degree amplitude. For example, while the plot for the longitudinal velocity, the velocity in the y direction, shows a sinusoidal pattern, and the peaks and troughs become smaller after 10 seconds because the aileron input ends after 10 seconds. Also, the plot of the angular velocity about the x-axis, the pitch rate, shows peaks and troughs that also become smaller once the aileron input ends. This suggests that the aircraft is stable with this input. The plot of the velocity in the vertical direction, the z direction, shows a sinusoidal pattern that terminates very quickly once the aileron input ends, meaning that the aircraft is stable in the vertical direction. The plot for the velocity in the x direction, the lateral direction, shows a very small sinusoidal pattern. However the amplitude of this pattern is very small and shows no signs of increasing once the aileron input ends. The aircraft also rotates slightly in a sinusoidal pattern about the y- and z-axes, but this amplitude of these patterns are very small and show no signs of increasing. Case 9 is the same simulation as Case 8, but it is the nonlinear case. The plots from the results of Case 9 can be viewed in the Appendix. There are no significant differences between the results for Cases 8 and 9. The aircraft is stable for both cases and the two cases' plots are very similar.

Case 10 is a linear type simulation with a sinusoidal aileron input performed on both wings with a 5 degree amplitude. Case 11 is a nonlinear version of Case 10. The aileron input and the results for Cases 10 and 11 can be viewed in the Appendix. There are no significant differences between the plots for Cases 10 and 11. Both cases suggest that the 8 meter X-HALE is stable for a sinusoidal aileron input with a 5 degree amplitude applied to both wings. The results for these cases are very similar to those of

Cases 8 and 9, which showed that the aircraft is stable for an aileron input of 2 degrees, except that plots show that the aileron input has a slightly more significant affect on the flight of the aircraft.

Cases 12 and 13 involve a 10 degree sinusoidal aileron input. The linear case, Case 12, suggests that the 8 meter X-HALE is stable for a sinusoidal aileron input with a 10 degree amplitude applied to both wings, while the nonlinear case, Case 13, suggests that the 8 meter X-HALE is unstable for this aileron input. The results for Case 12 are in Figure 46, Figure 47, Figure 48, Figure 49, Figure 50, Figure 51 and Figure 52, and the results for case 13 are in Figure 53, Figure 54, Figure 55, Figure 56, Figure 57, Figure 58 and Figure 59.

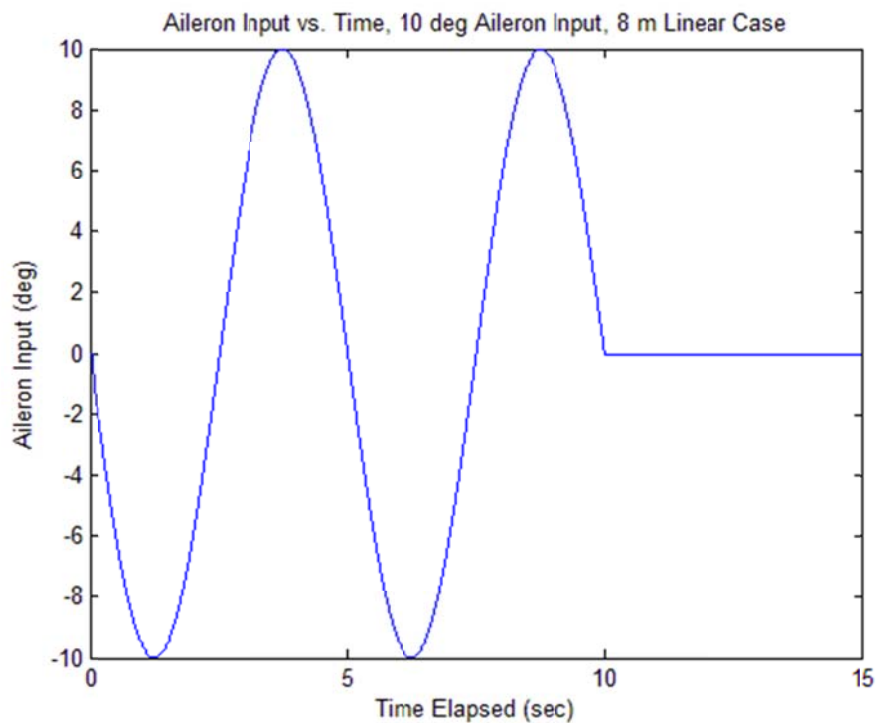


Figure 46. Case 12 Aileron Input versus Time

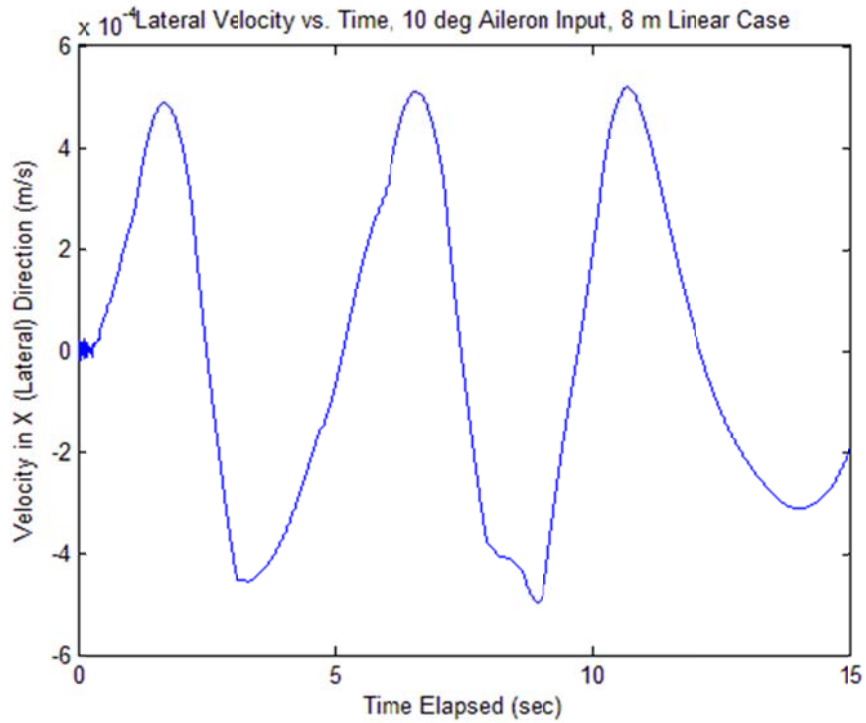


Figure 47. Case 12 Lateral Velocity v_x versus Time

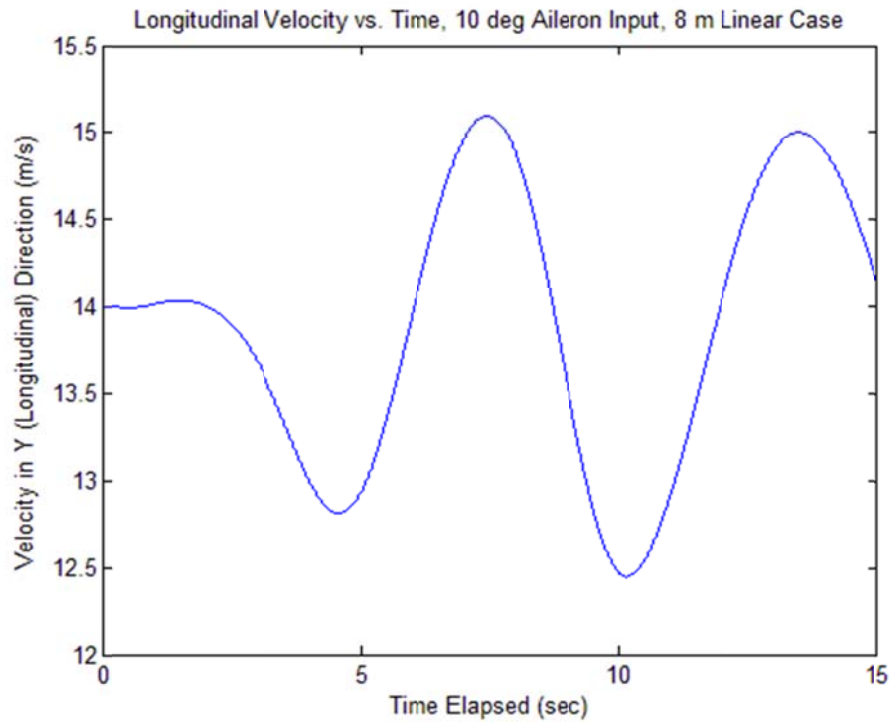


Figure 48. Case 12 Longitudinal Velocity v_y versus Time

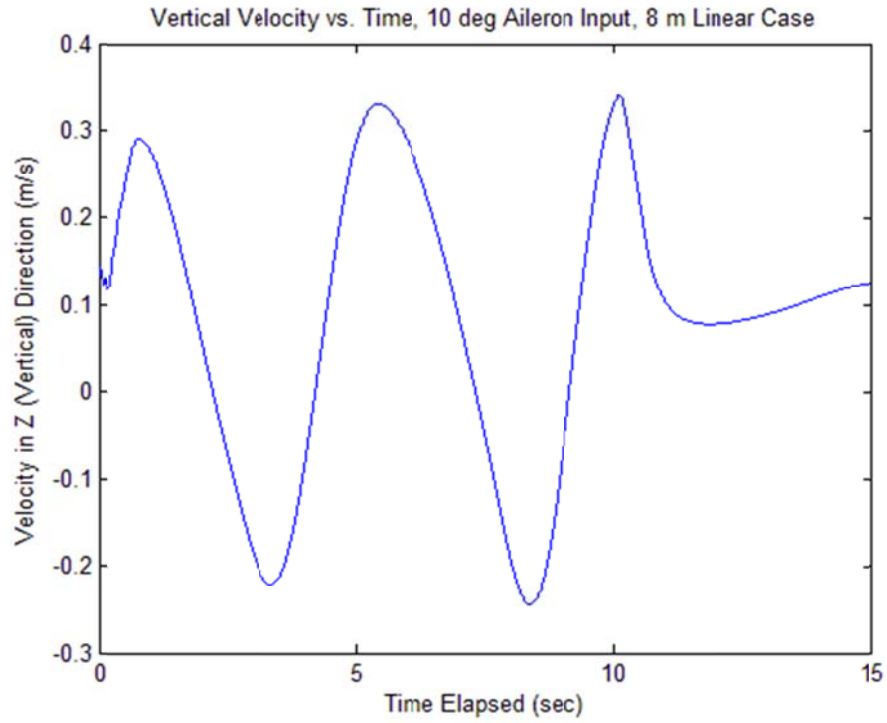


Figure 49. Case 12 Vertical Velocity v_z versus Time

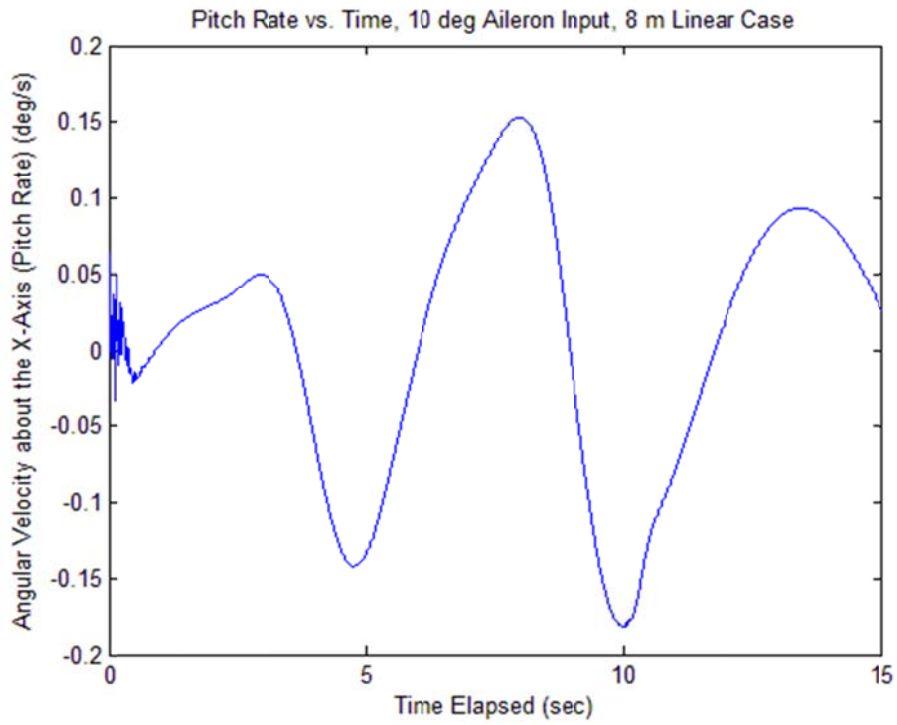


Figure 50. Case 12 Pitch Rate ω_x versus Time

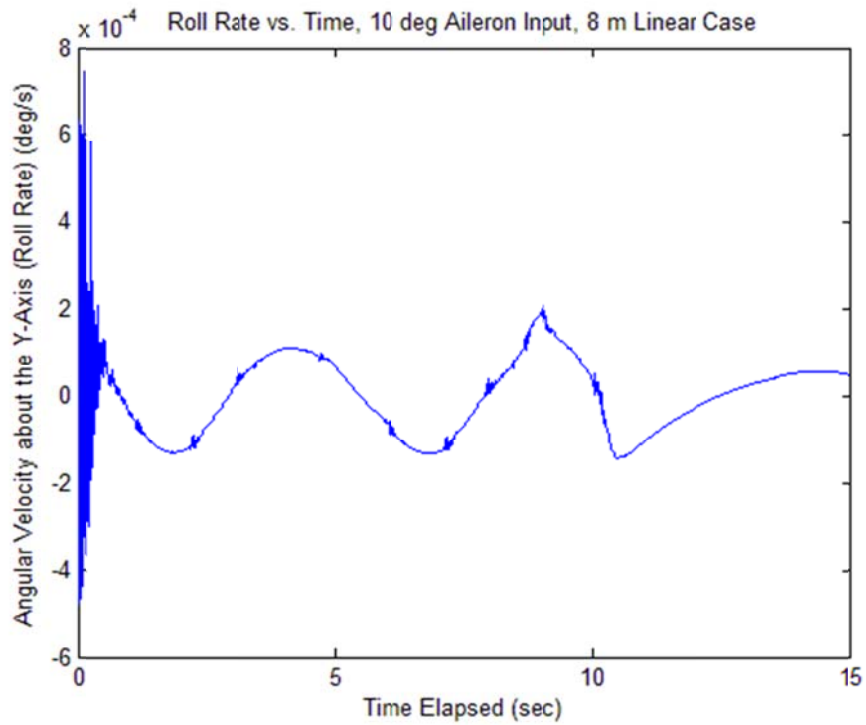


Figure 51. Case 12 Roll Rate ω_y versus Time

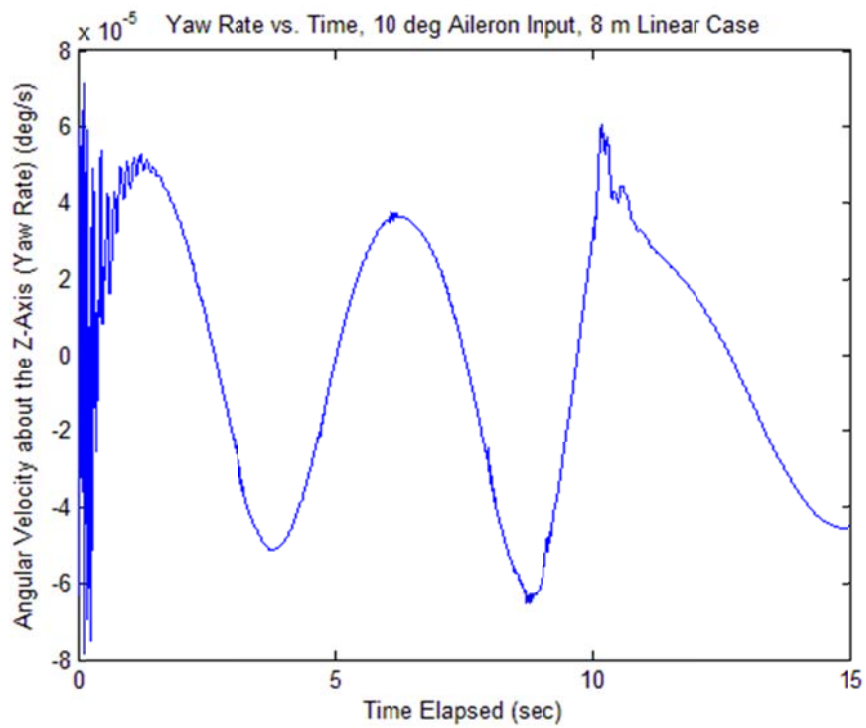


Figure 52. Case 12 Yaw Rate ω_z versus Time

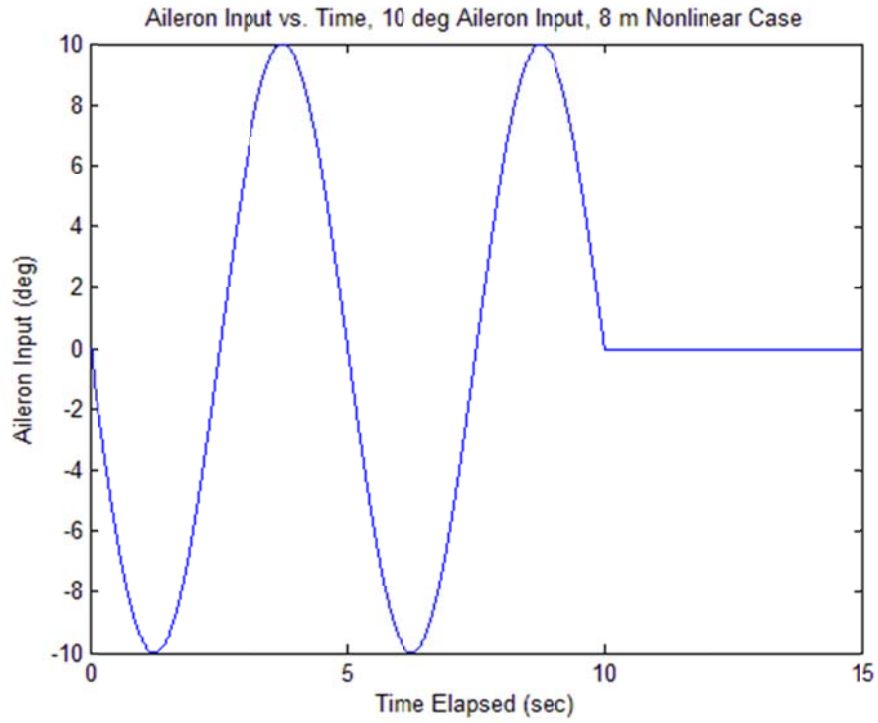


Figure 53. Case 13 Aileron Input versus Time

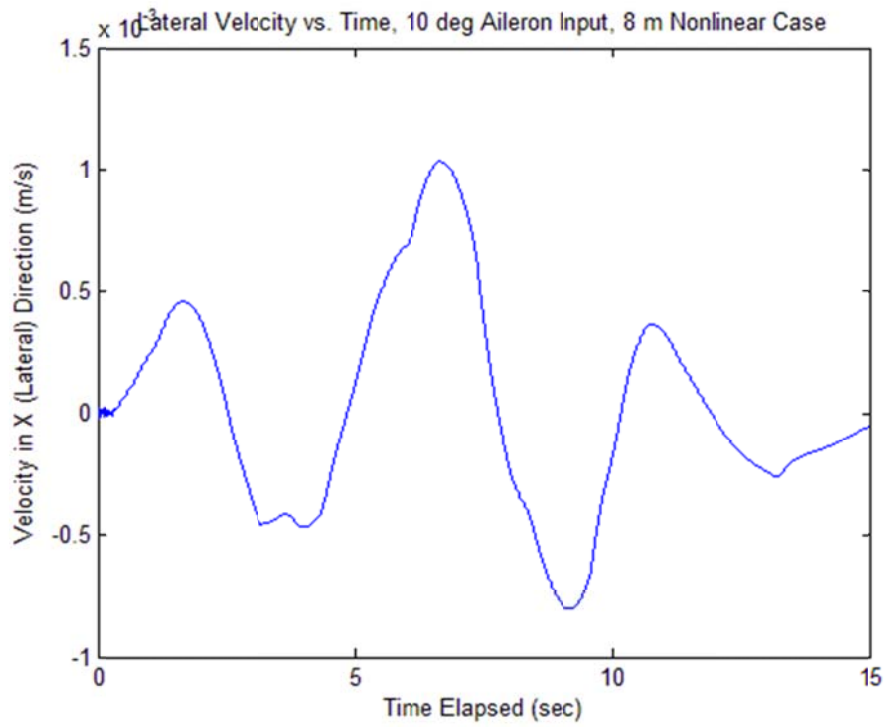


Figure 54. Case 13 Lateral Velocity v_x versus Time

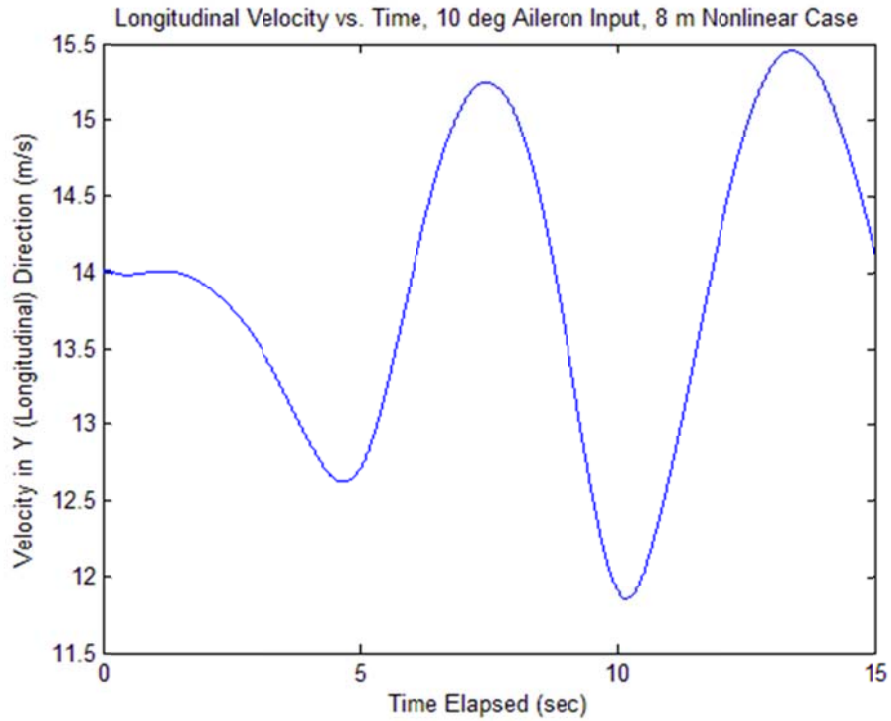


Figure 55. Case 13 Longitudinal Velocity v_y versus Time

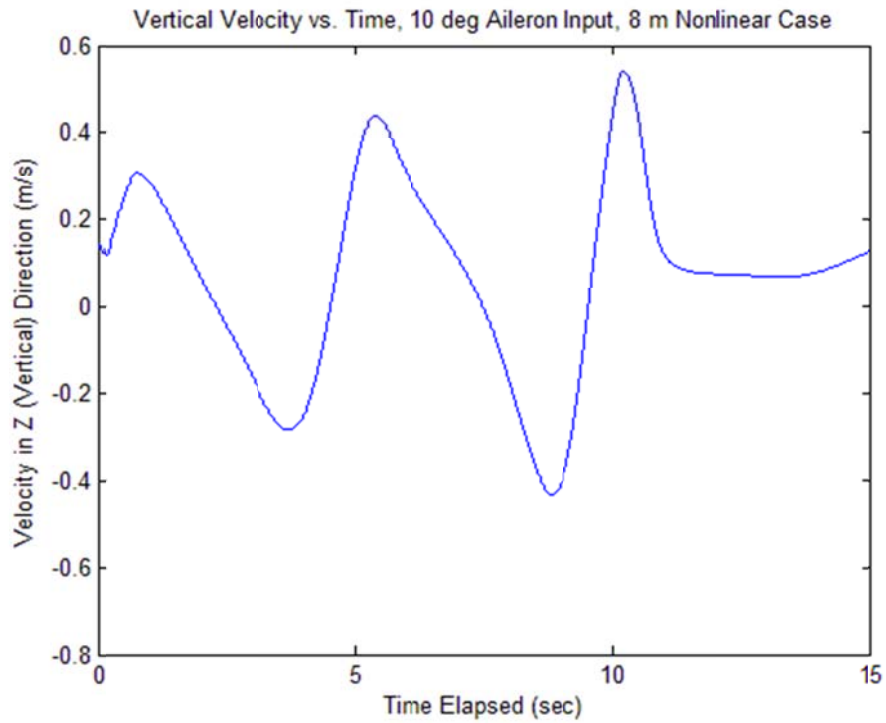


Figure 56. Case 13 Vertical Velocity v_z versus Time

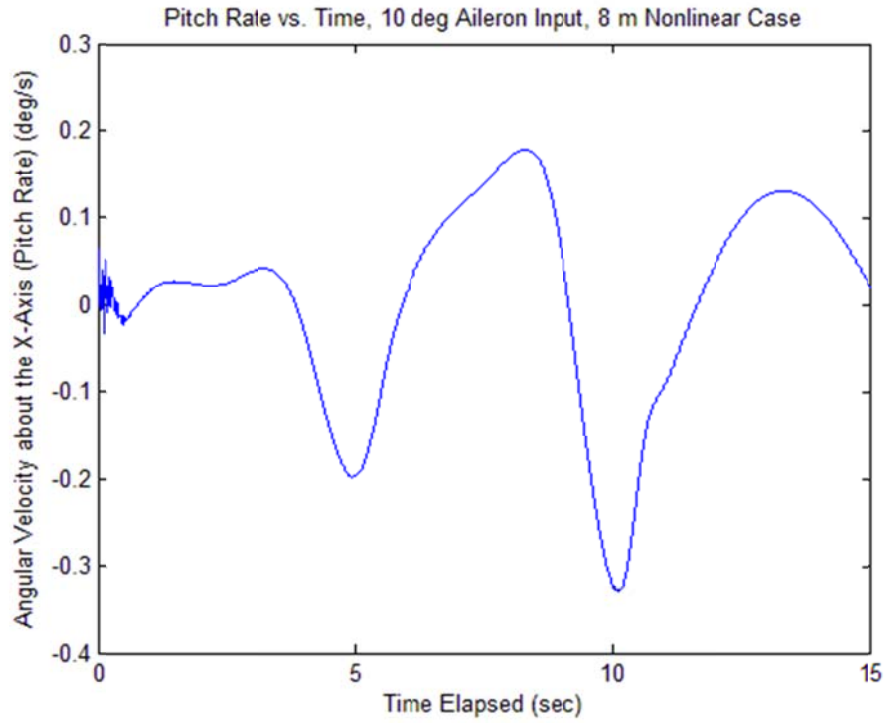


Figure 57. Case 13 Pitch Rate ω_x versus Time

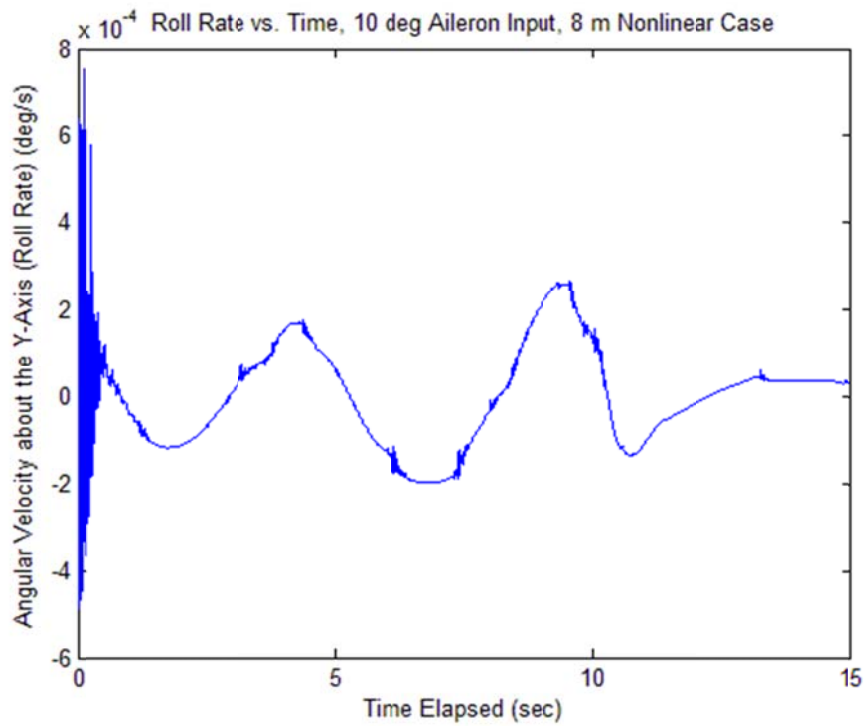


Figure 58. Case 13 Roll Rate ω_y versus Time

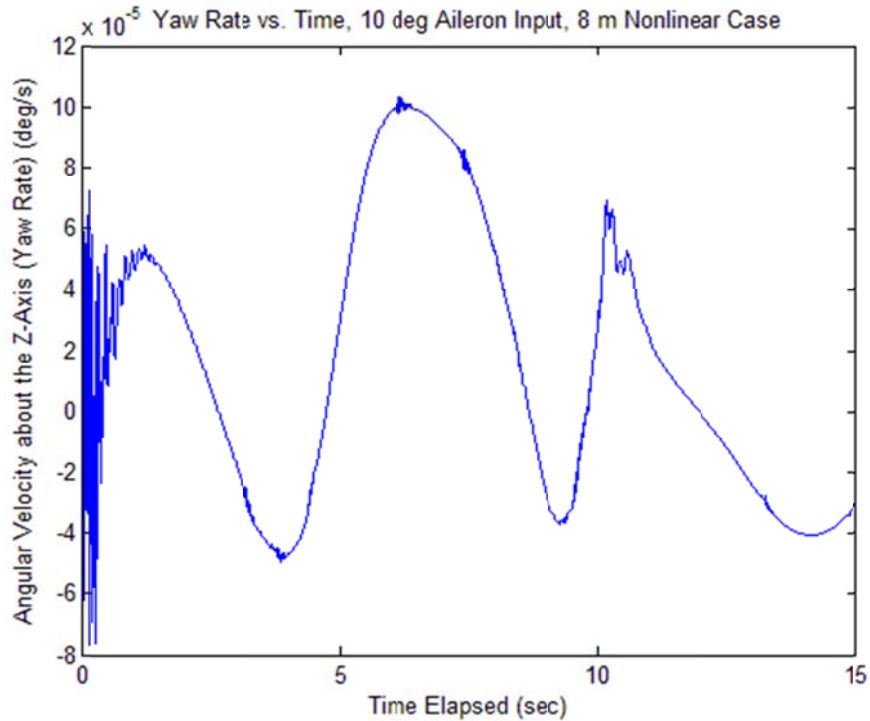


Figure 59. Case 13 Yaw Rate ω_z versus Time

The results for Case 12, a linear type simulation, show similar results to the cases for the 2 and 5 degree aileron input simulations; the aircraft shows minimal movement in the lateral direction, and recovers well from the aileron input in the longitudinal and vertical directions. Rotationally, the aircraft rotates slightly in a sinusoidal pattern about the x-axis but begins to recover after the input ends. The aircraft rotates slightly in a sinusoidal pattern about the y- and z-axes but these movements are very small. These results show stable flight.

However, the results for Case 13, a nonlinear type simulation and Case 12's nonlinear counterpart, suggest that the aircraft is unstable for an aileron input with a 10 degree amplitude. The results for Case 13 are similar to Case 12 except instead of recovering from the input in the longitudinal direction, the amplitude of the aircraft's sinusoidal longitudinal velocity continues to increase over time even though the aileron

input has terminated. This suggests unstable flight for an aileron input with a 10 degree amplitude. Therefore, while the linear case suggests stability, the nonlinear case suggests instability. Because the nonlinear simulation type models the nonlinear aeroelasticity and flight dynamics of an aircraft better than the linear simulation type does, the nonlinear simulation probably provides a more accurate depiction of the flight behavior of X-HALE.

Cases 14 and 15 involve a 15 degree sinusoidal aileron input. The results for Cases 14 can be viewed in Figure 60, Figure 61, Figure 62, Figure 63, Figure 64, Figure 65 and Figure 66, and the results for Case 15 can be viewed in Figure 67, Figure 68, Figure 69, Figure 70, Figure 71, Figure 71, Figure 72 and Figure 73. The linear case, Case 14, suggests that the 8 meter X-HALE is stable for this input, while the nonlinear case, Case 15, suggests that the 8 meter X-HALE is unstable for this aileron input.

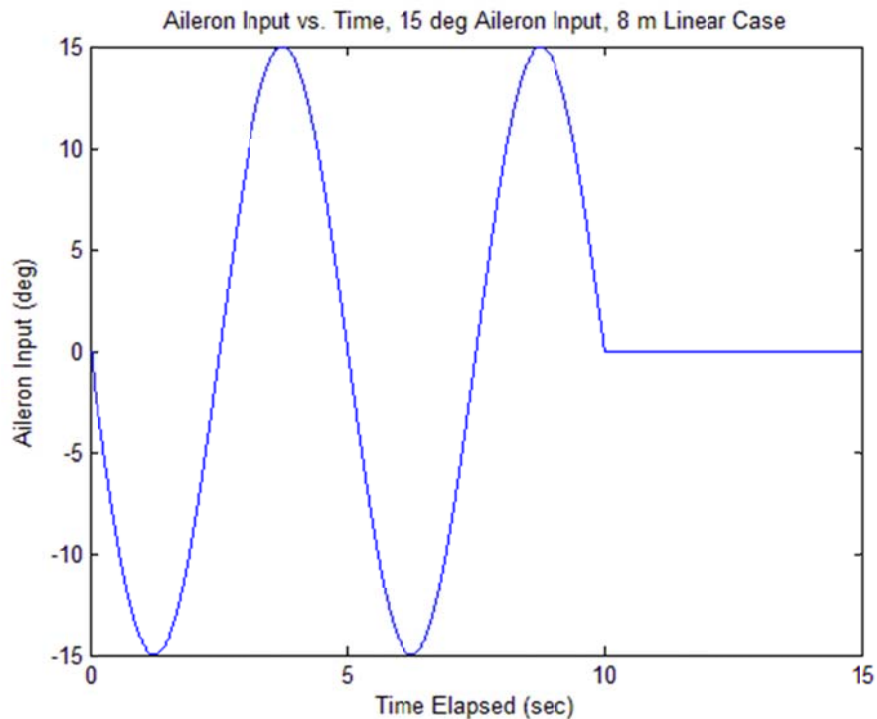


Figure 60. Case 14 Aileron Input versus Time

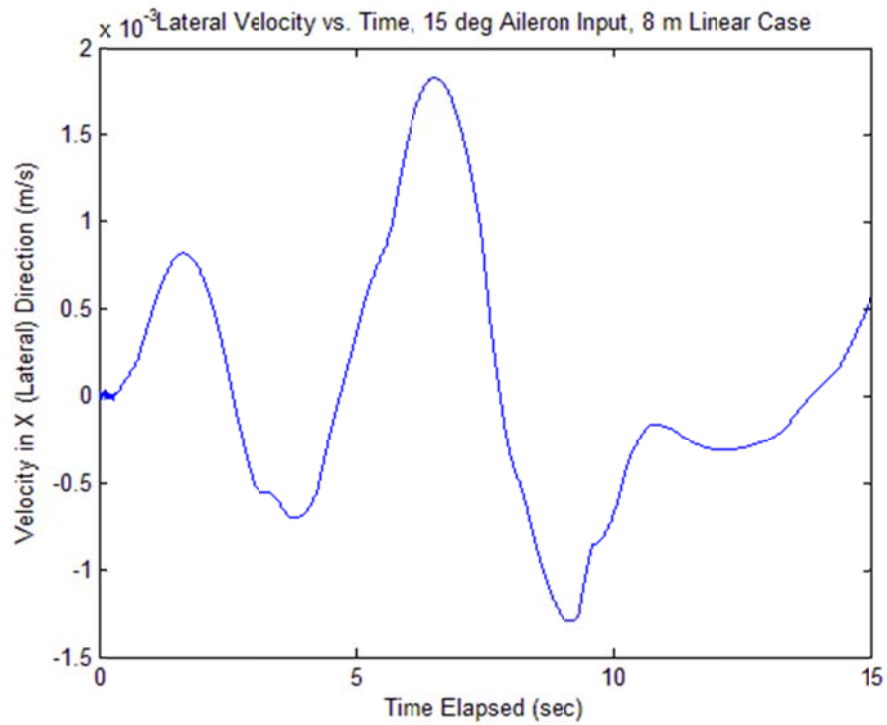


Figure 61. Case 14 Lateral Velocity v_x versus Time

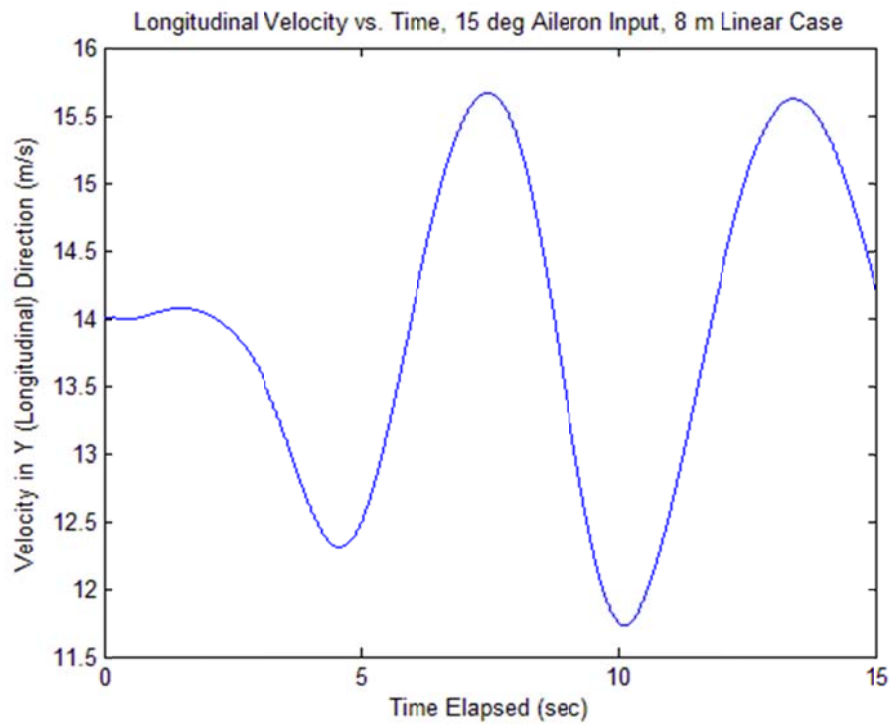


Figure 62. Case 14 Longitudinal Velocity v_y versus Time

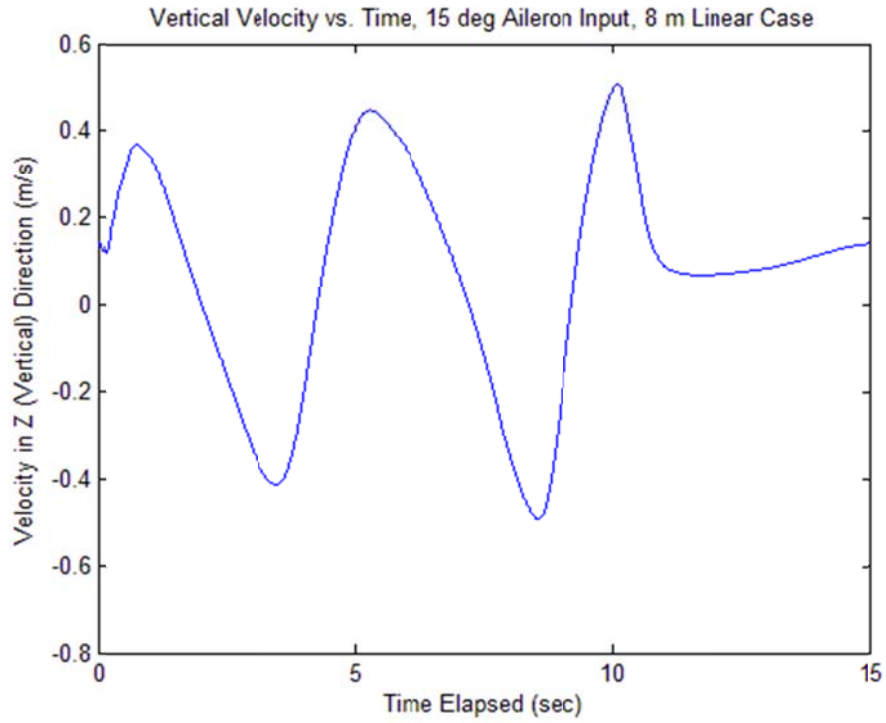


Figure 63. Case 14 Vertical Velocity v_z versus Time

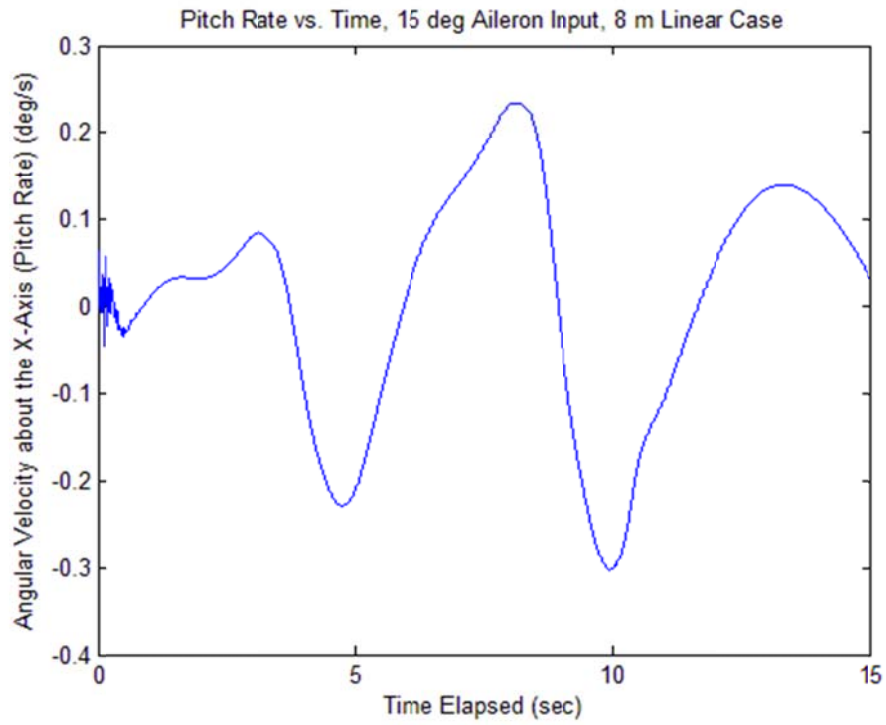


Figure 64. Case 14 Pitch Rate ω_x versus Time

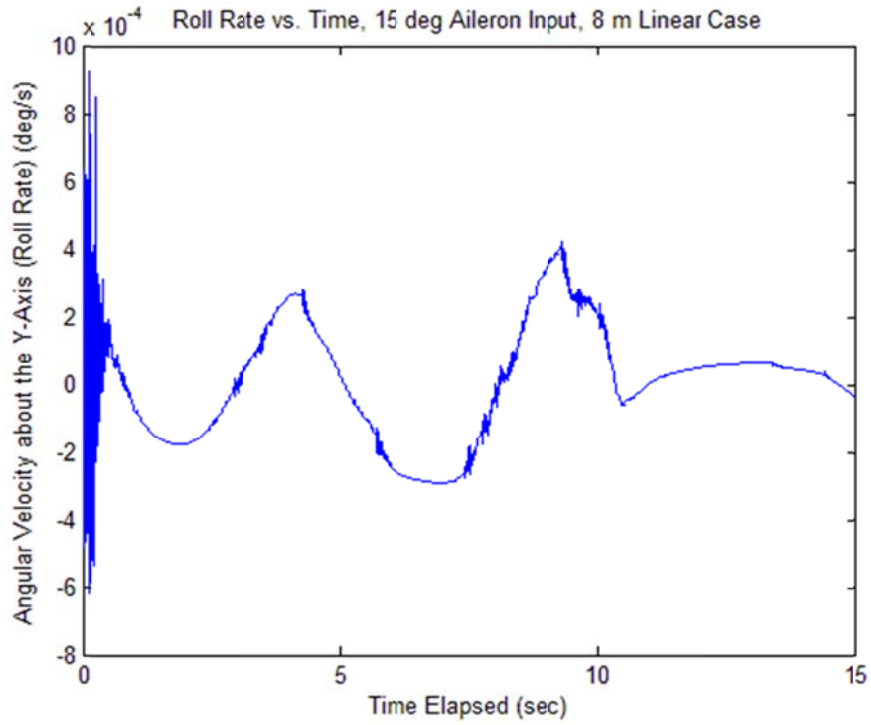


Figure 65. Case 14 Roll Rate ω_y versus Time

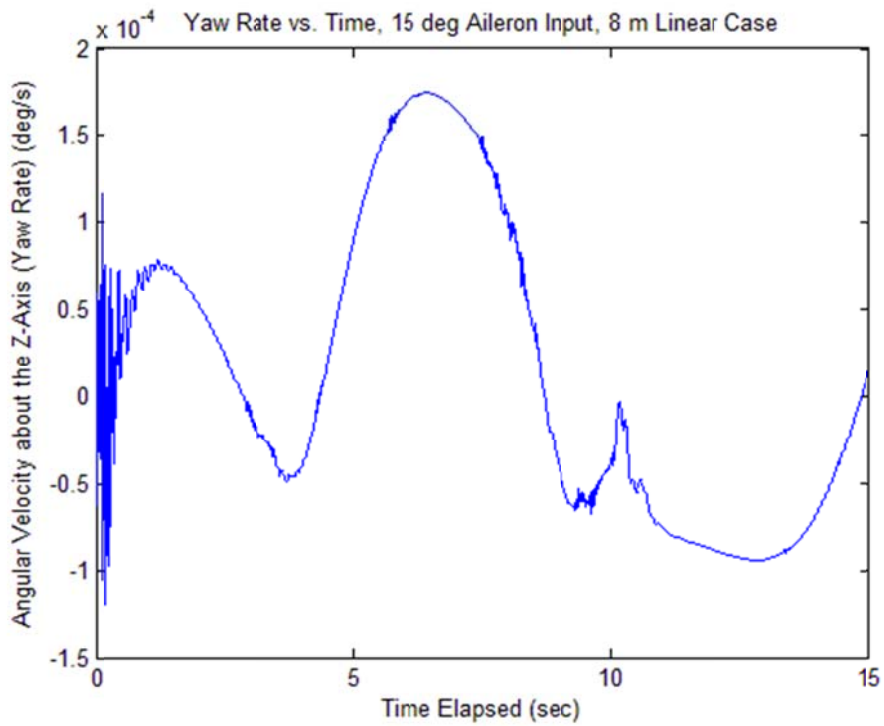


Figure 66. Case 14 Yaw Rate ω_z versus Time

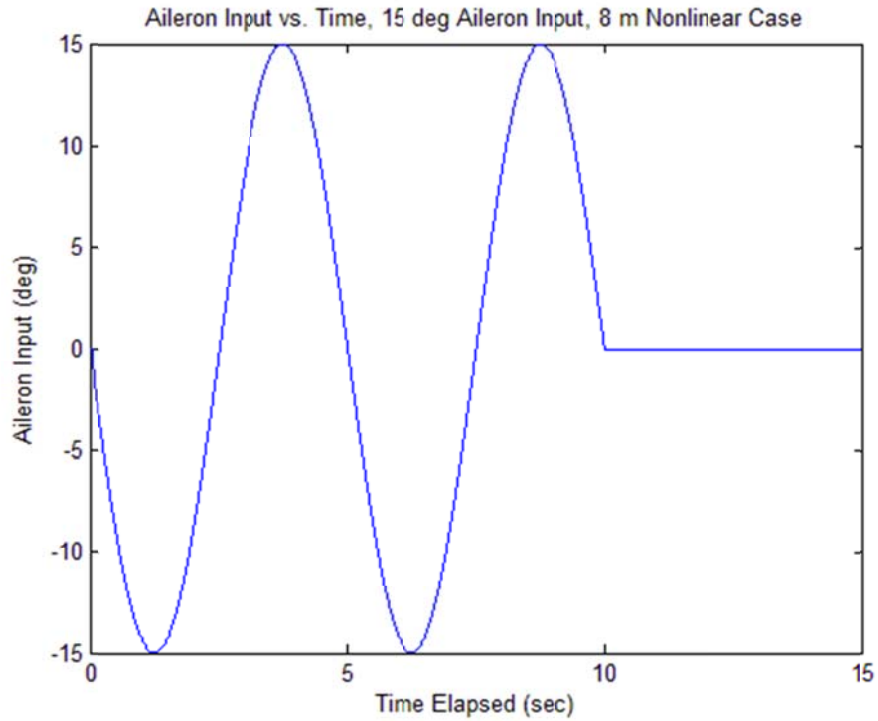


Figure 67. Case 15 Aileron Input versus Time

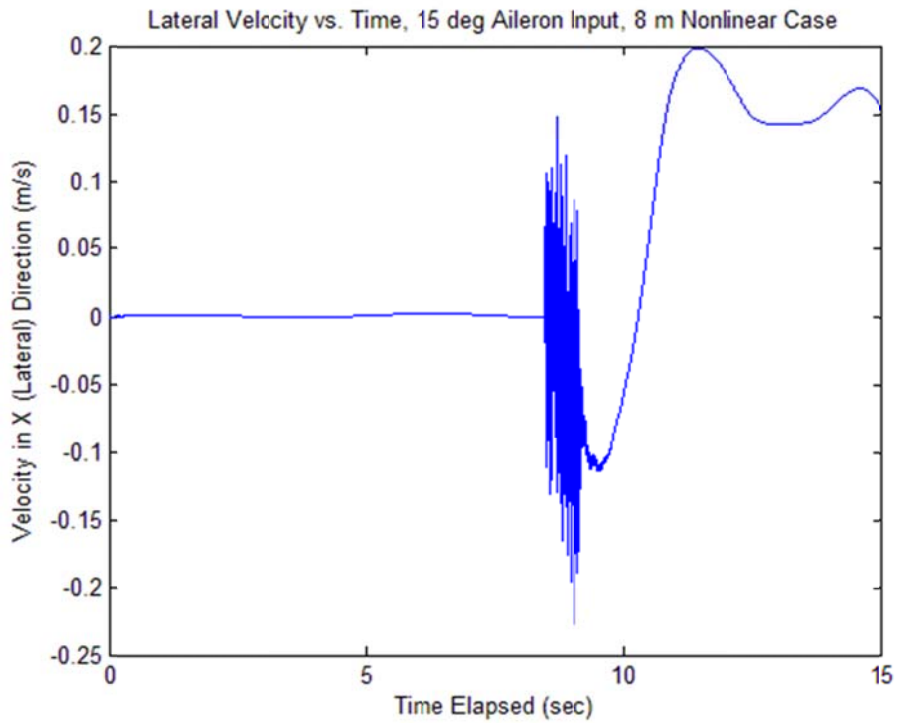


Figure 68. Case 15 Lateral Velocity v_x versus Time

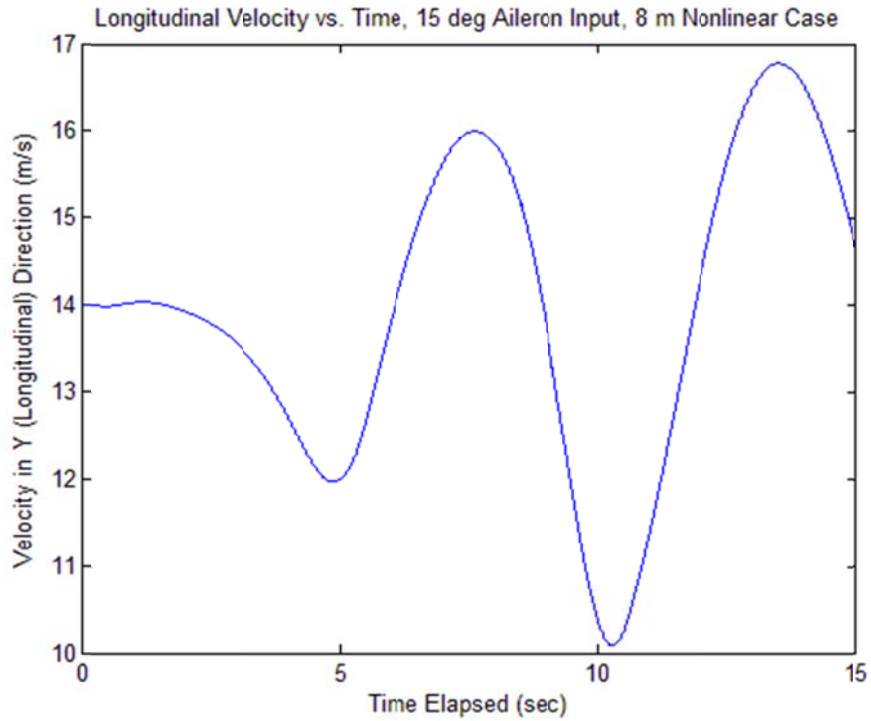


Figure 69. Case 15 Longitudinal Velocity v_y versus Time

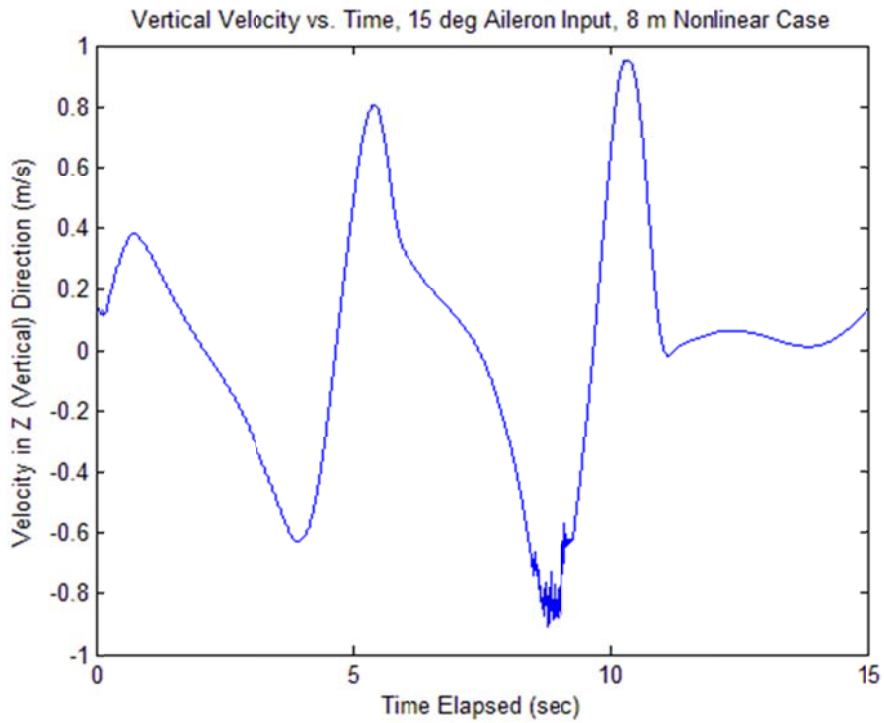


Figure 70. Case 15 Vertical Velocity v_z versus Time

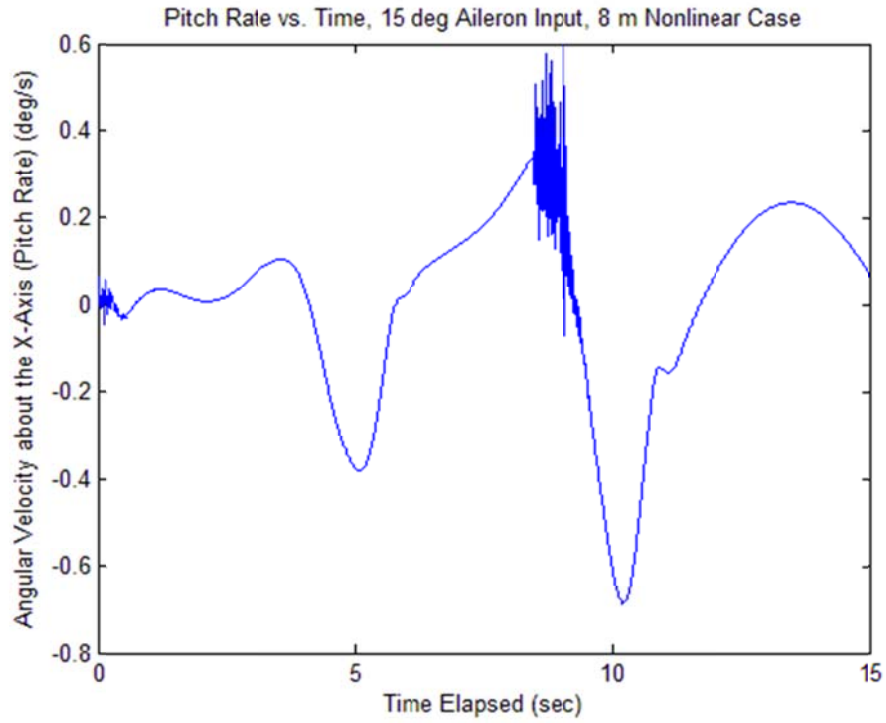


Figure 71. Case 15 Pitch Rate ω_x versus Time

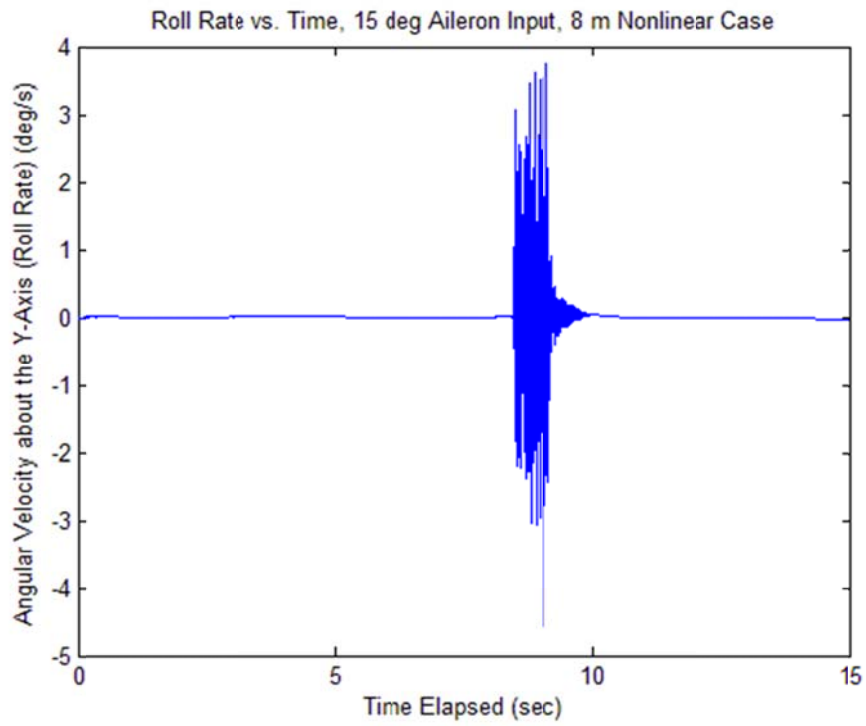


Figure 72. Case 15 Roll Rate ω_y versus Time

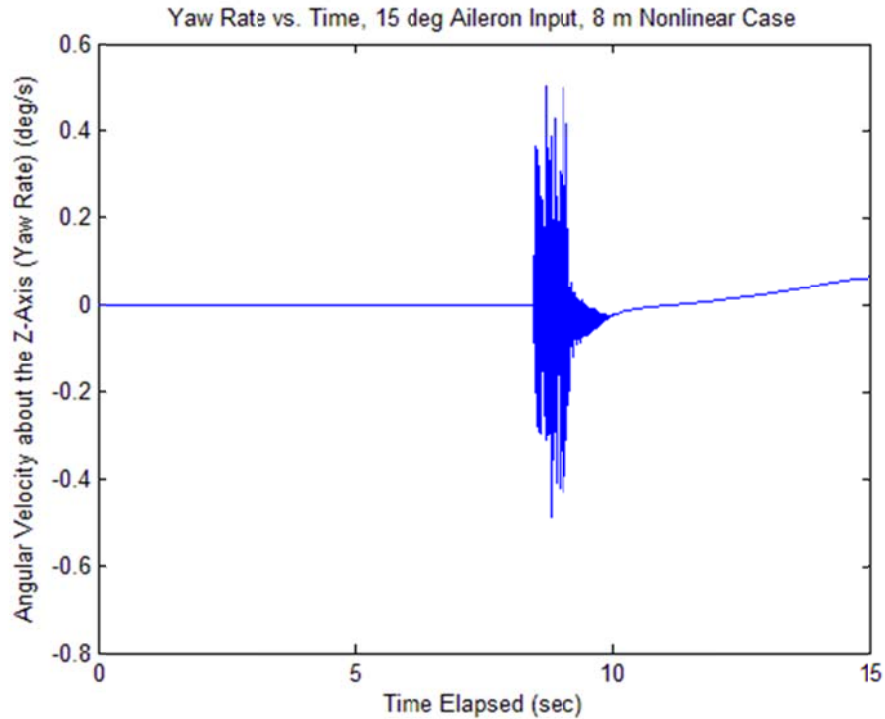


Figure 73. Case 15 Yaw Rate ω_z versus Time

For Case 14, the linear case, the plot for the longitudinal velocity, the velocity in the y direction, shows a sinusoidal pattern, and the peaks and troughs become smaller after 10 seconds because the aileron input ends after 10 seconds. Also, the plot of the angular velocity about the x-axis, the pitch rate, shows a very rough sinusoidal pattern, with peaks and troughs that also become smaller once the aileron input ends. The plot of the velocity in the vertical direction, the z direction, shows a sinusoidal pattern that terminates very quickly once the aileron input ends, meaning that the aircraft is stable in the vertical direction. The plot for the velocity in the x direction, the lateral direction, shows a vaguely sinusoidal pattern. However the amplitude of this pattern is very small and shows no signs of increasing once the aileron input ends. The aircraft also rotates slightly in vaguely sinusoidal patterns about the y- and z-axes, but this amplitude of these

patterns are very small. This all suggests that the aircraft is stable for a 15 degree aileron input.

However, Case 15, the nonlinear 15 degree amplitude aileron input case, suggests that the aircraft is unstable for this input. The aircraft shows minimal movement in the lateral direction until approximately 8 seconds, but this motion is still stable. The aircraft recovers from the aileron input in the vertical direction well. The longitudinal velocity plot suggests that aircraft does not recover from the aileron input in the longitudinal direction once the input ends after 10 seconds. This suggests that the aircraft is unstable for a 15 degree amplitude sinusoidal aileron input applied to both wings. Instead, the amplitude of the longitudinal velocity's sinusoidal pattern continues to grow larger. Rotationally, the aircraft recovers from the aileron input for all three axes. Note that several plots show some high frequency instabilities after approximately 8 seconds; however, this is not due to an actual instability of the aircraft but is due to numerical errors caused by the UM/NAST program.

Case 16 and 17 involve 20 and 25 degree amplitude sinusoidal aileron inputs, respectively. These are both linear type simulations. Both simulations suggest that the 8 meter X-HALE is unstable with these inputs. The nonlinear type versions of these simulations were attempted but these simulations failed most likely because the aircraft flight went extremely unstable. These attempts had the same time step (0.001 seconds), residual value (10) and time duration (15 seconds) as the other 8 meter X-HALE simulations. The results of Cases 16 and 17 can be viewed in the Appendix.

Case 16's results show minimal movement in the lateral direction. The aircraft recovers from the aileron input in the vertical direction, but the longitudinal velocity plot

suggests that aircraft does not recover from the aileron input in the longitudinal direction once the input ends after 10 seconds. Instead, the amplitude of the longitudinal velocity's sinusoidal pattern continues to grow larger. This suggests that the 8 meter X-HALE will be unstable for a 20 degree amplitude sinusoidal aileron input applied to both wings when test flown. The aircraft does show some small rotational movement about the x-axis, but this lessens once the aileron input ends. The aircraft also shows some rotational movement about the y- and z-axes; however, this movement is very small.

Case 17's results show minimal movement in the lateral direction. The aircraft recovers from the aileron input in the vertical direction, but the longitudinal velocity plot suggests that aircraft does not recover from the aileron input in the longitudinal direction once the input ends after 10 seconds. This suggests that the 8 meter X-HALE is unstable for a 25 degree amplitude sinusoidal aileron input applied to both wings. Instead, the amplitude of the longitudinal velocity's sinusoidal pattern continues to grow larger. Rotationally, the aircraft is stable and is minimally affected by the aileron input. Note that several plots for Case 17 show some high frequency instabilities after approximately 8 seconds; however, this is not due to an actual instability of the aircraft but is due to numerical errors caused by the UM/NAST program.

V. Conclusions and Recommendations

V.1 Conclusions

The results of the six 6 meter X-HALE simulations discussed suggest that the 6 meter X-HALE model is either unstable or that the simulations were set up incorrectly. Because Shearer, Cesnik and their co-workers designed both the 6 meter and the 8 meter models of X-HALE to be stable, it is unlikely that the actual 6 meter X-HALE aircraft is unstable. The most likely cause of the instabilities that the simulations show is that the trim conditions for the 6 meter simulations were poorly configured. More research must be done in order to determine the actual cause of the perceived instability of the aircraft. For now, no conclusion can be drawn about the stability of the aircraft. A summary of the results of the 6 meter X-HALE simulations discussed is given in Table 3.

Table 3. A Summary of Discussed 6 Meter X-HALE Simulations

Case	Simulation Type	Input	Duration (sec)/ Time Step (sec)/ Max Residual Value	Sinusoidal Aileron Input Data			Stability
				Period (sec)	Start/End Time (sec)	Amplitude (deg)	
1	6 Meter Linear	None	15/ 0.0025/ 0.1	N/A	N/A	N/A	Unstable
2	6 Meter Linear	None	10/ 0.0001/ 10	N/A	N/A	N/A	Unstable
3	6 Meter Nonlinear	None	10/ 0.0001/ 10	N/A	N/A	N/A	Unstable
4	6 Meter Linear	Aileron	10/ 0.0001/ 10	5	0.1/10	2	Unstable
5	6 Meter Linear	Aileron	10/ 0.0001/ 10	5	0.1/10	5	Unstable
6	6 Meter Linear	Aileron	10/ 0.0001/ 10	5	0.1/10	10	Unstable

The results of the 8 meter X-HALE simulations suggest that 8 meter X-HALE is stable for sinusoidal aileron inputs performed on both wings with 5 degrees of amplitude or less, and the aircraft is unstable for amplitudes of 10 degrees or more. The results also suggest that the aircraft is stable when no inputs are applied. Cesnik et al.'s results when performing UM/NAST simulations for the 8-meter X-HALE [4] suggest that when a single period of a left-wing-down sinusoidal aileron input is applied, the aircraft is stable for aileron inputs with a 2 degree amplitude, but not for inputs with a 5 degree amplitude or greater. Their results suggest that when a 1-cosine gust is symmetrically applied to the 8 meter X-HALE with a maximum gust speed of 4 m/s, while the nominal flight speed is

14 m/s at 30 m altitude, the aircraft is stable. This research build's off of Cesnik et al.'s results and predicts that, when test flown, the 8 meter X-HALE can be expected to be stable as long as any sinusoidal aileron inputs commanded on both wings has no more than 5 degrees of amplitude. A summary of the results of the 8 meter X-HALE simulations discussed is given in Table 4.

Table 4. A Summary of Discussed 8 Meter X-HALE Simulations

Case	Simulation Type	Input	Duration (sec)/ Time Step (sec)/ Max Residual Value	Sinusoidal Aileron Input Data			Stability
				Period (sec)	Start/End Time (sec)	Amplitude (deg)	
7	8 Meter Linear	None	15/ 0.001/ 10	N/A	N/A	N/A	Stable
8	8 Meter Linear	Aileron	15/ 0.001/ 10	5	0.1/10	2	Stable
9	8 Meter Nonlinear	Aileron	15/ 0.001/ 10	5	0.1/10	2	Stable
10	8 Meter Linear	Aileron	15/ 0.001/ 10	5	0.1/10	5	Stable
11	8 Meter Nonlinear	Aileron	15/ 0.001/ 10	5	0.1/10	5	Stable
12	8 Meter Linear	Aileron	15/ 0.001/ 10	5	0.1/10	10	Stable
13	8 Meter Nonlinear	Aileron	15/ 0.001/ 10	5	0.1/10	10	Unstable
14	8 Meter Linear	Aileron	15/ 0.001/ 10	5	0.1/10	15	Stable
15	8 Meter Nonlinear	Aileron	15/ 0.001/ 10	5	0.1/10	15	Unstable
16	8 Meter Linear	Aileron	15/ 0.001/ 10	5	0.1/10	20	Unstable
17	8 Meter Linear	Aileron	15/ 0.001/ 10	5	0.1/10	25	Unstable

V.2 Recommendations for Future Research

This research provides another step forward in the process of predicting the flight behavior of the X-HALE aircrafts when they are test flown for the purpose of potentially validating the UM/NAST code; however, more research is necessary to expand on the findings of this research. Unfortunately, the 6 meter X-HALE simulations run are probably not accurate models of the flight of the 6 meter X-HALE. More simulations should be done for the 6 meter model of X-HALE but this time the trim conditions should be properly configured. Ideally simulations would be run for at least a 15 second flight time. Simulations should be run using both the linear and nonlinear solution types. These simulations should include sinusoidal aileron inputs on both wings with various amplitudes, gust inputs of various speeds, and no inputs at all. Other simulations that may be helpful include turning simulations and climb and descent simulations. Additionally, simulations need to be run in order to predict the effect of flipping X-HALE's vertical tail on the 6 meter X-HALE. It is possible that the vertical tail may provide more stability, especially in the lateral direction. The 8 meter aircraft has more wing dihedral when the wings are flexed than the 6 meter aircraft because the aircraft is longer. This provides more lateral stability for the 8 meter aircraft. This may be why the 6 meter X-HALE appears to be less stable than the 8 meter X-HALE according to the results of this research.

Thankfully, the 8 meter X-HALE simulations performed in this research are more helpful. However, this research only performed simulations involving either sinusoidal aileron inputs on both wings or no inputs. Shearer, Cesnik and their co-workers performed simulations for the 8 meter X-HALE involving single period, left-wing-down

sinusoidal aileron inputs, and simulations with a 1-cosine gust symmetrically applied with a maximum gust speed of 4 m/s. There are plenty more simulations that can be run for the 8 meter version of X-HALE in order to help predict the aircraft's flight behavior such as turning simulations, and climb and descend simulations, and gust inputs of various speeds. Additionally, it may be helpful to run nonlinear type simulations for aileron inputs between 5 and 10 degrees of amplitude to pinpoint exactly what sinusoidal aileron input amplitude causes the aircraft to become unstable. Simulations also need to be run in order to predict the effect of flipping the 8 meter X-HALE's vertical tail.

Much of the initial difficulties experienced are due to the fact that the 6 meter simulations were probably improperly set up. However, future research can benefit from the findings of this research when it comes to the balance of the time step, the maximum residual value and the flight time. Future research should set up simulations with a time step of no more than 0.05 seconds (but at least 0.0001 seconds), a maximum residual value of no more than 10 (but at least 0.1) and a flight time of at least 15 seconds. A time step of no more than 0.05 seconds and a maximum residual value of no more than 10 will help to the simulations complete easily and to provide accurate results. A flight time of at least 15 seconds will help to ensure that enough information can be drawn from the results.

V.3 General Remarks

The recent crash of NASA's Helios aircraft (Figure 4), a forerunning HALE Remotely Piloted Aircraft (RPA), demonstrates that while previous research has been done on the problem of nonlinear aeroelasticity coupled with nonlinear flight dynamics, the problem is still not completely understood. Several codes have been developed for

the use of modeling nonlinear aeroelastic and flight dynamics of an aircraft, such as UM/NAST, NATASHA, ASWING and RCAS, but none have been completely validated with real flight data from a fixed-wing aircraft [4]. The goal of this research was to perform flight simulations with UM/NAST so as to make predictions about X-HALE's future test flights and subsequently uncover the strengths and weaknesses of UM/NAST when X-HALE is finally flown. Indeed, this research managed to make predictions about X-HALE's future test flights and is a step forward in potentially validating UM/NAST. This research, in conjunction with the UM/NAST code and the test flights of the X-HALE aircrafts should provide more information on the problem of nonlinear aeroelasticity coupled with nonlinear flight dynamics. Hopefully this knowledge can be put to use in the development of HALE aircraft. These HALE aircraft may include ISR platforms, such as US Air Force SensorCraft, network communication nodes for military or civilian purposes, or aircraft that will perform general atmospheric research.

Appendix A. Additional Figures

Case 1: 6 m Linear Type 15 sec Simulation, No Aileron Input

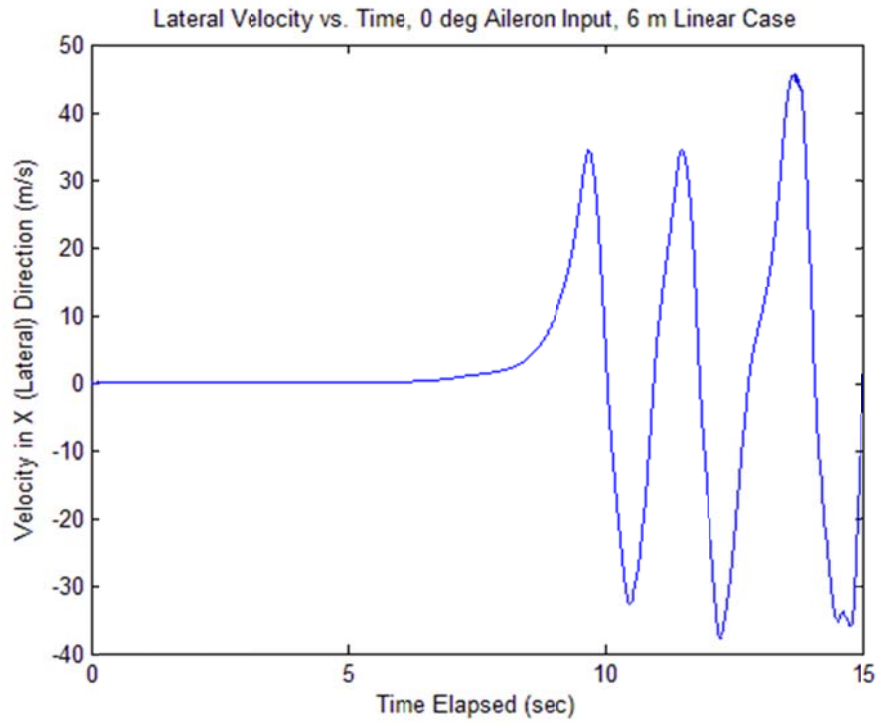


Figure 74. Case 1 Lateral Velocity v_x versus Time

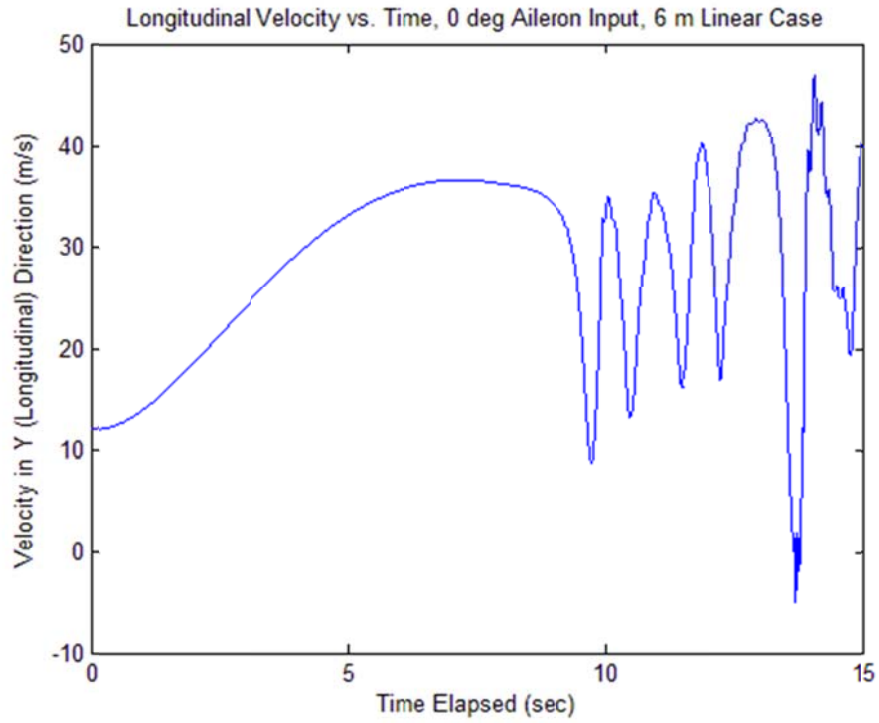


Figure 75. Case 1 Longitudinal Velocity v_y versus Time

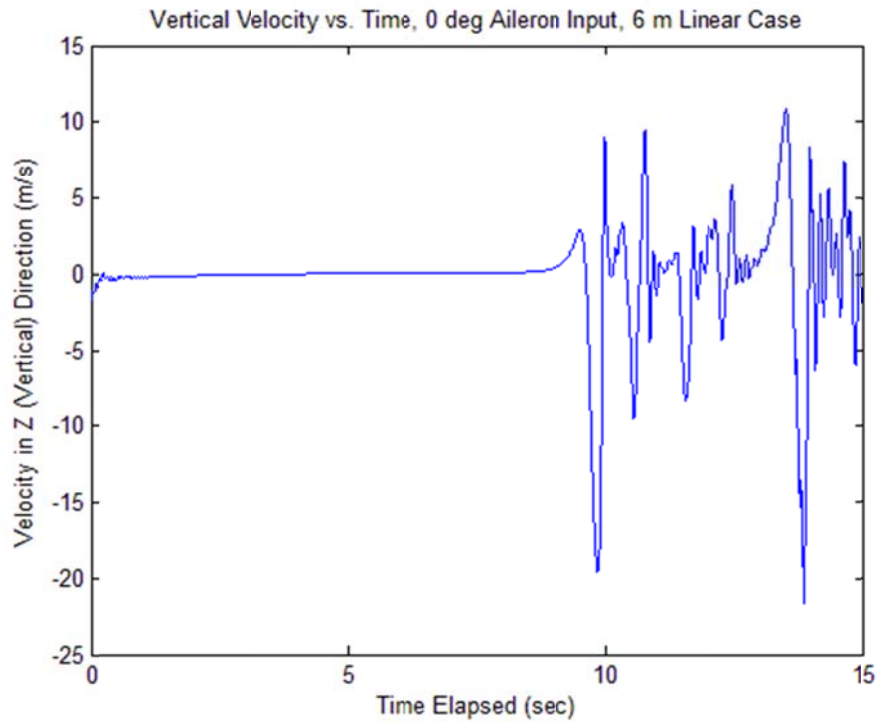


Figure 76. Case 1 Vertical Velocity v_z versus Time

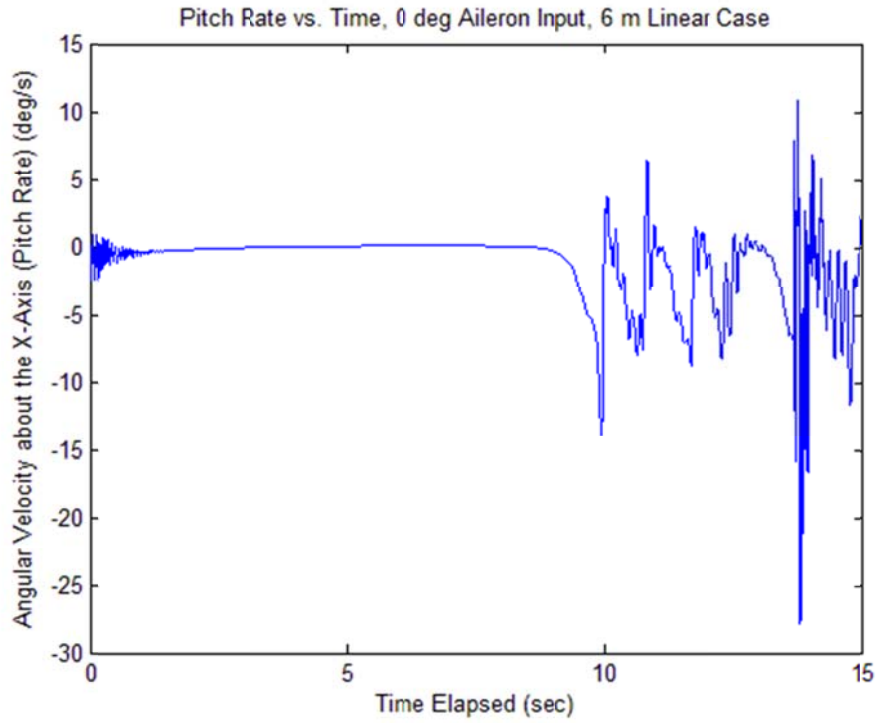


Figure 77. Case 1 Pitch Rate ω_x versus Time

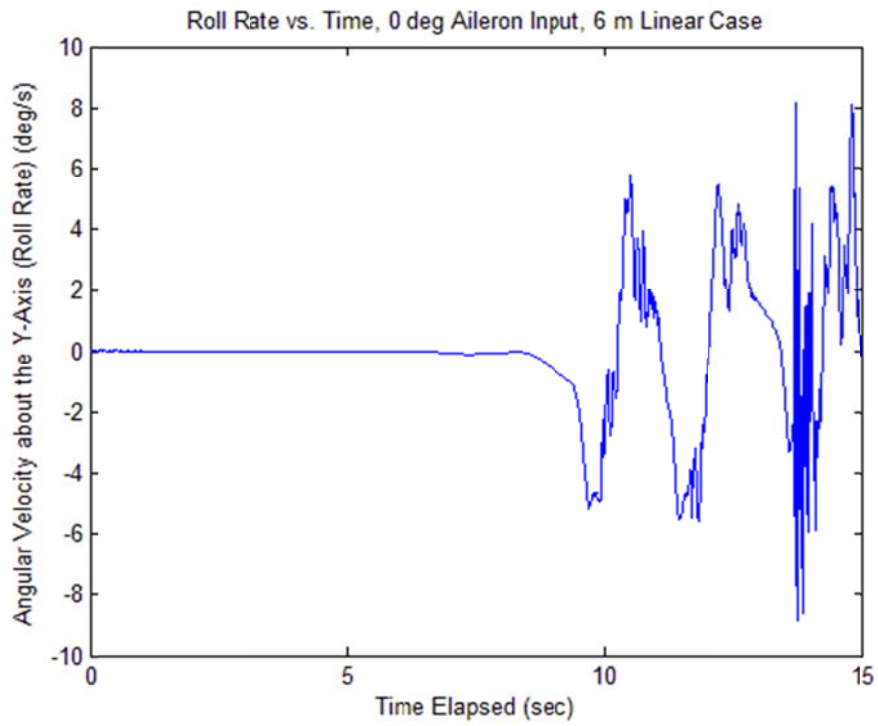


Figure 78. Case 1 Roll Rate ω_y versus Time

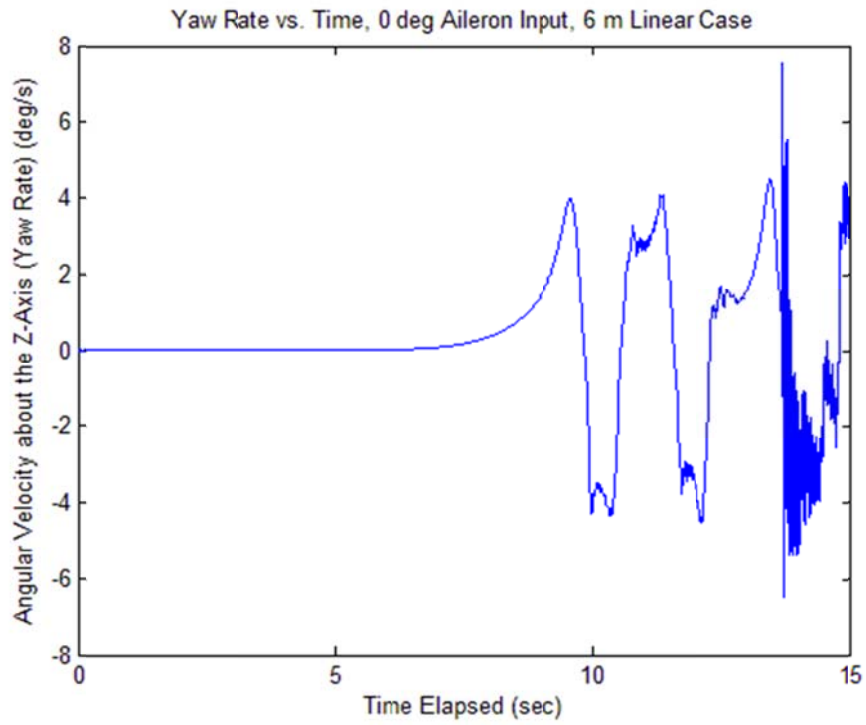


Figure 79. Case 1 Yaw Rate ω_z versus Time

Case 2: 6 m Linear Type 10 sec Simulation, No Aileron Input

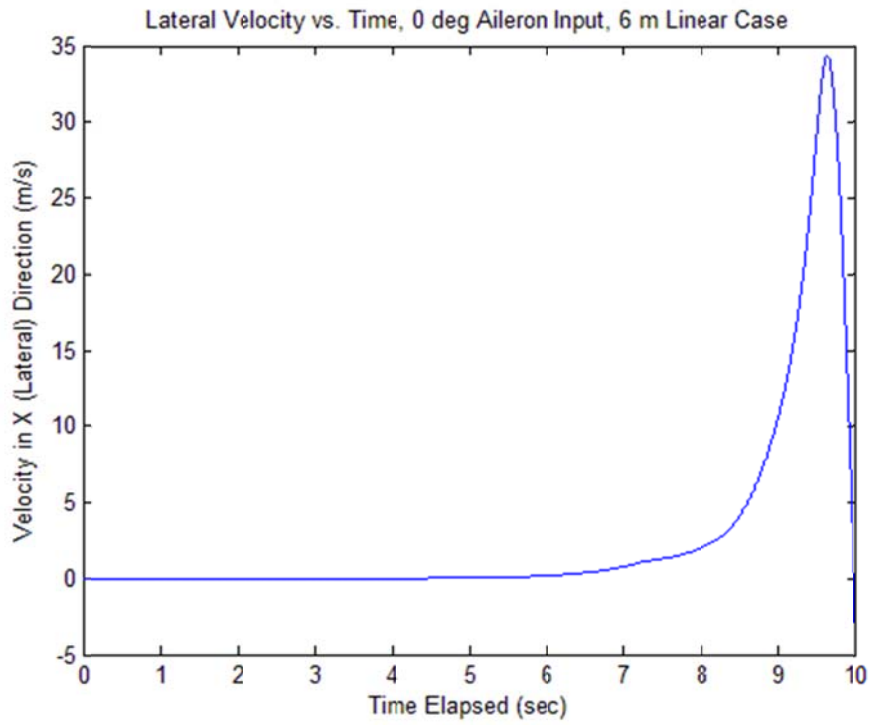


Figure 80. Case 2 Lateral Velocity v_x versus Time

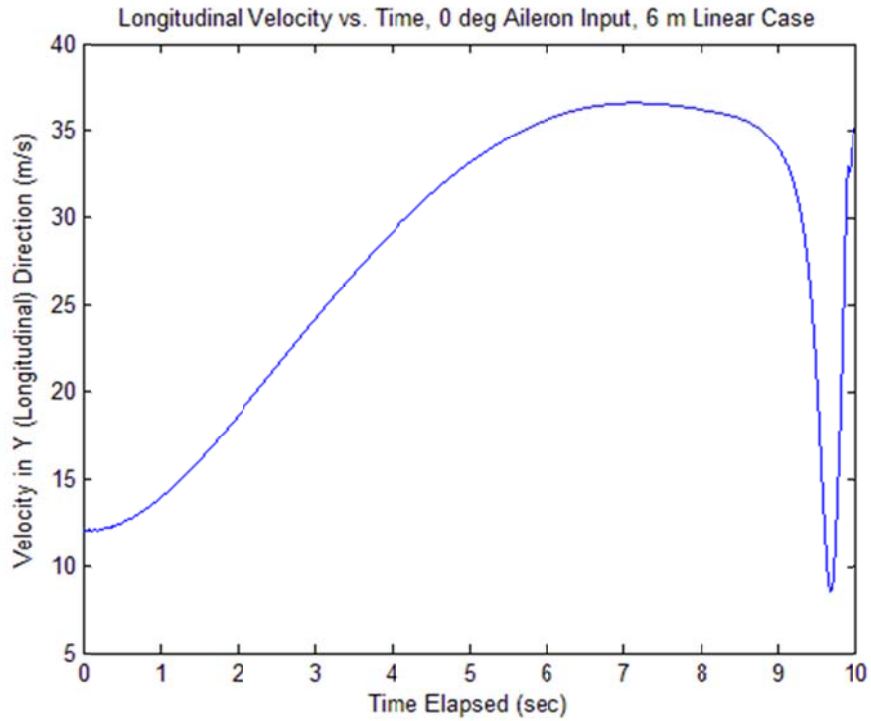


Figure 81. Case 2 Longitudinal Velocity v_y versus Time

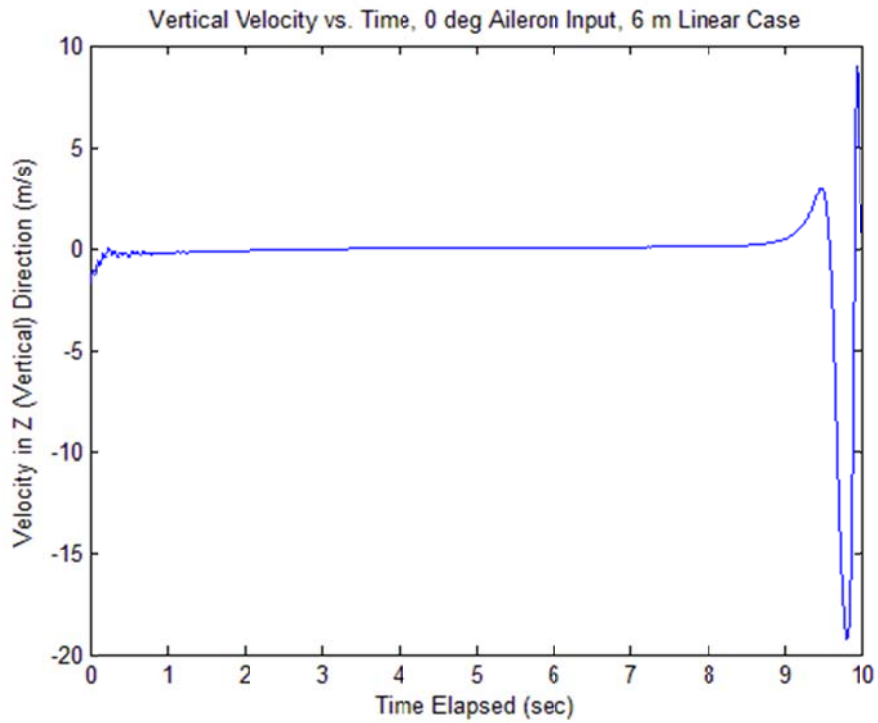


Figure 82. Case 2 Vertical Velocity v_z versus Time

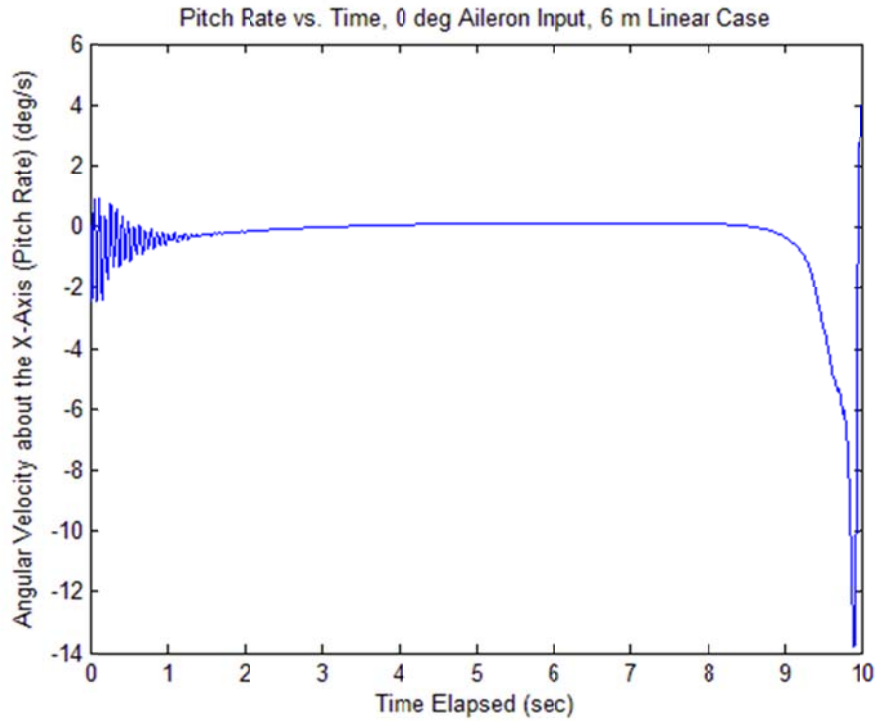


Figure 83. Case 2 Pitch Rate ω_x versus Time

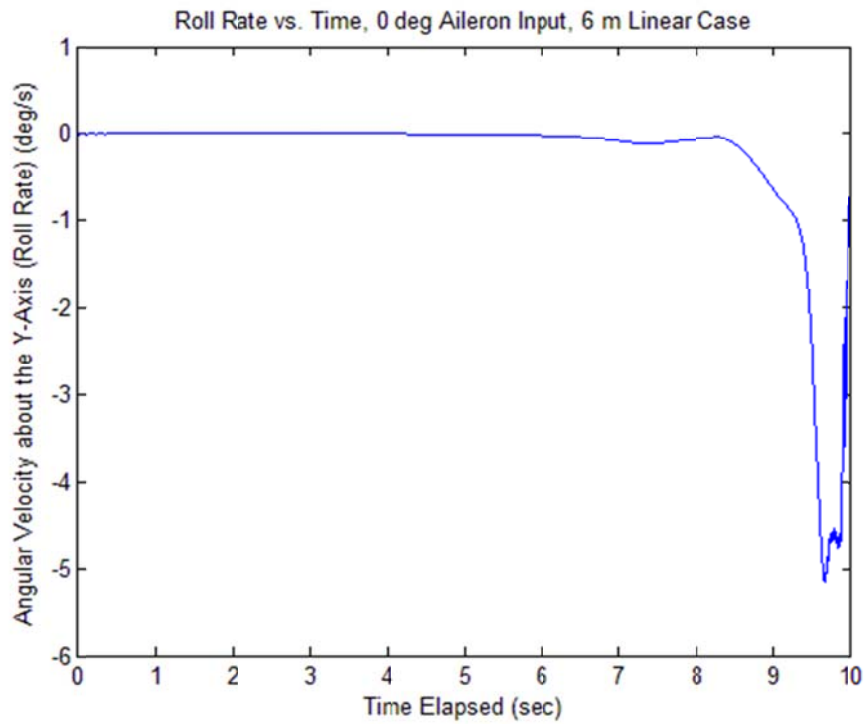


Figure 84. Case 2 Roll Rate ω_y versus Time

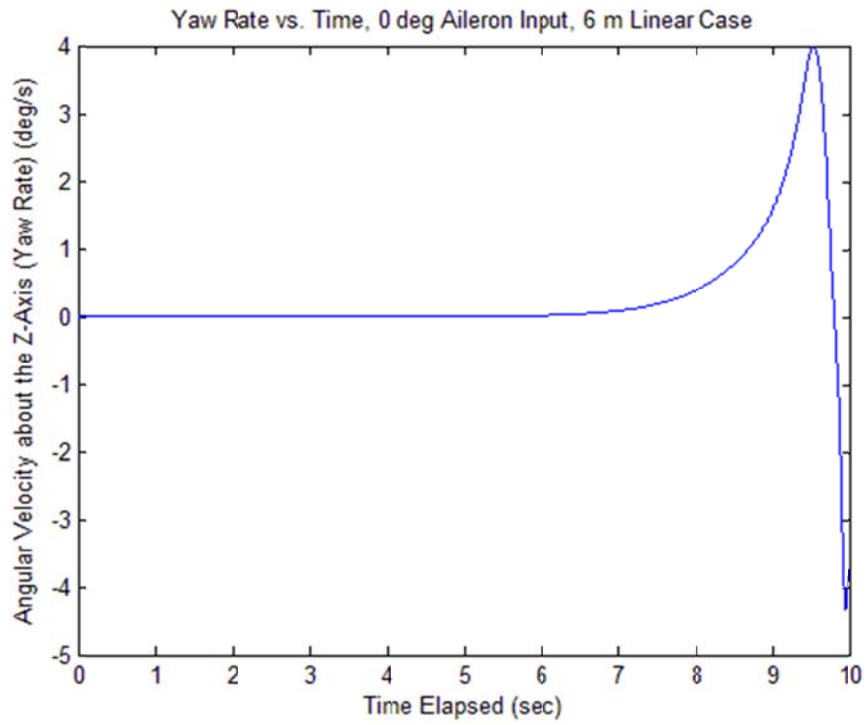


Figure 85. Case 2 Yaw Rate ω_z versus Time

Case 3: 6 m Nonlinear Type 10 sec Simulation, No Aileron Input

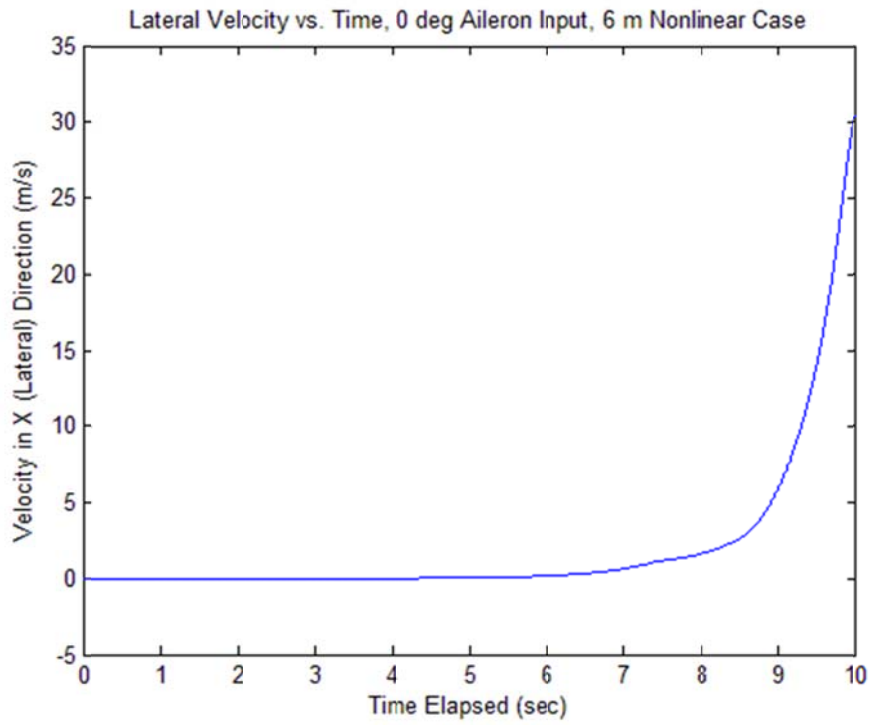


Figure 86. Case 3 Lateral Velocity v_x versus Time

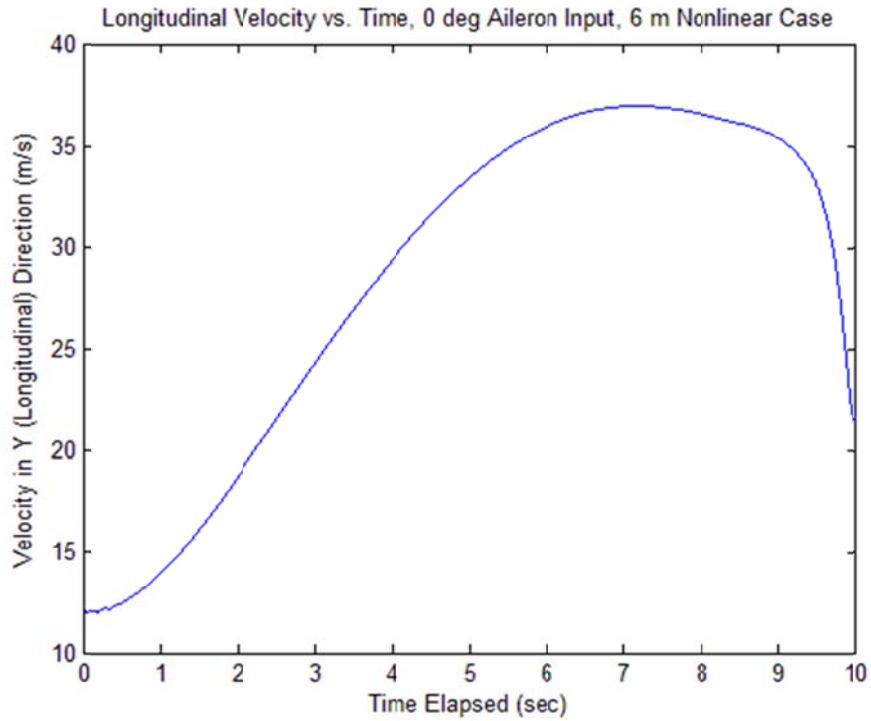


Figure 87. Case 3 Longitudinal Velocity v_y versus Time

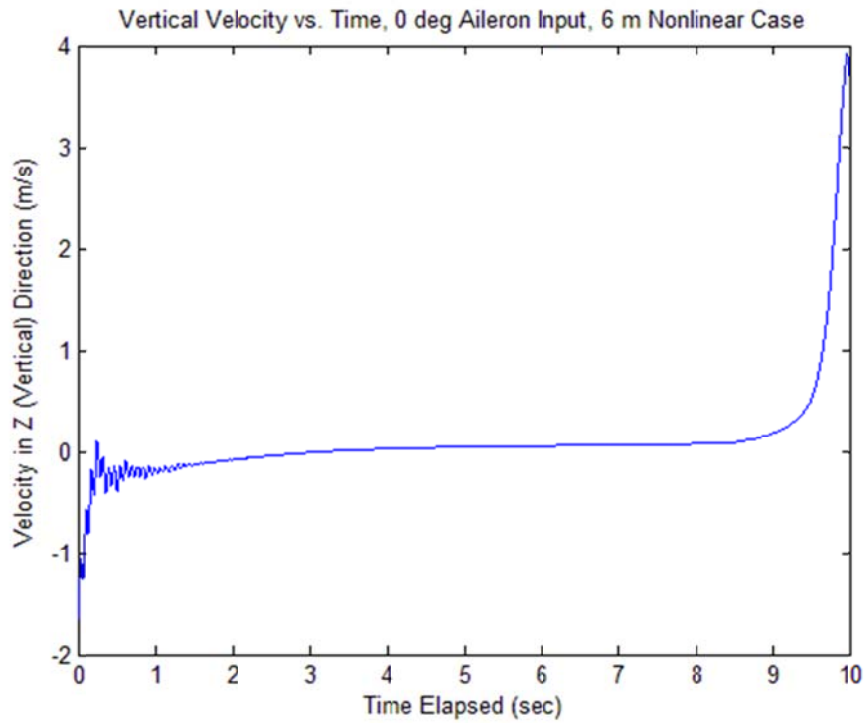


Figure 88. Case 3 Vertical Velocity v_z versus Time

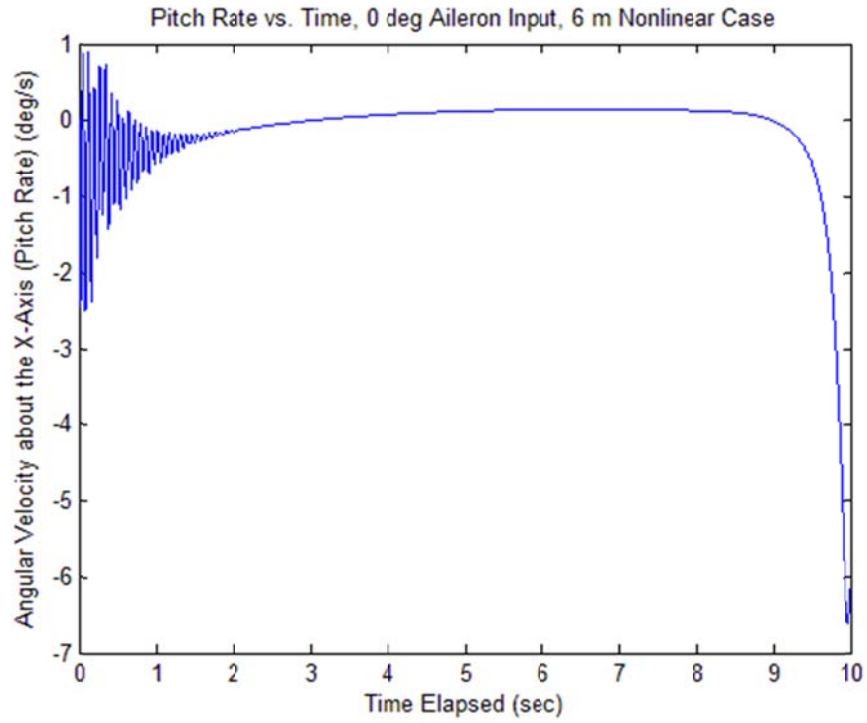


Figure 89. Case 3 Pitch Rate ω_x versus Time

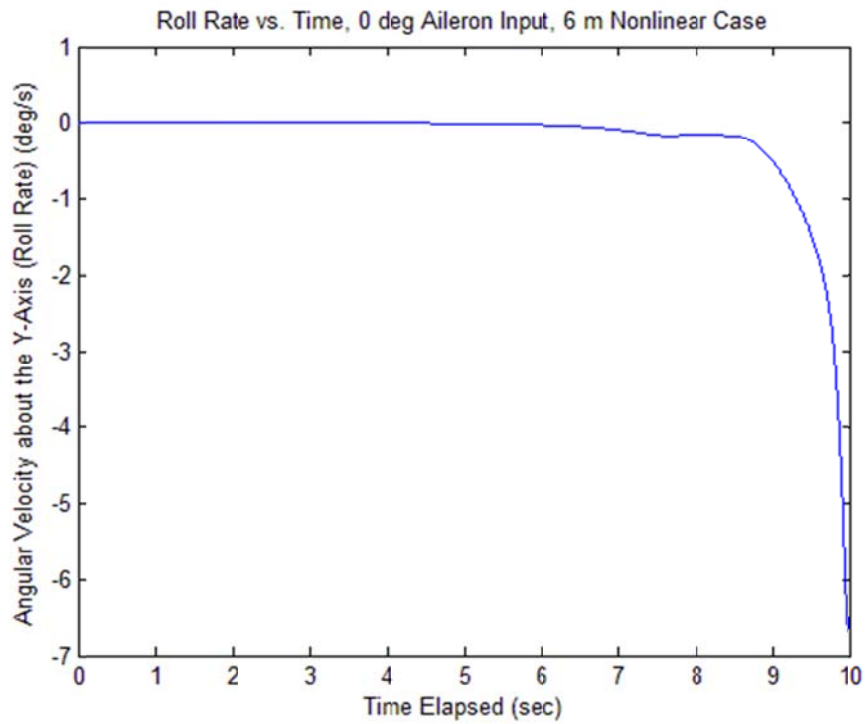


Figure 90. Case 3 Roll Rate ω_y versus Time

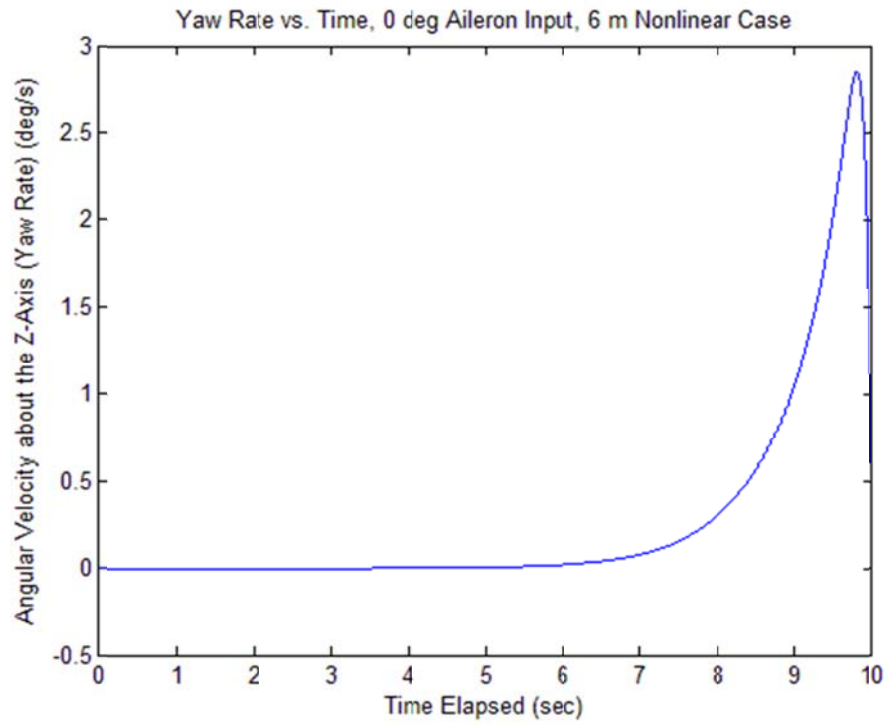


Figure 91. Case 3 Yaw Rate ω_z versus Time

Case 4: 6 m Linear Type 10 sec Simulation, 2 deg Aileron Input

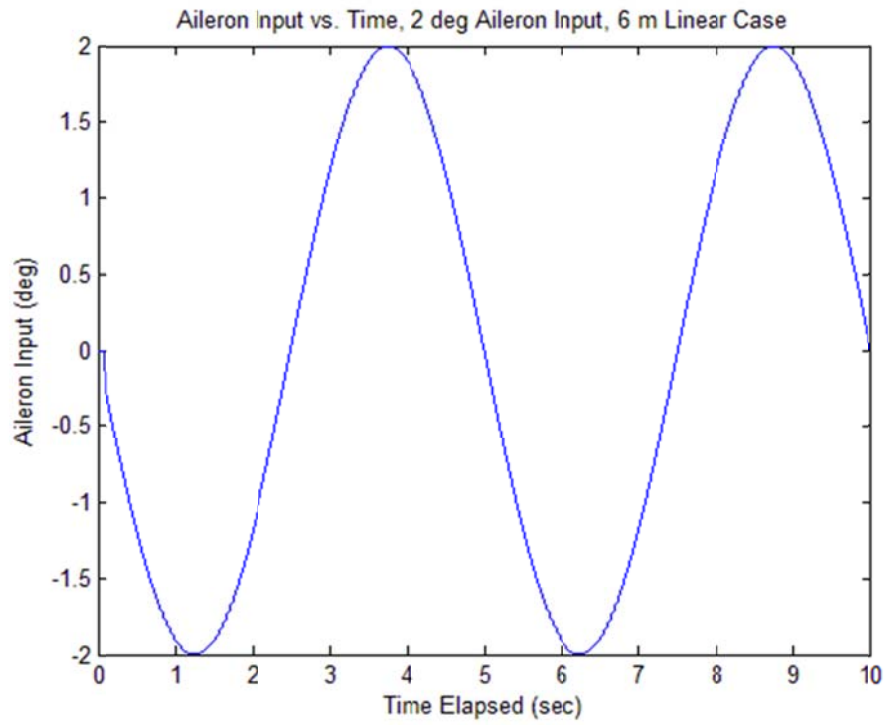


Figure 92. Case 4 Aileron Input versus Time

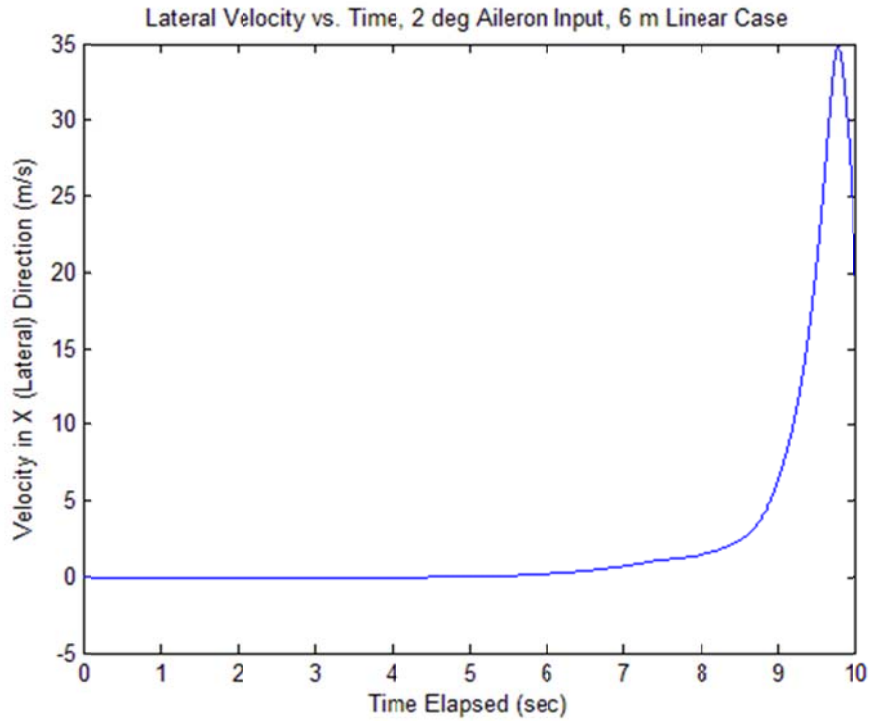


Figure 93. Case 4 Lateral Velocity v_x versus Time

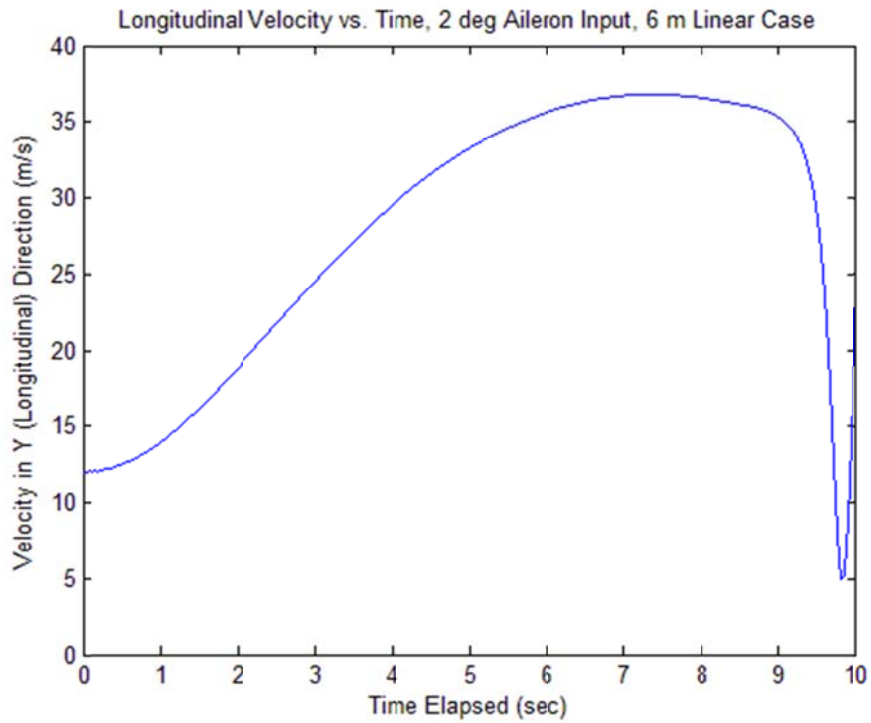


Figure 94. Case 4 Longitudinal Velocity v_y versus Time

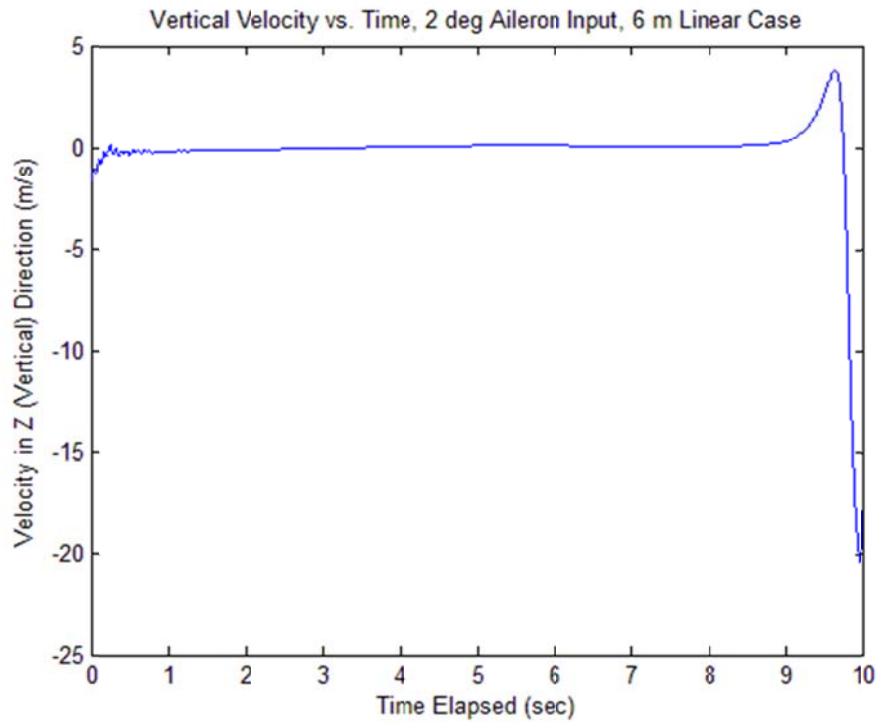


Figure 95. Case 4 Vertical Velocity v_z versus Time

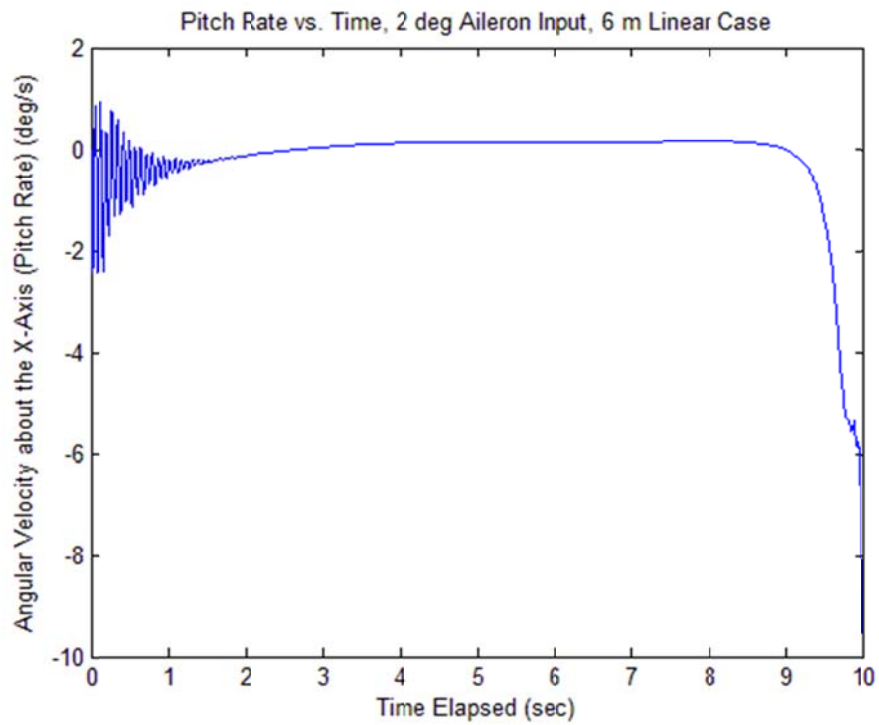


Figure 96. Case 4 Pitch Rate ω_x versus Time

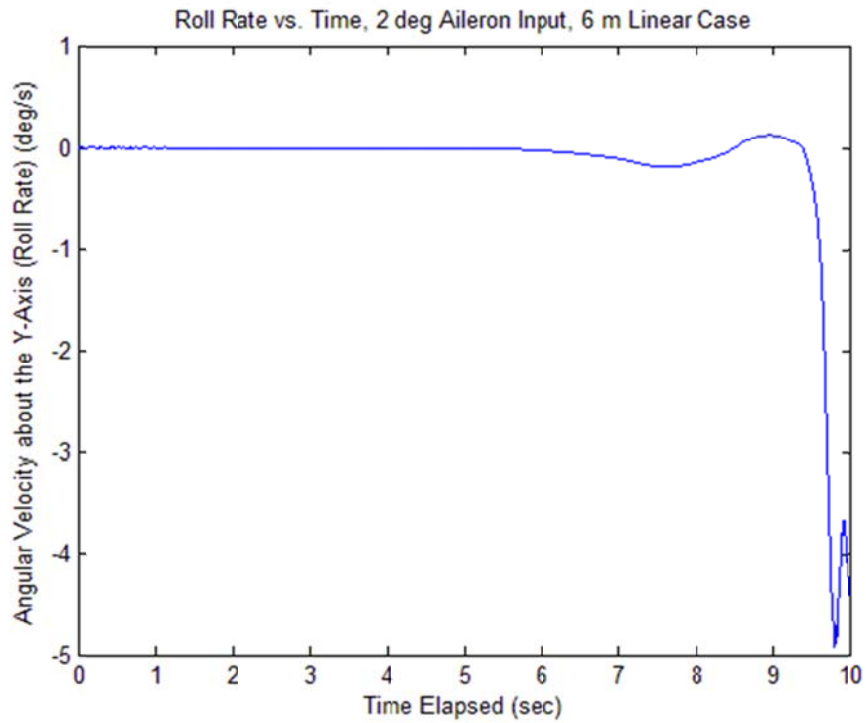


Figure 97. Case 4 Roll Rate ω_y versus Time

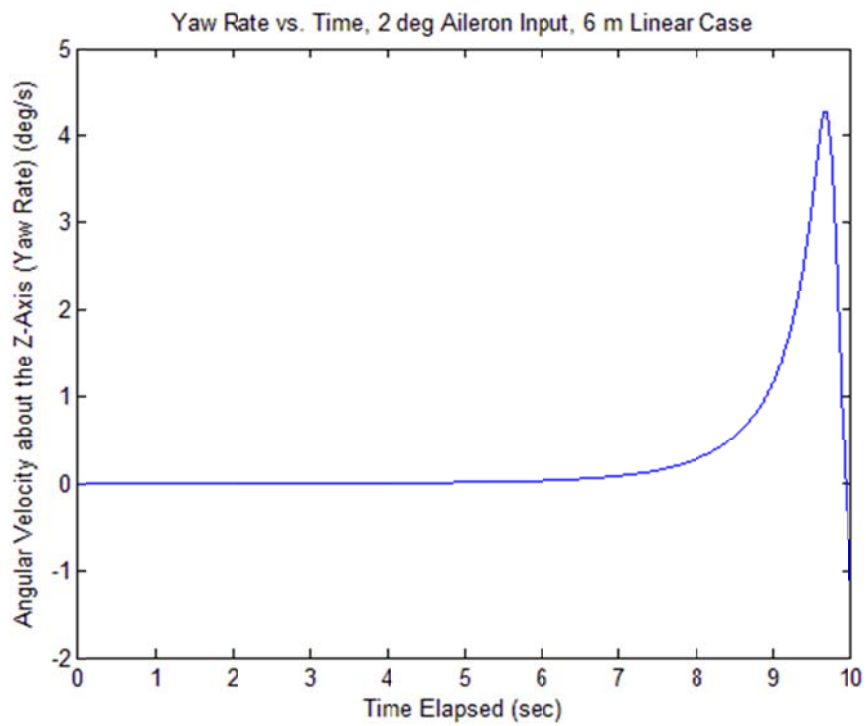


Figure 98. Case 4 Yaw Rate ω_z versus Time

Case 5: 6 m Linear Type 10 sec Simulation, 5 deg Aileron Input

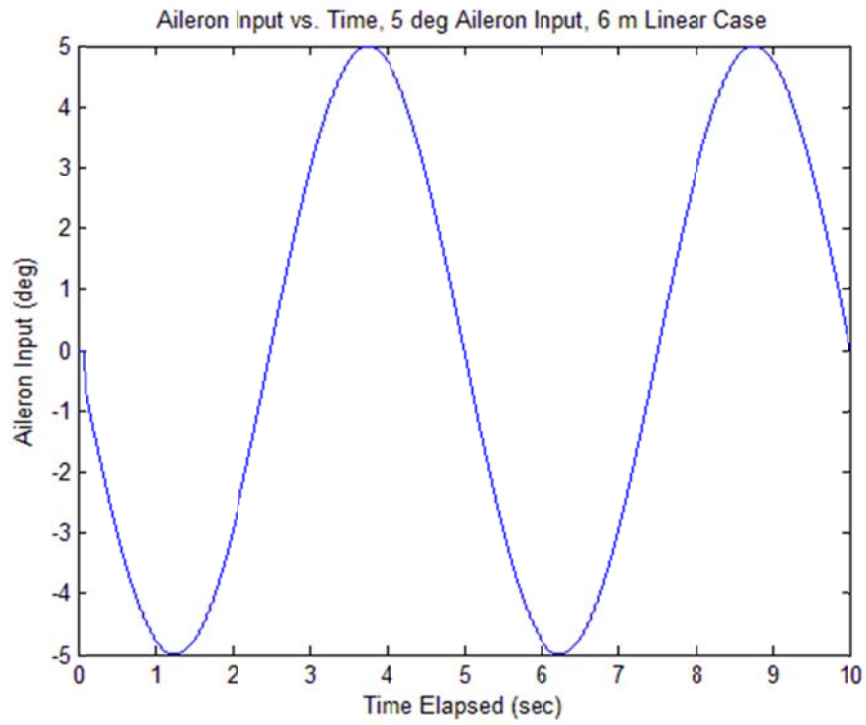


Figure 99. Case 5 Aileron Input versus Time

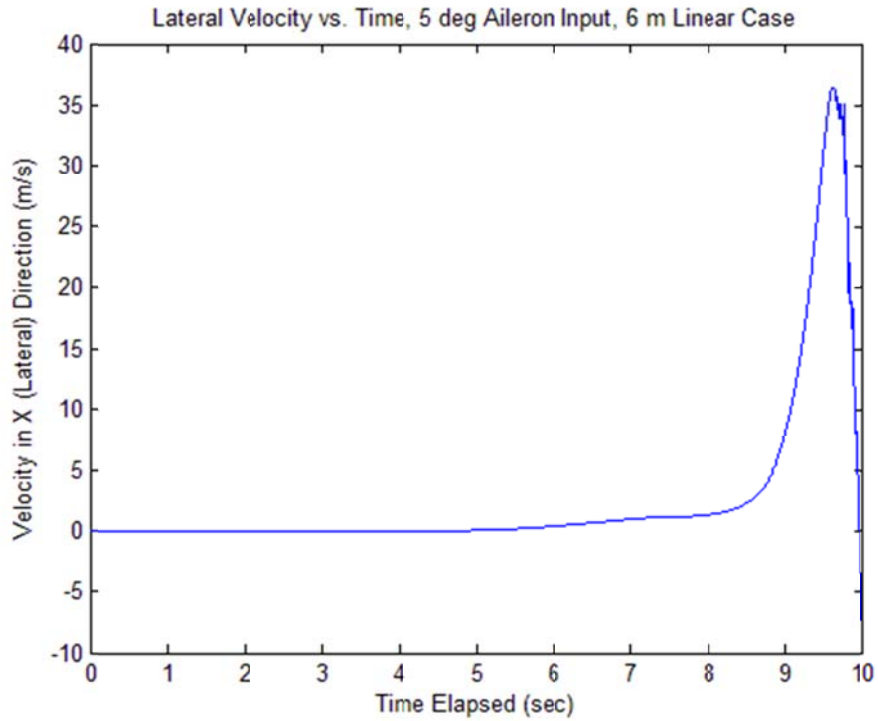


Figure 100. Case 5 Lateral Velocity v_x versus Time

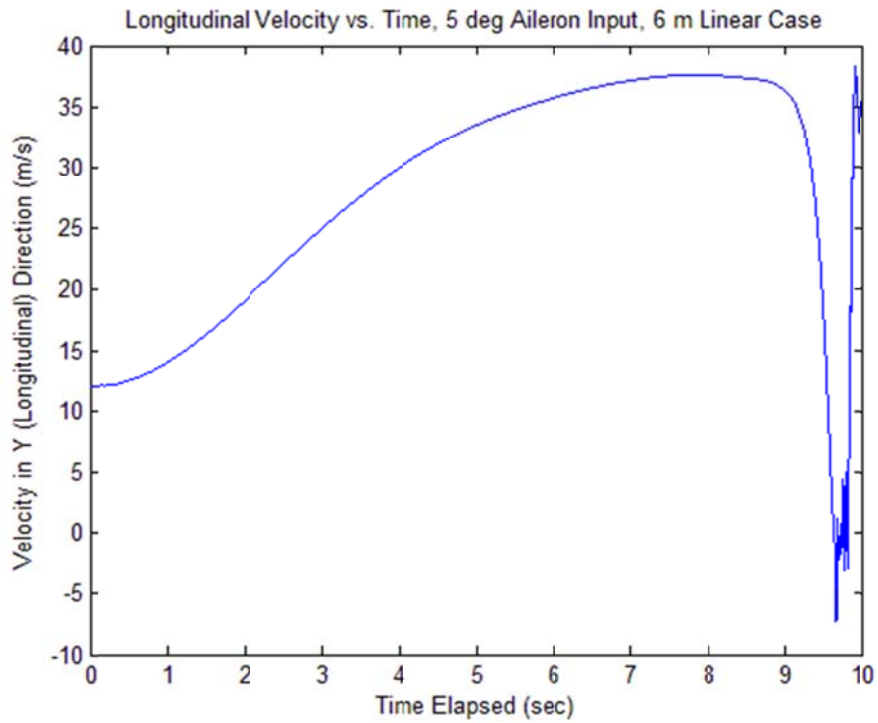


Figure 101. Case 5 Longitudinal Velocity v_y versus Time

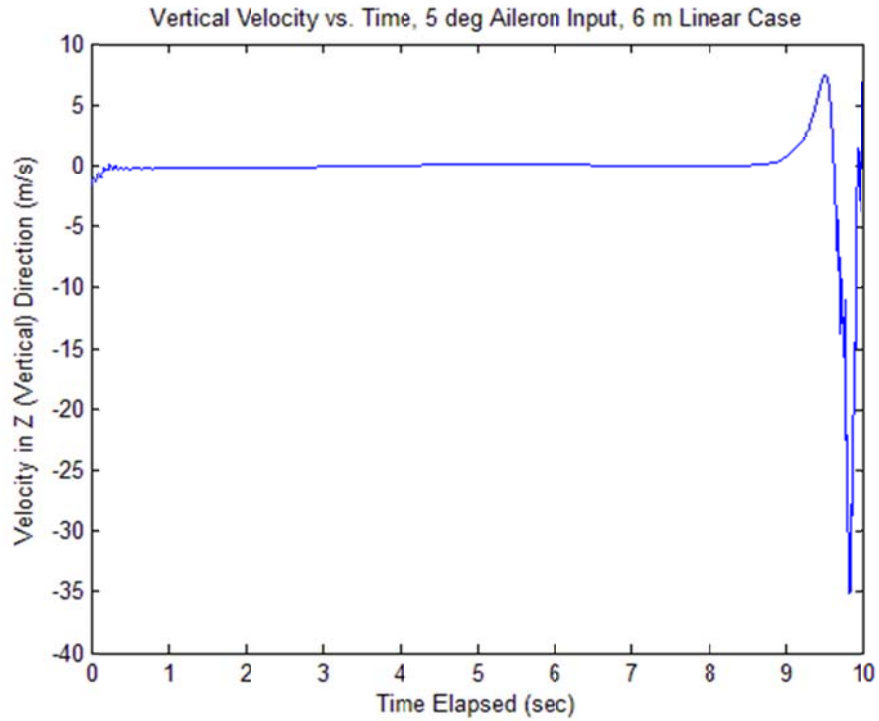


Figure 102. Case 5 Vertical Velocity v_z versus Time

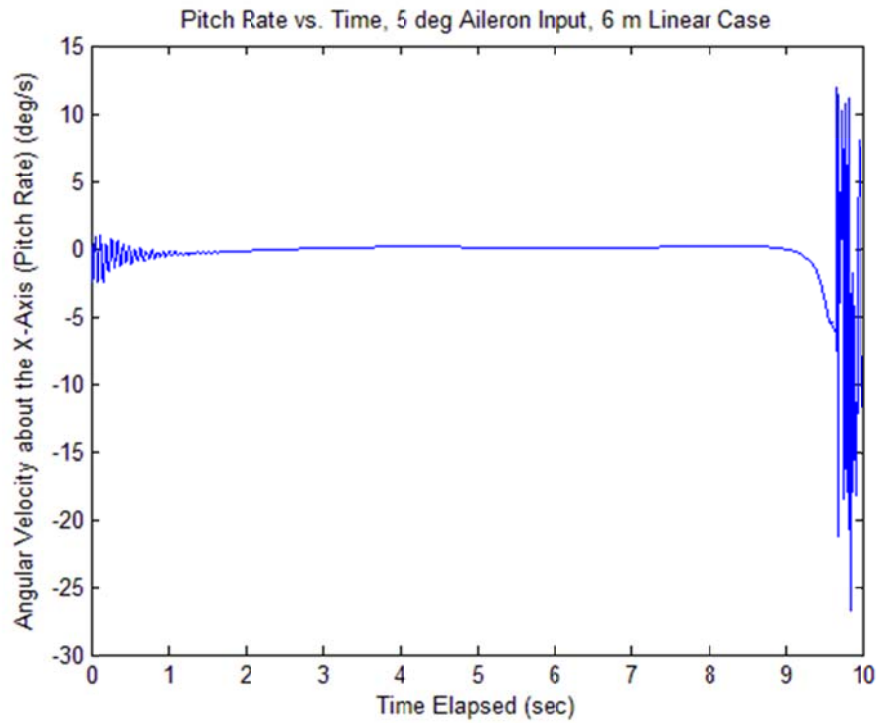


Figure 103. Case 5 Pitch Rate ω_x versus Time

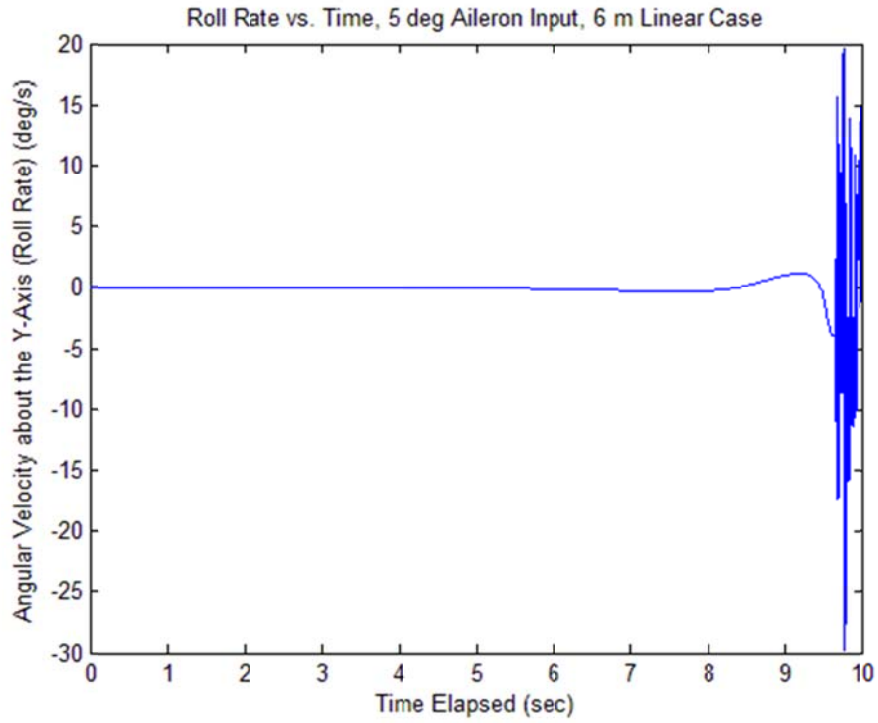


Figure 104. Case 5 Roll Rate ω_y versus Time

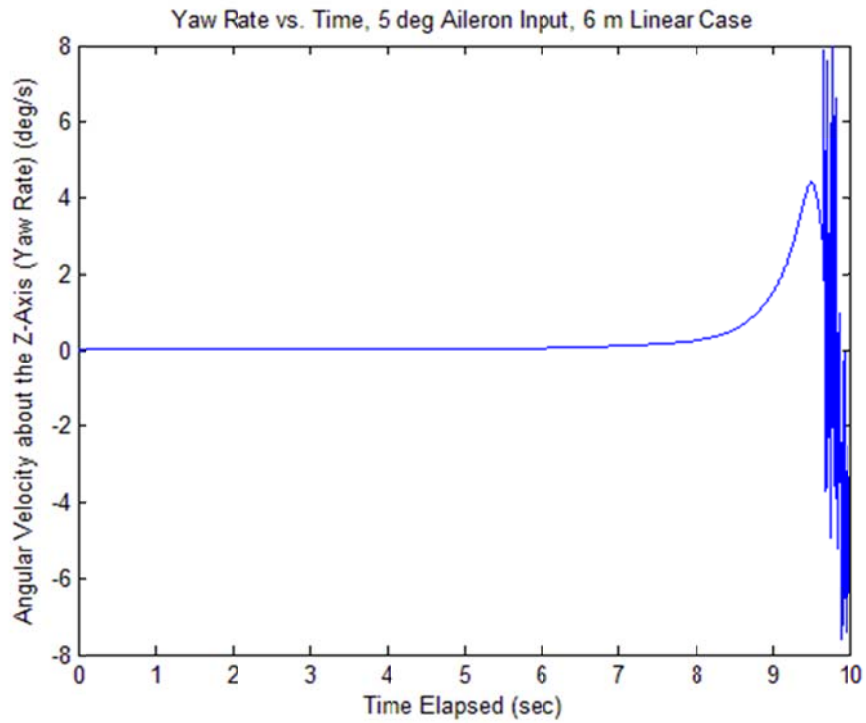


Figure 105. Case 5 Yaw Rate ω_z versus Time

Case 6: 6 m Linear Type 10 sec Simulation, 10 deg Aileron Input

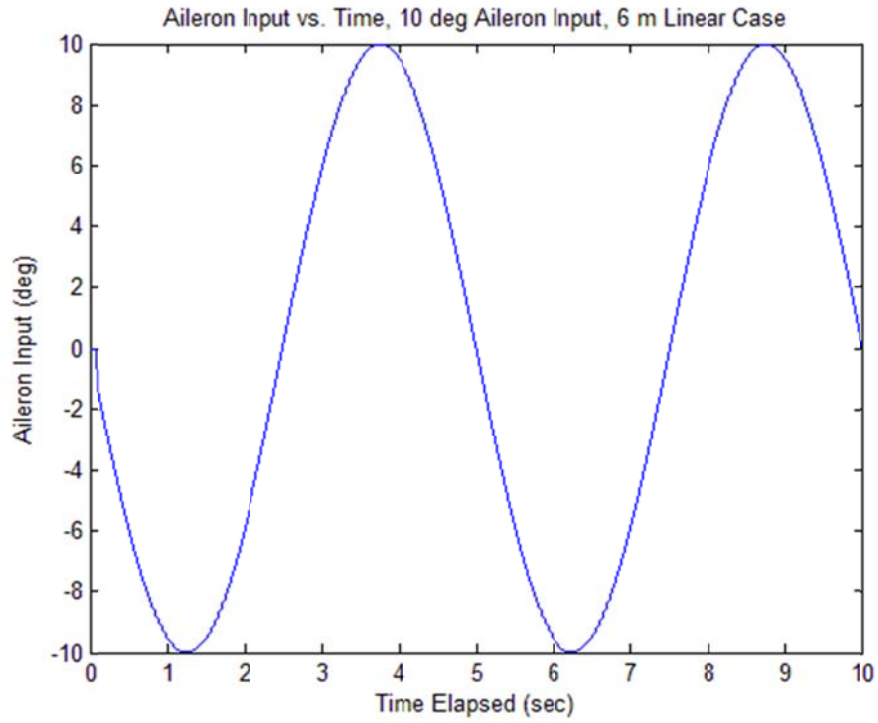


Figure 106. Case 6 Aileron Input versus Time

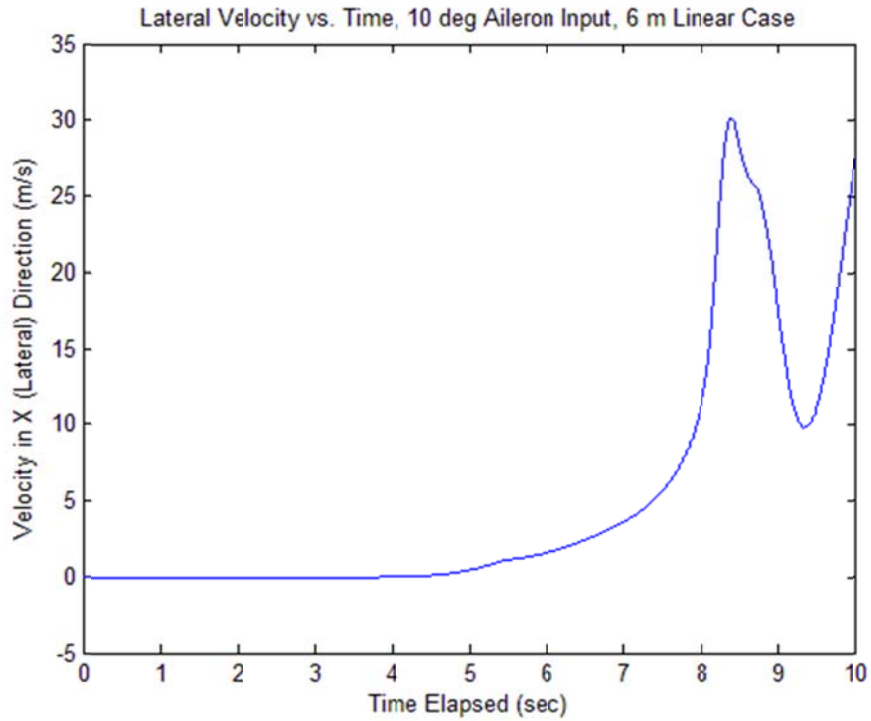


Figure 107. Case 6 Lateral Velocity v_x versus Time

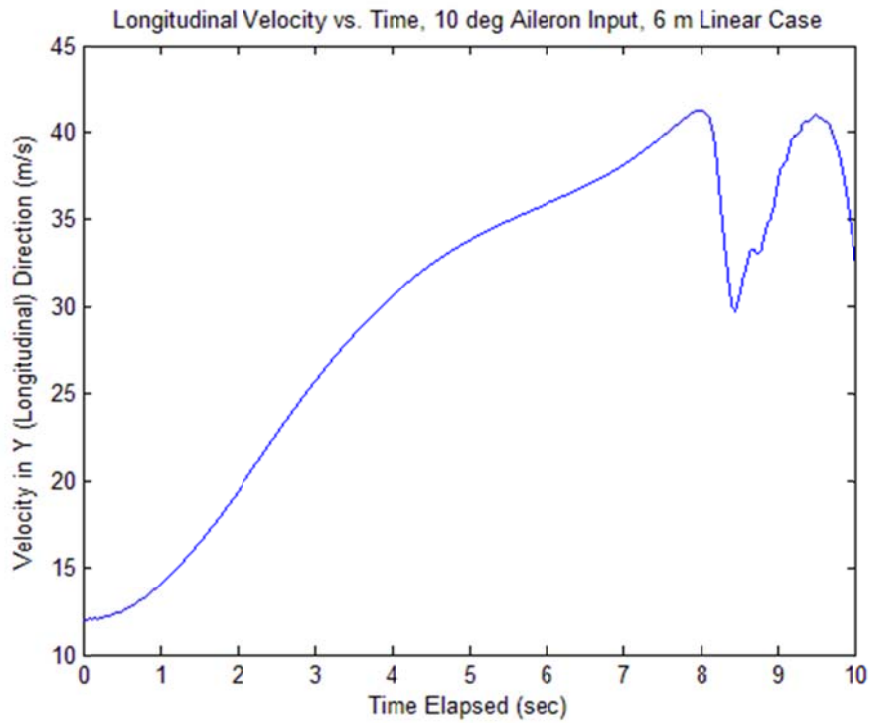


Figure 108. Case 6 Longitudinal Velocity v_y versus Time

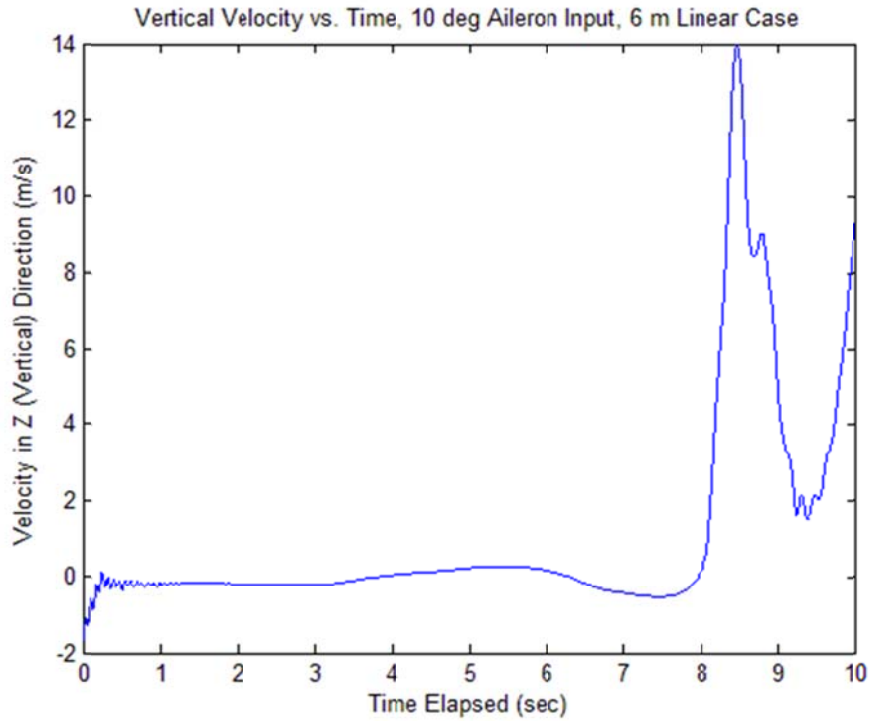


Figure 109. Case 6 Vertical Velocity v_z versus Time

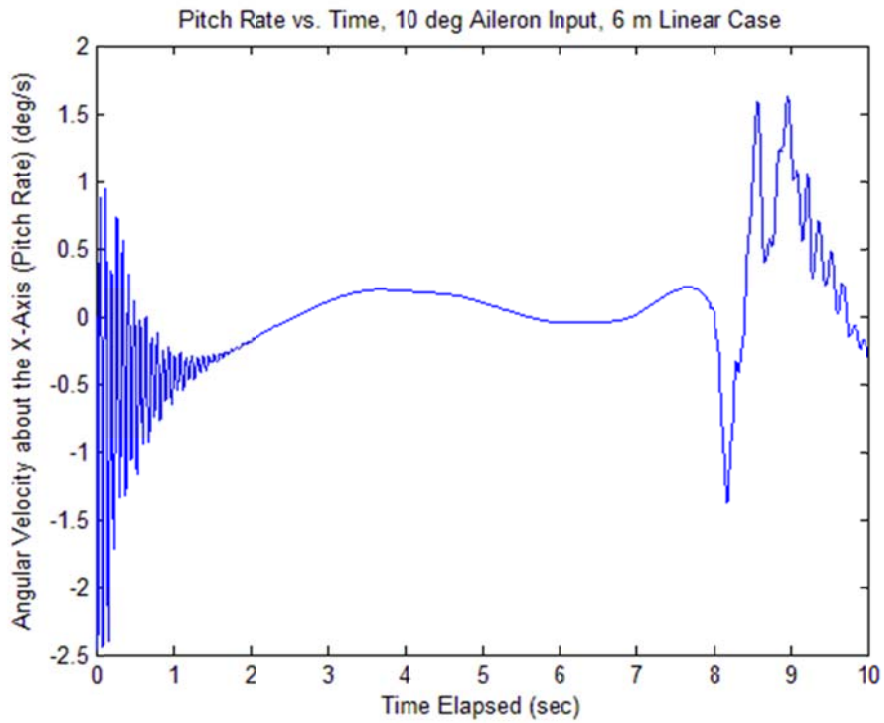


Figure 110. Case 6 Pitch Rate ω_x versus Time

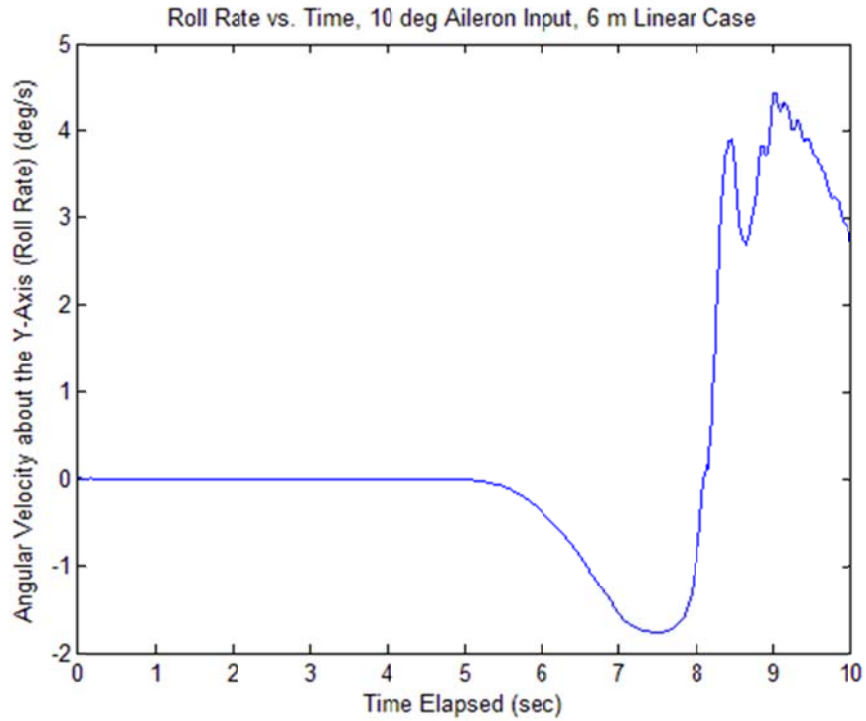


Figure 111. Case 6 Roll Rate ω_y versus Time

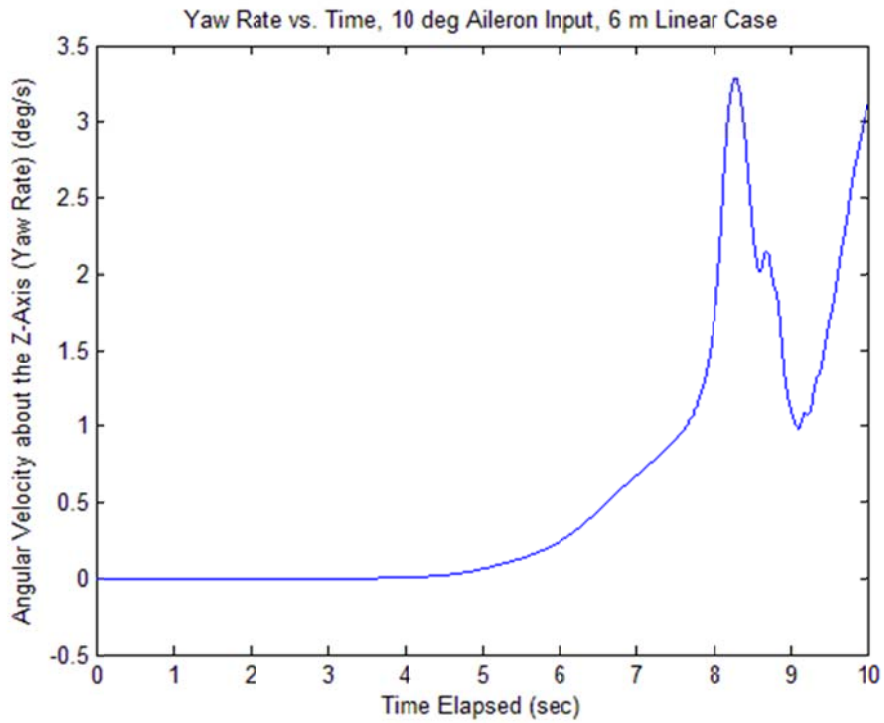


Figure 112. Case 6 Yaw Rate ω_z versus Time

Case 7: 8 m Linear Type 15 sec Simulation, No Aileron Input

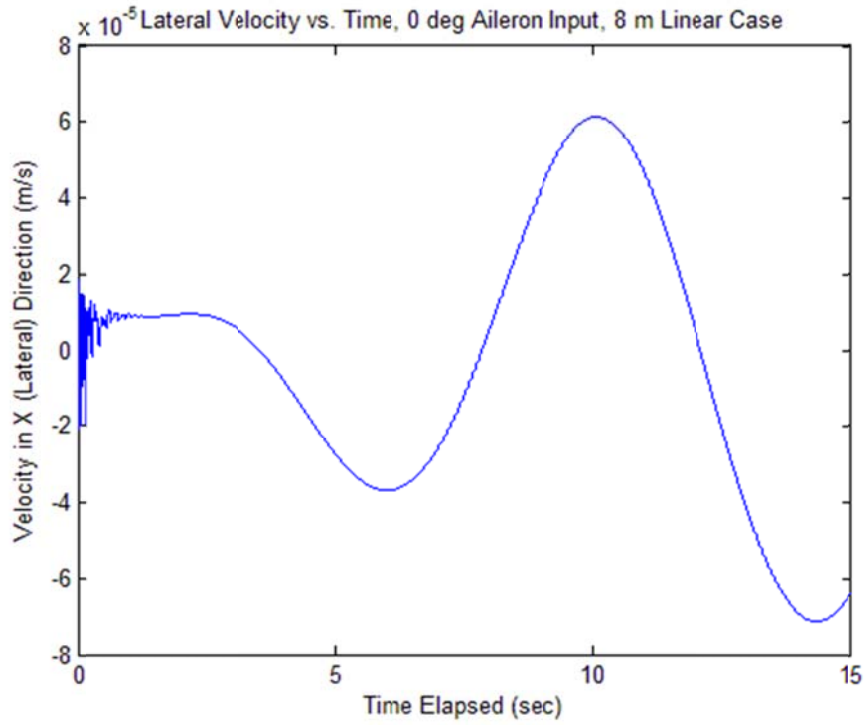


Figure 113. Case 7 Lateral Velocity v_x versus Time

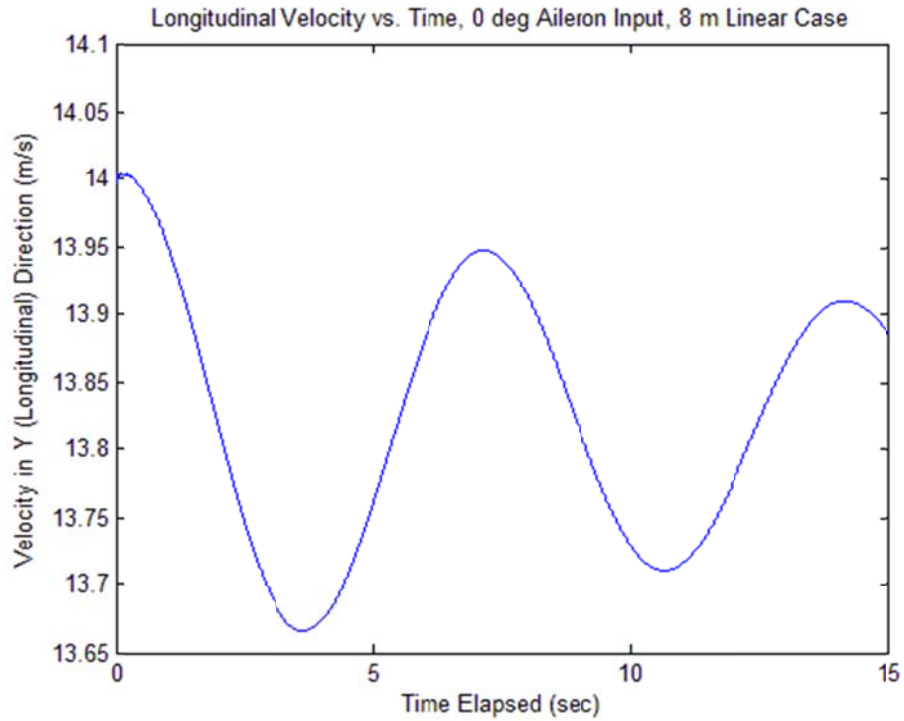


Figure 114. Case 7 Longitudinal Velocity v_y versus Time

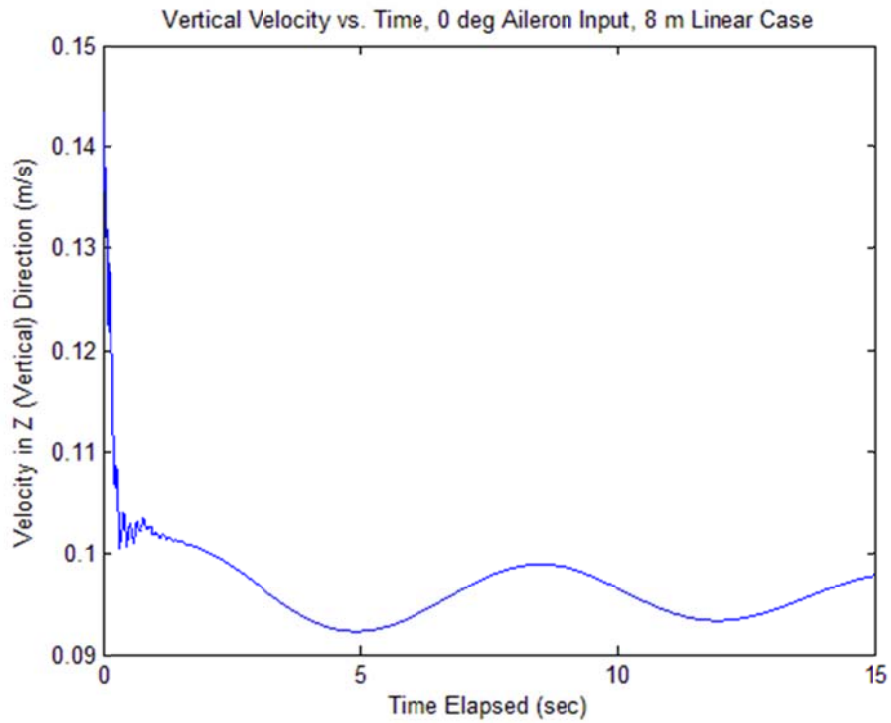


Figure 115. Case 7 Vertical Velocity v_z versus Time

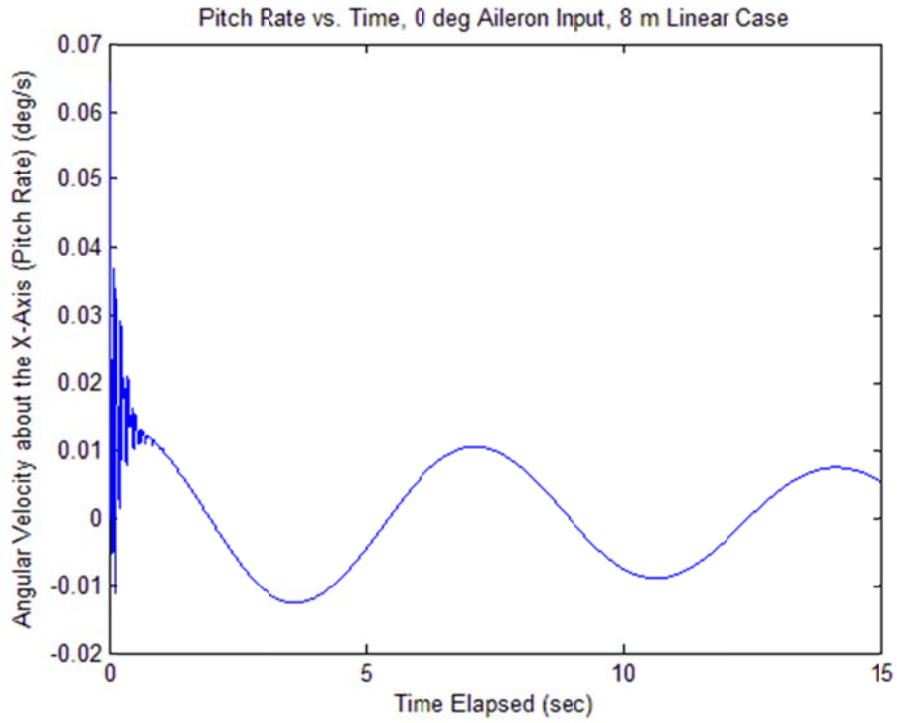


Figure 116. Case 7 Pitch Rate ω_x versus Time

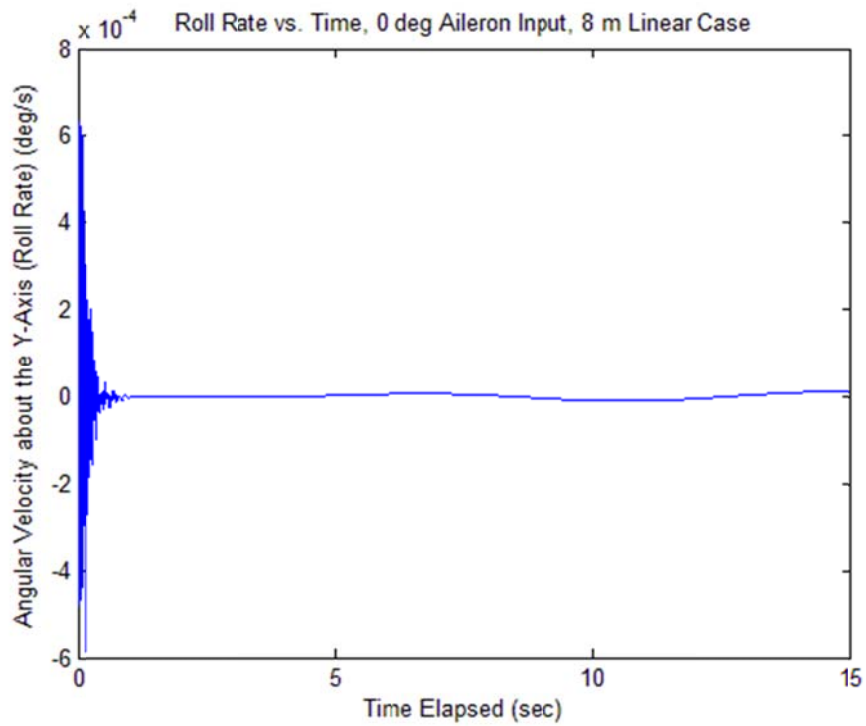


Figure 117. Case 7 Roll Rate ω_y versus Time

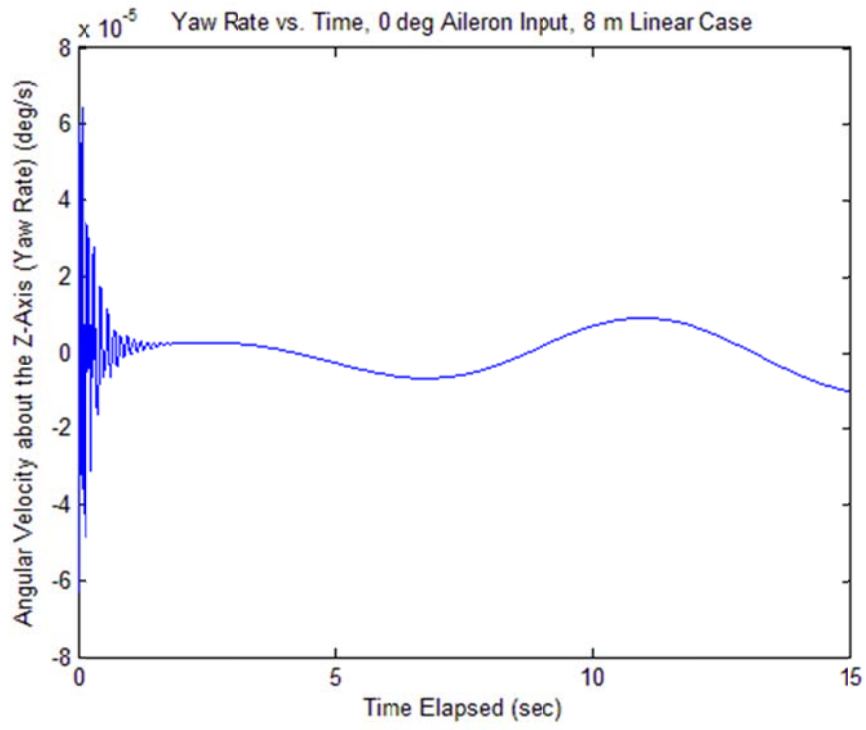


Figure 118. Case 7 Yaw Rate ω_z versus Time

Case 8: 8 m Linear Type 15 sec Simulation, 2 deg Aileron Input

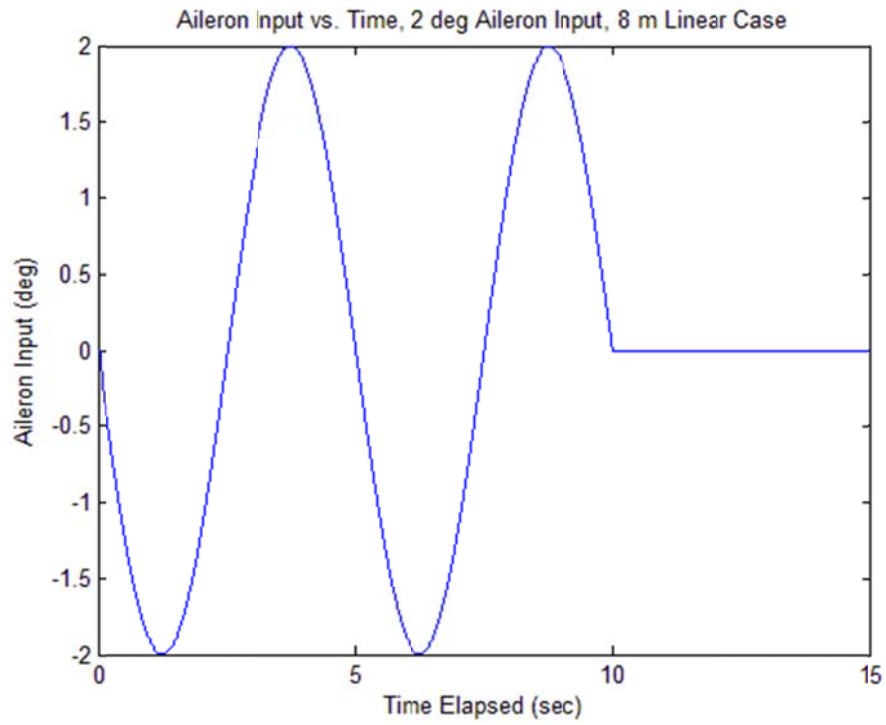


Figure 119. Case 8 Aileron Input versus Time

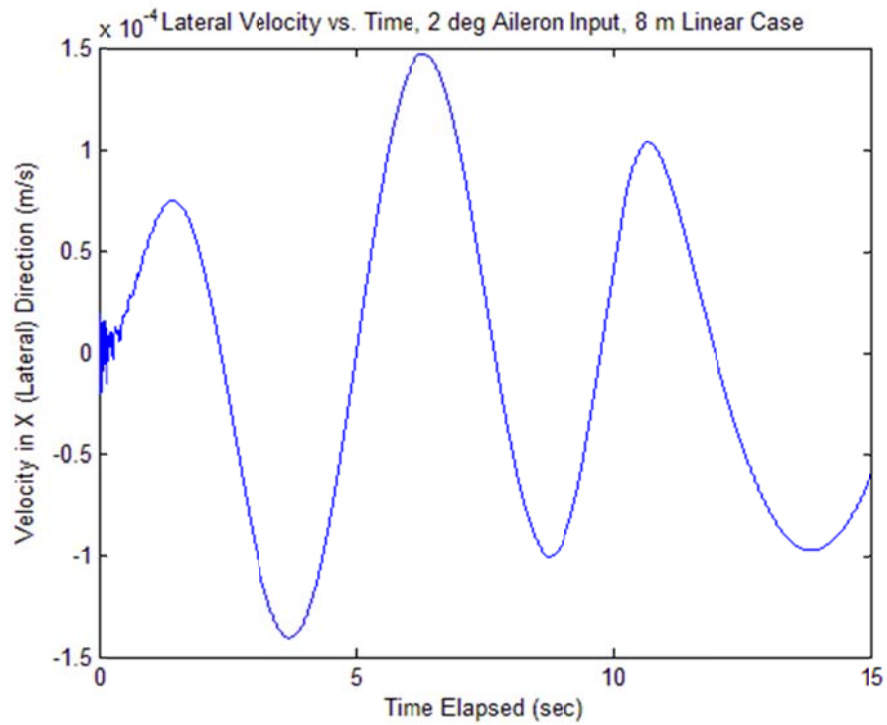


Figure 120. Case 8 Lateral Velocity v_x versus Time

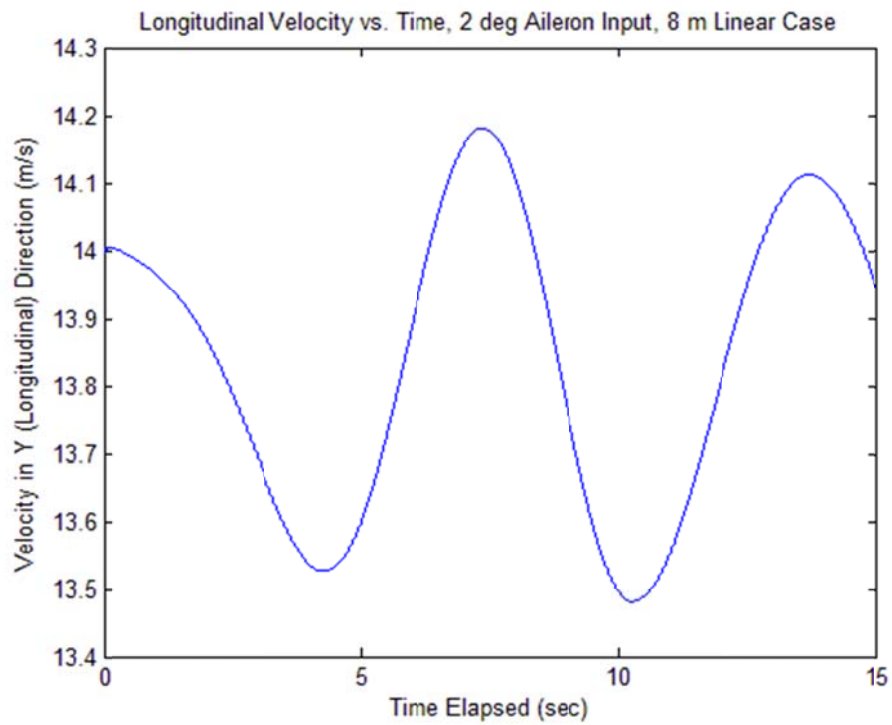


Figure 121. Case 8 Longitudinal Velocity v_y versus Time

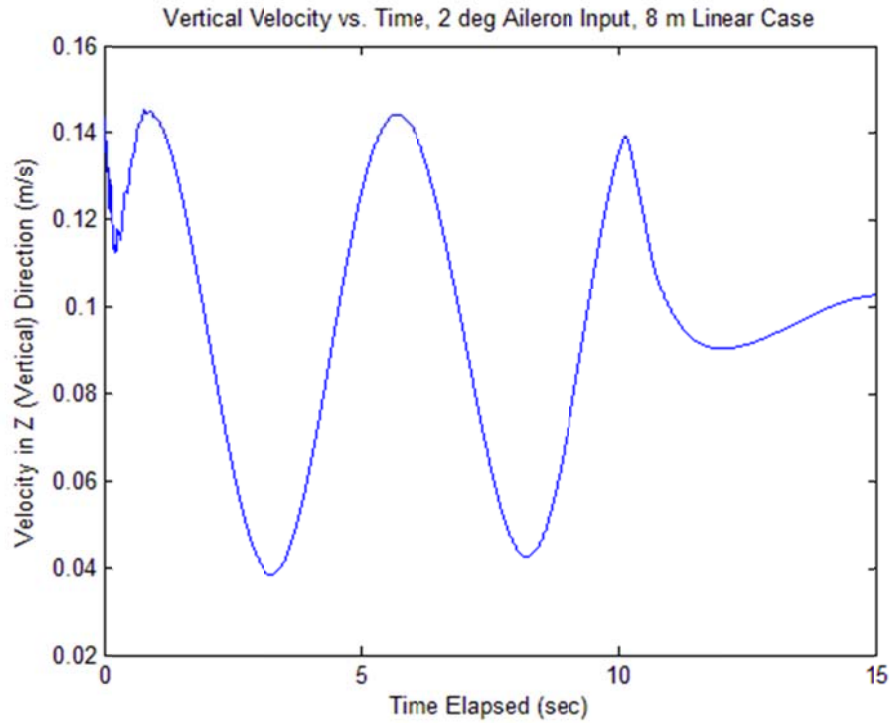


Figure 122. Case 8 Vertical Velocity v_z versus Time

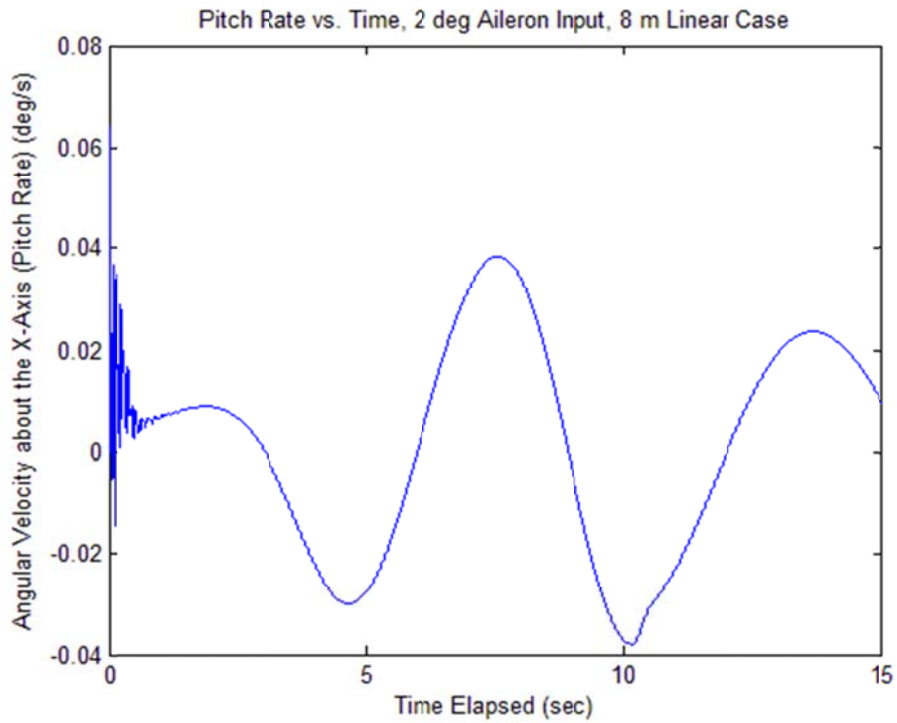


Figure 123. Case 8 Pitch Rate ω_x versus Time

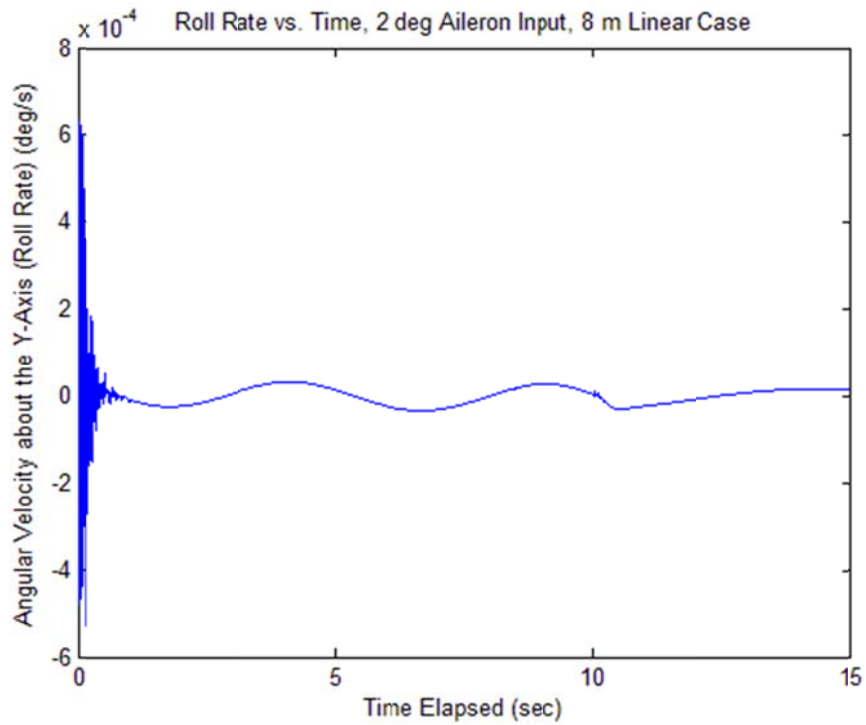


Figure 124. Case 8 Roll Rate ω_y versus Time

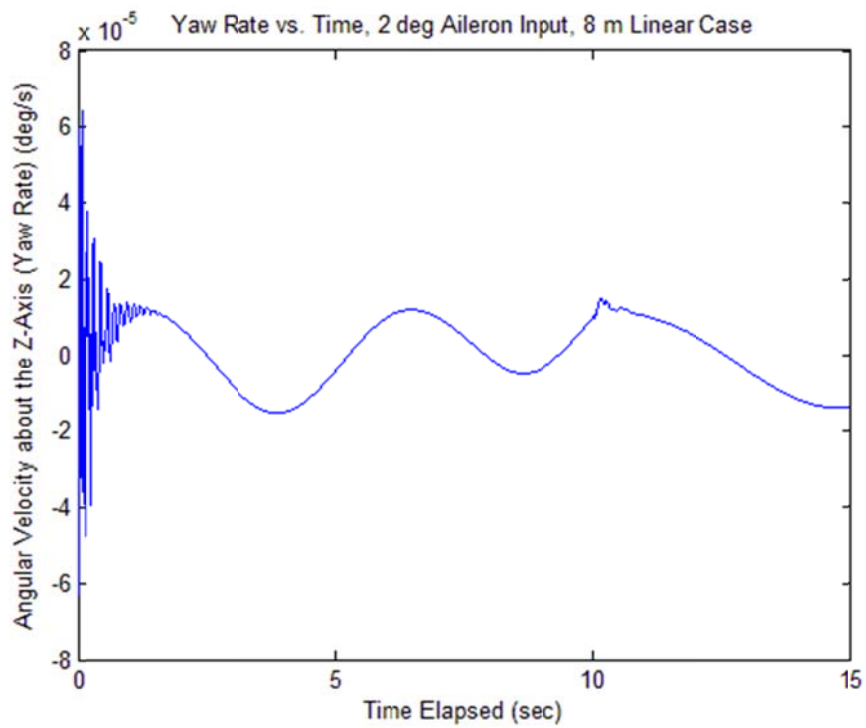


Figure 125. Case 8 Yaw Rate ω_z versus Time

Case 9: 8 m Nonlinear Type 15 sec Simulation, 2 deg Aileron Input

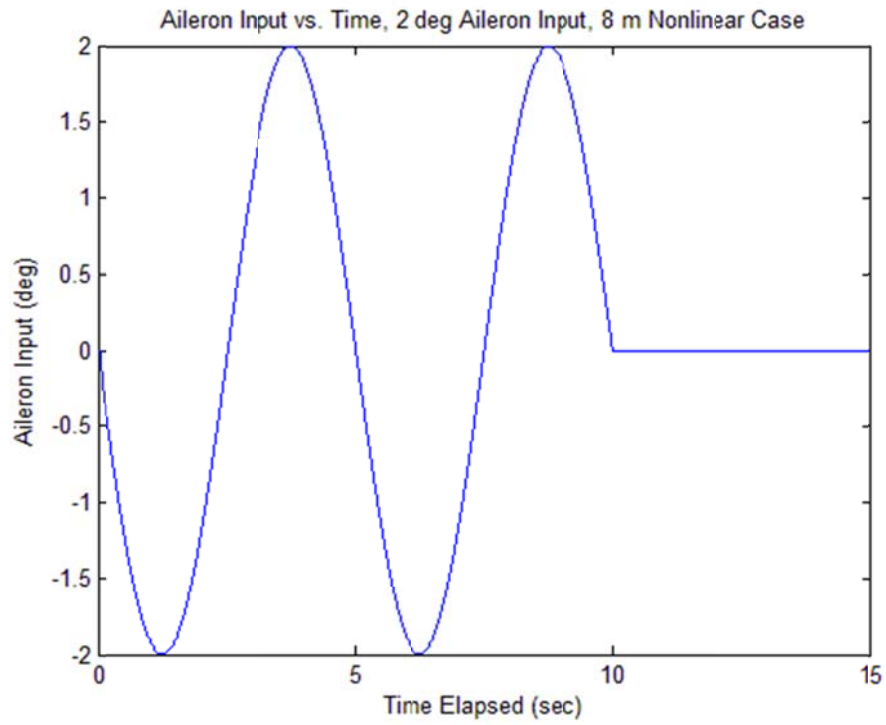


Figure 126. Case 9 Aileron Input versus Time

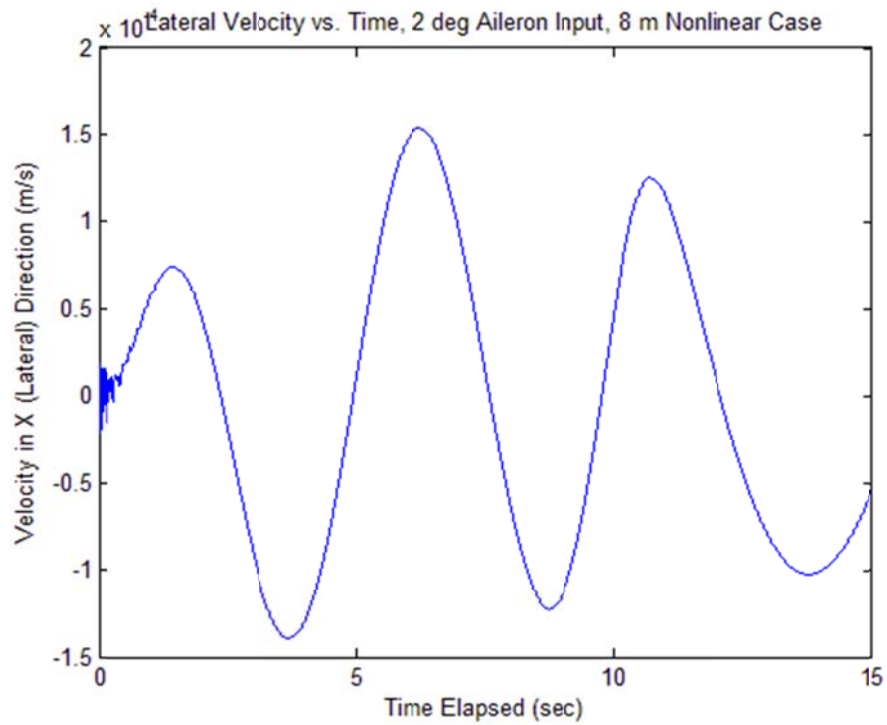


Figure 127. Case 9 Lateral Velocity v_x versus Time

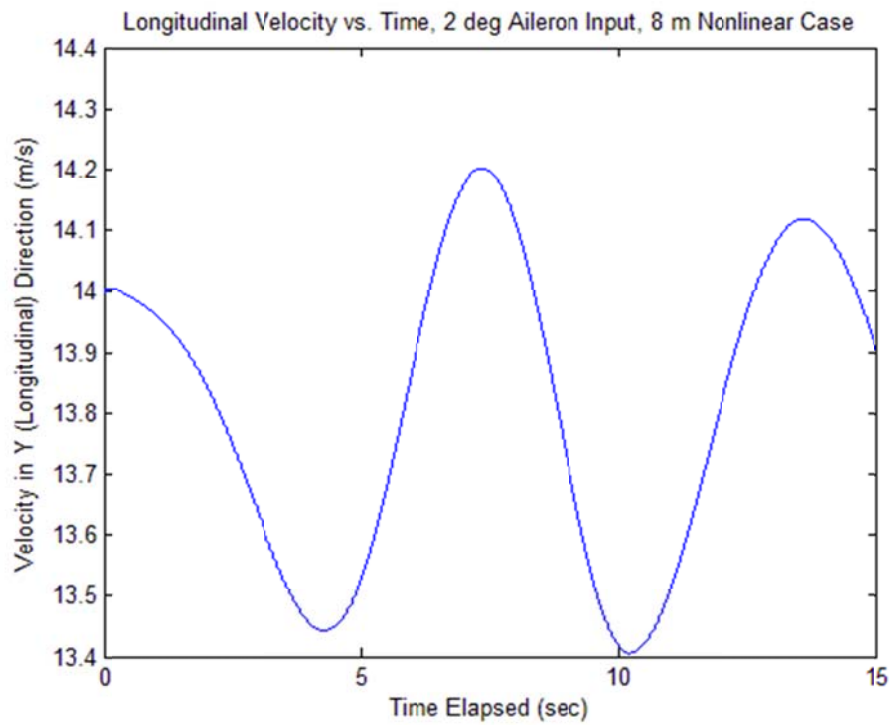


Figure 128. Case 9 Longitudinal Velocity v_y versus Time

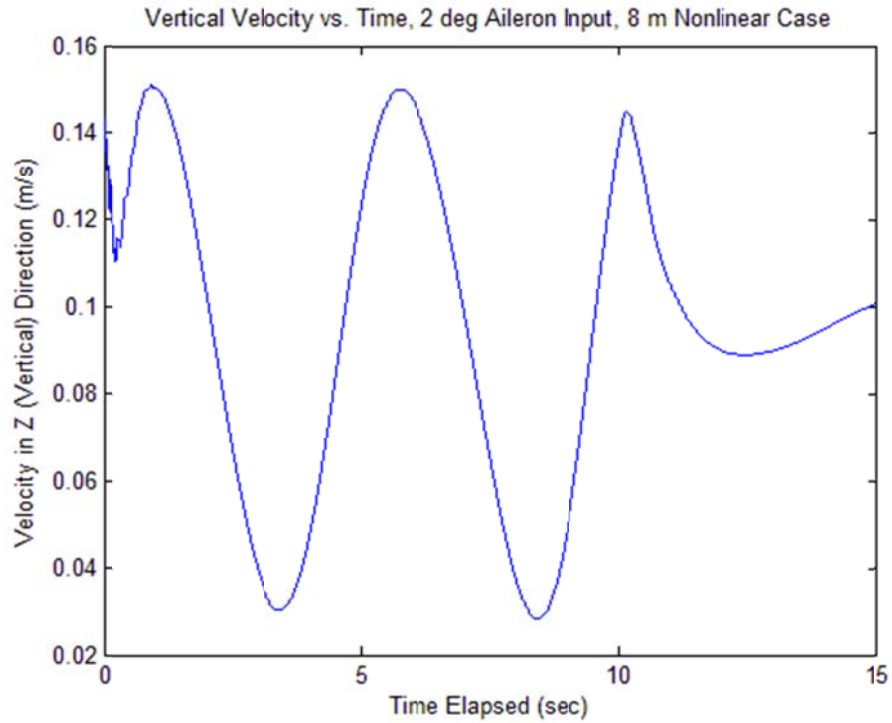


Figure 129. Case 9 Vertical Velocity v_z versus Time

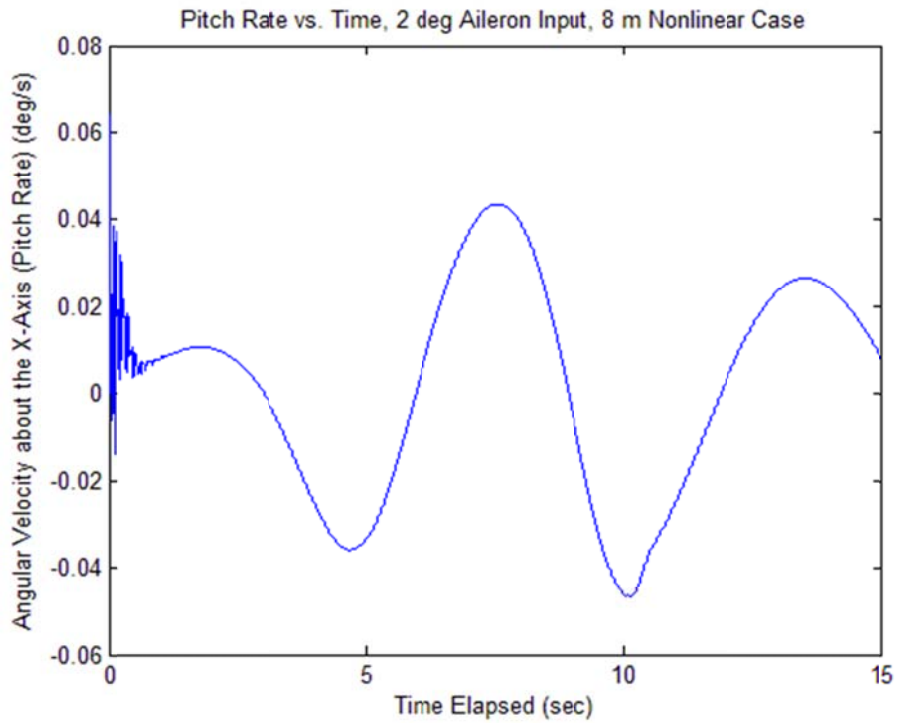


Figure 130. Case 9 Pitch Rate ω_x versus Time

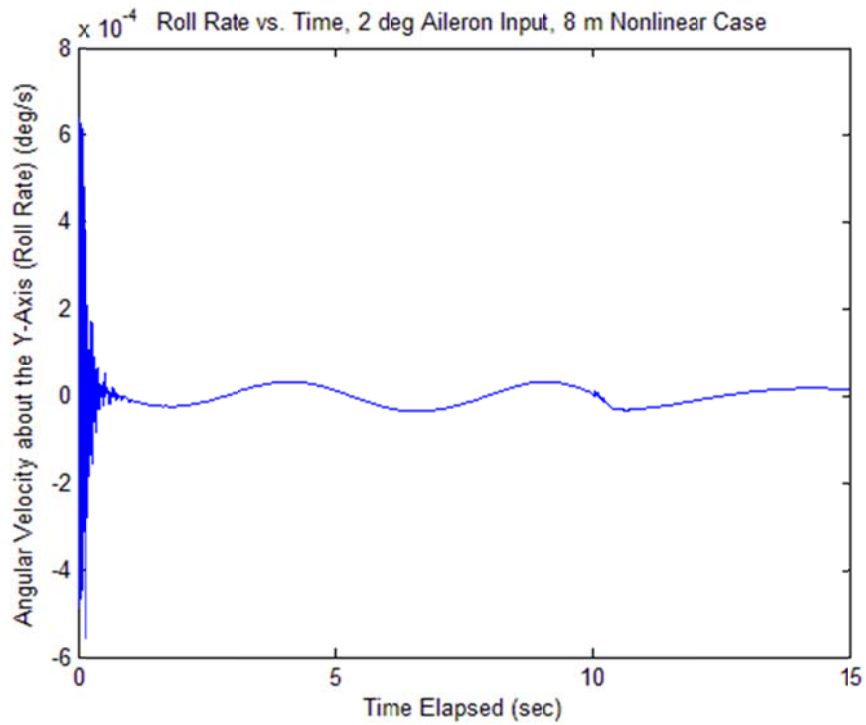


Figure 131. Case 9 Roll Rate ω_y versus Time

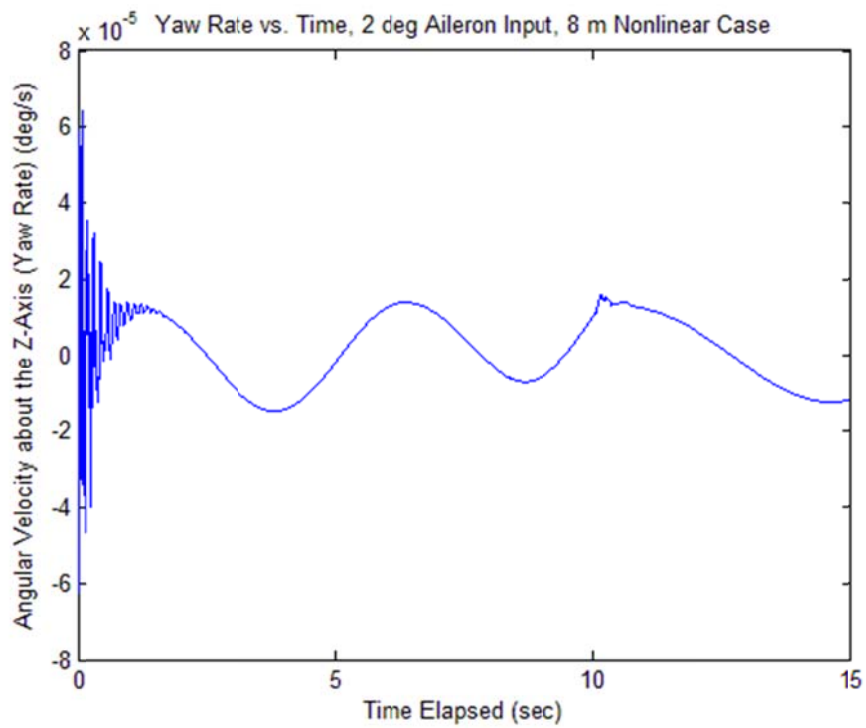


Figure 132. Case 9 Yaw Rate ω_z versus Time

Case 10: 8 m Linear Type 15 sec Simulation, 5 deg Aileron Input

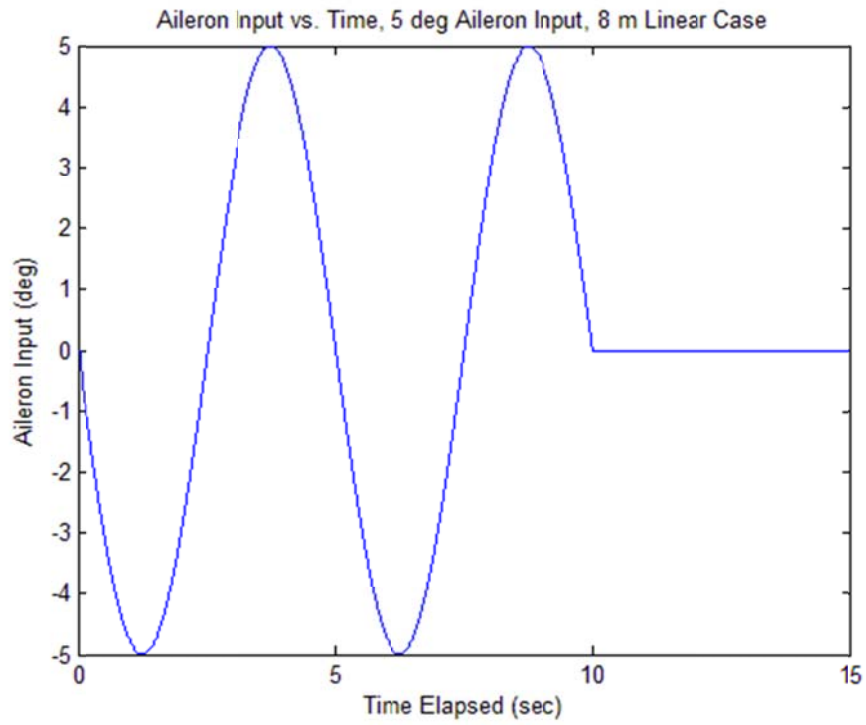


Figure 133. Case 10 Aileron Input versus Time

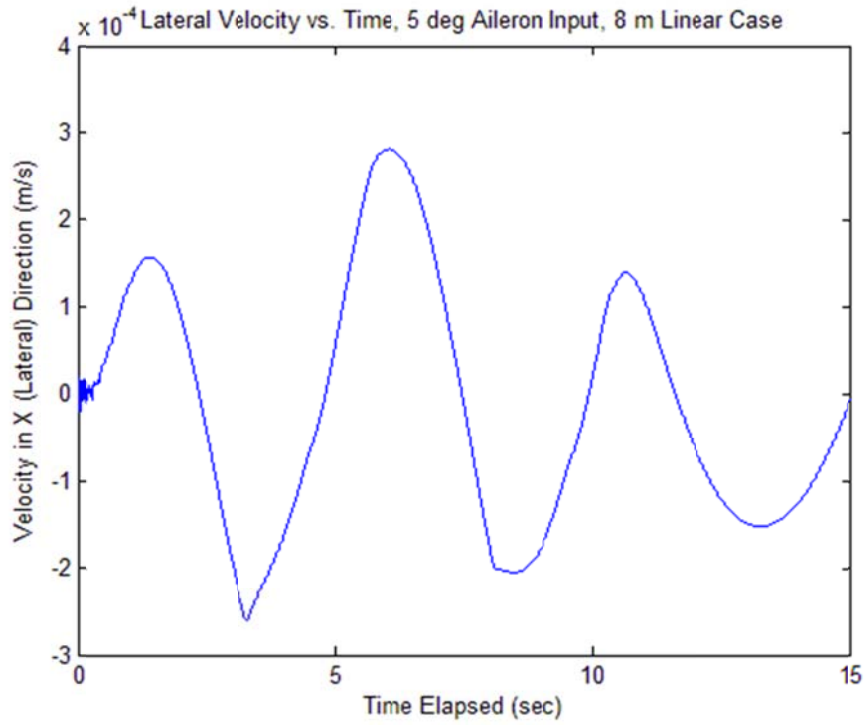


Figure 134. Case 10 Lateral Velocity v_x versus Time

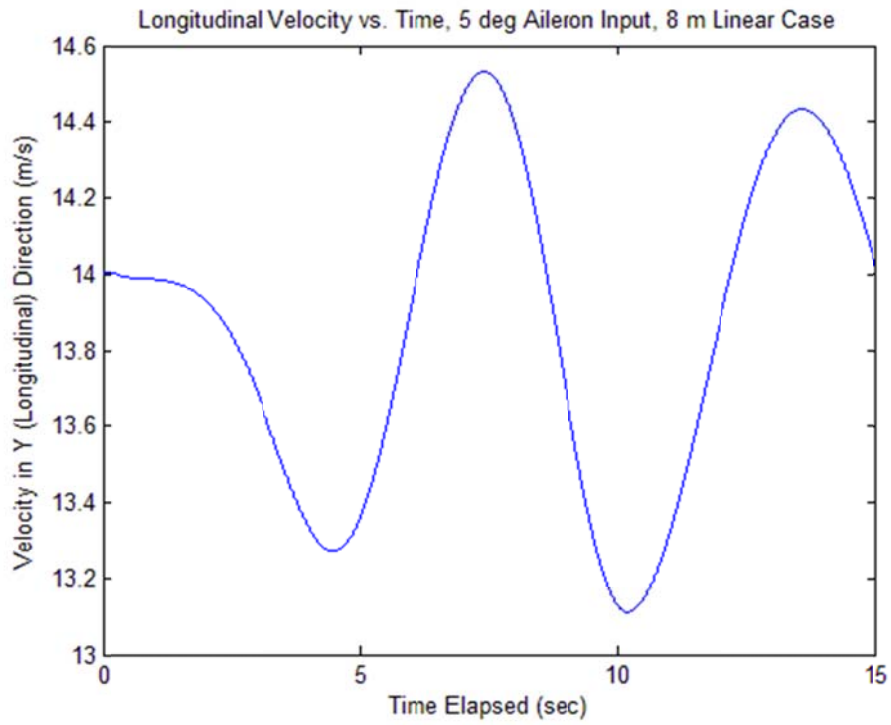


Figure 135. Case 10 Longitudinal Velocity v_y versus Time

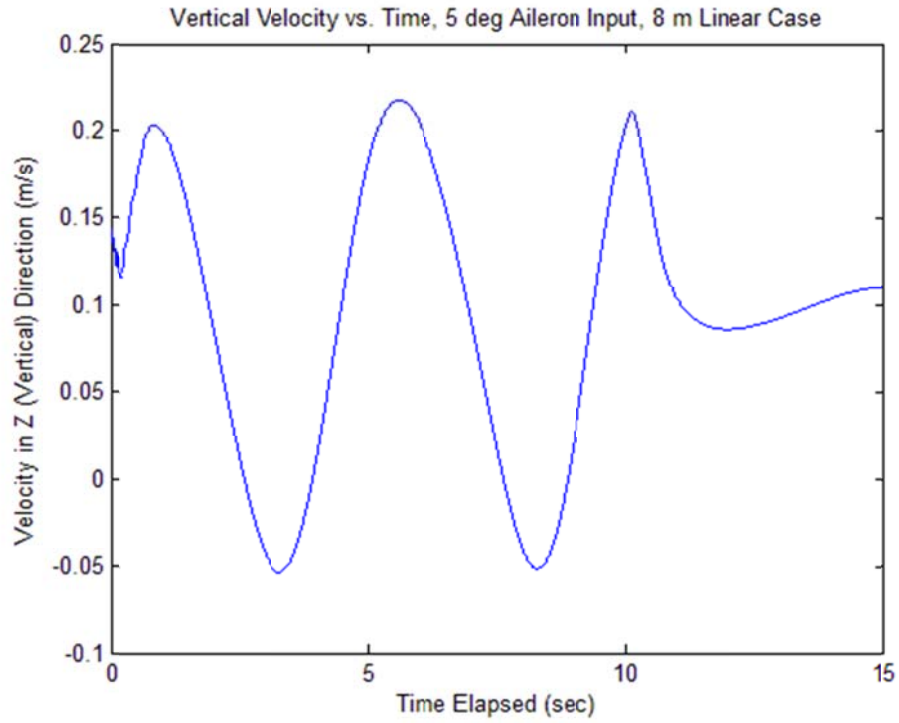


Figure 136. Case 10 Vertical Velocity v_z versus Time

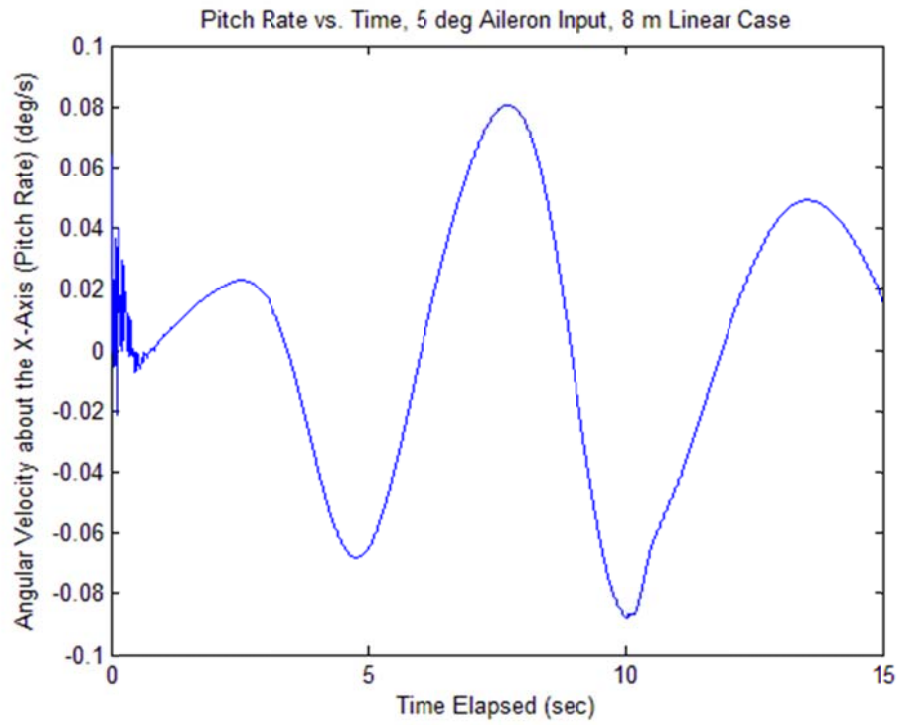


Figure 137. Case 10 Pitch Rate ω_x versus Time

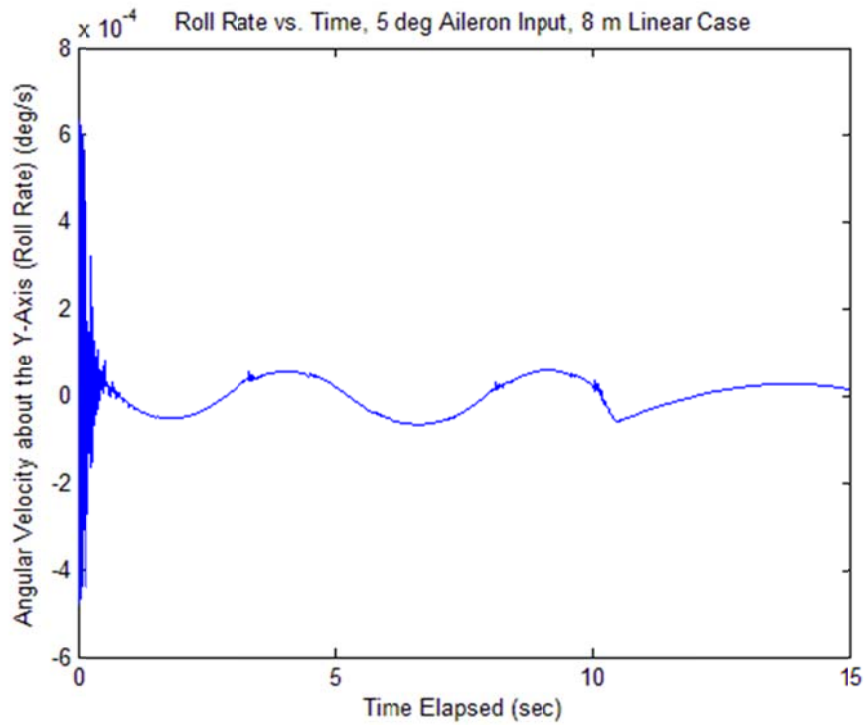


Figure 138. Case 10 Roll Rate ω_y versus Time

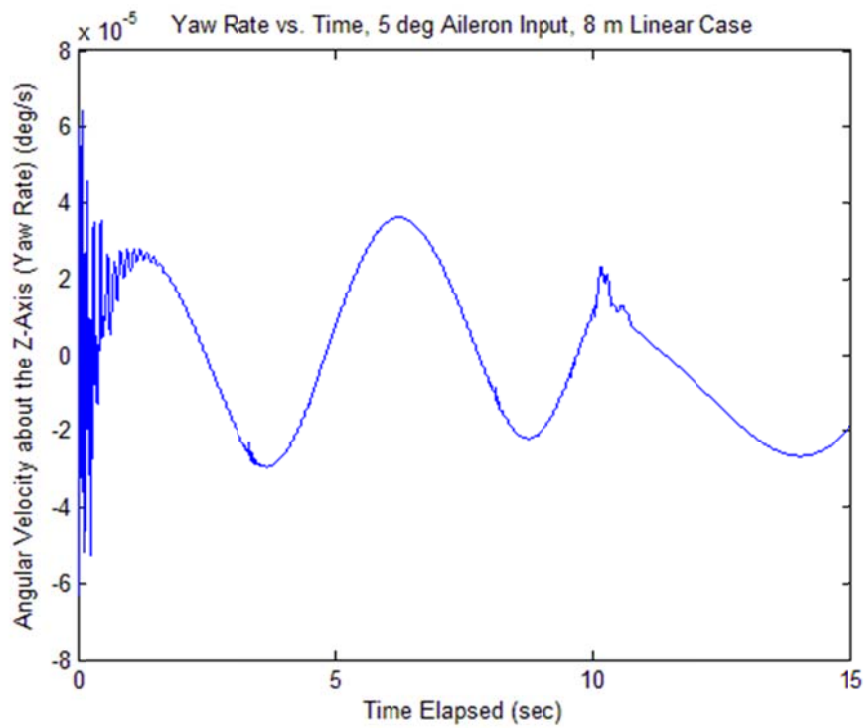


Figure 139. Case 10 Yaw Rate ω_z versus Time

Case 11: 8 m Nonlinear Type 15 sec Simulation, 5 deg Aileron Input

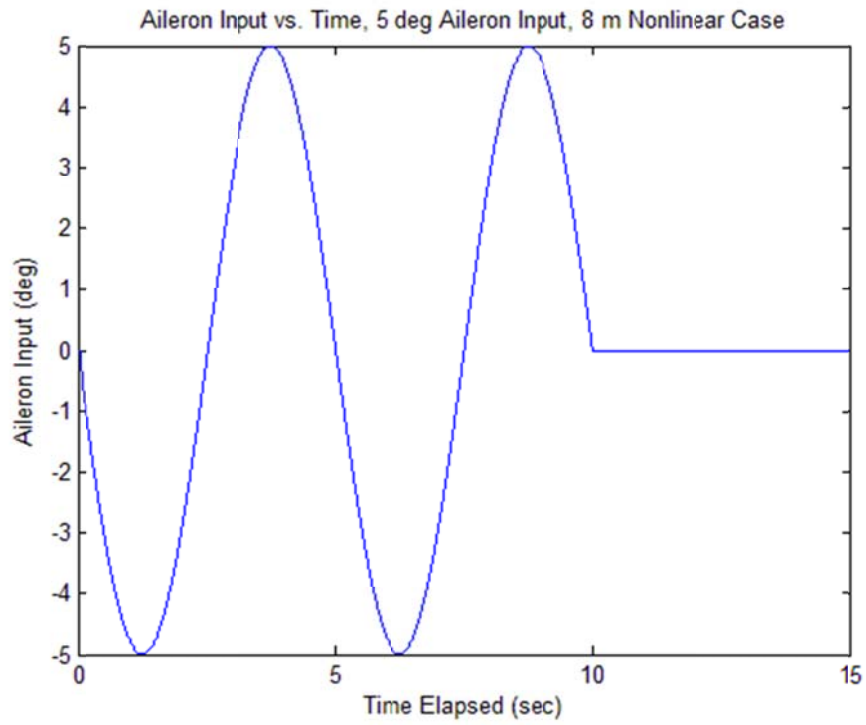


Figure 140. Case 11 Aileron Input versus Time

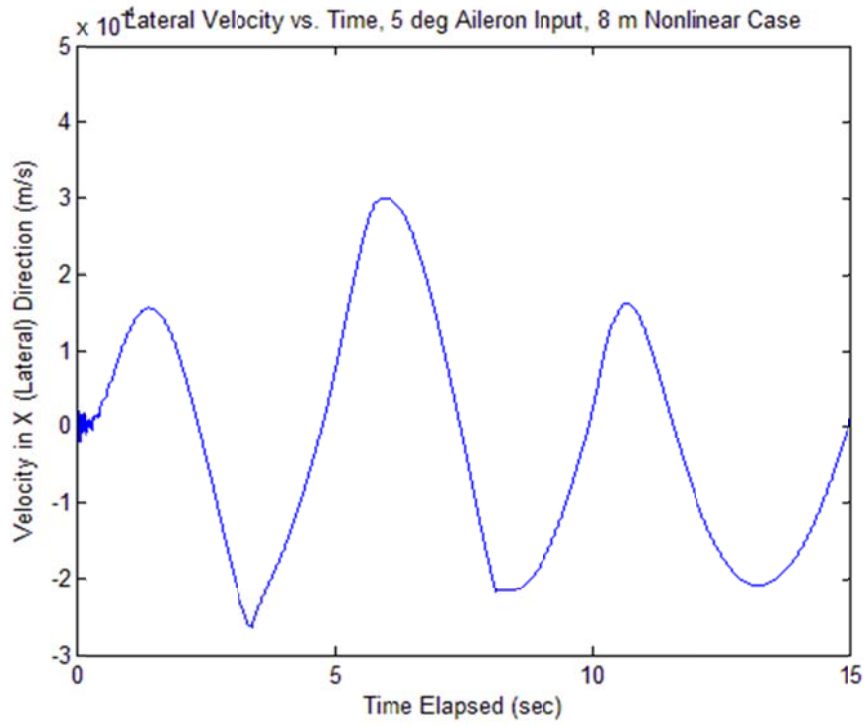


Figure 141. Case 11 Lateral Velocity v_x versus Time

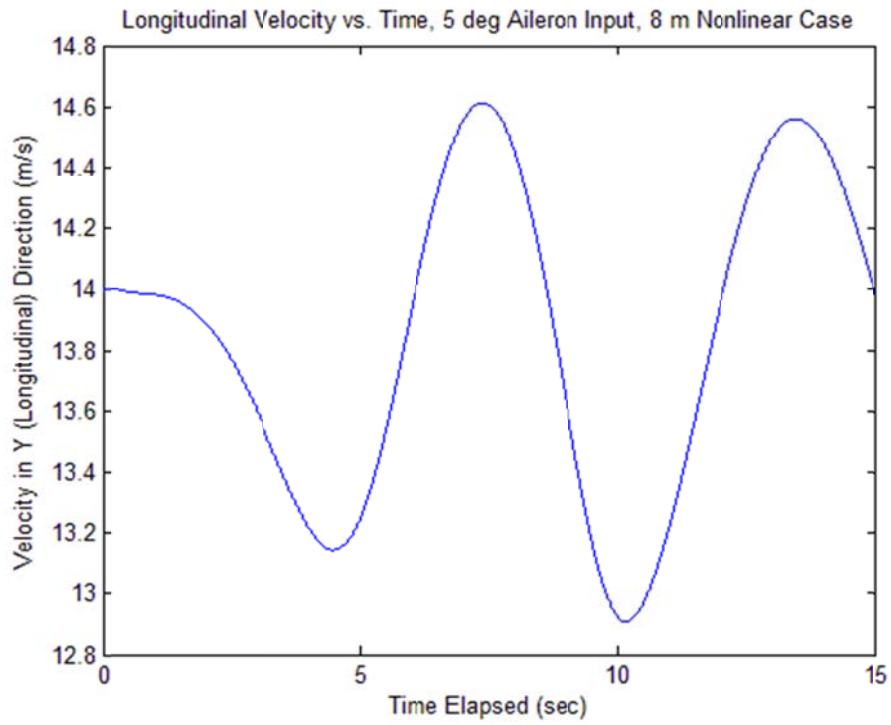


Figure 142. Case 11 Longitudinal Velocity v_y versus Time

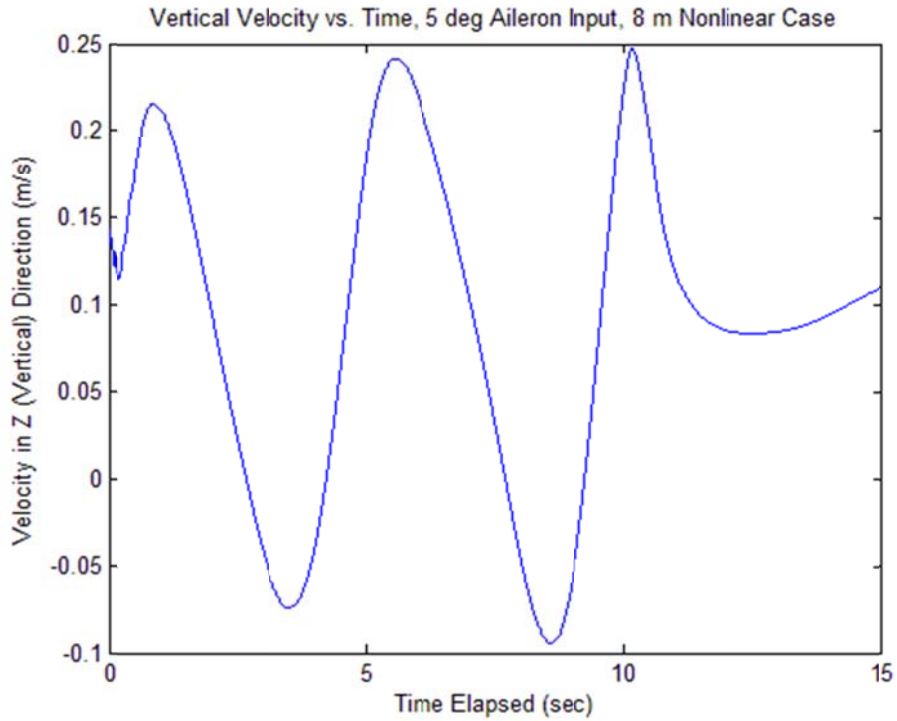


Figure 143. Case 11 Vertical Velocity v_z versus Time

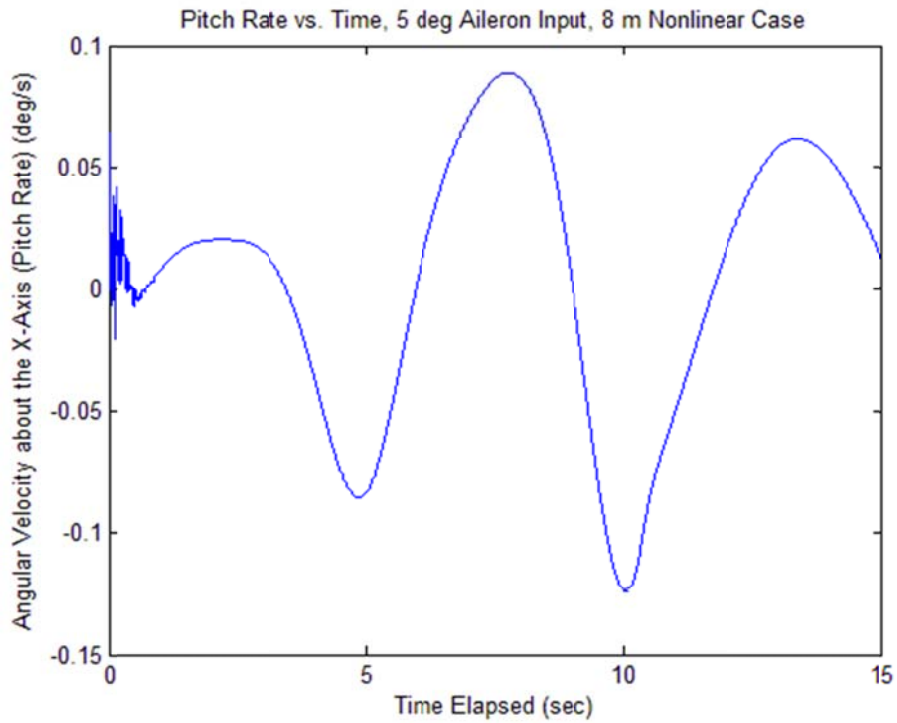


Figure 144. Case 11 Pitch Rate ω_x versus Time

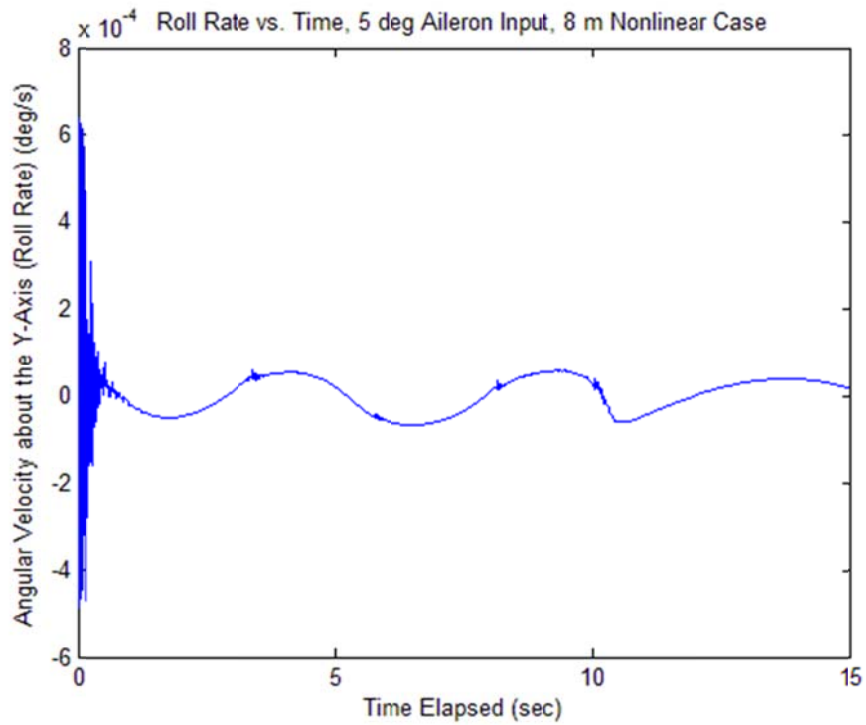


Figure 145. Case 11 Roll Rate ω_y versus Time

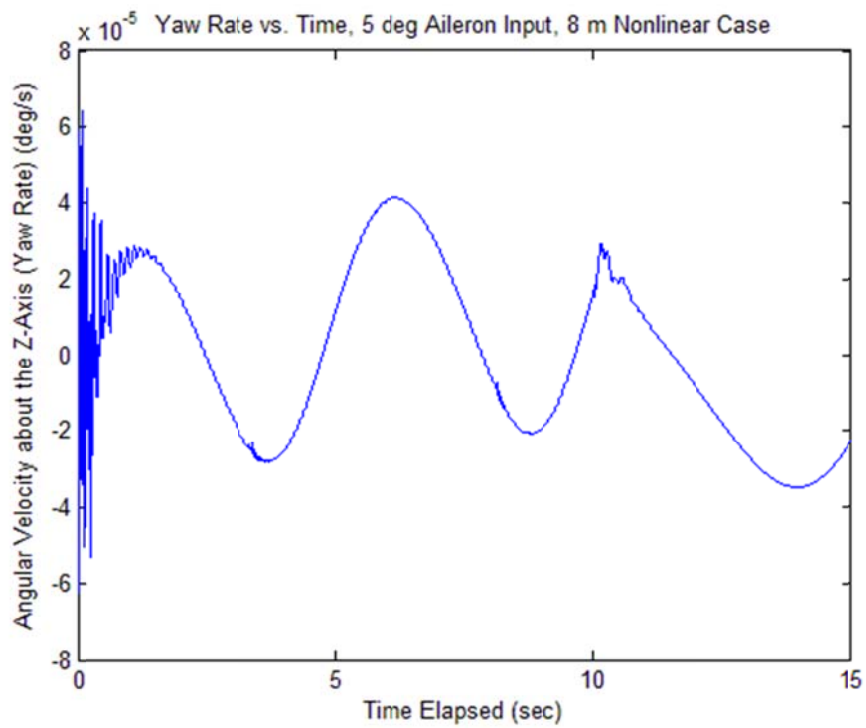


Figure 146. Case 11 Yaw Rate ω_z versus Time

Case 12: 8 m Linear Type 15 sec Simulation, 10 deg Aileron Input

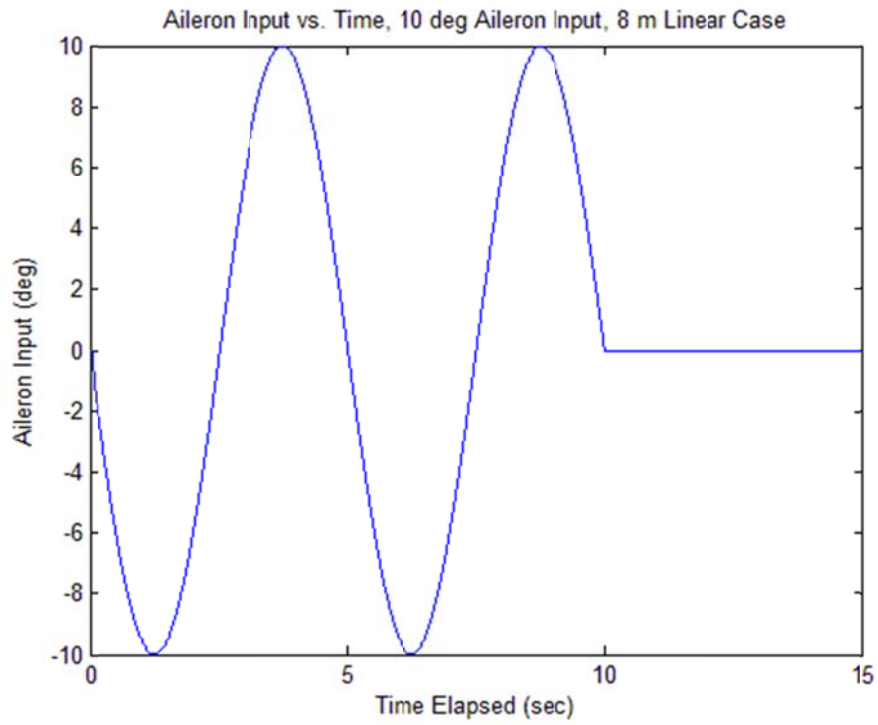


Figure 147. Case 12 Aileron Input versus Time

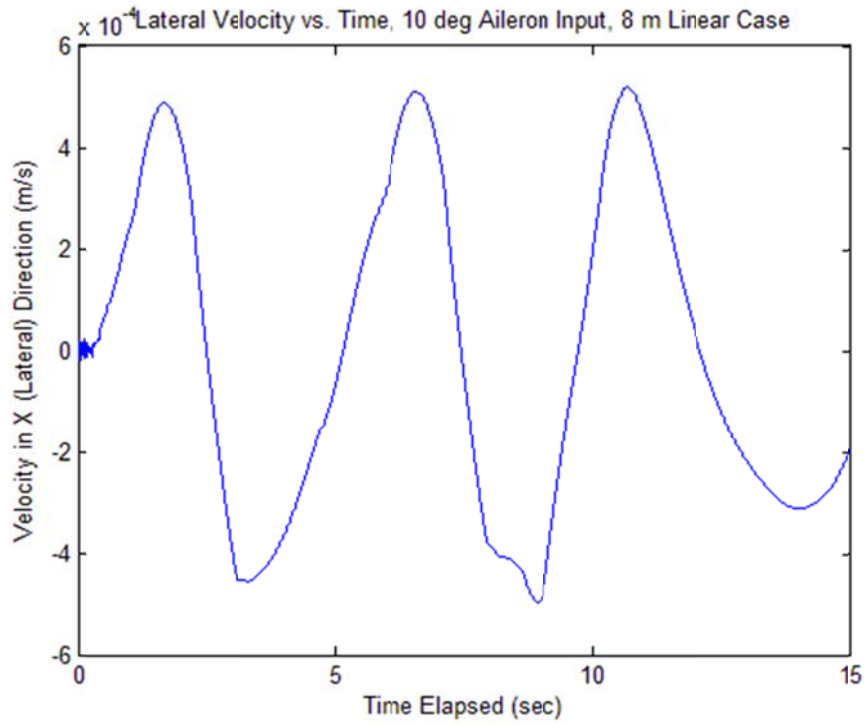


Figure 148. Case 12 Lateral Velocity v_x versus Time

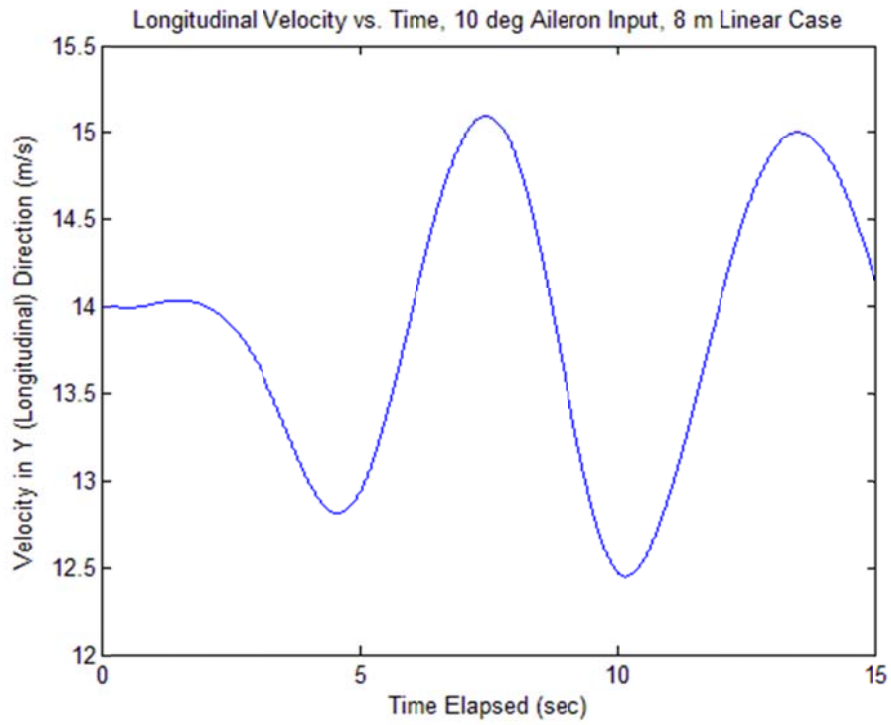


Figure 149. Case 12 Longitudinal Velocity v_y versus Time

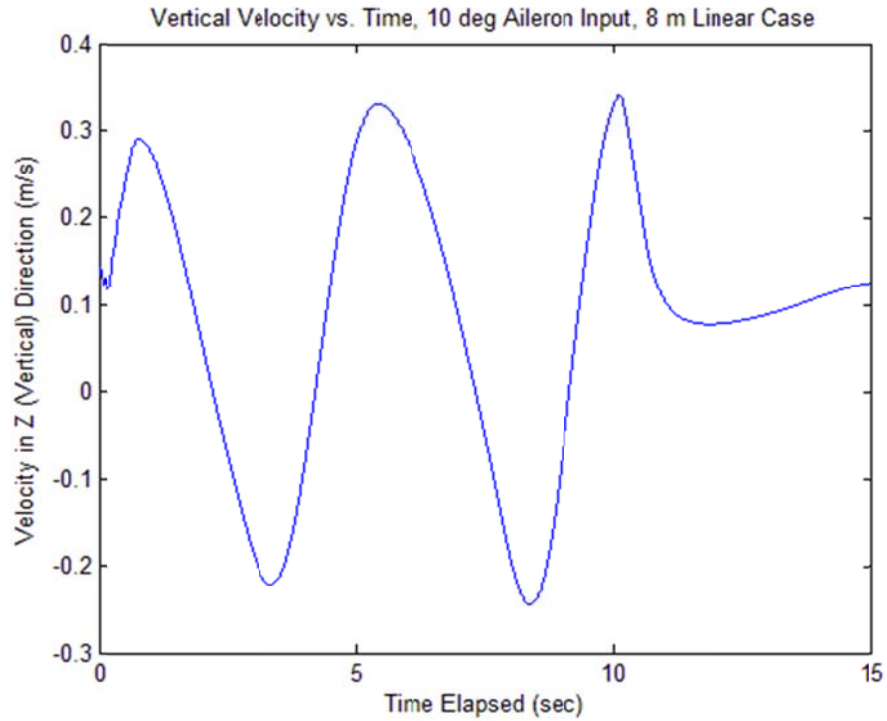


Figure 150. Case 12 Vertical Velocity v_z versus Time

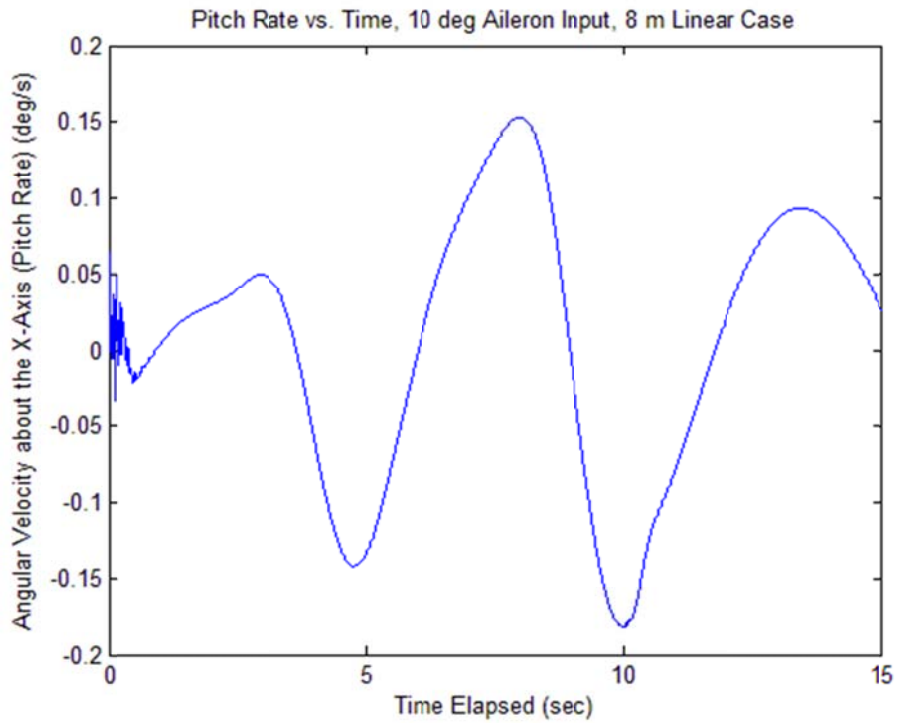


Figure 151. Case 12 Pitch Rate ω_x versus Time

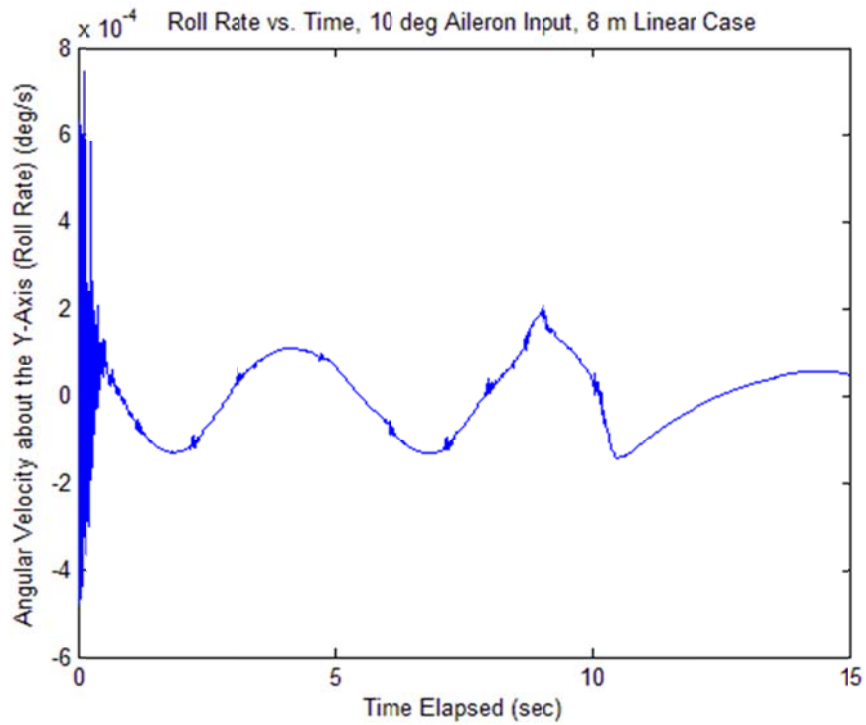


Figure 152. Case 12 Roll Rate ω_y versus Time

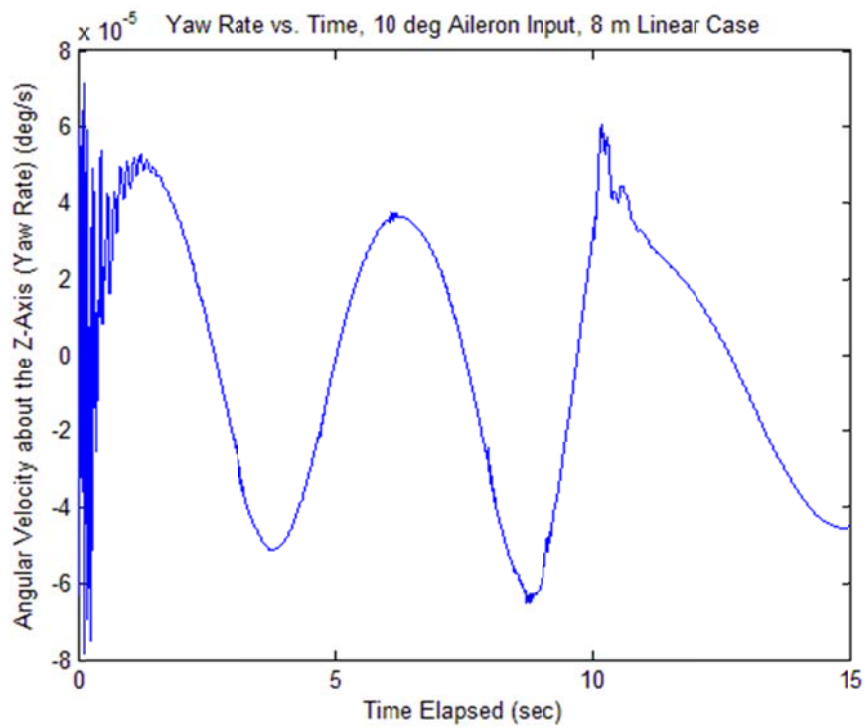


Figure 153. Case 12 Yaw Rate ω_z versus Time

Case 13: 8 m Nonlinear Type 15 sec Simulation, 10 deg Aileron Input

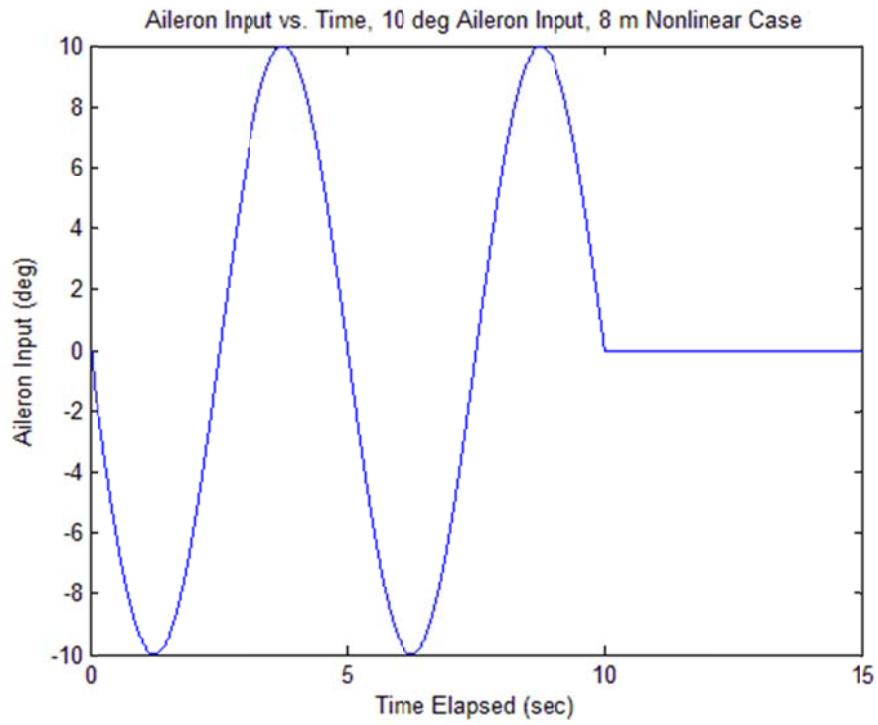


Figure 154. Case 13 Aileron Input versus Time

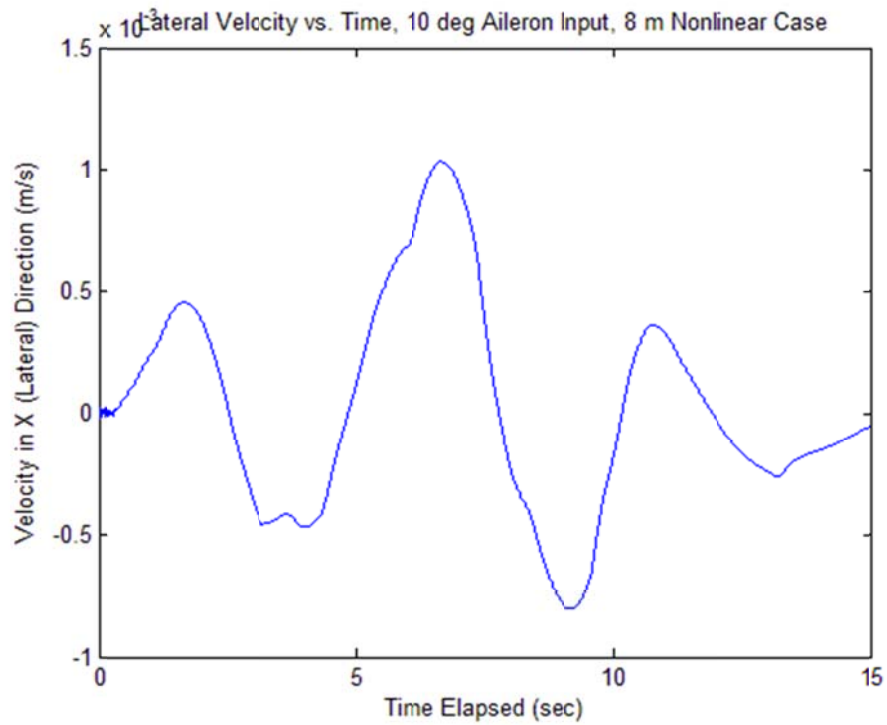


Figure 155. Case 13 Lateral Velocity v_x versus Time

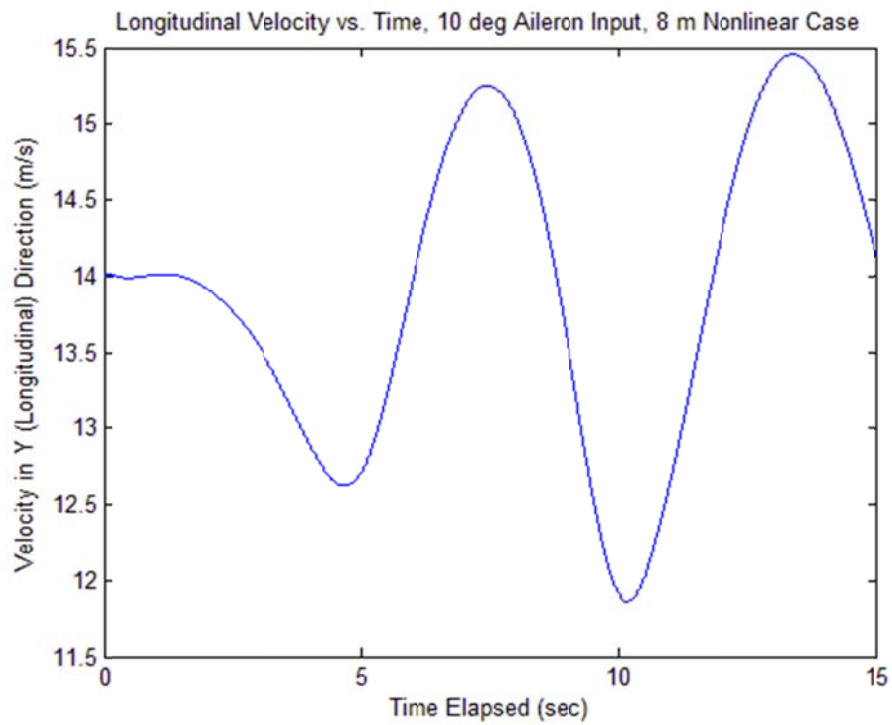


Figure 156. Case 13 Longitudinal Velocity v_y versus Time

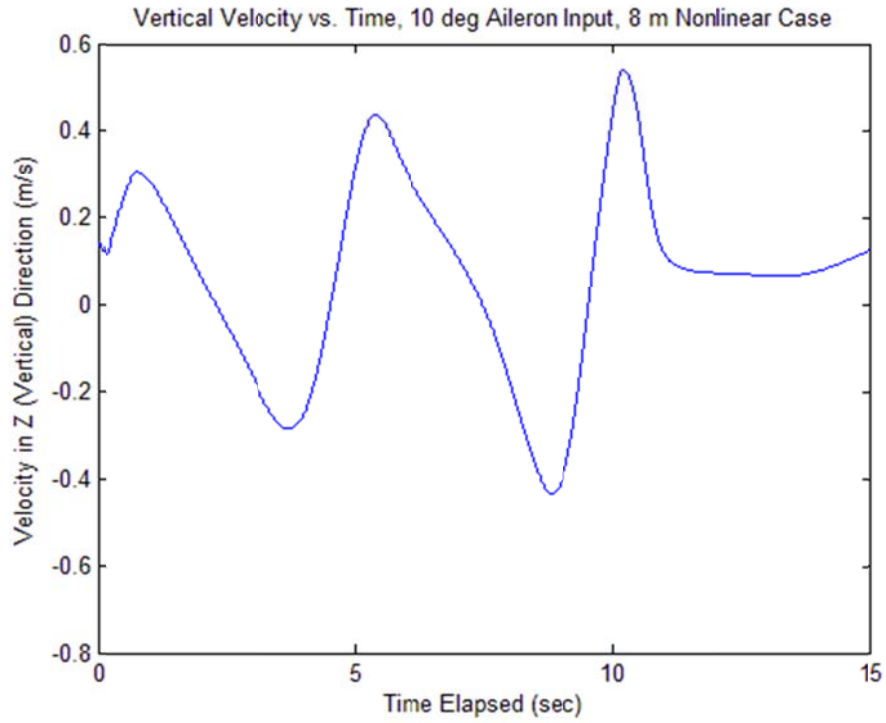


Figure 157. Case 13 Vertical Velocity v_z versus Time

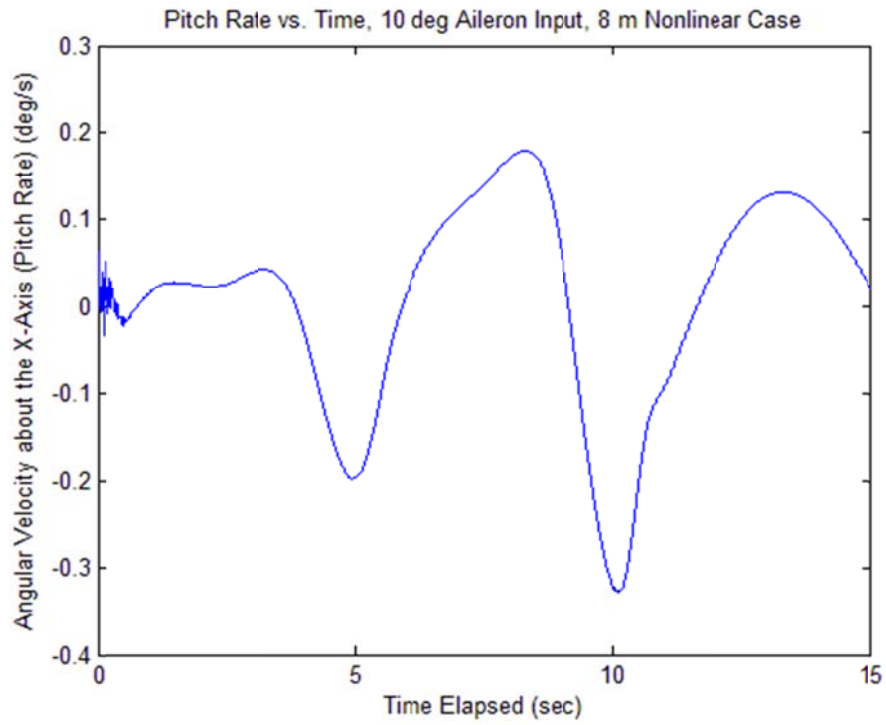


Figure 158. Case 13 Pitch Rate ω_x versus Time

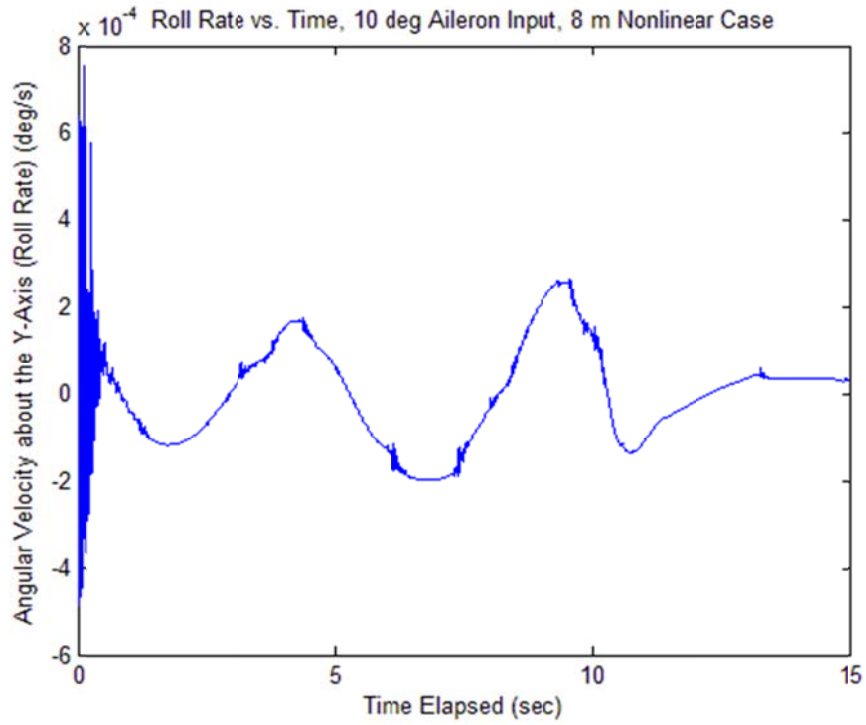


Figure 159. Case 13 Roll Rate ω_y versus Time

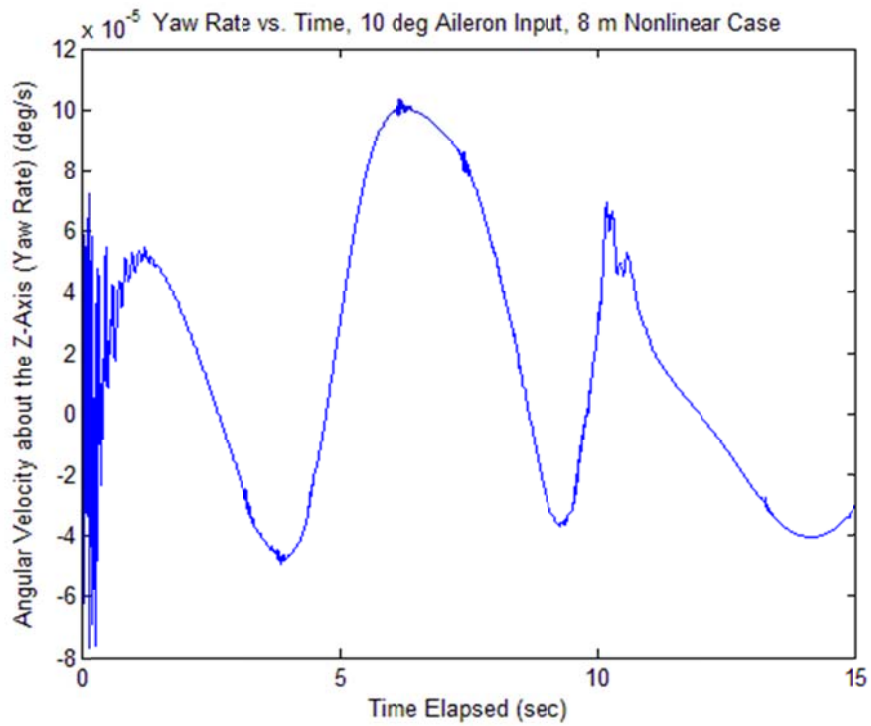


Figure 160. Case 13 Yaw Rate ω_z versus Time

Case 14: 8 m Linear Type 15 sec Simulation, 15 deg Aileron Input

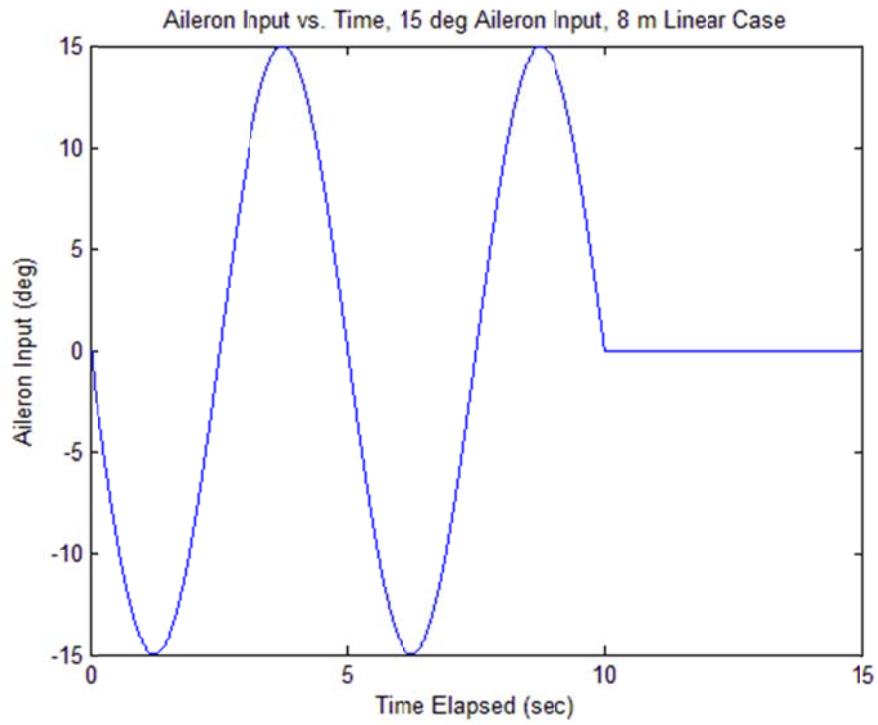


Figure 161. Case 14 Aileron Input versus Time

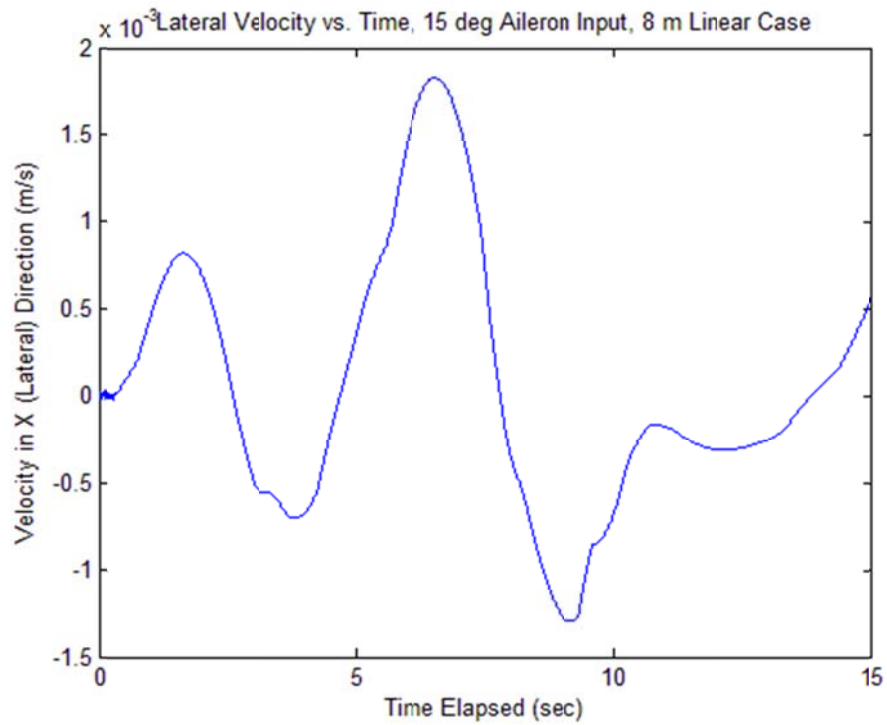


Figure 162. Case 14 Lateral Velocity v_x versus Time

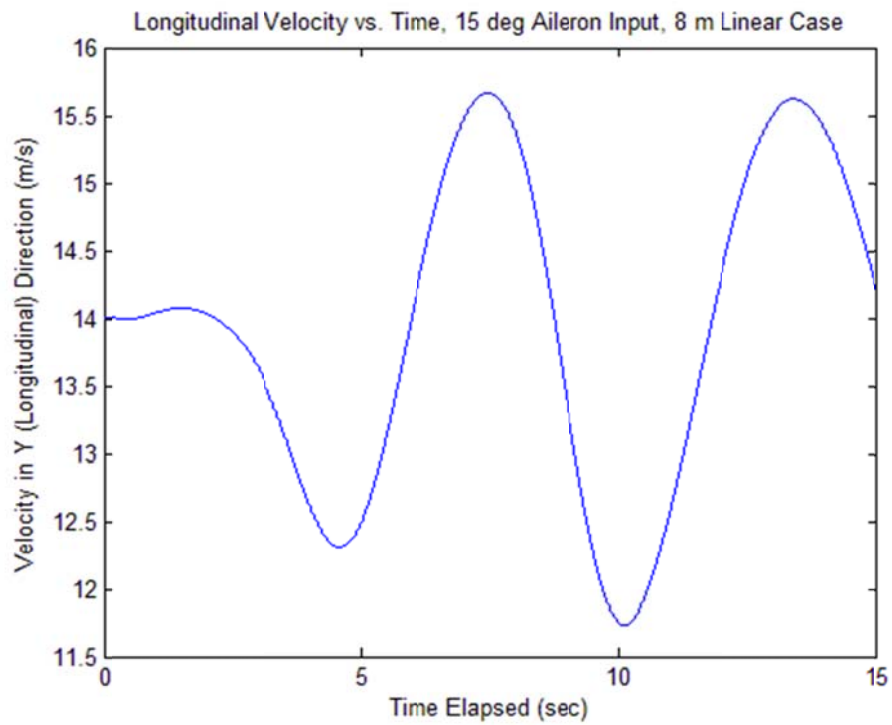


Figure 163. Case 14 Longitudinal Velocity v_y versus Time

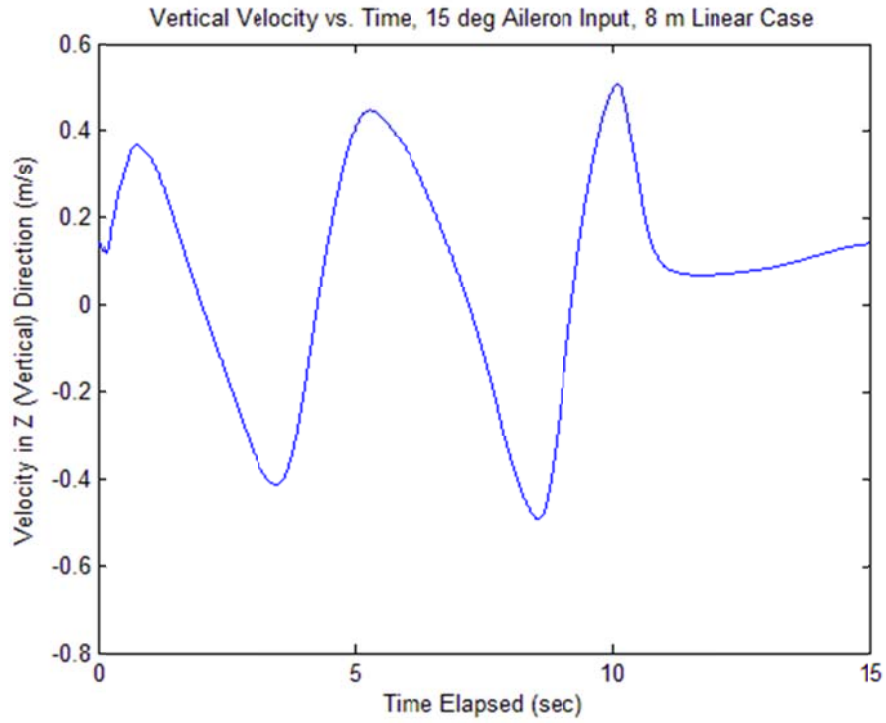


Figure 164. Case 14 Vertical Velocity v_z versus Time

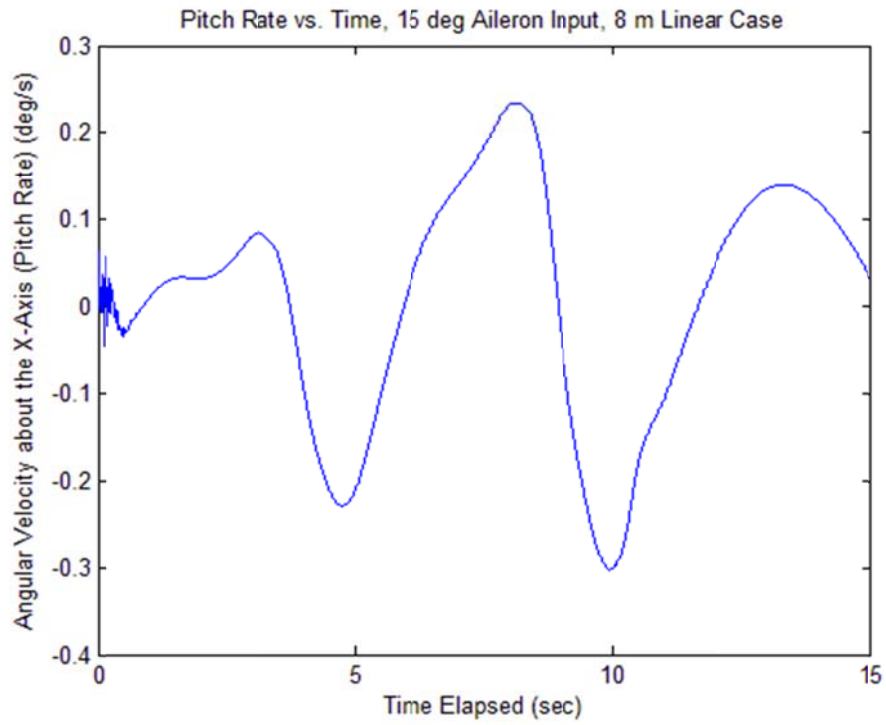


Figure 165. Case 14 Pitch Rate ω_x versus Time

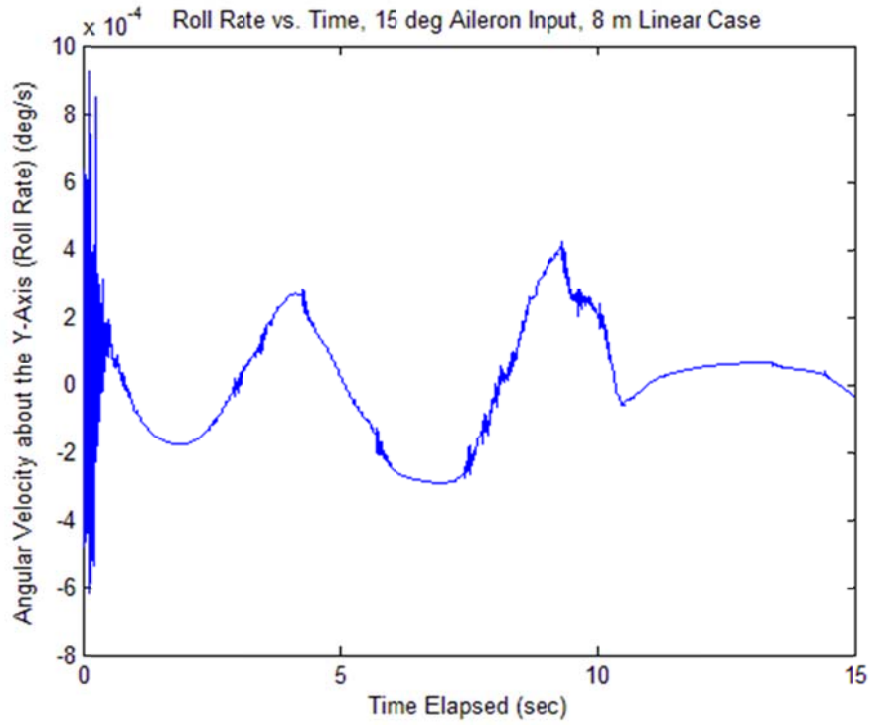


Figure 166. Case 14 Roll Rate ω_y versus Time

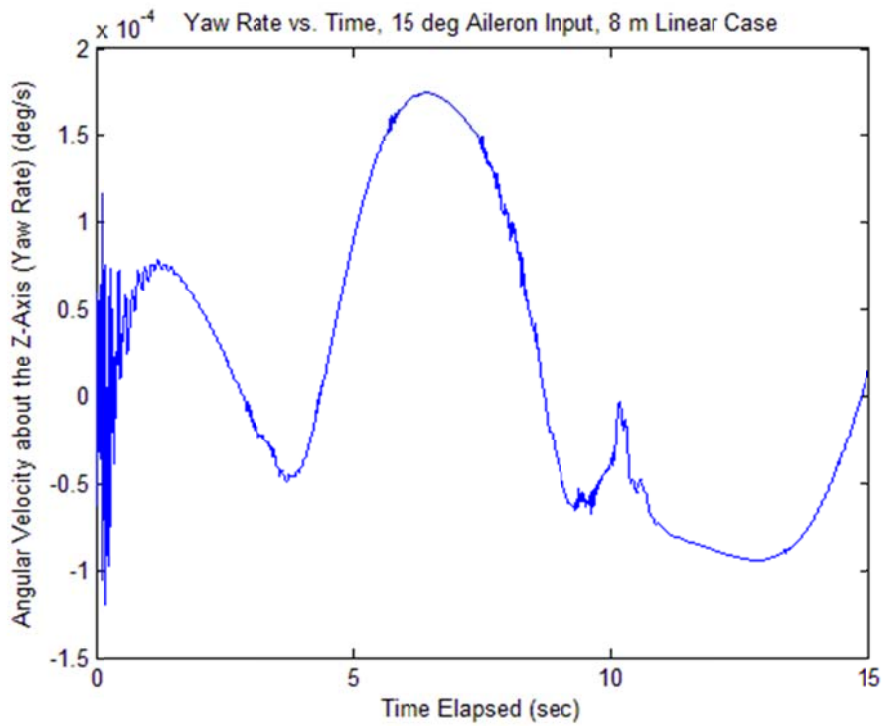


Figure 167. Case 14 Yaw Rate ω_z versus Time

Case 15: 8 m Nonlinear Type 15 sec Simulation, 15 deg Aileron Input

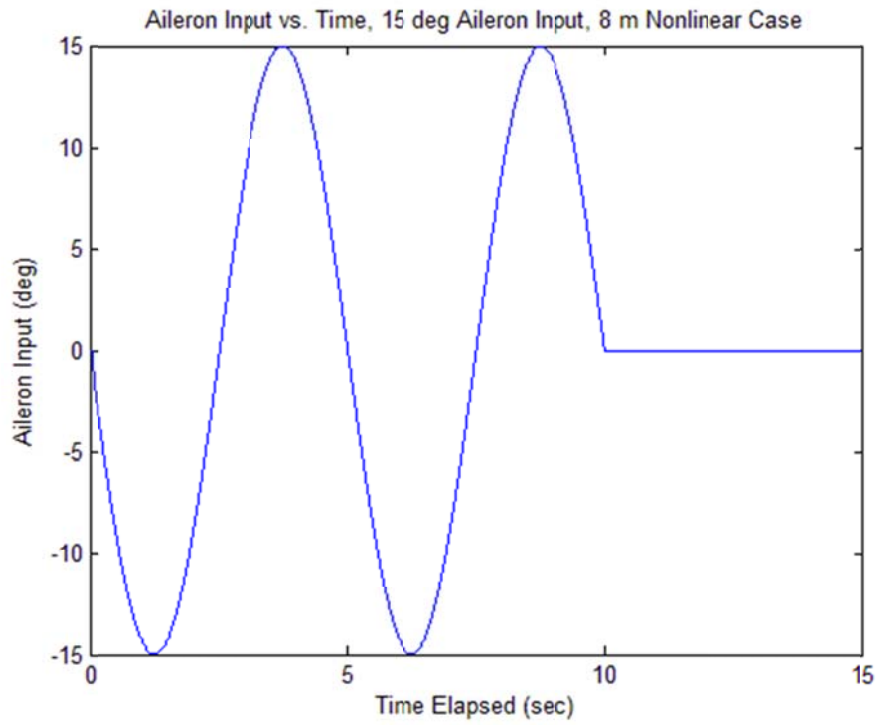


Figure 168. Case 15 Aileron Input versus Time

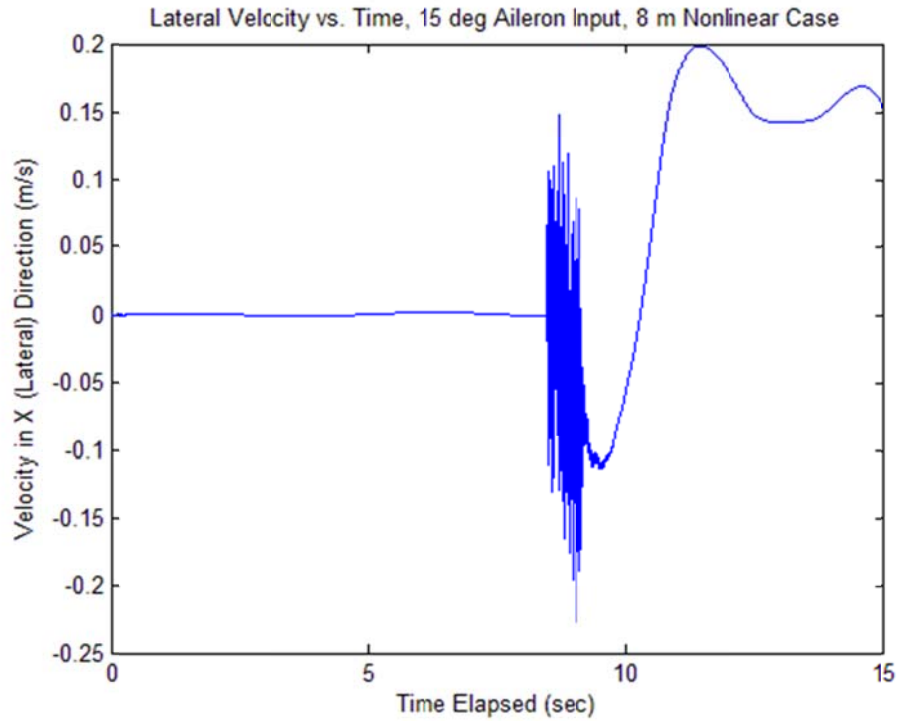


Figure 169. Case 15 Lateral Velocity v_x versus Time

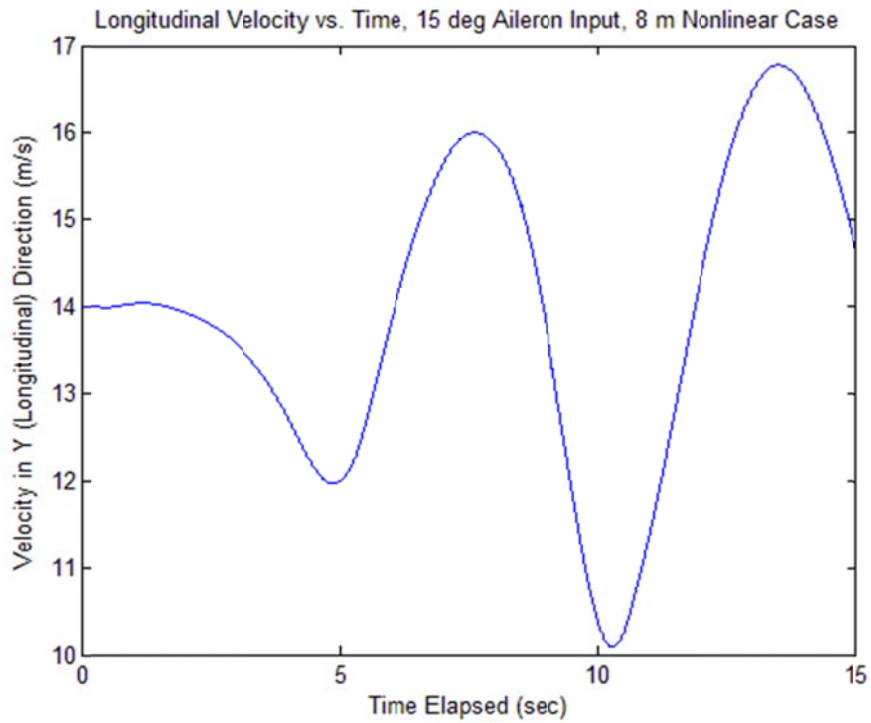


Figure 170. Case 15 Longitudinal Velocity v_y versus Time

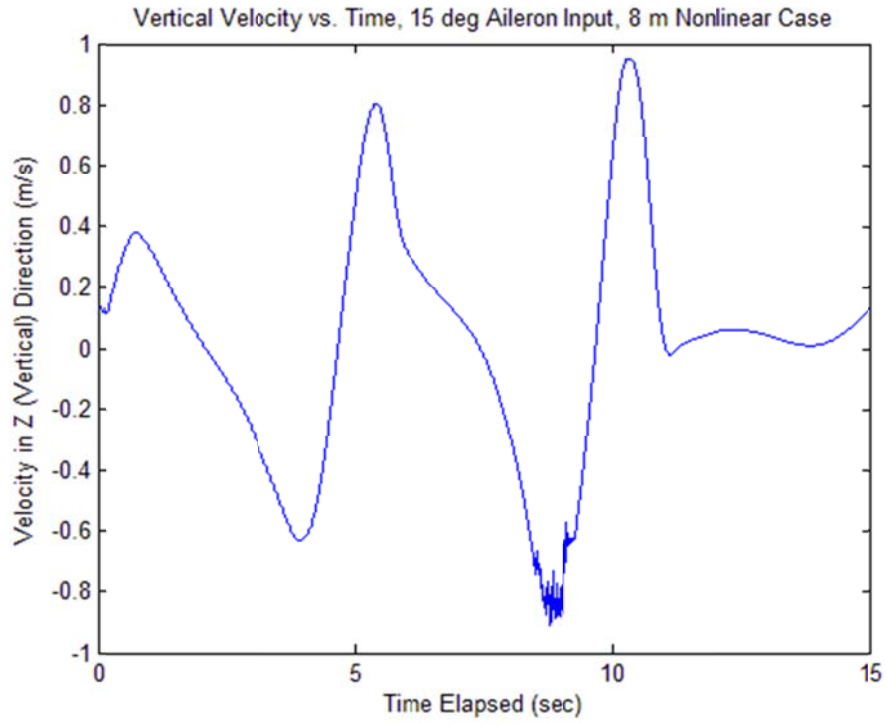


Figure 171. Case 15 Vertical Velocity v_z versus Time

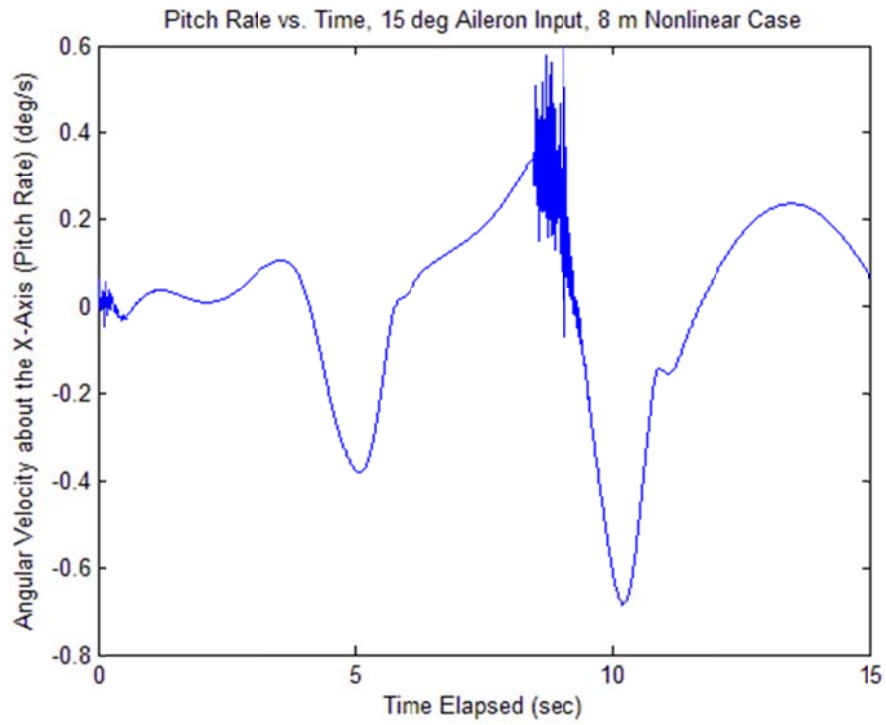


Figure 172. Case 15 Pitch Rate ω_x versus Time

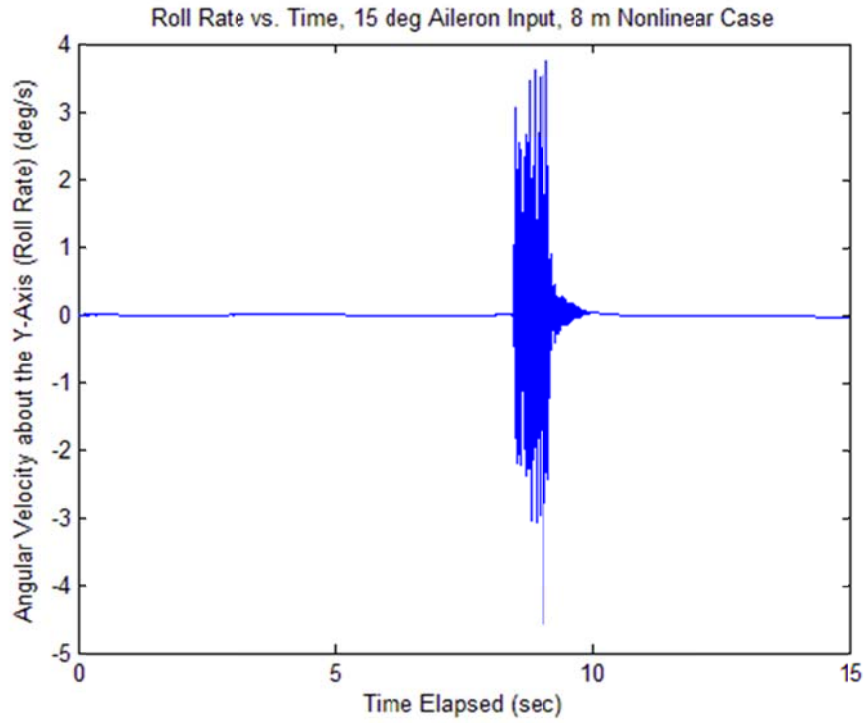


Figure 173. Case 15 Roll Rate ω_y versus Time

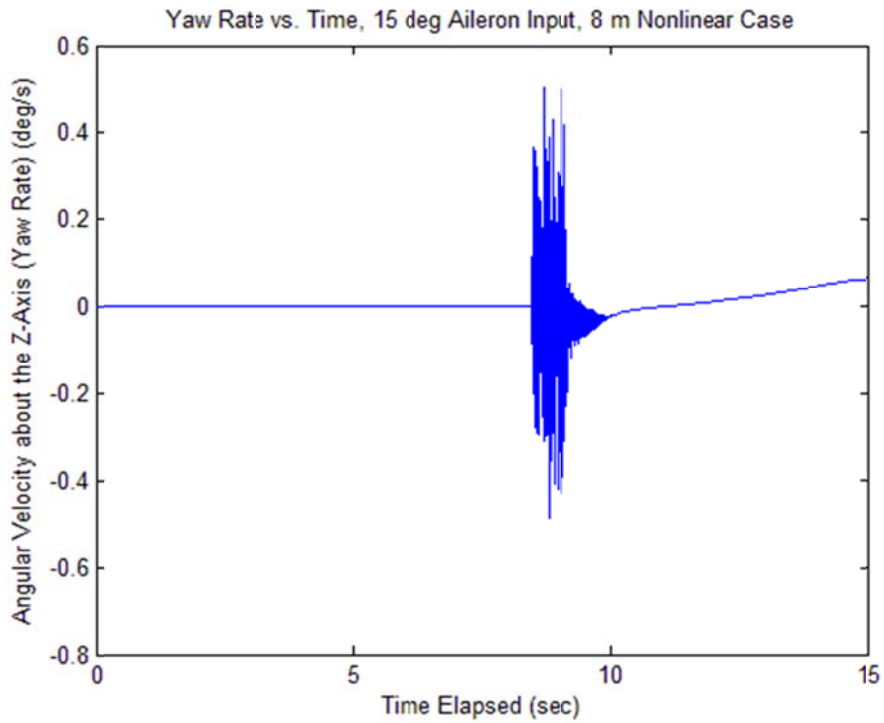


Figure 174. Case 15 Yaw Rate ω_z versus Time

Case 16: 8 m Linear Type 15 sec Simulation, 20 deg Aileron Input

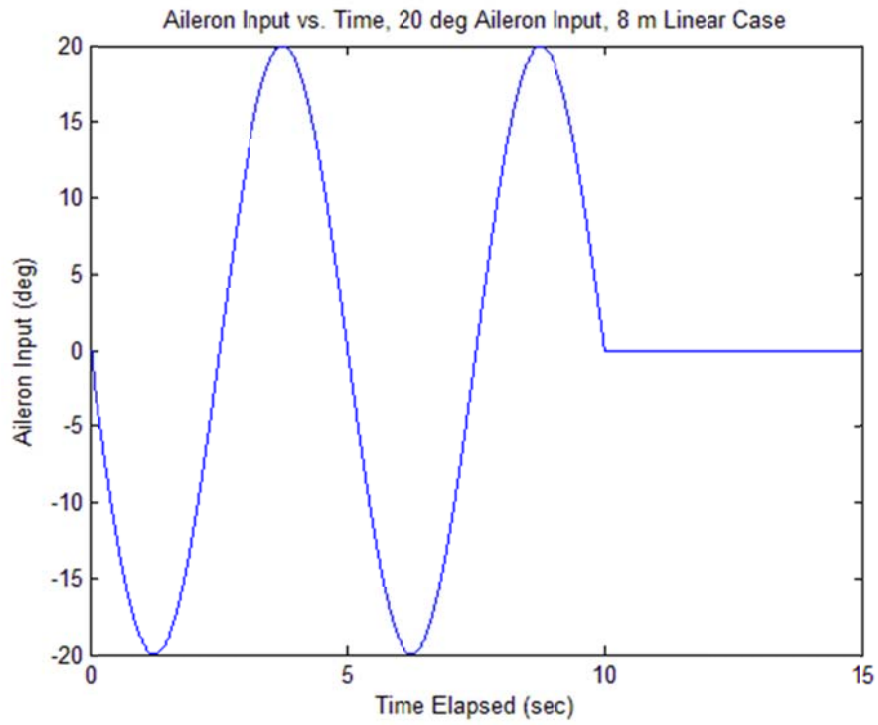


Figure 175. Case 16 Aileron Input versus Time

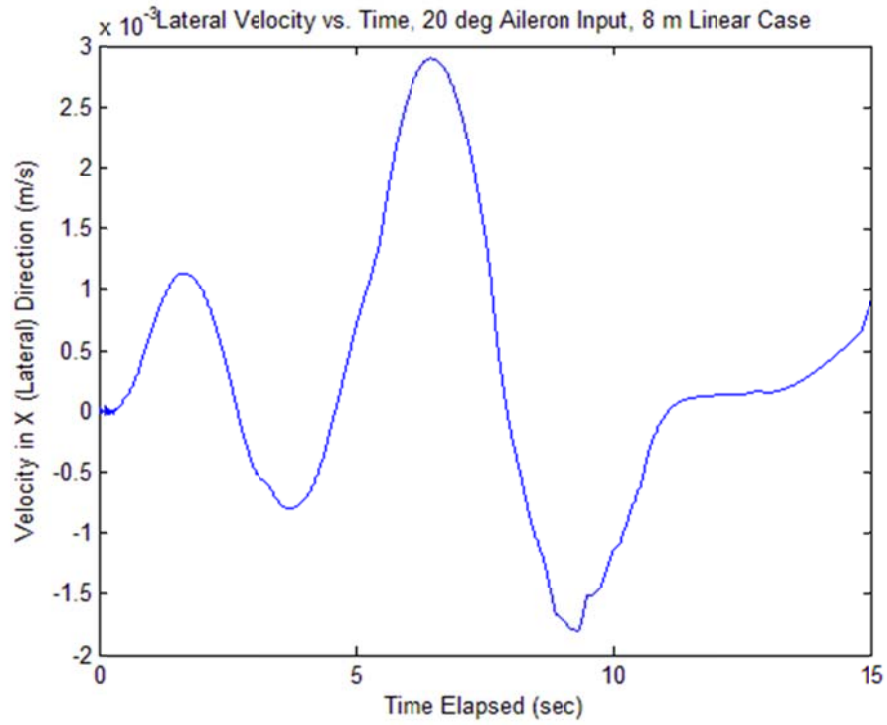


Figure 176. Case 16 Lateral Velocity v_x versus Time

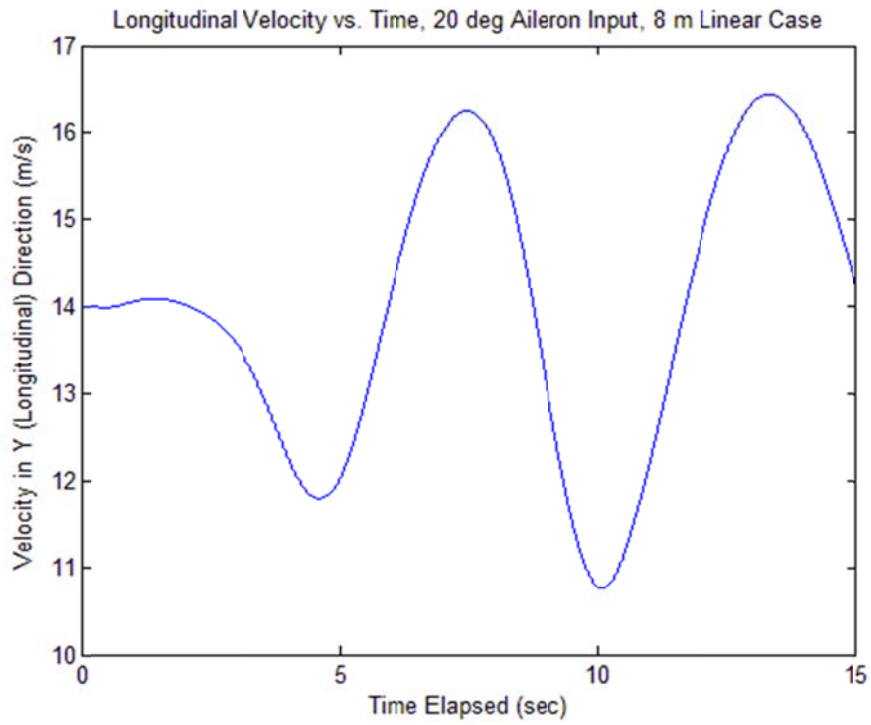


Figure 177. Case 16 Longitudinal Velocity v_y versus Time

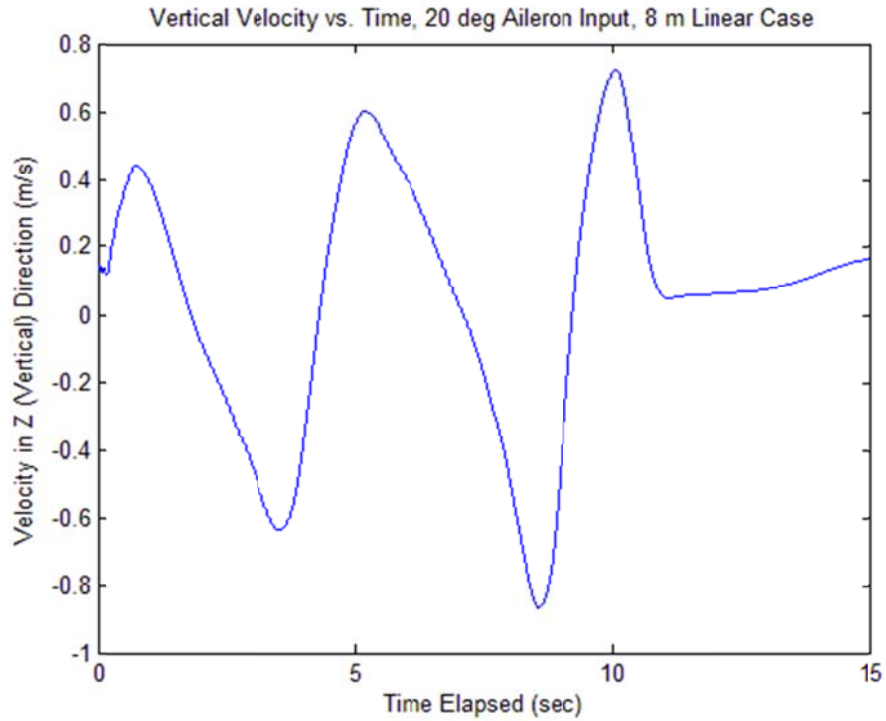


Figure 178. Case 16 Vertical Velocity v_z versus Time

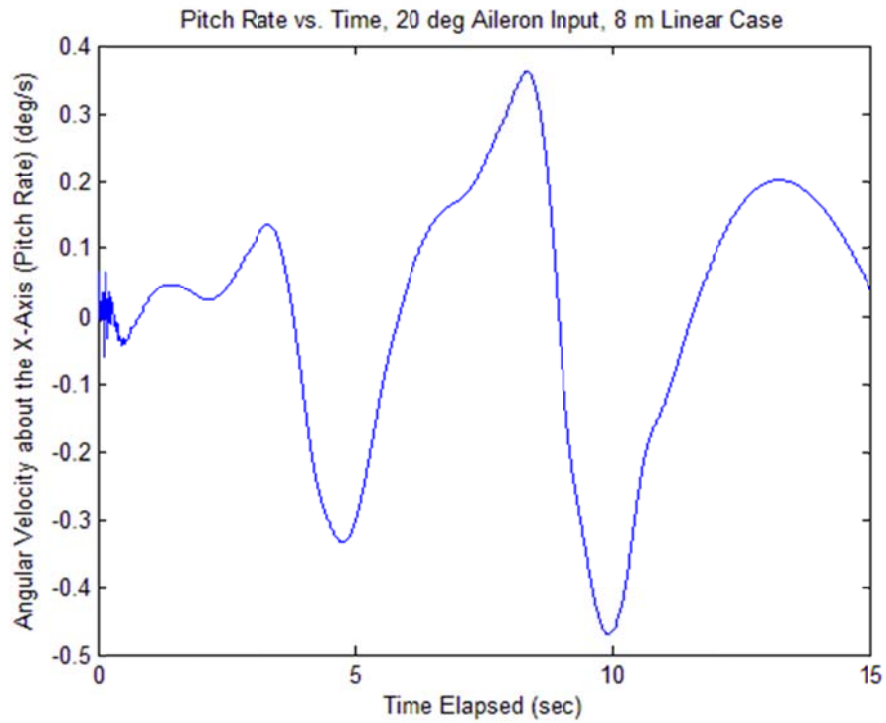


Figure 179. Case 16 Pitch Rate ω_x versus Time

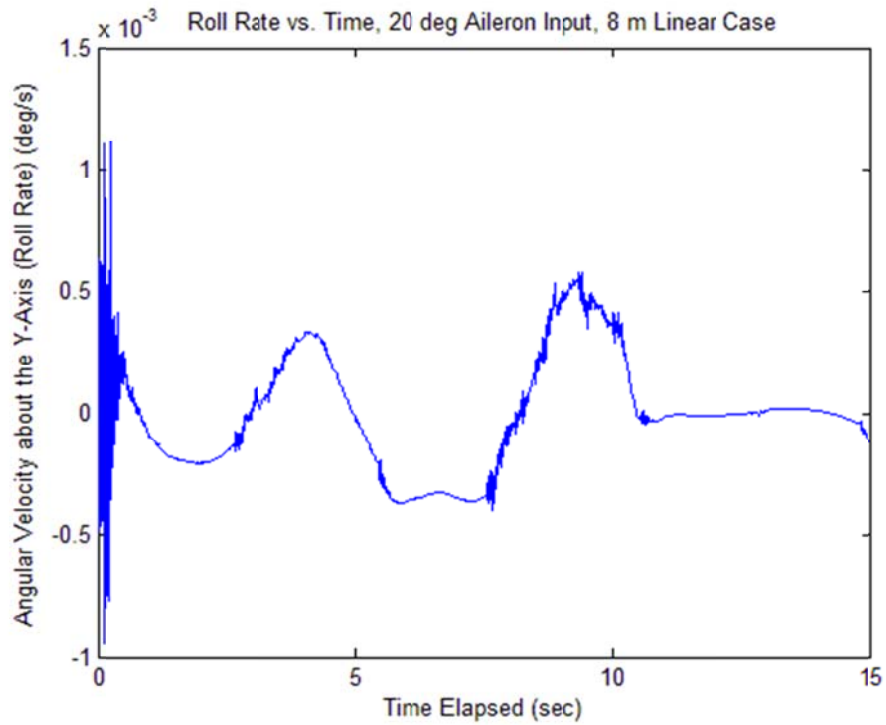


Figure 180. Case 16 Roll Rate ω_y versus Time

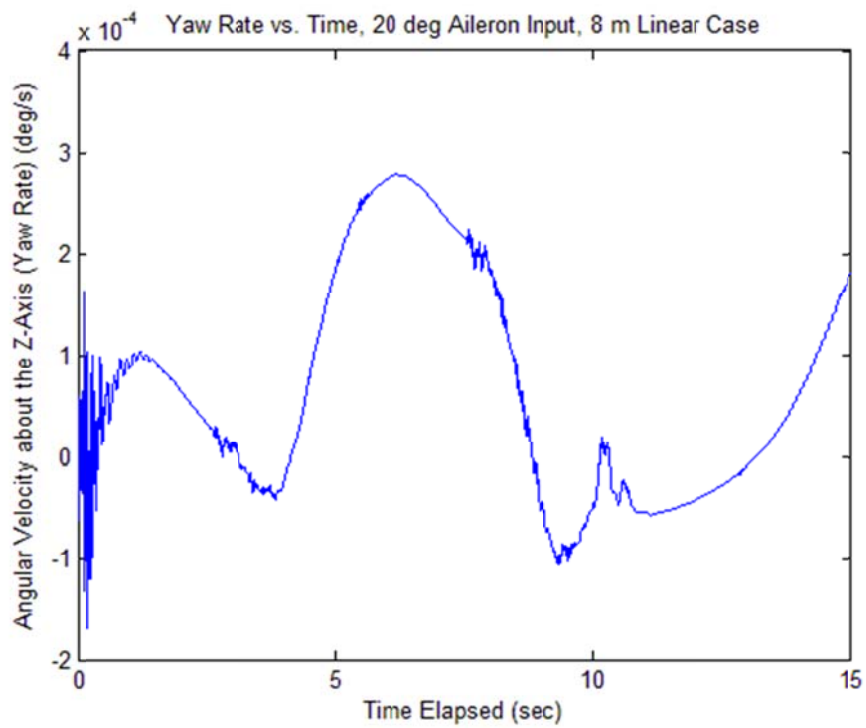


Figure 181. Case 16 Yaw Rate ω_z versus Time

Case 17: 8 m Linear Type 15 sec Simulation, 25 deg Aileron Input

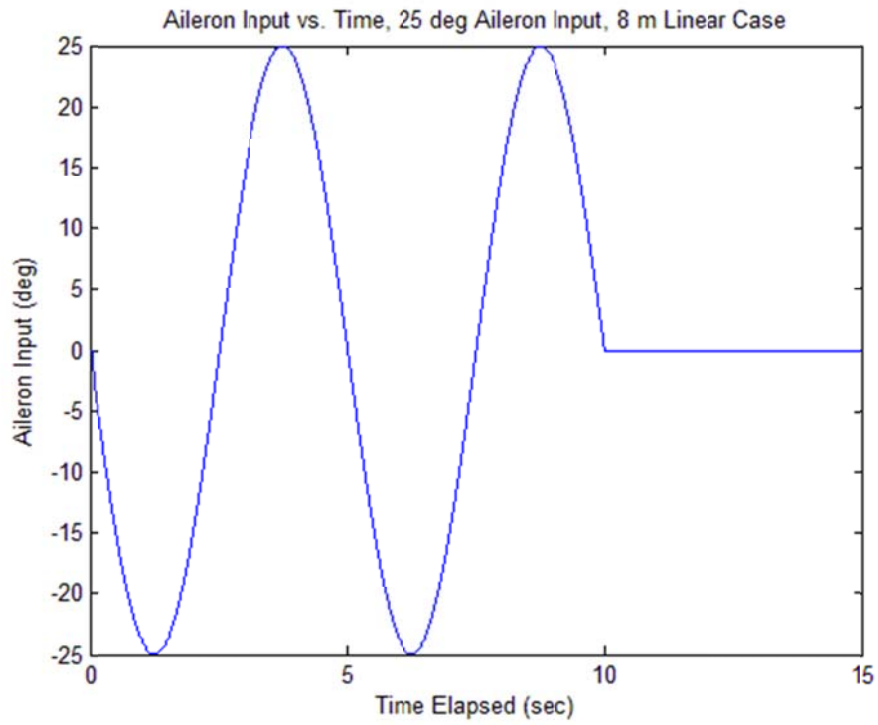


Figure 182. Case 17 Aileron Input versus Time

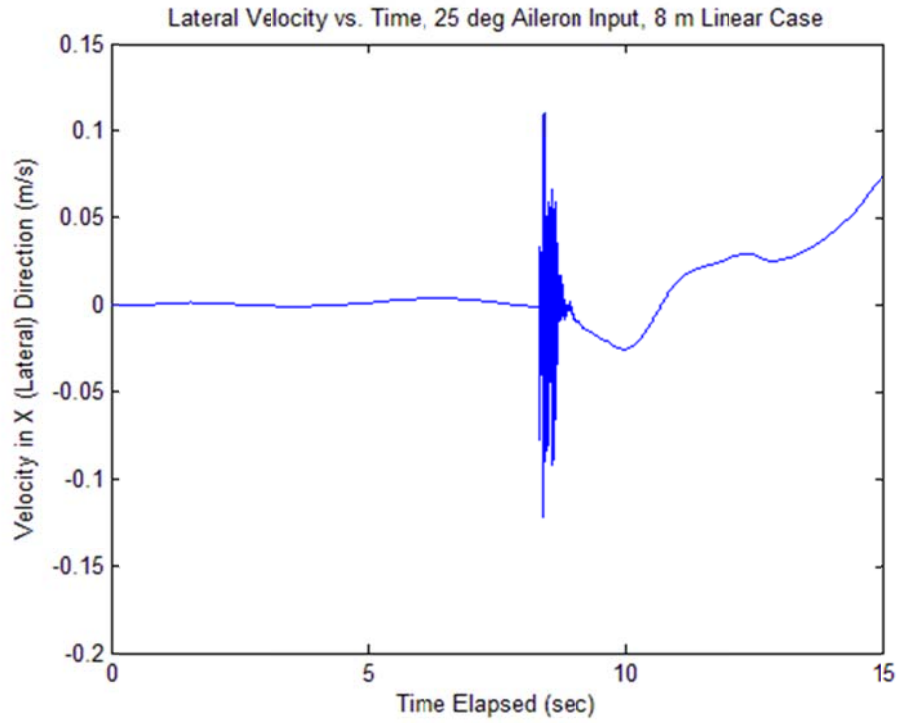


Figure 183. Case 17 Lateral Velocity v_x versus Time

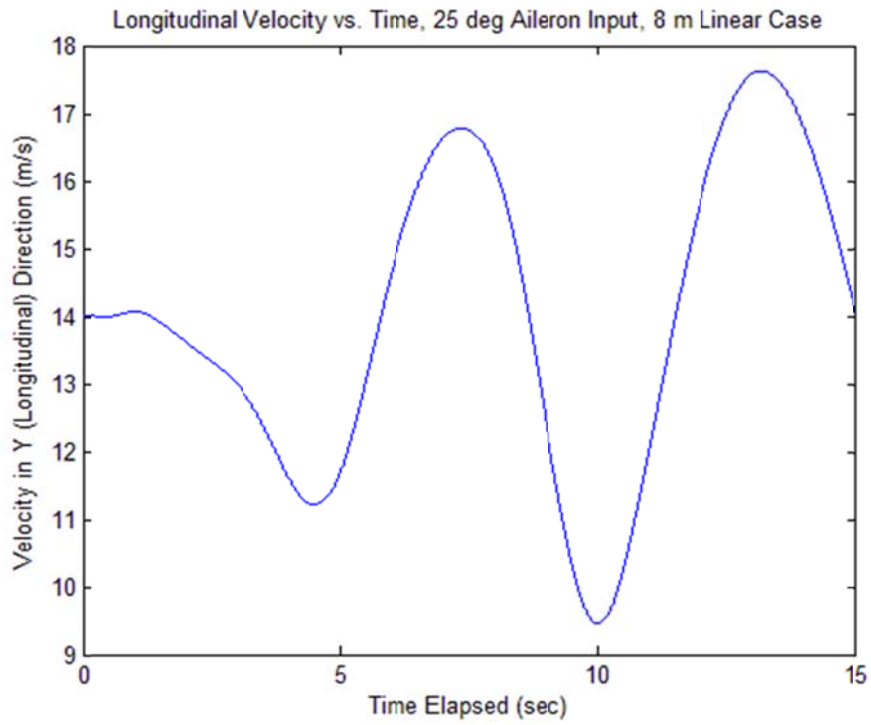


Figure 184. Case 17 Longitudinal Velocity v_y versus Time

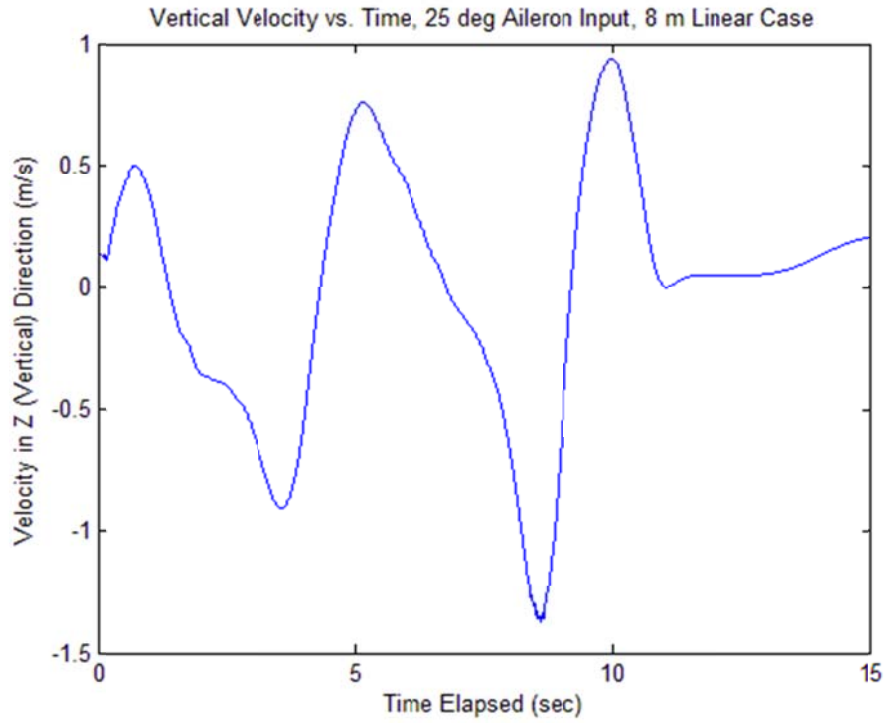


Figure 185. Case 17 Vertical Velocity v_z versus Time

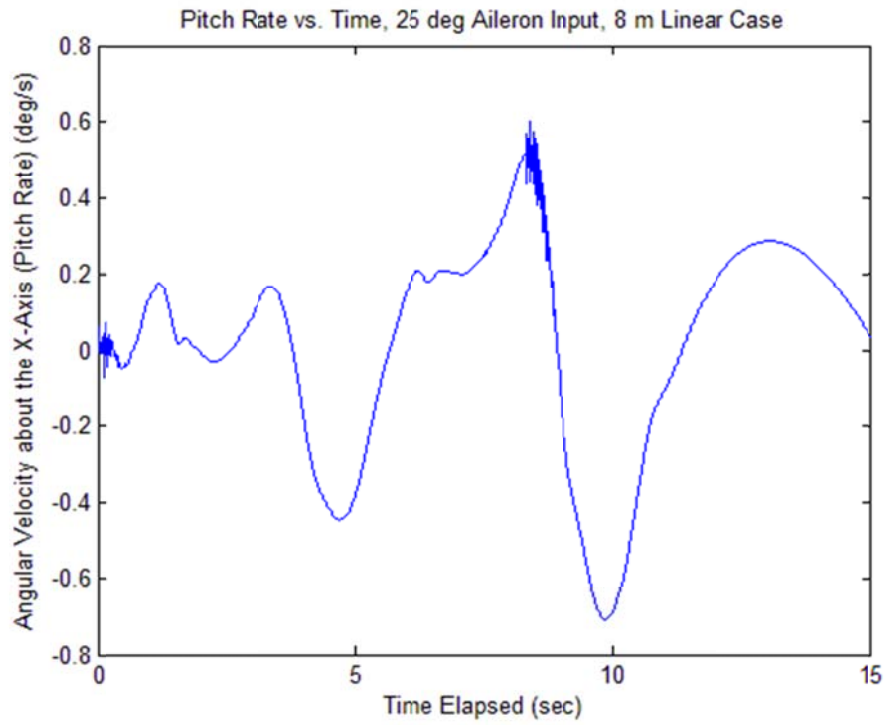


Figure 186. Case 17 Pitch Rate ω_x versus Time

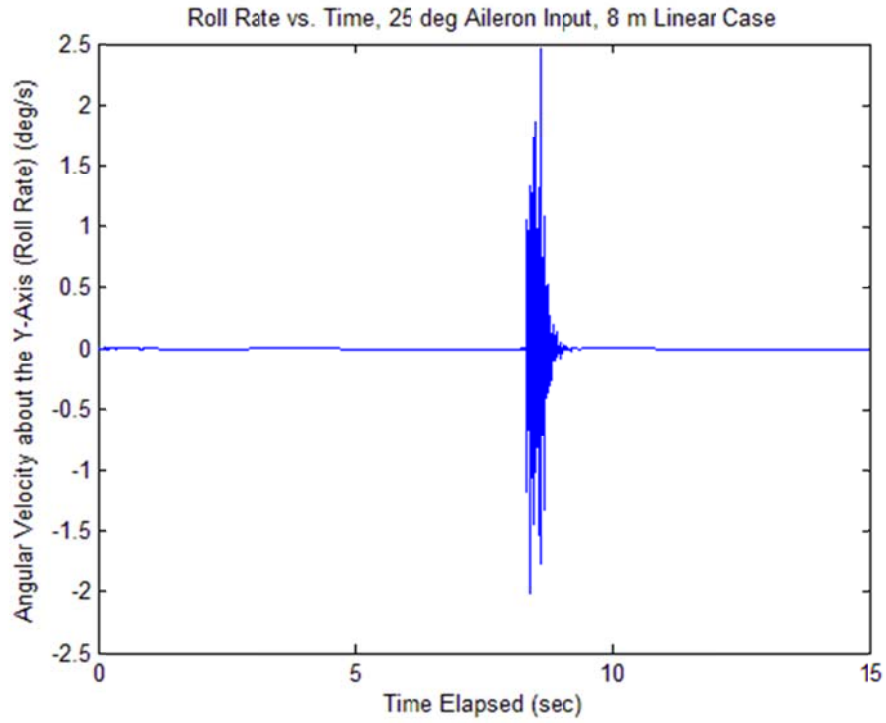


Figure 187. Case 17 Roll Rate ω_y versus Time

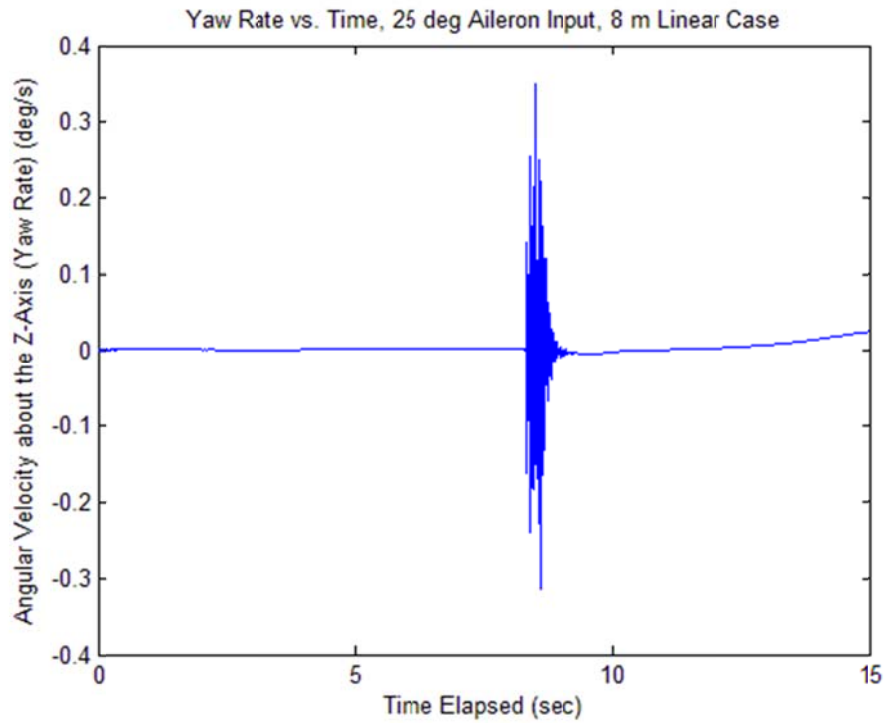


Figure 188. Case 17 Yaw Rate ω_z versus Time

Appendix B. Input File for the 6 Meter, 5 Degree Aileron Input Linear

Case, Case 5

```
%This is from the input flie 6_meter_baseline_case0.nin

title="XHALE_Dec2009_TEST"
filename="xHALE_dec_2009_test"

Aerodynamics {
    drag = 1 %or 0
    drag_derivatives = 1 %or 0
    inflow_forces = 1 %or 0
    inflow_expansion = 6
%    stall_model = "model_name"
    load_factor = 1
    pg_correction = 0
    nominal_mach = 0.3
    vertical_aero_load = 0
    stall_on = 0
    stall_model_type = 1
    reynolds_number = 150000
}

Flight Conditions {
    altitude = 30
    pressure =
    load_factor = 1 % gravmult
    density =
    velocity = 12
    gustx =
    gusty =
    gustz =
}
Pilot Input {
}
Structure {
    baoa = 7.828875834563730%7.828876272969460%7.828493098845625
    fuel_mass = 0;
    keypoints {
        0 0 0 %1 Center
        1 0 0 %2 kpt 1 on the right
        -1 0 0 %3 kpt 1 on the left
        2 0 0 %4 kpt-extension on the right
        -2 0 0 %5 kpt-extension on the right
        3.037 0 0.174 %6 kpt-extension on the right
        -3.037 0 0.174 %7 kpt-extension on the right
        1 0 -0.184 %8 R1 Pod down
        -1 0 -0.184 %9 L1 Pod down
        2 0 -0.184 %10 R2 Pod down
        -2 0 -0.184 %11 L2 Pod down
        1 -0.650 0 %12 R1 Tailboom
        0.7625 -0.650 0 %13 R1 Tail inner tip
        1.2375 -0.650 0 %14 R1 Tail outer tip
        -1 -0.650 0 %15 L1 Tailboom
    }
}
```

```

-0.7625 -0.650 0 %16 L1 Tail inner tip
-1.2375 -0.650 0 %17 L1 Tail outer tip
 2 -0.650 0 %18 R2 Tailboom
 1.7625 -0.650 0 %19 R2 Tail inner tip
 2.2375 -0.650 0 %20 R2 Tail outer tip
-2 -0.650 0 %21 L2 Tailboom
-1.7625 -0.650 0 %22 L2 Tail inner tip
-2.2375 -0.650 0 %23 L2 Tail outer tip
 0 0 -0.184 %24 Center pod down
 2.052 0 0 %25 kpt-extension on the right
-2.052 0 0 %26 kpt-extension on the right
}
members{
% [memb name, (key points ...), properti]
PODC 1 24 fairing_center %1
WR1 1 2 main_wing %2
POD1up 2 8 fairing_up_right%3
BR1 2 12 boom %4
TR1in 12 13 tail_in_right %5
TR1ou 12 14 tail_out_right %6
WR2 2 4 main_wing %7
POD3up 4 10 fairing_up_right%8
BR2 4 18 boom %9
TR2in 18 19 tail_in_right %10
TR2ou 18 20 tail_out_right %11
WR3 4 25 6 main_wing_dih %12
WL1 1 3 main_wing %13
POD2up 3 9 fairing_up_left %14
BL1 3 15 boom %15
TL1in 15 16 tail_in_left %16
TL1ou 15 17 tail_out_left %17
WL2 3 5 main_wing %18
POD4up 5 11 fairing_up_left %19
BL2 5 21 boom %20
TL2in 21 22 tail_in_left %21
TL2ou 21 23 tail_out_left %22
WL3 5 26 7 main_wing_dih %23
}

integration_direction= 1 1 1 -1 -1 1 1 1 -1 -1 1 1 -1 1 -1 1 -1 -1
1 -1 1 -1 -1
group{
grp1{
1
}
grp2{
2 3
2 4
4 5
4 6
2 7
7 8
7 9
9 10
9 11
7 12
}
}

```

```

grp3{
  13 14
  13 15
  15 16
  15 17
  13 18
  18 19
  18 20
  20 21
  20 22
  18 23
}
}
inter member constraint{
}
member properties {
  boom {
    type = "fuselage"
    diameter = 0.024 0.013
    number of elements = 1
    rigid_element = 1
    crosssection {
      reference axis      = 0.5 0    % location of ra from LE
                                % User may choose following
                                % type of input for variable
                                % reference axis locations
      mass_distribution = 0.119339623
                                % (mass units)/(unit span)
      center_of_gravity{
      }                                % Empty inputs means cg is
                                % located at ra
      inertia {
        Ixx= 2.914E-09
        Ixy= 0
        Ixz= 0
        Iyy= 1.457E-09
        Iyz= 0
        Izz= 1.457E-09
      }
      stiffness {                    % Be Set to rigid. These numbers
        K11= 5.390E+07 % extension stiffness [E*A]
        K12= 0          % extension twist coupling
        K13= 0          % extension bend y coupling
        K14= 0          % extension bend z coupling
        K22= 5.390E+07 % twist stiffness [G*J]
        K23= 0          % twist / bend y coupling
        K24= 0          % twist / bend z coupling
        K33= 5.390E+07 % bend y stiffness [E*I]
        K34= 0          % bend y / bend z coupling
        K44= 5.390E+07 % bend z stiffness
      }
    }
  }
}
main_wing {
  type = "wing"
  number of elements = 2
  control surface{

```

are dummy

```

    }
    airfoil      = NACA4415
    aero_coefficient = datatable
%   airfoilfile  = EMX07.dat
    AoA         = 0
%   rigid_element =
    aerodynamic_spanwise_distribution = 0
    fuel_percentage =
    chord        = 0.2          % Single value is used for
                                % constant chord length
                                % The user may specify
values
                                % at each Keypoint

    crosssection {
        reference axis      = 0.2878 0
                                % location of ra from LE
                                % User may choose following
                                % type of input for variable
                                % reference axis locations

        mass_distribution = 0.319
                                % (mass units)/(unit span)

        center_of_gravity{
                                % Empty inputs means cg is
            cgx = 0.0
            cgy = 0.00756      % @ c/4
            cgz = 0.0
        }
                                % located at ra
        inertia {
            Ixx= 8.089765E-04
            Ixy= -0.000000E+00
            Ixz= 0.000000E+00
            Iyy= 1.221712E-05
            Iyz= -6.493531E-06
            Izz= 7.967593E-04
        }
        stiffness {
            K11= 2.140827E+06   % extension stiffness [E*A]
            K12= 0.000000E+00   % extension twist coupling
            K13= 1.544115E+03   % extension bend y coupling
            K14= -4.905651E+04   % extension bend z coupling
            K22= 7.224739E+01   % twist stiffness [G*J]
            K23= -0.000000E+00   % twist / bend y coupling
            K24= 0.000000E+00   % twist / bend z coupling
            K33= 1.195708E+02   % bend y stiffness [E*I]
            K34= -4.634442E+01   % bend y / bend z coupling
            K44= 6.350796E+03   % bend z stiffness
        }
    }
}

main_wing_dih {
    type = "wing"
    number of elements = 1 2
    control surface{
        AilR = trail 0.25 2 3 WR3 % [name, percent of chord,
start element, end element]
        Aill = trail 0.25 2 3 WL3 % [name, percent of chord,
start element, end element]
    }
}

```

```

airfoil      = NACA4415
aero_coefficient = datatable
%
airfoilfile  = EMX07.dat
AoA          = 0 0 0
%
rigid_element =
aerodynamic_spanwise_distribution = 40
fuel_percentage =
chord        = 0.2          % Single value is used for
                        % constant chord length
                        % The user may specify
values
                        % at each Keypoint

crosssection {
  reference axis      = 0.2878 0
                        % location of ra from LE
                        % User may choose following
                        % type of input for variable
                        % reference axis locations

  mass_distribution = 0.319
                        % (mass units)/(unit span)

  center_of_gravity{
                        % Empty inputs means cg is
    cgx = 0.0
    cgy = 0.00756      % @ c/4
    cgz = 0.0
  }
                        % located at ra
  inertia {
    Ixx= 8.089765E-04
    Ixy= -0.000000E+00
    Ixz= 0.000000E+00
    Iyy= 1.221712E-05
    Iyz= -6.493531E-06
    Izz= 7.967593E-04
  }
  stiffness {
    K11= 2.140827E+06   % extension stiffness [E*A]
    K12= 0.000000E+00   % extension twist coupling
    K13= 1.544115E+03   % extension bend y coupling
    K14= -4.905651E+04  % extension bend z coupling
    K22= 7.224739E+01   % twist stiffness [G*J]
    K23= -0.000000E+00  % twist / bend y coupling
    K24= 0.000000E+00   % twist / bend z coupling
    K33= 1.195708E+02   % bend y stiffness [E*I]
    K34= -4.634442E+01  % bend y / bend z coupling
    K44= 6.350796E+03   % bend z stiffness
  }
}
}
tail_in_right {
  type = "wing"
  number of elements = 1
  control surface{
    % NM = [lead/trail(location),...
    %       percentage of chord,...
    %       start element,...
    %       end element,...
    %       memb label]

```



```

        Iyy = 2.282E-05
        Iyz = 2.644E-08
        Izz = 2.651E-05
    }
}
}
}
tail_out_right {
    type = "wing"
    number of elements = 1
    control surface{
        % NM = [lead/trail(location),...
        %     percentage of chord,...
        %     start element,...
        %     end element,...
        %     memb label]
        ELR1ou = trail 0.98 1 1 TR1ou % [name, percent of
chord, start element, end element]
        ELR2ou = trail 0.98 1 1 TR2ou % [name, percent of
chord, start element, end element]
    }
    airfoil = NACA0012
    aero_coefficient = datatable
    AoA = 0
    rigid_element = 1
    aerodynamic_spanwise_distribution = 40
    fuel_percentage =
chord = 0.11 % Single value is used for
% constant chord length
% The user may specify
% at each Keypoint
crosssection {
    reference axis = 0.3235 0% location of ra from LE
% User may choose following
% type of input for variable
% reference axis locations
% (mass units)/(unit span)
    mass_distribution = 0.129 % Empty inputs means cg is
center_of_gravity{
    cgx = 0.0 % @ c/4
    cgy = 0.008085
    cgz = 0.0
} % located at ra
inertia {
    Ixx= 1.597900E-04
    Ixy= -0.000000E+00
    Ixz= 0.000000E+00
    Iyy= 2.914098E-06
    Iyz= -1.688579E-22
    Izz= 1.568759E-04
}
stiffness { % Be Set to rigid. These
numbers are dummy
    K11= 3.214025E+06 % extension stiffness [E*A]
    K12= 0.000000E+00 % extension twist coupling
    K13= -3.714275E-04 % extension bend y coupling
    K14= -7.441697E+04 % extension bend z coupling

```

```

        K22=  2.138858E+01      % twist stiffness [G*J]
        K23= -0.000000E+00      % twist / bend y coupling
        K24=  0.000000E+00      % twist / bend z coupling
        K33=  9.098072E+01      % bend y stiffness [E*I]
        K34=  2.262609E-06      % bend y / bend z coupling
        K44=  4.274273E+03      % bend z stiffness
    }
    rigid_body{
        point_mass          = 1 % changed spelling
        nodes               = 1
        center_of_gravity = 0.0286 0.008395 0.0
        mass                = 0.02
        inertia{
            Ixx = 1.866E-07
            Ixy = 1.000E-10
            Ixz = 0.000E+00
            Iyy = 1.341E-06
            Iyz = 0.000E+00
            Izz = 1.311E-06
        }
    }
}
tail_in_left {
    type = "wing"
    number of elements = 1
    control surface{
        % NM = [lead/trail(location),...
        %       percentage of chord,...
        %       start element,...
        %       end element,...
        %       memb label]
        ELL1in = trail 0.98 1 1 TL1in % [name, percent of
chord, start element, end element]
        ELL2in = trail 0.98 1 1 TL2in % [name, percent of
chord, start element, end element]
    }
    airfoil          = NACA0012
    aero_coefficient = datatable
    AoA              = 0
    rigid_element    = 1
    aerodynamic_spanwise_distribution = 40
    fuel_percentage =
chord                = 0.11          % Single value is used for
                                % constant chord length
                                % The user may specify
                                % at each Keypoint
    crosssection {
        reference axis      = 0.3235 0% location of ra from LE
                                % User may choose following
                                % type of input for variable
                                % reference axis locations
        mass_distribution = 0.129 % (mass units)/(unit span)
        center_of_gravity{
            cgx = 0.0           % Empty inputs means cg is
            cgy = 0.008085     % @ c/4
        }
    }
}
values

```

```

        cgz = 0.0
    }
    inertia {
        Ixx= 1.597900E-04
        Ixy= -0.000000E+00
        Ixz= 0.000000E+00
        Iyy= 2.914098E-06
        Iyz= -1.688579E-22
        Izz= 1.568759E-04
    }
    stiffness {
numbers are dummy
        K11= 3.214025E+06
        K12= 0.000000E+00
        K13= -3.714275E-04
        K14= -7.441697E+04
        K22= 2.138858E+01
        K23= -0.000000E+00
        K24= 0.000000E+00
        K33= 9.098072E+01
        K34= 2.262609E-06
        K44= 4.274273E+03
    }
    rigid_body{
        point_mass      = 1 % changed spelling
        nodes           = 2
        center_of_gravity = -0.04575 4.95E-04 -0.0005
        mass            = 0.04873
        inertia{
            Ixx = 4.631E-06
            Ixy = -3.190E-06
            Ixz = -3.057E-07
            Iyy = 2.282E-05
            Iyz = 2.644E-08
            Izz = 2.651E-05
        }
    }
}
tail_out_left {
    type = "wing"
    number of elements = 1
    control surface{
        % NM = [lead/trail(location),...
        %     percentage of chord,...
        %     start element,...
        %     end element,...
        %     memb label]
        ELL1ou = trail 0.98 1 1 TL1ou % [name, percent of
chord, start element, end element]
        ELL2ou = trail 0.98 1 1 TL2ou % [name, percent of
chord, start element, end element]
    }
    airfoil      = NACA0012
    aero_coefficient = datatable
    AoA          = 0
    rigid_element = 1
}

```



```

number of elements = 1
airfoil            = NACA0018
aero_coefficient = datatable
%
airfoilfile       = mh78.dat
AoA               = 0
rigid_element     = 1
aerodynamic_spanwise_distribution = 40
fuel_percentage   =
chord = 0.37      % Single value is used for
                  % constant chord length
                  % The user may specify

values

                  % at each Keypoint

crosssection {
  reference axis= 0.6093 0%0 0%
  mass_distribution= 1.0e-8 % (mass units)/(unit span)
  inertia {
    Ixx= 1.0e-8
    Ixy= 0
    Ixz= 0
    Iyy= 1.0e-8
    Iyz= 0
    Izz= 1.0e-8
  }
  stiffness {      % Be Set to rigid. These numbers
are dummy
    K11= 5.390E+07 % extension stiffness [E*A]
    K12= 0          % extension twist coupling
    K13= 0          % extension bend y coupling
    K14= 0          % extension bend z coupling
    K22= 5.390E+07 % twist stiffness [G*J]
    K23= 0          % twist / bend y coupling
    K24= 0          % twist / bend z coupling
    K33= 5.390E+07 % bend y stiffness [E*I]
    K34= 0          % bend y / bend z coupling
    K44= 5.390E+07 % bend z stiffness
  }
  rigid_body{
    point_mass      = 2 % changed spelling
    nodes           = 1 2
    center_of_gravity{
      cgx{
        0% 0.0125 % 0.0125 % center pod battery
        0%-0.0031
      }
      cgy{
        -0.0009 % 0.0591 % center pod battery
        0.0431
      }
      cgz{
        -0.0689 %-0.0689 % center pod battery
        0.0116
      }
    }
  }
  mass{
    0.3960
    1.0248
  }
}

```


are dummy

```
stiffness {           % Be Set to rigid. These numbers
    K11= 5.390E+07    % extension stiffness [E*A]
    K12= 0            % extension twist coupling
    K13= 0            % extension bend y coupling
    K14= 0            % extension bend z coupling
    K22= 5.390E+07    % twist stiffness [G*J]
    K23= 0            % twist / bend y coupling
    K24= 0            % twist / bend z coupling
    K33= 5.390E+07    % bend y stiffness [E*I]
    K34= 0            % bend y / bend z coupling
    K44= 5.390E+07    % bend z stiffness
}
rigid_body{
    point_mass        = 2 % changed spelling
    nodes              = 1 2
    center_of_gravity{
        cgx{
            0.0125 % 0.0125 % right pods battery
            -0.0062
        }
        cgy{
            -0.0009 % 0.0591 % right pods battery
            0.0662
        }
        cgz{
            -0.0689 %-0.0689 % right pods battery
            0.0066
        }
    }
}
mass{
    0.3960
    1.0571
}
inertia{
    Ixx{
        1.160E-03
        1.134E-02
    }
    Ixy{
        0.000E+00
        -1.212E-03
    }
    Ixz{
        0.000E+00
        1.055E-05
    }
    Iyy{
        9.485E-05
        3.209E-03
    }
    Iyz{
        0.000E+00
        4.595E-05
    }
    Izz{
        1.098E-03
    }
}
```



```

Ixx= 1.0e-8
Ixy= 0
Ixz= 0
Iyy= 1.0e-8
Iyz= 0
Izz= 1.0e-8
}
are dummy stiffness {           % Be Set to rigid. These numbers
K11= 5.390E+07 % extension stiffness [E*A]
K12= 0         % extension twist coupling
K13= 0         % extension bend y coupling
K14= 0         % extension bend z coupling
K22= 5.390E+07 % twist stiffness [G*J]
K23= 0         % twist / bend y coupling
K24= 0         % twist / bend z coupling
K33= 5.390E+07 % bend y stiffness [E*I]
K34= 0         % bend y / bend z coupling
K44= 5.390E+07 % bend z stiffness
}
rigid_body{
point_mass      = 2 % changed spelling
nodes          = 1 2
center_of_gravity{
cgx{
0.0 % 0.0125 % right pods battery
0.0
}
cgy{
-0.0109 % 0.0591 % right pods battery
0.0562
}
cgz{
-0.0689 %-0.0689 % right pods battery
0.0066
}
}
}
mass{
0.3960
0.4000
}
inertia{
Ixx{
1.160E-04
1.134E-03
}
Ixy{
0.000E+00
-1.212E-03
}
Ixz{
0.000E+00
1.055E-05
}
Iyy{
9.485E-05
3.209E-03
}
}

```



```

% (6): time-independent value
% (7): time-independent value (OPTIONAL)
% (8): start time (OPTIONAL)
% (9): stop time (OPTIONAL)
% FD1 = force_dist MB 1 20 z 50*sin(40*t)+25
% [(1) (2) (3) (4) (5) (6) OPTIONAL (7) OPTIONAL (8)]
% (1): load type (moment)
% (2): member designation
% (3): location type(keypoint or node)
% (4): location number
% (5): cartesian direction
% (6): time-independent value
% (7): time-independent value (OPTIONAL)
% (8): start time (OPTIONAL)
% (9): stop time (OPTIONAL)
% M1 = moment MB node 60 x 50
% [(1) (2) (3) (4) (5) (6) OPTIONAL (7) OPTIONAL (8)]
% (1): load type (moment_dist)
% (2): member designation
% (3): starting element
% (4): ending element
% (5): cartesian direction
% (6): time-independent value
% (7): time-independent value (OPTIONAL)
% (8): start time (OPTIONAL)
% (9): stop time (OPTIONAL)
% MD1 = moment_dist MB 9 10 z 50
% [load type, member designation, element start, element end,
mode, voltage value, OPTIONAL--> start time, stop time,...] % NEED TO
COMPLETE
% VA1 = actuator_volt VA1 1 10
% [(1) (2) (3) OPTIONAL (4) OPTIONAL (5)]
% (1): load type (control_surf)
% (2): control surface designation
% (3): time-independent value
% (4): time-independent value (OPTIONAL)
% (5): start time (OPTIONAL)
% (6): stop time (OPTIONAL)
DEFTAIL1= control_surf ELR1in -7.830535569853027%-
7.830535463594316%-7.830173052395354 %12*sin(2*pi/6.3*t)% 0.01 0.11
DEFTAIL2= control_surf ELR1ou -7.830535569853027%-
7.830535463594316%-7.830173052395354 %12*sin(2*pi/6.3*t)% 0.01 0.11
DEFTAIL3= control_surf ELR2in -7.830535569853027%-
7.830535463594316%-7.830173052395354 %12*sin(2*pi/6.3*t)% 0.01 0.11
DEFTAIL4= control_surf ELR2ou -7.830535569853027%-
7.830535463594316%-7.830173052395354 %12*sin(2*pi/6.3*t)% 0.01 0.11
DEFTAIL5= control_surf ELL1in -7.830535569853027%-
7.830535463594316%-7.830173052395354 %12*sin(2*pi/6.3*t)% 0.01 0.11
DEFTAIL6= control_surf ELL1ou -7.830535569853027%-
7.830535463594316%-7.830173052395354 %12*sin(2*pi/6.3*t)% 0.01 0.11
DEFTAIL7= control_surf ELL2in -7.830535569853027%-
7.830535463594316%-7.830173052395354 %12*sin(2*pi/6.3*t)% 0.01 0.11
DEFTAIL8= control_surf ELL2ou -7.830535569853027%-
7.830535463594316%-7.830173052395354 %12*sin(2*pi/6.3*t)% 0.01 0.11
DEFAiLR= control_surf AiLR 0 -5*sin(2*pi/5*t) 0.1 10
DEFAiLL= control_surf AiLL 0 -5*sin(2*pi/5*t) 0.1 10
}

```

```

}

Simulation {
    mode = "new"
    type = "dynamic"

    % Model Construction Parameters
    structural damping = 1e-4           % Structural damping
parameter                               % (set to 0 for no
structure                               % damping)
    first mode damping = -1e-4        % First mode damping (set
to                                       % negative value to use the
                                           % given alphD)

    % Steady State Simulation Parameters
    sssim{
        sim_type          = "nonlinear" % "nonlinear" or
"linearized"
        relative tolerance = .001      % Relative tolerance for
static                                       % solution convergence
        numerical damping  = .8        % Numerical damping
parameter
        max iterations     = 100       % for static solution
iterations                               % Maximum number of
state                                     % allowed in each steady
                                           % solution
    }
    % Time Simulation Parameters
    timesim{
        integration_type   = "Gen-Alpha" % "Trapz" or
sim_type                 = "linear" % "nonlinear" or "linear" /
"reduced_order"
        time_duration      = 10
        time_step          = 0.0001    % or time_divisions=4000
% restart_filename       = "wbt_smp1" % ??????
        rho_inf_1          = 0.999
        rho_inf_2          = 0.999
        time_step_save     = 100
        start_time_flag    = 0 % put a 1 to start from previous
conditions fresh simulations require 0
        n_sub_add_time_step = 1
        error_states_0     = []
        gust_input         = 0
        local_wrinkling    = 0
        ref_val_1          = 1e10
        ref_val_2          = 1e10
        time_sim_tol       = 1e1
        no_rigidbody_dof   = 0
    }
    % Flutter Analysis Parameters
    flutsim{

```

```

    flight_index      = 2          % Flight indices where
vehicle              % stability is calculated
                    = 30 30      % Altitudes at each index
    altitude
    fuel_mass        = 0 0        % Fuel mass
    body_angle       = -2.681822255727332 -8.483437184110727
                    % Body angle will come from
trim solution and have same number of inputs as speeds sep by spaces
    flap_angle       = 2.487111475290816 7.597875750046539
                    % Flap angle
    thrust           = 1.043348116498814 1.960989314382431
                    % Thrust force
    U_predict        = 12 8 20    % lower, step, and upper
    rb_const         = 0          % Type of rigid body
constraint           % 0: No rb constraint
                    % 1: Full rb constraint
                    % 2: only plunging is free
                    % 3: only pitching is free
                    % 4: plunging and pitching
free
    re_trim          = 1          % Flag to indicate retrim
                    % during the speed
increment
    load_update_flag = Mot1 Mot2 Mot3 Mot4 Mot5 DEFTAIL1
DEFTAIL2 DEFTAIL3 DEFTAIL4 DEFTAIL5 DEFTAIL6 DEFTAIL7 DEFTAIL8
    } % Note about flutter analysis:
    % altitude and fuel_mass are n by 1 column matrices, where n is
the
    % number of index
    % body_angle, flap_angle, and thrust are also n by 1 column
matrices
    % only when re_trim = 0 (no retrim is considered). They are
usually
    % n by m matrices where m equals the span of speed increment
    % Modal Analysis Parameters
    modalsim{
        config       = free      % and/or deformed_shape
                    % Modal analysis using
                    % different criteria
                    % free vibration (in
vacuum)              % deformed vibration (under
                    % prescribed load)
    }
    % Trim Module Parameters
    trimsim{
        trim_count   = 1          % Number of
trim solutions to be performed
        altitude     = 30 % Altitudes at each index
        U_trim       = 12 % Flight Speed at each index
        fuel_mass    = 0 % Fuel mass at each index
        trimoption   = 0 % 0: static trim (use forces) 1: dynamic trim
        (use accel.)
        tol_trim     = 1e-8 % Tolerance to converge

```

```

        parameters {      % They override the values set in the previous
sections (as in Loads Structure)
        baoa      7.828876272969460 0.01      % Body angle of attack,
initial guess, increment
        DEFTAIL1 -7.830535463594316 0.01      % CS name, initial guess,
increment
        Mot1      0.987101042245488 0.01      % Load name (pt load),
initial guess, increment
        Mot2      0.987101042245488 0.01
        Mot3      0.987101042245488 0.01
        Mot4      0.987101042245488 0.01
        Mot5      0.987101042245488 0.01
        DEFTAIL2 -7.830535463594316 0.01      % CS name, initial guess,
increment
        DEFTAIL3 -7.830535463594316 0.01      % CS name, initial guess,
increment
        DEFTAIL4 -7.830535463594316 0.01      % CS name, initial guess,
increment
        DEFTAIL5 -7.830535463594316 0.01      % CS name, initial guess,
increment
        DEFTAIL6 -7.830535463594316 0.01      % CS name, initial guess,
increment
        DEFTAIL7 -7.830535463594316 0.01      % CS name, initial guess,
increment
        DEFTAIL8 -7.830535463594316 0.01      % CS name, initial guess,
increment
        }
}
Screen Output{
    refgeom{
        undeformed_geometry = 0
        sketch_plot         = 0
        color_style         = "gray" % "spring" or "summer" or
"autumn" or "winter" or "gray"
    }
    sssim{
        static_deformed_geometry = 0
        no_force_lines           = 0
        text                     = 1
        print_lift_moment        = 1
        figure_position          = 0.05 0.05 0.60 0.60
        figure_color             = 0
        view                     = 160 45
        animate_response         = 1
        movie                    =
        iteration_output         = 1
    }
    timesim{
        time_step_output        = 1
        iteration_output         = 1
        progress_bar            = 0
    }
    flutsim{
        plot_poles              = 1
    }
}
modalsim {

```

```

        numberofmodes          = 10          % Number of modes to be
displayed on screen
        scale                   = 1          % Factor to scale the mode
shapes NOTE: No normalization is done with the modes
    }
    trimsim{
    }
% print_to_file{
%     stiffness_matrix          = 1
%     interial_matrix          = 1
%     trim_input                = 1
%     trim_output              = 1
%     modal_analysis            = frequency
% }
% generate_input_treeI         = 1
% generate_input_treeC         = 1
% response_plot {
%     keypoint 2 pos_z
%     keypoint 2 vel_z
% }
% load_plot                    = FL1 F1
}

```

```

File Output{
    % Time Simulation File Output Request
    timesim{
        bframe_flight_path      = 1
        bframe_flight_velocity  = 1
        euler_angles            = 1
        displacement{
            WR3 node 9
            WR3 node 6
            WR3 node 3
            WR3 node 1
            WR2 node 3
            WR2 node 1
            WR1 node 3
            WR1 node 1
            WL3 node 9
            WL3 node 6
            WL3 node 3
            WL3 node 1
            WL2 node 3
            WL2 node 1
            WL1 node 3
            WL1 node 1
        }
        displacement{
        %     all
        % }
        displacementsort        = "node"    % "node" or "time"
        liftdist{
        %     all
        % }
    }
}

```

Appendix C. Input File for the 8 Meter, No Aileron Input Linear Case,

Case 7

```
% This is from the input flie 8_meter_ailerons_case0.nin
title="XHALE_Dec2009_TEST"
filename="xHALE_dec_2009_test"

Aerodynamics {
    drag = 1 %or 0
    drag_derivatives = 1 %or 0
    inflow_forces = 0 %or 0
    inflow_expansion = 6
%    stall_model = "model_name"
    load_factor = 1
    pg_correction = 0
    nominal_mach = 0.3
    vertical_aero_load = 0
    stall_on = 0
    stall_model_type = 1
    reynolds_number = 150000
}

Flight Conditions {
    altitude = 30
    pressure =
    load_factor = 1 % gravmult
    density =
    velocity = 14
    gustx =
    gusty =
    gustz =
}

Pilot Input {
}

Structure {
    baaa = -0.587176915651974%-0.046047309451146%-
0.045987813505220
    fuel_mass = 0;
    keypoints {
        0 0 0 %1 Center
        1 0 0 %2 kpt 1 on the right
        -1 0 0 %3 kpt 1 on the left
        2 0 0 %4 kpt-extension on the right
        -2 0 0 %5 kpt-extension on the right
        4.037 0 0.174 %6 kpt-extension on the right
        -4.037 0 0.174 %7 kpt-extension on the right
        1 0 -0.184 %8 R1 Pod down
        -1 0 -0.184 %9 L1 Pod down
        2 0 -0.184 %10 R2 Pod down
        -2 0 -0.184 %11 L2 Pod down
    }
}
```

```

    1      -0.650  0      %12 R1 Tailboom
    0.7625 -0.650  0      %13 R1 Tail inner tip
    1.2375 -0.650  0      %14 R1 Tail outer tip
    -1      -0.650  0      %15 L1 Tailboom
    -0.7625 -0.650  0      %16 L1 Tail inner tip
    -1.2375 -0.650  0      %17 L1 Tail outer tip
    2       -0.650  0      %18 R2 Tailboom
    1.7625 -0.650  0      %19 R2 Tail inner tip
    2.2375 -0.650  0      %20 R2 Tail outer tip
    -2      -0.650  0      %21 L2 Tailboom
    -1.7625 -0.650  0      %22 L2 Tail inner tip
    -2.2375 -0.650  0      %23 L2 Tail outer tip
    0       0      -0.184 %24 Center pod down
    3       0      0      %25 kpt-extension on the right
    -3      0      0      %26 kpt-extension on the right
    3.052   0      0      %27 kpt-extension on the right
    -3.052  0      0      %28 kpt-extension on the right
}
members{
% [memb name, (key points ...), propertiy]
PODC    1 24      fairing_center %1
WR1     1 2      main_wing      %2
POD1up  2 8      fairing_up_right%3
BR1     2 12     boom           %4
TR1in   12 13    tail_in_right  %5
TR1ou   12 14    tail_out_right %6
WR2     2 4      main_wing      %7
POD3up  4 10     fairing_up_right%8
BR2     4 18     boom           %9
TR2in   18 19    tail_in_right  %10
TR2ou   18 20    tail_out_right %11
WR3     4 25     main_wing      %12
WR4     25 27 6   main_wing_dih  %13
WL1     1 3      main_wing      %14
POD2up  3 9      fairing_up_left %15
BL1     3 15     boom           %16
TL1in   15 16    tail_in_left   %17
TL1ou   15 17    tail_out_left  %18
WL2     3 5      main_wing      %19
POD4up  5 11     fairing_up_left %20
BL2     5 21     boom           %21
TL2in   21 22    tail_in_left   %22
TL2ou   21 23    tail_out_left  %23
WL3     5 26     main_wing      %24
WL4     26 28 7   main_wing_dih  %25
}

integration_direction= 1 1 1 -1 -1 1 1 1 -1 -1 1 1 1 -1 1 -1 1 -1 -
1 1 -1 1 -1 -1 -1
group{
grp1{
1
}
grp2{
2 3
2 4
4 5
}
}

```

```

4 6
2 7
7 8
7 9
9 10
9 11
7 12
12 13
}
grp3{
14 15
14 16
16 17
16 18
14 19
19 20
19 21
21 22
21 23
19 24
24 25
}
}
inter member constraint{
}
member properties {
boom {
type = "fuselage"
diameter = 0.024 0.013
number of elements = 1
rigid_element = 1
crosssection {
reference axis = 0.5 0 % location of ra from LE
% User may choose following
% type of input for variable
% reference axis locations

mass_distribution = 0.01%0.119339623
% (mass units)/(unit span)

center_of_gravity{
} % Empty inputs means cg is
% located at ra
inertia {
Ixx= 2.914E-09
Ixy= 0
Ixz= 0
Iyy= 1.457E-09
Iyz= 0
Izz= 1.457E-09
}
stiffness { % Be Set to rigid. These numbers

are dummy
K11= 5.390E+07 % extension stiffness [E*A]
K12= 0 % extension twist coupling
K13= 0 % extension bend y coupling
K14= 0 % extension bend z coupling
K22= 5.390E+07 % twist stiffness [G*J]
K23= 0 % twist / bend y coupling
K24= 0 % twist / bend z coupling

```

```

        K33= 5.390E+07 % bend y stiffness [E*I]
        K34= 0         % bend y / bend z coupling
        K44= 5.390E+07 % bend z stiffness
    }
}
}
main_wing {
    type = "wing"
    number of elements = 2
    control surface{
    }
    airfoil      = NACA4415
    aero_coefficient = datatable
%   airfoilfile  = EMX07.dat
%   AoA          = 5
%   rigid_element =
    aerodynamic_spanwise_distribution = 0
    fuel_percentage =
    chord           = 0.2          % Single value is used for
                                % constant chord length
                                % The user may specify
                                % at each Keypoint
values
    crosssection {
        reference axis      = 0.2878 0
                                % location of ra from LE
                                % User may choose following
                                % type of input for variable
                                % reference axis locations
        mass_distribution = 0.319
                                % (mass units)/(unit span)
        center_of_gravity{
            cgx = 0.0
            cgy = 0.00756
            cgz = 0.0
                                % @ c/4
                                % located at ra
        }
        inertia {
            Ixx= 8.089765E-04
            Ixy= -0.000000E+00
            Ixz= 0.000000E+00
            Iyy= 1.221712E-05
            Iyz= -6.493531E-06
            Izz= 7.967593E-04
        }
        stiffness {
            K11= 2.140827E+06 % extension stiffness [E*A]
            K12= 0.000000E+00 % extension twist coupling
            K13= 1.544115E+03 % extension bend y coupling
            K14= -4.905651E+04 % extension bend z coupling
            K22= 7.224739E+01 % twist stiffness [G*J]
            K23= -0.000000E+00 % twist / bend y coupling
            K24= 0.000000E+00 % twist / bend z coupling
            K33= 1.195708E+02 % bend y stiffness [E*I]
            K34= -4.634442E+01 % bend y / bend z coupling
            K44= 6.350796E+03 % bend z stiffness
        }
    }
}

```

```

}
main_wing_dih {
    type = "wing"
    number of elements = 1 2
    control surface{
        AilR = trail 0.40 2 3 WR4 % [name, percent of chord,
start element, end element]
        AilL = trail 0.40 2 3 WL4 % [name, percent of chord,
start element, end element]
    }
    airfoil = NACA4415
    aero_coefficient = datatable
%
    airfoilfile = EMX07.dat
    AoA = 5 5 5
%
    rigid_element =
    aerodynamic_spanwise_distribution = 40
    fuel_percentage =
    chord = 0.2 % Single value is used for
% constant chord length
% The user may specify
values % at each Keypoint

    crosssection {
        reference axis = 0.2878 0 % location of ra from LE
% User may choose following
% type of input for variable
% reference axis locations

        mass_distribution = 0.319 % (mass units)/(unit span)

        center_of_gravity{
            cgx = 0.0 % Empty inputs means cg is
            cgy = 0.00756 % @ c/4
            cgz = 0.0
        } % located at ra

        inertia {
            Ixx= 8.089765E-04
            Ixy= -0.000000E+00
            Ixz= 0.000000E+00
            Iyy= 1.221712E-05
            Iyz= -6.493531E-06
            Izz= 7.967593E-04
        }

        stiffness {
            K11= 2.140827E+06 % extension stiffness [E*A]
            K12= 0.000000E+00 % extension twist coupling
            K13= 1.544115E+03 % extension bend y coupling
            K14= -4.905651E+04 % extension bend z coupling
            K22= 7.224739E+01 % twist stiffness [G*J]
            K23= -0.000000E+00 % twist / bend y coupling
            K24= 0.000000E+00 % twist / bend z coupling
            K33= 1.195708E+02 % bend y stiffness [E*I]
            K34= -4.634442E+01 % bend y / bend z coupling
            K44= 6.350796E+03 % bend z stiffness
        }
    }
}
}

```

```

tail_in_right {
  type = "wing"
  number of elements = 1
  control surface{
    % NM = [lead/trail(location),...
    %       percentage of chord,...
    %       start element,...
    %       end element,...
    %       memb label]
    ELR1in = trail 0.98 1 1 TR1in % [name, percent of
chord, start element, end element]
    ELR2in = trail 0.98 1 1 TR2in % [name, percent of
chord, start element, end element]
  }
  airfoil      = NACA0012
  aero_coefficient = datatable
  AoA          = 0
  rigid_element = 1
  aerodynamic_spanwise_distribution = 40
  fuel_percentage =
chord          = 0.11          % Single value is used for
                                % constant chord length
                                % The user may specify
                                % at each Keypoint
values
crosssection {
  reference axis      = 0.3235 0% location of ra from LE
                                % User may choose following
                                % type of input for variable
                                % reference axis locations
  mass_distribution = 0.129 % (mass units)/(unit span)
  center_of_gravity{
    cgx = 0.0
    cgy = 0.008085 % @ c/4
    cgz = 0.0
  } % located at ra
  inertia {
    Ixx= 1.597900E-04
    Ixy= -0.000000E+00
    Ixz= 0.000000E+00
    Iyy= 2.914098E-06
    Iyz= -1.688579E-22
    Izz= 1.568759E-04
  }
  stiffness {
numbers are dummy
    K11= 3.214025E+06 % extension stiffness [E*A]
    K12= 0.000000E+00 % extension twist coupling
    K13= -3.714275E-04 % extension bend y coupling
    K14= -7.441697E+04 % extension bend z coupling
    K22= 2.138858E+01 % twist stiffness [G*J]
    K23= -0.000000E+00 % twist / bend y coupling
    K24= 0.000000E+00 % twist / bend z coupling
    K33= 9.098072E+01 % bend y stiffness [E*I]
    K34= 2.262609E-06 % bend y / bend z coupling
    K44= 4.274273E+03 % bend z stiffness
  }
}

```

```

rigid_body{
  point_mass      = 1 % changed spelling
  nodes           = 2
  center_of_gravity = 0.04575 4.95E-04 -0.0005
  mass            = 0.04873
  inertia{
    Ixx = 4.631E-06
    Ixy = -3.190E-06
    Ixz = -3.057E-07
    Iyy = 2.282E-05
    Iyz = 2.644E-08
    Izz = 2.651E-05
  }
}
}
}
tail_out_right {
  type = "wing"
  number of elements = 1
  control surface{
    % NM = [lead/trail(location),...
    %       percentage of chord,...
    %       start element,...
    %       end element,...
    %       memb label]
    ELR1ou = trail 0.98 1 1 TR1ou % [name, percent of
chord, start element, end element]
    ELR2ou = trail 0.98 1 1 TR2ou % [name, percent of
chord, start element, end element]
  }
  airfoil      = NACA0012
  aero_coefficient = datatable
  AoA          = 0
  rigid_element = 1
  aerodynamic_spanwise_distribution = 40
  fuel_percentage =
chord          = 0.11          % Single value is used for
                                % constant chord length
                                % The user may specify
                                % at each Keypoint
values
crosssection {
  reference axis      = 0.3235 0% location of ra from LE
                                % User may choose following
                                % type of input for variable
                                % reference axis locations
  mass_distribution = 0.129 % (mass units)/(unit span)
  center_of_gravity{
    cgx = 0.0 % Empty inputs means cg is
    cgy = 0.008085 % @ c/4
    cgz = 0.0
  } % located at ra
  inertia {
    Ixx= 1.597900E-04
    Ixy= -0.000000E+00
    Ixz= 0.000000E+00
    Iyy= 2.914098E-06

```

```

        Iyz= -1.688579E-22
        Izz=  1.568759E-04
    }
    stiffness {
numbers are dummy
        K11=  3.214025E+06    % extension stiffness [E*A]
        K12=  0.000000E+00    % extension twist coupling
        K13= -3.714275E-04    % extension bend y coupling
        K14= -7.441697E+04    % extension bend z coupling
        K22=  2.138858E+01    % twist stiffness [G*J]
        K23= -0.000000E+00    % twist / bend y coupling
        K24=  0.000000E+00    % twist / bend z coupling
        K33=  9.098072E+01    % bend y stiffness [E*I]
        K34=  2.262609E-06    % bend y / bend z coupling
        K44=  4.274273E+03    % bend z stiffness
    }
    rigid_body{
        point_mass          = 1 % changed spelling
        nodes                = 1
        center_of_gravity   = 0.0286 0.008395 0.0
        mass                 = 0.02
        inertia{
            Ixx = 1.866E-07
            Ixy = 1.000E-10
            Izx = 0.000E+00
            Iyy = 1.341E-06
            Iyz = 0.000E+00
            Izz = 1.311E-06
        }
    }
}
tail_in_left {
    type = "wing"
    number of elements = 1
    control surface{
        % NM = [lead/trail(location),...
        %       percentage of chord,...
        %       start element,...
        %       end element,...
        %       memb label]
        ELL1in = trail 0.98 1 1 TL1in % [name, percent of
chord, start element, end element]
        ELL2in = trail 0.98 1 1 TL2in % [name, percent of
chord, start element, end element]
    }
    airfoil          = NACA0012
    aero_coefficient = datatable
    AoA              = 0
    rigid_element    = 1
    aerodynamic_spanwise_distribution = 40
    fuel_percentage =
    chord            = 0.11          % Single value is used for
                                     % constant chord length
                                     % The user may specify
values
                                     % at each Keypoint

```

```

crosssection {
  reference axis      = 0.3235 0% location of ra from LE
                        % User may choose following
                        % type of input for variable
                        % reference axis locations
  mass_distribution = 0.129 % (mass units)/(unit span)
  center_of_gravity{
    cgx = 0.0 % Empty inputs means cg is
    cgy = 0.008085 % @ c/4
    cgz = 0.0
  } % located at ra
  inertia {
    Ixx= 1.597900E-04
    Ixy= -0.000000E+00
    Ixz= 0.000000E+00
    Iyy= 2.914098E-06
    Iyz= -1.688579E-22
    Izz= 1.568759E-04
  }
  stiffness { % Be Set to rigid. These
numbers are dummy
    K11= 3.214025E+06 % extension stiffness [E*A]
    K12= 0.000000E+00 % extension twist coupling
    K13= -3.714275E-04 % extension bend y coupling
    K14= -7.441697E+04 % extension bend z coupling
    K22= 2.138858E+01 % twist stiffness [G*J]
    K23= -0.000000E+00 % twist / bend y coupling
    K24= 0.000000E+00 % twist / bend z coupling
    K33= 9.098072E+01 % bend y stiffness [E*I]
    K34= 2.262609E-06 % bend y / bend z coupling
    K44= 4.274273E+03 % bend z stiffness
  }
  rigid_body{
    point_mass      = 1 % changed spelling
    nodes           = 2
    center_of_gravity = -0.04575 4.95E-04 -0.0005
    mass            = 0.04873
    inertia{
      Ixx = 4.631E-06
      Ixy = -3.190E-06
      Ixz = -3.057E-07
      Iyy = 2.282E-05
      Iyz = 2.644E-08
      Izz = 2.651E-05
    }
  }
}
tail_out_left {
  type = "wing"
  number of elements = 1
  control surface{
    % NM = [lead/trail(location),...
    %       percentage of chord,...
    %       start element,...
    %       end element,...
    %       memb label]

```

```

        ELL1ou = trail 0.98 1 1 TL1ou % [name, percent of
chord, start element, end element]
        ELL2ou = trail 0.98 1 1 TL2ou % [name, percent of
chord, start element, end element]
    }
    airfoil          = NACA0012
    aero_coefficient = datatable
    AoA              = 0
    rigid_element    = 1
    aerodynamic_spanwise_distribution = 40
    fuel_percentage  =
chord                = 0.11          % Single value is used for
                                     % constant chord length
                                     % The user may specify
values
                                     % at each Keypoint
    crosssection {
        reference axis    = 0.3235 0% location of ra from LE
                                     % User may choose following
                                     % type of input for variable
                                     % reference axis locations
        mass_distribution = 0.129 % (mass units)/(unit span)
        center_of_gravity{
            cgx = 0.0
            cgy = 0.008085 % @ c/4
            cgz = 0.0
        } % located at ra
        inertia {
            Ixx= 1.597900E-04
            Ixy= -0.000000E+00
            Ixz= 0.000000E+00
            Iyy= 2.914098E-06
            Iyz= -1.688579E-22
            Izz= 1.568759E-04
        }
        stiffness {
numbers are dummy
            K11= 3.214025E+06 % extension stiffness [E*A]
            K12= 0.000000E+00 % extension twist coupling
            K13= -3.714275E-04 % extension bend y coupling
            K14= -7.441697E+04 % extension bend z coupling
            K22= 2.138858E+01 % twist stiffness [G*J]
            K23= -0.000000E+00 % twist / bend y coupling
            K24= 0.000000E+00 % twist / bend z coupling
            K33= 9.098072E+01 % bend y stiffness [E*I]
            K34= 2.262609E-06 % bend y / bend z coupling
            K44= 4.274273E+03 % bend z stiffness
        }
        rigid_body{
            point_mass      = 1 % changed spelling
            nodes           = 1
            center_of_gravity = -0.0286 0.008395 0.0
            mass            = 0.02
            inertia{
                Ixx = 1.866E-07
                Ixy = 1.000E-10
                Ixz = 0.000E+00
            }
        }
    }

```

```

        Iyy = 1.341E-06
        Iyz = 0.000E+00
        Izz = 1.311E-06
    }
}
}
}
}
fairing_center {
    type = "vtail"
    number of elements = 1
    airfoil = NACA0018
    aero_coefficient = datatable
%   airfoilfile = mh78.dat
    AoA = 0
    rigid_element = 1
    aerodynamic_spanwise_distribution = 40
    fuel_percentage =
    chord = 0.37 % Single value is used for
                % constant chord length
                % The user may specify
                % at each Keypoint
values
crosssection {
    reference axis= 0.6093 0%0 0%
    mass_distribution= 1.0e-8 % (mass units)/(unit span)
    inertia {
        Ixx= 1.0e-8
        Ixy= 0
        Ixz= 0
        Iyy= 1.0e-8
        Iyz= 0
        Izz= 1.0e-8
    }
    stiffness { % Be Set to rigid. These numbers
        K11= 5.390E+07 % extension stiffness [E*A]
        K12= 0 % extension twist coupling
        K13= 0 % extension bend y coupling
        K14= 0 % extension bend z coupling
        K22= 5.390E+07 % twist stiffness [G*J]
        K23= 0 % twist / bend y coupling
        K24= 0 % twist / bend z coupling
        K33= 5.390E+07 % bend y stiffness [E*I]
        K34= 0 % bend y / bend z coupling
        K44= 5.390E+07 % bend z stiffness
    }
}
rigid_body{
    point_mass = 2 % changed spelling
    nodes = 1 2
    center_of_gravity{
        cgx{
            0% 0.0125 % 0.0125 % center pod battery
            0%-0.0031
        }
        cgy{
            0.0591 % 0.0591 % center pod battery
            0.0431
}

```


are dummy

```
inertia {
  Ixx= 1.0e-8
  Ixy= 0
  Ixz= 0
  Iyy= 1.0e-8
  Iyz= 0
  Izz= 1.0e-8
}
stiffness {          % Be Set to rigid. These numbers

  K11= 5.390E+07 % extension stiffness [E*A]
  K12= 0          % extension twist coupling
  K13= 0          % extension bend y coupling
  K14= 0          % extension bend z coupling
  K22= 5.390E+07 % twist stiffness [G*J]
  K23= 0          % twist / bend y coupling
  K24= 0          % twist / bend z coupling
  K33= 5.390E+07 % bend y stiffness [E*I]
  K34= 0          % bend y / bend z coupling
  K44= 5.390E+07 % bend z stiffness
}
rigid_body{
  point_mass      = 2 % changed spelling
  nodes           = 1 2
  center_of_gravity{
    cgx{
      0.0125 % 0.0125 % right pods battery
      -0.0062
    }
    cgy{
      0.0591 % 0.0591 % left pods battery
      0.0662
    }
    cgz{
      -0.0689 %-0.0689 % right pods battery
      0.0066
    }
  }
}
mass{
  0.3960
  1.0571
}
inertia{
  Ixx{
    1.160E-03
    1.134E-02
  }
  Ixy{
    0.000E+00
    -1.212E-03
  }
  Ixz{
    0.000E+00
    1.055E-05
  }
  IYY{
    9.485E-05
  }
}
```



```

% (4): location number
% (5): cartesian direction
% (6): time-independent value
% (7): time-independent value (OPTIONAL)
% (8): start time (OPTIONAL)
% (9): stop time (OPTIONAL)
Mot1 = force PODC node 1 y
1.381910189857558%1.393017135044694%1.397558812228706
%1.179272806499928%2.076274838533569 -0.5*sin(2*pi/0.10*(t-0.01))
0.01 0.11
Mot2 = force POD1up node 1 y
1.381910189857558%1.393017135044694%1.397558812228706
%1.179272806499928%2.076274838533569 -0.5*sin(2*pi/0.10*(t-0.01))
0.01 0.11
Mot3 = force POD2up node 1 y
1.381910189857558%1.393017135044694%1.397558812228706
%1.179272806499928%2.076274838533569 -0.5*sin(2*pi/0.10*(t-0.01))
0.01 0.11
Mot4 = force POD3up node 1 y
1.381910189857558%1.393017135044694%1.397558812228706
%1.179272806499928%2.076274838533569 -0.5*sin(2*pi/0.10*(t-0.01))
0.01 0.11
Mot5 = force POD4up node 1 y
1.381910189857558%1.393017135044694%1.397558812228706
%1.179272806499928%2.076274838533569 -0.5*sin(2*pi/0.10*(t-0.01))
0.01 0.11
D1 = force PODC node 2 y -0.4408
D2 = force POD1up node 2 y -0.4408
D3 = force POD2up node 2 y -0.4408
D4 = force POD3up node 2 y -0.4408
D5 = force POD4up node 2 y -0.4408
% Fexample = force WL1 node 60 z 30*sin(20*t)
% [(1) (2) (3) (4) (5) (6) OPTIONAL (7) OPTIONAL (8)]
% (1): load type (force_dist)
% (2): member designation
% (3): starting element
% (4): ending element
% (5): cartesian direction
% (6): time-independent value
% (7): time-independent value (OPTIONAL)
% (8): start time (OPTIONAL)
% (9): stop time (OPTIONAL)
% FD1 = force_dist MB 1 20 z 50*sin(40*t)+25
% [(1) (2) (3) (4) (5) (6) OPTIONAL (7) OPTIONAL (8)]
% (1): load type (moment)
% (2): member designation
% (3): location type(keypoint or node)
% (4): location number
% (5): cartesian direction
% (6): time-independent value
% (7): time-independent value (OPTIONAL)
% (8): start time (OPTIONAL)
% (9): stop time (OPTIONAL)
% M1 = moment MB node 60 x 50
% [(1) (2) (3) (4) (5) (6) OPTIONAL (7) OPTIONAL (8)]
% (1): load type (moment_dist)
% (2): member designation

```

```

% (3): starting element
% (4): ending element
% (5): cartesian direction
% (6): time-independent value
% (7): time-independent value (OPTIONAL)
% (8): start time (OPTIONAL)
% (9): stop time (OPTIONAL)
% MD1 = moment_dist MB 9 10 z 50
% [load type, member designation, element start, element end,
mode, voltage value, OPTIONAL--> start time, stop time,...] % NEED TO
COMPLETE
% VAL = actuator_volt VAL 1 10
% [(1) (2) (3) OPTIONAL (4) OPTIONAL (5)]
% (1): load type (control_surf)
% (2): control surface designation
% (3): time-independent value
% (4): time-independent value (OPTIONAL)
% (5): start time (OPTIONAL)
% (6): stop time (OPTIONAL)
DEFTAIL1= control_surf ELR1in 0.255459746972205%-
0.797452909688008%-0.798991452122181% 12*sin(2*pi/7.4*t) %-
0.5*sin(2*pi/0.10*(t-0.01)) 0.01 0.11
DEFTAIL2= control_surf ELR1ou 0.255459746972205%-
0.797452909688008%-0.798991452122181% 12*sin(2*pi/7.4*t) %-
0.5*sin(2*pi/0.10*(t-0.01)) 0.01 0.11
DEFTAIL3= control_surf ELR2in 0.255459746972205%-
0.797452909688008%-0.798991452122181% 12*sin(2*pi/7.4*t) %-
0.5*sin(2*pi/0.10*(t-0.01)) 0.01 0.11
DEFTAIL4= control_surf ELR2ou 0.255459746972205%-
0.797452909688008%-0.798991452122181% 12*sin(2*pi/7.4*t) %-
0.5*sin(2*pi/0.10*(t-0.01)) 0.01 0.11
DEFTAIL5= control_surf ELL1in 0.255459746972205%-
0.797452909688008%-0.798991452122181% -12*sin(2*pi/7.4*t) %-
0.5*sin(2*pi/0.10*(t-0.01)) 0.01 0.11
DEFTAIL6= control_surf ELL1ou 0.255459746972205%-
0.797452909688008%-0.798991452122181% -12*sin(2*pi/7.4*t) %-
0.5*sin(2*pi/0.10*(t-0.01)) 0.01 0.11
DEFTAIL7= control_surf ELL2in 0.255459746972205%-
0.797452909688008%-0.798991452122181% -12*sin(2*pi/7.4*t) %-
0.5*sin(2*pi/0.10*(t-0.01)) 0.01 0.11
DEFTAIL8= control_surf ELL2ou 0.255459746972205%-
0.797452909688008%-0.798991452122181% -12*sin(2*pi/7.4*t) %-
0.5*sin(2*pi/0.10*(t-0.01)) 0.01 0.11
DEFAilR = control_surf AilR 0 %-25*sin(2*pi/5*t)% 0.1 10
DEFAilL = control_surf AilL 0 %-25*sin(2*pi/5*t)% 0.1 10
}
}

Simulation {
mode = "new"
type = "dynamic"

% Model Construction Parameters
structural damping = 1e-4 % Structural damping
parameter

```

```

structure
    first mode damping = -1e-4
to
    % (set to 0 for no
    % damping)
    % First mode damping (set
    % negative value to use the
    % given alphD)

    % Steady State Simulation Parameters
    sssim{
        sim_type = "nonlinear" % or "linearized"
        relative tolerance = .001 % Relative tolerance for
static
        numerical damping = .8 % solution convergence
parameter % Numerical damping

        max iterations = 100 % for static solution
iterations % Maximum number of
state % allowed in each steady
% solution
    }
    % Time Simulation Parameters
    timesim{
        integration_type = "Gen-Alpha" % "Trapz" % or
        sim_type = "linear" % "nonlinear" or "linear" /
"reduced_order"
        time_duration = 15
        time_step = 0.001 % or time_divisions=4000
% restart_filename = "wbt_smpl" % ??????
        rho_inf_1 = 0.999
        rho_inf_2 = 0.999
        time_step_save = 100
        start_time_flag = 0 % put a 1 to start from previous
conditions fresh simulations require 0
        n_sub_add_time_step = 1
        error_states_0 = []
        gust_input = 0
        local_wrinkling = 0
        ref_val_1 = 1e10
        ref_val_2 = 1e10
        time_sim_tol = 1e1
        no_rigidbody_dof = 0
    }
    % Flutter Analysis Parameters
    flutsim{
vehicle
        flight_index = 5 % Flight indices where
% stability is calculated
        altitude = 30 30 30 30 30 % Altitudes at each index
        fuel_mass = 0 0 0 0 0 % Fuel mass
        body_angle = 2.205322913566195 -0.045987813505220 -
1.443354591065910 -2.368166336699205 -3.011227170417016
% Body angle will come from
trim solution and have same number of inputs as speeds sep by spaces

```

```

        flap_angle          = -4.489285620262512 -0.798991452122181
1.274654009819700 2.561879489113293 3.425940725693468
                                % Flap angle
        thrust              = 1.175649523636680 1.397558812228706
1.640699000413539 1.919182700376490 2.229785787025574
                                % Thrust force
        U_predict           = 12 2 20          % lower, step, and upper
        rb_const            = 0              % Type of rigid body
constraint
                                % 0: No rb constraint
                                % 1: Full rb constraint
                                % 2: only plunging is free
                                % 3: only pitching is free
                                % 4: plunging and pitching
free
        re_trim             = 1              % Flag to indicate retrim
                                % during the speed
increment
        load_update_flag    = Mot1 Mot2 Mot3 Mot4 Mot5 DEFTAIL1
DEFTAIL2 DEFTAIL3 DEFTAIL4 DEFTAIL5 DEFTAIL6 DEFTAIL7 DEFTAIL8
    } % Note about flutter analysis:
        % altitude and fuel_mass are n by 1 column matrices, where n is
the
        % number of index
        % body_angle, flap_angle, and thrust are also n by 1 column
matrices
        % only when re_trim = 0 (no retrim is considered). They are
usually
        % n by m matrices where m equals the span of speed increment
        % Modal Analysis Parameters
        modalsim{
            config           = free          % and/or deformed_shape
                                % Modal analysis using
                                % different criteria
                                % free vibration (in
vacuum)
                                % deformed vibration (under
                                % prescribed load)
        }
        % Trim Module Parameters
        trimsim{
            trim_count       = 1%5          % Number
of trim solutions to be performed
            altitude         = 30%30 30 30 30 30% Altitudes at each index
            U_trim           = 14%12 14 16 18 20% Flight Speed at each index
            fuel_mass        = 0%0 0 0 0 0  % Fuel mass at each
index
            trimoption       = 0%0 0 0 0 0  % 0: static trim (use
forces) 1: dynamic trim (use accel.)
            tol_trim         = 1e-2%1e-2 1e-2 1e-2 1e-2 1e-2  % Tolerance to
converge
            parameters {      % They override the values set in the previous
sections (as in Loads Structure)
                baoa        2 0.1          % Body angle of attack, initial guess,
increment
                Mot1       4 0.1          % Load name (pt load), initial guess,
increment

```

```

    Mot2      4 0.1
    Mot3      4 0.1
    Mot4      4 0.1
    Mot5      4 0.1
    DEFTAIL1  2 0.1    % CS name, initial guess, increment
    DEFTAIL2  2 0.1    % CS name, initial guess, increment
    DEFTAIL3  2 0.1    % CS name, initial guess, increment
    DEFTAIL4  2 0.1    % CS name, initial guess, increment
    DEFTAIL5  2 0.1    % CS name, initial guess, increment
    DEFTAIL6  2 0.1    % CS name, initial guess, increment
    DEFTAIL7  2 0.1    % CS name, initial guess, increment
    DEFTAIL8  2 0.1    % CS name, initial guess, increment
  }
}
Screen Output{
  refgeom{
    undeformed_geometry = 1
    sketch_plot          = 1
    color_style          = "gray" % "spring" or "summer" or
"autumn" or "winter" or "gray"
  }
  sssim{
    static_deformed_geometry = 1
    no_force_lines           = 0
    text                     = 1
    print_lift_moment        = 1
    figure_position          = 0.05 0.05 0.60 0.60
    figure_color              = 0
    view                     = 160 45
    animate_response         = 1
    movie                    =
    iteration_output         = 1
  }
  timesim{
    time_step_output        = 1
    iteration_output        = 1
    progress_bar            = 0
  }
  flutsim{
    plot_poles              = 0
  }
  modalsim {
    numberofmodes          = 10      % Number of modes to be
displayed on screen
    scale                   = 1      % Factor to scale the mode
shapes NOTE: No normalization is done with the modes
  }
  trimsim{
  }
% print_to_file{
%   stiffness_matrix       = 1
%   interial_matrix       = 1
%   trim_input            = 1
%   trim_output           = 1
%   modal_analysis        = frequency
% }

```

```

% generate_input_treeI      = 1
% generate_input_treeC      = 1
% response_plot {
%     keypoint 2 pos_z
%     keypoint 2 vel_z
% }
% load_plot                  = FL1 F1
% }

```

```

File Output{
% Time Simulation File Output Request
timesim{
    bframe_flight_path      = 1
    bframe_flight_velocity  = 1
    euler_angles            = 1
    displacement{
        WR4 node 9
        WR4 node 6
        WR4 node 3
        WR3 node 6
        WR3 node 3
        WR2 node 6
        WR2 node 3
        WR1 node 6
        WR1 node 3
        WR1 node 1
        WL4 node 9
        WL4 node 6
        WL4 node 3
        WL3 node 6
        WL3 node 3
        WL2 node 6
        WL2 node 3
        WL1 node 6
        WL1 node 3
        WL1 node 1
    }
% displacement{
%     all
% }
    displacementsort        = "node"    % "node" or "time"
% liftddist{
%     all
% }
}
}

```

Bibliography

1. Blair, Maxwell and Robert A. Canfield. “A Joined-Wing Structural Weight Modeling Study.” (AIAA 2002-1337), 2002.
2. Brown, E.L. “Integrated Strain Actuation in Aircraft with Highly Flexible Composite Wings.” Ph.D. Dissertation. Massachusetts Institute of Technology, Boston, MA, June 2003.
3. Cesnik, Carlos E.S. and E.L. Brown. “Active Warping Control of a Joined-Wing Airplane Configuration.” (AIAA 2002-1719), 2002.
4. Cesnik, Carlos E.S., Senatore, Patrick J., Su, Weihua, Atkins, Ella M., Shearer, Christopher M. and Nathan A. Pitcher. “X-HALE: A Very Flexible UAV for Nonlinear Aeroelastic Tests.” (AIAA 2010-2715), April 2010.
5. Cesnik, Carlos E. S. and Weihua Su. “Nonlinear Aeroelastic Modeling and Analysis of Fully Flexible Aircraft.” (AIAA 2005–2169), 2005.
6. Drela, M. “Integrated Simulation Model for Preliminary Aerodynamic, Structural, and Control-Law Design of Aircraft.” (AIAA 1999-1394), 1999.
7. Dowell, E.H., and D. Tang. “Nonlinear Aeroelasticity and Unsteady Aerodynamics.” *AIAA Journal* (Volume 40 Number 9), September 2002.
8. Garcia, J.A. “Numerical Investigation of Nonlinear Aeroelastic Effects on Flexible High-Aspect-Ratio Wings.” *Journal of Aircraft* (Volume 42 Number 4), July-August 2005.
9. González P., Oscar E., Boschetti, Pedro J., Cardenas, Elsa M. and Andrea Amerio. “Static-Stability Analysis of an Unmanned Airplane as a Flexible-Body.” (AIAA 2010-8230), 2010.
10. Jansen, K. E., Whiting, C. H., and G.M. Hulbert. “A Generalized- α Method for Integrating the Filtered Navier–Stokes Equations with a Stabilized Finite Element Method.” *Computer Methods in Applied Mechanics and Engineering* (Volume 190 Numbers 3–4), October 2000.
11. Jones, R.I. “The Design and Challenge of High Altitude Long Endurance (Hale) Unmanned Aircraft.” *The Aeronautical Journal* (Volume 27 Number 10), 1999.
12. Kaszynski, Alexander A. “X-HALE: The Development of a Research Platform for the Validation of Nonlinear Aeroelastic Codes.” Master’s Degree Thesis. Air Force Institute of Technology, Wright-Patterson Air Force Base, OH, March 2011.

13. Love, Michael H., Zink, P. Scott, Weisemann, Paul A. and Harold Youngren. "Body Freedom Flutter of High Aspect Ratio Flying Wings." (AIAA 2005-1947), 2005.
14. Noll, T.E., Brown, J.M., Perez-Davis, M.E., Ishmael, S.D., Tiffany, G.C. and M Gaier. "Investigation of the Helios Prototype Aircraft Mishap." Tech. Rep., NASA, January 2004.
15. Palacios, R. and Carlos E.S. Cesnik. "Static Nonlinear Aeroelasticity Flexible Slender Wings in Compressible Flow." (AIAA 2005-1945), 2005.
16. Patil, M.J., Hodges, D.H. and C.E.S. Cesnik. "Nonlinear Aeroelasticity and Flight Dynamics of High Altitude Long-Endurance Aircraft." *Journal of Aircraft* (Volume 38 Number 1), 2000.
17. Patil, M.J. and D.H. Hodges. "Flight Dynamics of Highly Flexible Flying Wings." *Journal of Aircraft* (Volume 43 Number 6), 2006.
18. Patil, M.J. and D.J. Taylor. "Gust Response of Highly Flexible Aircraft." (AIAA 2006-1638), 2006.
19. Peters, D. and M.J. Johnson. "Finite-State Airloads for Deformable Airfoils on Fixed and Rotating Wings." *Aeroelasticity and Fluid/Structure Interaction, American Society of Mechanical Engineers*. New York, November 1994.
20. Richards, Jenner, Suleman, Afzal, Aarons, Tyler and Robert Canfield. "Multidisciplinary Design for the Flight Test of a Scaled Joined Wing SensorCraft." (AIAA 2010-9351), 2010.
21. Saberi, Hossein, Khoshlahjeh, Maryam, Ormiston, Robert A., Rutkowski, Michael J. "Overview of RCAS and Application to Advanced Rotorcraft Problems." AHS 4th Decennial Specialist's Conference on Aeromechanics, San Francisco, California, January 2004.
22. Shearer, Christopher M. and Carlos E.S. Cesnik. "Modified Generalized- α Method for Integrating Governing Equations of Very Flexible Aircraft." (AIAA 2006-1747), 2006.
23. Shearer, Christopher M. and Carlos E.S. Cesnik. "Nonlinear Flight Dynamics of Very Flexible Aircraft." *Journal of Aircraft* (Volume 44 Number 5), 2007.
24. Shearer, Christopher M. and Carlos E.S. Cesnik. "Trajectory Control for Very Flexible Aircraft." *Journal of Guidance, Control, and Dynamics* (Volume 31 Number 2), March-April 2008.

25. Shearer, C. M. and C. E. S. Cesnik. "X-HALE_TestPlan_v19_19Oct2010." Ann Arbor, 19 Oct. 2010. DOC.
26. Sotoudeh, Zahra and Dewey H. Hodges. "Nonlinear Aeroelastic Analysis of Joined-Wing Aircraft with Fully Intrinsic Equations." (AIAA 2009-2464), 2009.
27. Sotoudeh, Zahra and Dewey H. Hodges. "Parametric Study of Joined-Wing Aircraft Geometry." (AIAA 2010-2718), 2010.
28. Sotoudeh, Zahra, Hodges, Dewey H. and Chong-Seok Chang. "Validation Studies for Aeroelastic Trim and Stability Analysis of Highly Flexible Aircraft," *Journal of Aircraft* (Volume 47 Number 4), 2010.
29. Stevens, B.L. and F.L. Lewis. *Aircraft Control and Simulation*. Wiley, New York, 2002.
30. Strawn, Roger C., Nygaard, Tor, Bhagwat, Mahendra J., Dimanlig, Arsenio, Saberi, Hossein, Ormiston, Robert A, and Mark Potsdam. "Integrated Computational Fluid and Structural Dynamics Analyses for Comprehensive Rotorcraft Analysis." (AIAA 2007-6575), 2007.
31. Su, Weihua and Carlos E.S. Cesnik. "Dynamic Response of Highly Flexible Flying Wings." (AIAA 2006-1636), 2006.
32. Su, Weihua and Carlos E.S. Cesnik. "Nonlinear Aeroelastic Simulations of a Flapping Wing Micro Air Vehicle Using Two Unsteady Aerodynamic Formulations." (AIAA 2010-2887), 2010.
33. Tang, D., Conner, M.D. and E.H. Dowell. "Reduced-Order Aerodynamic Model and Its Application to a Nonlinear Aeroelastic System." *Journal of Aircraft* (Volume 35 Number 2), March-April 1998.
34. Tang, D. and E.H. Dowell. "Experimental and Theoretical Study on Aeroelastic Response of High-Aspect-Ratio Wings." *Journal of Aircraft* (Volume 39 Number 8), August 2001.
35. Tilmann, C.P., Flick, P.M, Martin, C.A. and M.H. Love, "High-Altitude Long Endurance Technologies for SensorCraft." RTO AVT Symposium on "Novel Vehicle Concepts and Emerging Vehicle Technologies," Brussels, Belgium, April 7-10 2003, MP-104-P-26-1.
36. Van Schoor, M.C. and A.H. von Flotow. "Aeroelastic Characteristics of a Highly Flexible Aircraft," *Journal of Aircraft* (Volume 27 Number 10), October 1990.

37. Wang, Z., Chen, P.C., Liu, D.D., Mook, D.T. and M.J. Patil. "Time Domain Nonlinear Aeroelastic Analysis for HALE Wings." (AIAA 2006-1640), May 2006.
38. Weishaar, T.A. and D. Lee. "Aeroelastic Tailoring of Joined-Wing Configurations." (AIAA 2002-1207), April 2002.
39. Whitson, S. "The Proteus, Giving Shape to Forms Unknown," Private Pilot (Volume 33 Number 12), December 1998.
40. Wilson, J.R. "Fly Like a Vulture," Aerospace America (Volume 46 Number 11), November 2008.

REPORT DOCUMENTATION PAGE				<i>Form Approved</i> OMB No. 074-0188	
The public reporting burden for this collection of information is estimated to average 1 hour per response, including the time for reviewing instructions, searching existing data sources, gathering and maintaining the data needed, and completing and reviewing the collection of information. Send comments regarding this burden estimate or any other aspect of the collection of information, including suggestions for reducing this burden to Department of Defense, Washington Headquarters Services, Directorate for Information Operations and Reports (0704-0188), 1215 Jefferson Davis Highway, Suite 1204, Arlington, VA 22202-4302. Respondents should be aware that notwithstanding any other provision of law, no person shall be subject to a penalty for failing to comply with a collection of information if it does not display a currently valid OMB control number. PLEASE DO NOT RETURN YOUR FORM TO THE ABOVE ADDRESS.					
1. REPORT DATE (DD-MM-YYYY) 16 June 2011		2. REPORT TYPE Master's Thesis		3. DATES COVERED (From - To) March 2010 - June 2011	
4. TITLE AND SUBTITLE Simulations for the Test Flight of an Experimental HALE Aircraft				5a. CONTRACT NUMBER	
				5b. GRANT NUMBER	
				5c. PROGRAM ELEMENT NUMBER	
6. AUTHOR(S) Brooke E. Kaszynski, 2 nd Lieutenant, USAF				5d. PROJECT NUMBER	
				5e. TASK NUMBER	
				5f. WORK UNIT NUMBER	
7. PERFORMING ORGANIZATION NAMES(S) AND ADDRESS(S) Air Force Institute of Technology Graduate School of Engineering and Management (AFIT/EN) 2950 Hobson Way, Building 640 WPAFB OH 45433-8865				8. PERFORMING ORGANIZATION REPORT NUMBER AFIT/GAE/ENY/11-J02	
9. SPONSORING/MONITORING AGENCY NAME(S) AND ADDRESS(ES) Edward J. Alyanak, AFRL/RBSD 2210 8th St, Building 20146, Room 220 Wright-Patterson AFB, OH 45431 Edward.Alyanak@wpafb.af.mil 937-848-7565				10. SPONSOR/MONITOR'S ACRONYM(S) AFRL/RBSD	
				11. SPONSOR/MONITOR'S REPORT NUMBER(S)	
12. DISTRIBUTION/AVAILABILITY STATEMENT APPROVED FOR PUBLIC RELEASE; DISTRIBUTION UNLIMITED.					
13. SUPPLEMENTARY NOTES This material is declared a work of the U.S. Government and is not subject to copyright protection in the United States.					
14. ABSTRACT Recent events, such as the crash of NASA's Helios aircraft during a test flight, show that more must be known about the nonlinear control of HALE aircraft. Shearer, Cesnik and their co-workers have developed a code that is a practical solution to the coupled nonlinear aeroelasticity and flight dynamics of very flexible aircraft called the University of Michigan's Nonlinear Aeroelastic Simulation Toolbox (UM/NAST). They are also in the process of developing a model HALE aircraft called X-HALE which will be used to validate this code experimentally. This research performs flight simulations with UM/NAST so as to make predictions about X-HALE's future test flights and subsequently uncover the strengths and weaknesses of UM/NAST when X-HALE is finally flown. These simulations include simulations of straight and level flight and rolling flight. Rolling simulations involve periodic changes in the angle of the ailerons. Both the 6 meter and the 8 meter models of X-HALE are studied. Two control models are compared. These include the linear and non-linear models of UM/NAST.					
15. SUBJECT TERMS Aircraft, flexible coupling, high altitude, long endurance, HALE, UM/NAST, RPV, simulations					
16. SECURITY CLASSIFICATION OF:			17. LIMITATION OF ABSTRACT UU	18. NUMBER OF PAGES 205	19a. NAME OF RESPONSIBLE PERSON Christopher Shearer, Lt Col, USAF
a. REPORT U	b. ABSTRACT U	c. THIS PAGE U			19b. TELEPHONE NUMBER (Include area code) (937) 255-1179 (christopher.shearer@wpafb.af.mil)

